External Control in Atom Transfer Radical Polymerization

Sajjad Dadashi Silab

Carnegie Mellon University

Department of Chemistry

July 2021

In partial fulfillment of the requirements for the Ph.D. degree in Chemistry

Abstract

This dissertation describes the advances in external control in atom transfer radical polymerization (ATRP). Chapter 1 provides an overview of the fundamentals and advances of reversible deactivation radical polymerization (RDRP) techniques. In particular, the development of ATRP and the advances in use of external means for initiating the ATRP catalytic systems are highlighted.

In Chapter 2, I presented an in-depth mechanistic analysis of various ATRP systems regarding temporal control with external stimuli. Temporal control was studied in ATRP using zerovalent metals, light, and chemical redox agents. The effect of polymerization components in providing temporal control was studied. The effect of the activity of the Cu catalysts was highlighted to demonstrate the importance of developing highly active catalytic systems for achieving excellent temporal and on-demand control over polymerization. Results of this research offered a deep mechanistic understanding of the contribution of ATRP components in polymerizations induced by external stimuli. Furthermore, we developed a redox switchable ATRP system that enabled on demand control over the activity of the Cu catalyst and hence the polymerization. By applying reducing or oxidizing agents such as ascorbic acid and ferrocenium salts or air, the Cu catalyst was switched on or off, respectively. As a result, the polymerization was switched multiple times between on and off states.

As discussed in Chapter 2, we investigated photoinduced ATRP which was triggered using UV light. To explore new possibilities for carrying out photoinduced ATRP and address challenges associated with the use of UV light (*i.e.*, high energy and low depth of penetration), developing photocatalytic systems based on visible or near infrared (NIR) light is necessary. Chapter 3 presented our research in advancing photoinduced ATRP systems by taking advantage of the visible or NIR lights. We explored dual photoredox catalytic systems comprised of suitable photocatalysts used for generation of the Cu activators under visible light irradiation (green or red). In the first section of this chapter, I showed the development of a heterogeneous photocatalyst comprised of conjugated microporous polymers of phenothiazine as a highly versatile photocatalyst for activating copper-catalyzed ATRP. Using dimethoxybenzene as a crosslinker under Friedel-Crafts reaction offered the photocatalyst of being heterogeneous in nature as well as extending the conjugation throughout the network via aromatic linkages. The

heterogeneous photocatalyst enabled performing copper-catalyzed ATRP under green or red-light irradiation, and offered reusability for several reactions with high photocatalytic efficiency.

In subsequent chapters, the development of new catalytic systems for external control in ATRP other than Cu complexes is presented. Although Cu-based catalysts provide excellent control over ATRP, developing new catalytic systems would open new possibilities for the enhanced ATRP performance. For example, iron-based complexes are of great importance because of the abundance of iron on earth's crust and its involvement in biological events. These features offer a great opportunity for developing environmentally benign iron-based catalytic systems for ATRP.

In Chapter 4, I first reviewed the fundamentals and possibilities of using iron catalysts in ATRP. Next, I presented our research on development of an iron-based photoinduced ATRP system, which provided well-controlled polymerization of methacrylate monomers using ppm levels of the iron catalyst under blue light irradiation. We showed that irradiation of the catalyst with $FeBr_4^-$ anion under blue light promoted a ligand-to-metal charge transfer that resulted in a homolytic cleavage of the Fe-Br bond. Therefore, the activator Fe^{II} was generated photochemically to start the polymerization. This system was studied in detail regarding the photoreduction mechanism, the scope of applicable monomers such as fluorinated and non-fluorinated methacrylates in synthesis of homo and block copolymers, and temporal control. Subsequently, I studied the effect of halogen and reaction medium in polymerization control in iron-catalyzed ATRP in the presence of halide anions as ligands. Because of the stronger Fe-Cl bond in the Cl-based initiating systems, inefficient deactivation led to poorly controlled polymers with high dispersity. However, Br-based initiating systems provided well-controlled ATRP because of the fast and efficient Br exchange (dispersity <1.2). Moreover, we discovered that the high stability of the anionic deactivator $FeBr_4^-$ in polar solvents led to diminished rates of deactivation and therefore polymers with large dispersity values were obtained (>1.6).

Chapter 5 discussed use of organic photoredox catalysts in ATRP. Organo-catalyzed ATRP (O-ATRP) systems provide the possibility of eliminating the use of metal-based catalysts. The photocatalysts in the excited state activate the dormant chain ends via an electron transfer. The excited state photocatalyst is much more reducing than a ground state. In this work we extended the use of phenothiazine as a visible light photocatalyst in O-ATRP of methacrylate monomers.

We showed that extended conjugation imparted by introducing a phenyl ring to the catalyst's core resulted in a red shift in the absorption of the photocatalyst and thus enabled ATRP under visible light irradiation. Well-controlled polymerization of various methacrylate monomers was observed with excellent temporal control modulated by light on/off periods.

In Chapter 6, I presented a new concept in catalyzing ATRP by using iodine-based initiating systems. The alkyl iodide initiator was generated in situ by a halogen exchange reaction using iodide salts and a bench-top stable alkyl bromide, ethyl α-bromophenylacetate. The alkyl iodide was activated by visible light irradiation in the presence of iodide salts as catalysts. We studied iodine-mediated photoATRP in aqueous media which enabled fast and well-controlled ATRP of a water-soluble methacrylate monomer under blue, green, or yellow light irradiation. We found that this system offered excellent control over the kinetics of polymerization that occurred only under light irradiation. The complexation of with the iodide salts with the chain ends provided labile bonds for photochemical generation of radicals. Moreover, we demonstrated that this system was oxygen tolerant as polymerizations were well-controlled in the presence of residual oxygen without the need for deoxygenation processes. The results of this chapter offered new possibilities in designing ATRP catalytic systems that can be carried out under mild conditions and controlled by photochemical processes.

Finally in Chapter 7, I summarized the results of research studies presented in this dissertation on development of ATRP catalytic systems controlled by external stimuli. I also provided an outlook for possible implications of these findings as well as new directions for advancing the field of RDRP in general and specifically for ATRP systems controlled by external stimuli.

Acknowledgements

First, I would like to sincerely thank Prof. Krzysztof (Kris) Matyjaszewski for the incredible support during my PhD research at Carnegie Mellon University. I am extremely grateful for the opportunity to join his group and carry out my graduate research under his tutelage. Kris has always been a great source of learning, support, and inspiration in many aspects. His mentorship and trust allowed me to explore and shape my ideas and advance in my research journey. I learned a great deal about science, polymers, how to critically approach problems, develop research ideas, and more importantly, how to be a successful and responsible scientist. Thank you, Kris! This dissertation would not have been possible without your continued support and guidance.

I would like to thank my friends and collaborators within the Matyjaszewski group. Thank you to Dr. Xiangcheng Pan, Dr. Marco Fantin, Dr. Francesca Lorandi, Dr. Greg Szczepaniak, Michael Martinez, Dr. Yi Wang, Dr. Sushil Lathwal, Mingkang Sun, Dr. Tom Ribelli, Khidong Kim and many more members of the MatyLab with whom I had a chance to interact and do science together.

I am also thankful to all my collaborators outside the Matyjaszewski group. I thank Prof. Craig Hawker, Prof. Athina Anastasaki, Prof. Dominik Konkolewicz, Dr. In-Hwan Lee, and my other collaborators for the work on investigating temporal control in photoinduced ATRP, which resulted in an important contribution to my PhD dissertation. In addition, I thank Prof. Eddy Benetti (ETH Zurich), Prof. Nitash Balsara and Neel Shah (UC Berkeley), and Prof. Eva Harth (University of Houston) for the opportunity to collaborate on many interesting projects beyond the scope of this dissertation.

I also thank my committee members Prof. Kevin Noonan and Prof. Newell Washburn, and Prof. Brent Sumerlin (external examiner) for their invaluable input during my research and graduate program. I am thankful to the faculty and staff within the Department of Chemistry at Carnegie Mellon University who always offered their help and support. In particular, I acknowledge Prof. Stefan Benrhard, Prof. Tomek Kowalewski, and Prof. Bruce Armitage for useful discussion, input, and their support. I acknowledge the John and Nancy Harrison Legacy Graduate Fellowship in Chemistry and Biochemistry.

Finally, I would like to dedicate this dissertation to my family. I would like to especially thank my parents, Hamid Dadashi Silab and Fariba (Zahra) Lotfi Silab and my siblings, Ammar, Somaye, and Ozra for their continued support, love, and encouragement in pursuing my education. Thank you!

Table of Contents

Table of Figures

Table of Schemes

Chapter 1.   Introduction to External Control in ATRP

Reversible deactivation radical polymerization (RDRP) techniques have been at the forefront of recent advances in polymer science.[1-3] RDRP methods offer precise control over the molecular weight, dispersity, sequence, composition, and architecture of the polymeric materials which would not be accessible in conventional radical polymerization systems. In RDRP, control over polymerization is achieved by a dynamic exchange of the polymer chains between active (radical) and dormant (capped) states. A rapid and efficient exchange between the dormant and active species is desired for efficient polymerization and minimizing the fraction of terminated chains.

Common RDRP approaches developed for controlling the activation-deactivation equilibria of polymer chains include use of stable free-radicals as controlling agents, degenerative transfer processes, or catalytic transfer of capping agents (for example, halogen atoms) (Scheme 1). For example, nitroxide mediated polymerization (NMP) uses stable nitroxide radicals to mediate the growth of polymer chains.[4] The labile alkoxyamine C-ON bond can be cleaved at elevated temperatures to form C-centered radicals to start the polymerization. Moreover, stable nitroxide radicals are generated which can reversibly trap the propagating radicals and hence exert control over polymerization.

In degenerative transfer processes, chain transfer agents (CTAs) are used to control polymerization via the degenerative transfer of radicals formed from conventional radical initiators. For example, thiocarbonylthio compounds are used as CTAs in reversible addition-fragmentation chain transfer (RAFT) polymerizations.[5] Addition of radicals to a thiocarbonylthio group forms an intermediate radical species, which can further fragment at the weak C-S bond and form a dormant polymer chain capped with the thiocarbonylthio group as well as a new propagating radical. In conventional approaches, RAFT polymerization was performed by using radical initiators to start the polymerization and gain control via the degenerate process. In recent years, the RAFT systems have been advanced by developing other external means to initiate the polymerization process.[6] The thiocarbonylthio chain transfer agents can be activated via photoinduced electron/energy transfer processes in the presence of suitable photocatalysts/photosensitizers. The photochemical activation of the CTAs generates radicals to initiate polymerization.

In addition to the RAFT process in the presence of thiocarbonylthio CTAs, iodine transfer polymerization can also undergo the degenerative transfer process.[7-9] However, due to its low transfer efficiency, iodine transfer polymerization provides moderate control over the growth of polymer chains. In the presence of suitable catalytic species, the iodine transfer can also become catalytic thus increasing the efficiency of polymerization and achieving better control.[10]

Atom transfer radical polymerization is a catalytic process involving activator and deactivator catalytic species to reversibly activate alkyl halide initiators via halogen atom transfer. Activation of the initiators by the activator catalyst (L/Cu^I) in its lower oxidation state generates initiating/propagating radicals while also forming the catalyst with a higher oxidation state bonded to a halogen atom (L/Cu^{II}-X).[2] This species acts as the deactivator for propagating radicals. Copper-based complexes are the most efficient and well-studied catalysts in ATRP. The efficiency of halogen atom transfer depends on the C-X bond dissociation energy, affinity of the Cu activator towards halogen atom (halogenophilicity) as well as high affinity of the halides for L/Cu^{II} to ensure fast deactivation of growing radicals and to afford well-controlled polymerizations.
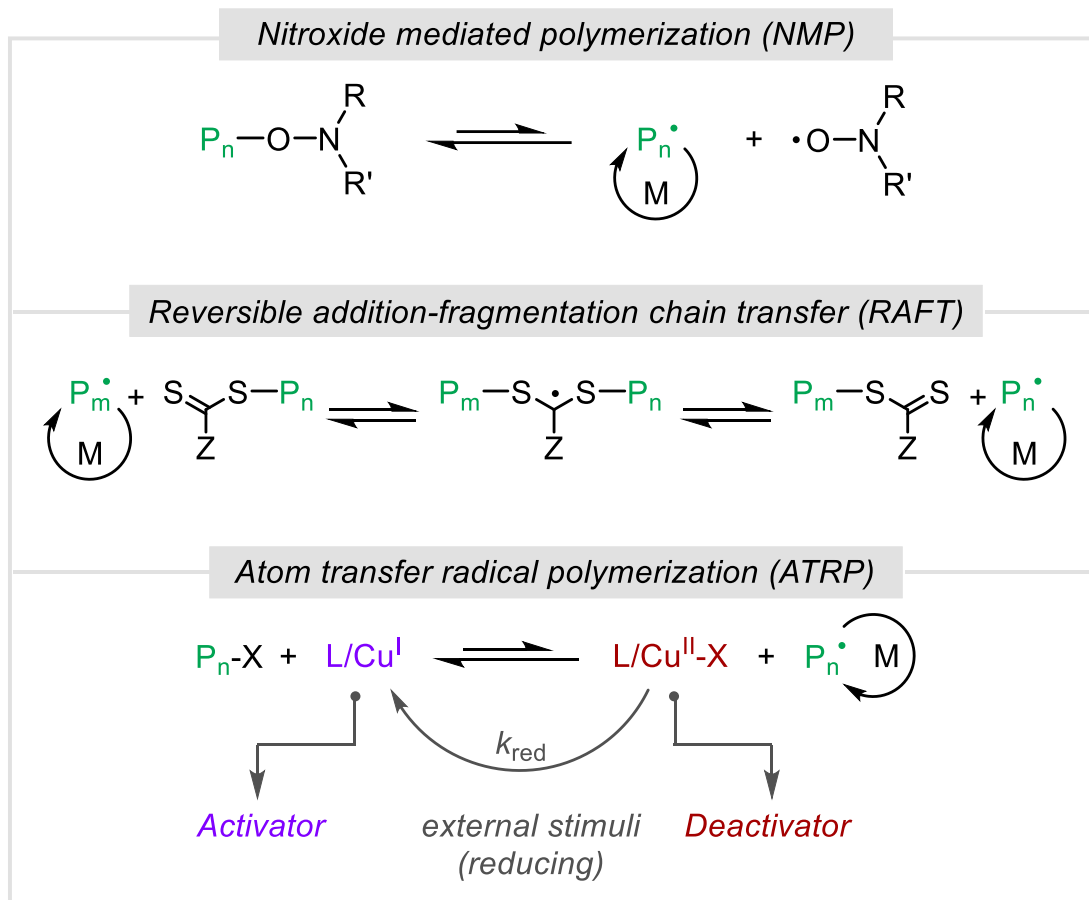
Scheme 1. Mechanism of most common RDRP methods: NMP, RAFT polymerization and ATRP.

The first generation of ATRP catalysts employed Cu complexes with 2,2'-bipyridine (bpy) ligands of relatively low catalytic activity.[11] Advances in mechanistic understanding of the ATRP processes and designing new catalytic systems have enabled increasing the activity of the Cu-based ATRP catalysts over one billion times larger than the initial Cu/bpy systems.[12] This increase in the activity of the Cu complexes offered new opportunities in controlling the ATRP processes. Use of ligands with increased electron-donating properties is one of the crucial factors for influencing the activity of the corresponding Cu catalysts. For example, substitution of the tris(2-pyridylmethyl)amine (TPMA) ligand scaffold with electron donating groups resulted in an over 3 orders of magnitude increase in the activity of the Cu catalyst.[13-15] The reduction potential of the Cu complexes with electron donating ligands shifted to more negative values and therefore increased their catalytic activity. There is a linear correlation between the reduction potential of

the Cu catalysts and the ATRP equilibrium constant (K_{ATRP}), which increases as the reduction potential of the catalyst is shifted toward more negative values (Figure 1).
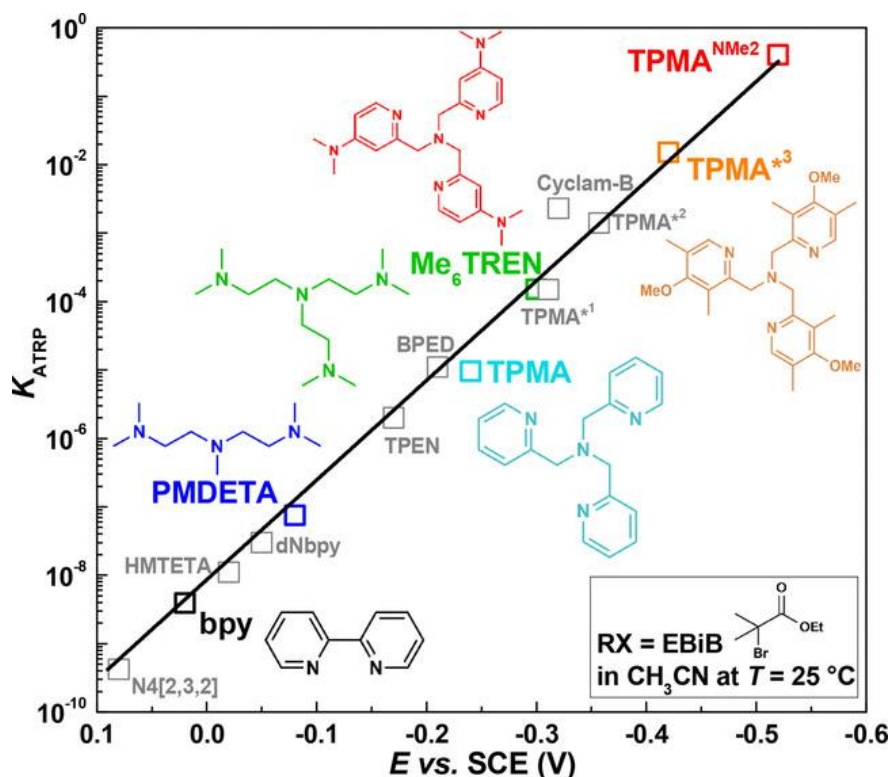
Figure 1. Correlation between the standard reduction potential of L/Cu^{II}-Br catalysts, measured by cyclic voltammetry, and the corresponding K_{ATRP} values, measured by spectroscopic methods (or predicted in the case of TPMA^{NMe2}=tris [(4-dimethylaminopyridyl) methyl] amine), in acetonitrile at 25 °C, for RX = ethyl α-bromoisobutyrate (EBiB). Adapted with permission from ref[16].

Initial attempts in development of ATRP catalysis used Cu complexes in equimolar ratios with respect to the initiator, in a process known as normal ATRP. However, use of the Cu catalyst in large quantities may not be cost effective and can cause additional challenges in purification of the final product. Decreasing the amount of required catalyst for achieving a well-controlled and efficient polymerization would need the in situ generation of the activator complex. As in any radical process, termination of radicals in ATRP results in an irreversible conversion of activator L/Cu^{I} to L/Cu^{II}-Br and thus a decrease in the rate or stop of polymerization. Therefore, advances in ATRP catalysis have been focused on the development of new initiating/catalytic systems that use various regeneration techniques to form activators in situ. In addition, because of the high

sensitivity of the L/Cu^I complexes to air and therefore difficulties associated with their handling, it is desired to start with L/Cu^{II} as it is stable and easy to handle under ambient conditions.

A variety of regeneration techniques have been developed to realize the reduction of L/Cu^{II}-Br and regeneration of the activator L/Cu^I catalysts.[17] For example, an exogeneous radical source such as azobisisobutyronitrile (AIBN), in a process known as initiators for continuous activator regeneration (ICAR) ATRP, generates radicals capable of reducing L/Cu^{II}-Br to L/Cu^I and thus initiating the polymerization.[18, 19] Chemical reducing agents such as ascorbic acid, tin(II) compounds, glucose, silver wire, and hydrazine can generate activators via reduction of L/Cu^{II}-Br to L/Cu^I in activators regenerated by electron transfer (ARGET) ATRP.[20] Zerovalent metals such as Cu^0 [21, 22] or the liquid metal eutectic Ga–In (EGaIn) alloy,[23] in addition to the regeneration of the activator, can also activate the alkyl halide dormant chains, in a process known as supplemental activator and reducing agent (SARA) ATRP.[24, 25] In mechanochemically induced ATRP, piezoelectric nanoparticles were used to reduce L/Cu^{II}-Br to L/Cu^I via electron transfer effected by applying mechanical force.[26, 27]

Electrochemistry was used to generate activator catalysts for carrying out the ATRP process.[28, 29] In addition, electrochemistry is a powerful technique for studying the properties of the ATRP catalysts and polymerization systems. Photoinduced ATRP was developed to use the energy light for performing ATRP via regeneration of the activator catalysts.[30] Different modes of activation in photoinduced ATRP can be achieved depending on the nature of the catalytic system.

All these regeneration techniques enable control over the regeneration of the activator catalytic species and therefore offer the opportunity to control the kinetics of polymerization via external means.[17] For example, application of photochemistry in ATRP processes has allowed a facile approach for gaining temporal control over the kinetics of polymerization and fabricate patterned structures whereby areas exposed to light can undergo polymerization as opposed to masked area that remain unreacted (Figure 2).
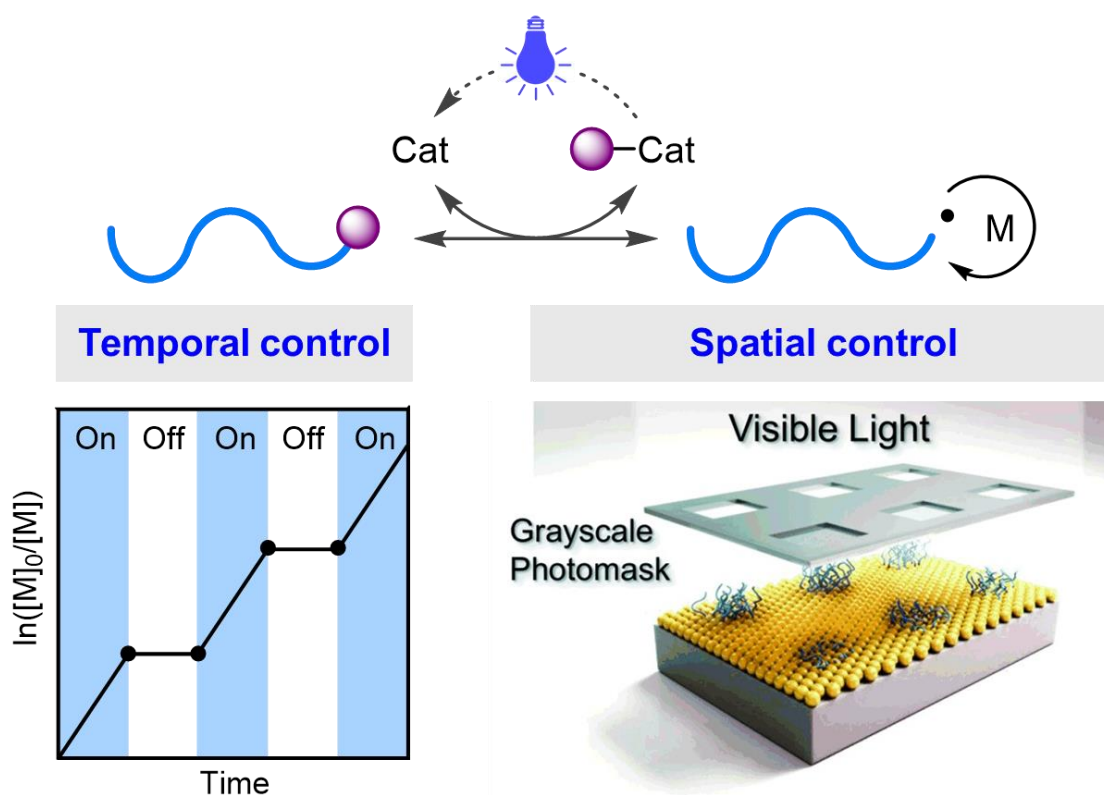
Figure 2. Light-mediated radical polymerizations offer temporal control over kinetics of the reaction as well spatial control in fabrication of patterned materials.

Photoinduced ATRP was initially conducted under UV light irradiation (<400 nm).[31-35] Photoexcitation of the L/Cu^{II} complex followed by an electron transfer from the electron donor was proposed to be a major pathway for the reduction of the Cu catalyst and regeneration of the activators (Scheme 2). Although there might be some other pathways for generation of initiating species such as direct activation of the alkyl halide *etc.*, their contribution was estimated to be minor compared to the excitation and electron transfer to the Cu catalyst.[36] The ATRP catalytic cycle was accomplished by the Cu catalyst operating in the ground state, whereas photoexcitation was required for the reduction and regeneration of the activator L/Cu^{I}. Alkylamines (including excess ligand) served as electron donors to promote the photoreduction.

Another class of photoinduced ATRP uses photoredox catalysts to mediate the activation and deactivation processes by a photocatalyst.[37, 38] The photoredox catalyzed ATRP is distinct in its underlying mechanism in which the activation of the dormant chain ends was realized by the excited state photocatalysts, as opposed to the ground state activation by the Cu catalysts. Photoredox catalysts are strongly reducing in the excited state capable of activating dormant

chains via a photoinduced electron transfer. As a result, initiating radicals are formed which is accompanied by the generation of the oxidized form of the photoredox catalyst with a halide anion ($PC^{\bullet+}/Br^-$). This species serves as a deactivator of the growing radicals, which generates the initial, ground state photocatalyst and thus completing the photocatalytic cycle.

Ir complexes were initially developed as efficient photoredox catalysts for ATRP.[39] Subsequently developed, organic-based photocatalysts offer a transition metal-free approach in catalyzing ATRP. These compounds include phenothiazines, phenoxazines, dihydrophenazines and more.[40-46] A great deal of research has been devoted in expanding the repertoire of catalytic systems as well as understanding their mechanism regarding the activation and deactivation processes.

A third class of photoinduced ATRP systems involves use of Cu complexes combined with photoredox catalysts that possess a wide range of photophysical properties and photoactivation modes. The photoredox catalysts can be used to generate the activator Cu^I via photoinduced electron/energy transfer processes. The dual photoredox catalysis enables extension of photoinduced ATRP to visible or NIR light and therefore offers new possibilities in controlling the ATRP process. For example, NIR active dyes were used as a photosensitizer in activating Cu-catalyzed ATRP under NIR light irradiation.[47] Moreover, up-conversion nanoparticles could convert the energy of NIR light to emit in the UV region.[48] The UV light emitted from the nanoparticles excited the Cu catalyst, which after a reductive quenching in the presence of electron donors generated activating species. Use of visible or NIR light for driving ATRP is advantageous over high energy UV light, which has a low depth of penetration and may pose challenges in applications where mild conditions are needed.
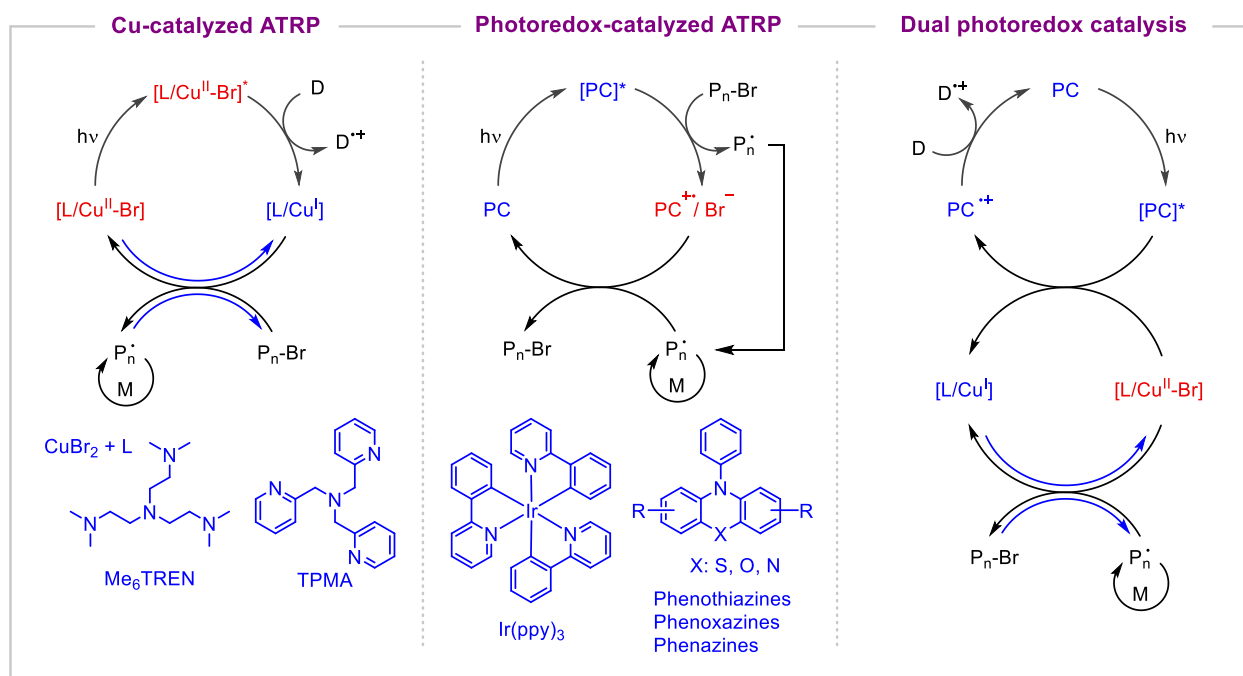
Scheme 2. Light in ATRP: (left) photoinduced ATRP via photoexcitation of the L/Cu^{II} complexes under UV light followed by a reductive quenching in the presence of electron donors to generate activators. (middle) Photoredox-catalyzed ATRP in the presence of photocatalysts to mediate polymerization via excited state activation of dormant chains. (right) Dual photoredox catalyzed ATRP using visible or NIR light active photocatalysts to generate the activator L/Cu^{I} species to start and mediate the polymerization by the Cu complexes.

A distinct feature of photochemical processes is the ability to control the kinetics of polymerization by applying or removal of light stimuli.[49] As the photoredox catalyzed ATRP operates in the excited state for the activation of the dormant chain ends and considering the low concentration of the excited state species, excellent temporal control can be achieved with an instant response to switching the light on/off. However, in Cu-catalyzed ATRP systems, temporal control is not directly achieved upon switching the light off. In these systems, the L/Cu^{I} activator is generated via photoinduced electron transfer reactions. Removal of light only stops the photoreduction and regeneration process. However, as the polymerization is catalyzed by the Cu catalysts in the ground state, the presence of residual L/Cu^{I} activator may lead to further activation of polymer chains in the dark. The extent of polymerization in the dark depends on the concentration of the activator which is modulated by the ATRP equilibrium and the activity of

the Cu catalysts. Temporal control in Cu-catalyzed ATRP systems is achieved upon consumption of the activator via radical termination reactions leading the polymerization to stop.

Therefore, to achieve excellent temporal control in Cu-catalyzed ATRP, it is important to develop highly active catalytic systems. The low concentration of the activator in the presence of highly active systems, would be quickly consumed by radical termination reactions. By contrast the low active systems the high concentration of the activator may continue polymerization further in the dark before all the activator is completely converted to L/Cu^{II}-Br deactivators.

Another approach to assert on-demand control over the activity of the catalysts and hence kinetics of polymerization would require modulation of the oxidation state of the Cu catalyst between L/Cu^{I} and L/Cu^{II} as activator and deactivator species.

Electrochemically mediated ATRP enables both reduction and oxidation of the catalyst and switching the polymerization on/off by applying reducing or oxidizing currents or potentials.[28, 50-52] Applying a reducing current switched the polymerization on by generating L/Cu^{I} activator. In the presence of oxidizing current, the catalyst was switched off by oxidizing L/Cu^{I} to L/Cu^{II}, and polymerization stopped. Using orthogonal dual stimuli that enable on demand switching of the Cu catalyst between L/Cu^{I} and L/Cu^{II} states can provide efficient temporal control over ATRP in a broad range of catalytic systems.
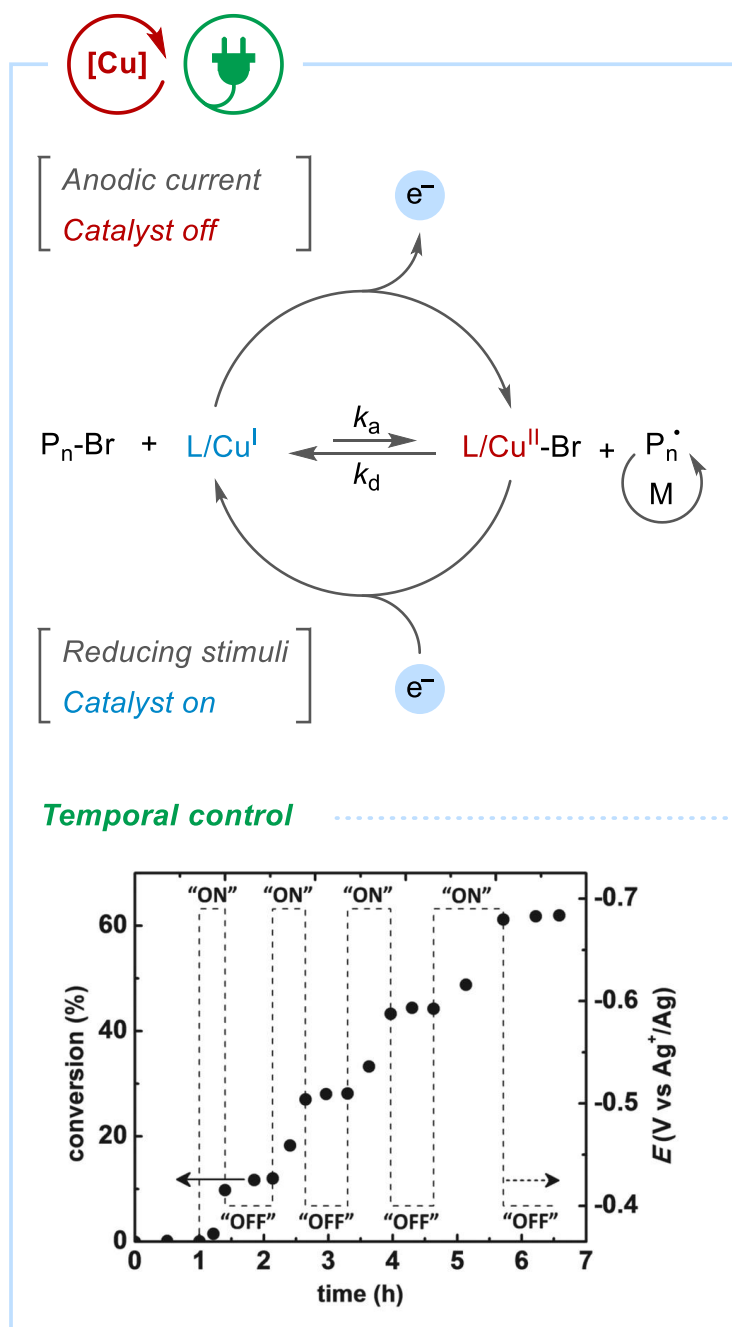
Scheme 3. Electrochemically-mediated ATRP enabling reduction and oxidation of the Cu catalyst to impart temporal control by modulating the oxidation state of the catalyst, adapted from ref[28].

Despite the advances in use of external means in ATRP prior to this PhD dissertation, more research is needed to provide a deep mechanistic understanding of all these processes as well as discover new scope for a wide range of catalytic systems. In this dissertation, I present a unified

and in-depth analysis of various ATRP initiating/catalytic systems in the presence of external stimuli. Temporal control studies shed light on the importance and contribution of polymerization components in achieving temporal control in response to application of external stimuli. In particular, the studies conducted in this dissertation pointed to the crucial role of Cu catalysts and their catalytic activity in ATRP for understanding the effect of external stimuli in providing temporal control. Different classes of ATRP catalytic systems including copper-catalyzed, iron-catalyzed, organo-catalyzed, and iodine-mediated ATRP have been studied. New directions were explored for photoinduced copper-catalyzed ATRP that involved the development of photoredox catalytic systems active under green or red light irradiation for activation of the Cu catalysts. New reactivities were developed for carrying out photoinduced ATRP in the presence of iron catalysts that rely on a unique photochemical generation of the activator compared to Cu complexes. The ligand-to-metal charge transfer under visible light enabled homolysis of the Fe-Br bond. This bond photolysis generated the Fe^{II} activator and a Br-based initiating radical. Iron catalysis was studied in a wide range of monomers as well as the mechanistic understanding of iron catalysts. In search of new reactivities for light-mediated polymerizations, an organo-catalyzed ATRP system was developed using a visible light active phenothiazine as a photoredox catalyst. Finally, the iodine-mediated photoATRP in aqueous media enabled facile and rapid polymerization of a water-soluble methacrylate monomer. The polymerization was mediated in the presence of iodide salts, acting as a catalyst complexed with the iodine chain end to activate under blue, green, or yellow light irradiation.

References

1. Corrigan, N.; Jung, K.; Moad, G.; Hawker, C. J.; Matyjaszewski, K.; Boyer, C. Reversible-deactivation radical polymerization (Controlled/living radical polymerization): From discovery to materials design and applications. *Prog. Polym. Sci.* **2020,** 111, 101311.

2. Matyjaszewski, K.; Xia, J. Atom Transfer Radical Polymerization. *Chem. Rev.* **2001,** 101 (9), 2921-2990.

3. Parkatzidis, K.; Wang, H. S.; Truong, N. P.; Anastasaki, A. Recent Developments and Future Challenges in Controlled Radical Polymerization: A 2020 Update. *Chem* **2020,** 6 (7), 1575-1588.

4. Nicolas, J.; Guillaneuf, Y.; Lefay, C.; Bertin, D.; Gigmes, D.; Charleux, B. Nitroxide-mediated polymerization. *Prog. Polym. Sci.* **2013,** 38 (1), 63-235.

5. Perrier, S. 50th Anniversary Perspective: RAFT Polymerization—A User Guide. *Macromolecules* **2017,** 50 (19), 7433-7447.

6. Hill, M. R.; Carmean, R. N.; Sumerlin, B. S. Expanding the Scope of RAFT Polymerization: Recent Advances and New Horizons. *Macromolecules* **2015,** 48 (16), 5459-5469.

7. Gaynor, S. G.; Wang, J.-S.; Matyjaszewski, K. Controlled Radical Polymerization by Degenerative Transfer: Effect of the Structure of the Transfer Agent. *Macromolecules* **1995,** 28 (24), 8051-8056.

8. Iovu, M. C.; Matyjaszewski, K. Controlled/Living Radical Polymerization of Vinyl Acetate by Degenerative Transfer with Alkyl Iodides. *Macromolecules* **2003,** 36 (25), 9346-9354.

9. Matyjaszewski, K.; Gaynor, S.; Wang, J.-S. Controlled Radical Polymerizations: The Use of Alkyl Iodides in Degenerative Transfer. *Macromolecules* **1995,** 28 (6), 2093-2095.

10. Wang, C.-G.; Chong, A. M. L.; Pan, H. M.; Sarkar, J.; Tay, X. T.; Goto, A. Recent development in halogen-bonding-catalyzed living radical polymerization. *Polym. Chem.* **2020,** 11 (35), 5559-5571.

11. Wang, J.-S.; Matyjaszewski, K. Controlled/"living" radical polymerization. atom transfer radical polymerization in the presence of transition-metal complexes. *J. Am. Chem. Soc.* **1995,** 117 (20), 5614-5615.

12. Ribelli, T. G.; Lorandi, F.; Fantin, M.; Matyjaszewski, K. Atom Transfer Radical Polymerization: Billion Times More Active Catalysts and New Initiation Systems. *Macromol. Rapid Commun.* **2019,** 40 (1), 1800616.

13. Ribelli, T. G.; Fantin, M.; Daran, J.-C.; Augustine, K. F.; Poli, R.; Matyjaszewski, K. Synthesis and Characterization of the Most Active Copper ATRP Catalyst Based on Tris[(4-dimethylaminopyridyl)methyl]amine. *J. Am. Chem. Soc.* **2018,** 140 (4), 1525-1534.

14. Enciso, A. E.; Lorandi, F.; Mehmood, A.; Fantin, M.; Szczepaniak, G.; Janesko, B. G.; Matyjaszewski, K. p-Substituted Tris(2-pyridylmethyl)amines as Ligands for Highly Active ATRP Catalysts: Facile Synthesis and Characterization. *Angew. Chem. Int. Ed.* **2020,** 59 (35), 14910-14920.

15. Schröder, K.; Mathers, R. T.; Buback, J.; Konkolewicz, D.; Magenau, A. J. D.; Matyjaszewski, K. Substituted Tris(2-pyridylmethyl)amine Ligands for Highly Active ATRP Catalysts. *ACS Macro Lett.* **2012,** 1 (8), 1037-1040.

16. Lorandi, F.; Matyjaszewski, K. Why Do We Need More Active ATRP Catalysts? *Isr. J. Chem.* **2020,** 60, 108-123.

17. Pan, X.; Fantin, M.; Yuan, F.; Matyjaszewski, K. Externally controlled atom transfer radical polymerization. *Chem. Soc. Rev.* **2018,** 47 (14), 5457-5490.

18. Matyjaszewski, K.; Jakubowski, W.; Min, K.; Tang, W.; Huang, J.; Braunecker, W. A.; Tsarevsky, N. V. Diminishing catalyst concentration in atom transfer radical polymerization with reducing agents. *Proc. Natl. Acad. Sci. U.S.A.* **2006,** 103 (42), 15309-15314.

19. Konkolewicz, D.; Magenau, A. J. D.; Averick, S. E.; Simakova, A.; He, H. K.; Matyjaszewski, K. ICAR ATRP with ppm Cu Catalyst in Water. *Macromolecules* **2012,** 45 (11), 4461-4468.

20. Matyjaszewski, K.; Jakubowski, W.; Min, K.; Tang, W.; Huang, J. Y.; Braunecker, W. A.; Tsarevsky, N. V. Diminishing catalyst concentration in atom transfer radical polymerization with reducing agents. *Proc. Natl. Acad. Sci. U.S.A.* **2006,** 103 (42), 15309-15314.

21. Matyjaszewski, K.; Tsarevsky, N. V.; Braunecker, W. A.; Dong, H.; Huang, J.; Jakubowski, W.; Kwak, Y.; Nicolay, R.; Tang, W.; Yoon, J. A. Role of Cu0 in Controlled/"Living" Radical Polymerization. *Macromolecules* **2007,** 40 (22), 7795-7806.

22. Matyjaszewski, K.; Coca, S.; Gaynor, S. G.; Wei, M.; Woodworth, B. E. Zerovalent Metals in Controlled/"Living" Radical Polymerization. *Macromolecules* **1997,** 30 (23), 7348-7350.

23. Wei, Q.; Sun, M.; Lorandi, F.; Yin, R.; Yan, J.; Liu, T.; Kowalewski, T.; Matyjaszewski, K. Cu-Catalyzed Atom Transfer Radical Polymerization in the Presence of Liquid Metal Micro/Nanodroplets. *Macromolecules* **2021,** 54 (4), 1631-1638.

24. Konkolewicz, D.; Wang, Y.; Zhong, M. J.; Krys, P.; Isse, A. A.; Gennaro, A.; Matyjaszewski, K. Reversible-Deactivation Radical Polymerization in the Presence of Metallic Copper. A Critical Assessment of the SARA ATRP and SET-LRP Mechanisms. *Macromolecules* **2013,** 46 (22), 8749-8772.

25. Konkolewicz, D.; Wang, Y.; Krys, P.; Zhong, M.; Isse, A. A.; Gennaro, A.; Matyjaszewski, K. SARA ATRP or SET-LRP. End of controversy? *Polym. Chem.* **2014,** 5 (15), 4396-4417.

26. Wang, Z.; Pan, X.; Yan, J.; Dadashi-Silab, S.; Xie, G.; Zhang, J.; Wang, Z.; Xia, H.; Matyjaszewski, K. Temporal Control in Mechanically Controlled Atom Transfer Radical Polymerization Using Low ppm of Cu Catalyst. *ACS Macro Lett.* **2017,** 6 (5), 546-549.

27. Mohapatra, H.; Kleiman, M.; Esser-Kahn, A. P. Mechanically controlled radical polymerization initiated by ultrasound. *Nat. Chem.* **2017,** 9 (2), 135-139.

28. Magenau, A. J. D.; Strandwitz, N. C.; Gennaro, A.; Matyjaszewski, K. Electrochemically Mediated Atom Transfer Radical Polymerization. *Science* **2011,** 332 (6025), 81-84.

29. Chmielarz, P.; Fantin, M.; Park, S.; Isse, A. A.; Gennaro, A.; Magenau, A. J. D.; Sobkowiak, A.; Matyjaszewski, K. Electrochemically mediated atom transfer radical polymerization (eATRP). *Prog. Polym. Sci.* **2017,** 69, 47-78.

30. Dadashi-Silab, S.; Tasdelen, M. A.; Yagci, Y. Photoinitiated Atom Transfer Radical Polymerization: Current Status and Future Perspectives. *J. Polym. Sci., Part A: Polym. Chem.* **2014,** 52 (20), 2878-2888.

31. Konkolewicz, D.; Schröder, K.; Buback, J.; Bernhard, S.; Matyjaszewski, K. Visible Light and Sunlight Photoinduced ATRP with ppm of Cu Catalyst. *ACS Macro Lett.* **2012,** 1 (10), 1219-1223.

32. Anastasaki, A.; Nikolaou, V.; Zhang, Q.; Burns, J.; Samanta, S. R.; Waldron, C.; Haddleton, A. J.; McHale, R.; Fox, D.; Percec, V.; Wilson, P.; Haddleton, D. M. Copper(II)/Tertiary Amine Synergy in Photoinduced Living Radical Polymerization: Accelerated Synthesis of ω-Functional and α,ω-Heterofunctional Poly(acrylates). *J. Am. Chem. Soc.* **2014,** 136 (3), 1141-1149.

33. Dadashi-Silab, S.; Atilla Tasdelen, M.; Yagci, Y. Photoinitiated atom transfer radical polymerization: Current status and future perspectives. *J. Polym. Sci., Part A: Polym. Chem.* **2014,** 52 (20), 2878-2888.

34. Tasdelen, M. A.; Uygun, M.; Yagci, Y. Photoinduced Controlled Radical Polymerization in Methanol. *Macromol. Chem. Phys.* **2010,** 211 (21), 2271-2275.

35. Mosnáček, J.; Ilčíková, M. Photochemically Mediated Atom Transfer Radical Polymerization of Methyl Methacrylate Using ppm Amounts of Catalyst. *Macromolecules* **2012,** 45 (15), 5859-5865.

36. Ribelli, T. G.; Konkolewicz, D.; Bernhard, S.; Matyjaszewski, K. How are Radicals (Re)Generated in Photochemical ATRP? *J. Am. Chem. Soc.* **2014,** 136 (38), 13303-13312.

37. Theriot, J. C.; McCarthy, B. G.; Lim, C.-H.; Miyake, G. M. Organocatalyzed Atom Transfer Radical Polymerization: Perspectives on Catalyst Design and Performance. *Macromol. Rapid Commun.* **2017,** 38 (13), 1700040.

38. Discekici, E. H.; Anastasaki, A.; Read de Alaniz, J.; Hawker, C. J. Evolution and Future Directions of Metal-Free Atom Transfer Radical Polymerization. *Macromolecules* **2018,** 51 (19), 7421-7434.

39. Fors, B. P.; Hawker, C. J. Control of a Living Radical Polymerization of Methacrylates by Light. *Angew. Chem. Int. Ed.* **2012,** 51 (35), 8850-8853.

40. Treat, N. J.; Fors, B. P.; Kramer, J. W.; Christianson, M.; Chiu, C.-Y.; Read de Alaniz, J.; Hawker, C. J. Controlled Radical Polymerization of Acrylates Regulated by Visible Light. *ACS Macro Lett.* **2014,** 3 (6), 580-584.

41. Treat, N. J.; Sprafke, H.; Kramer, J. W.; Clark, P. G.; Barton, B. E.; Read de Alaniz, J.; Fors, B. P.; Hawker, C. J. Metal-Free Atom Transfer Radical Polymerization. *J. Am. Chem. Soc.* **2014,** 136 (45), 16096-16101.

42. Pan, X.; Fang, C.; Fantin, M.; Malhotra, N.; So, W. Y.; Peteanu, L. A.; Isse, A. A.; Gennaro, A.; Liu, P.; Matyjaszewski, K. Mechanism of Photoinduced Metal-Free Atom Transfer Radical Polymerization: Experimental and Computational Studies. *J. Am. Chem. Soc.* **2016,** 138 (7), 2411-2425.

43. Pan, X.; Lamson, M.; Yan, J.; Matyjaszewski, K. Photoinduced Metal-Free Atom Transfer Radical Polymerization of Acrylonitrile. *ACS Macro Lett.* **2015,** 4 (2), 192-196.

44. Theriot, J. C.; Lim, C. H.; Yang, H.; Ryan, M. D.; Musgrave, C. B.; Miyake, G. M. Organocatalyzed atom transfer radical polymerization driven by visible light. *Science* **2016,** 352 (6289), 1082-1086.

45. Pearson, R. M.; Lim, C. H.; McCarthy, B. G.; Musgrave, C. B.; Miyake, G. M. Organocatalyzed Atom Transfer Radical Polymerization Using N-Aryl Phenoxazines as Photoredox Catalysts. *J. Am. Chem. Soc.* **2016,** 138 (35), 11399-11407.

46. Cole, J. P.; Federico, C. R.; Lim, C.-H.; Miyake, G. M. Photoinduced Organocatalyzed Atom Transfer Radical Polymerization Using Low ppm Catalyst Loading. *Macromolecules* **2019,** 52 (2), 747-754.

47. Kütahya, C.; Schmitz, C.; Strehmel, V.; Yagci, Y.; Strehmel, B. Near-Infrared Sensitized Photoinduced Atom-Transfer Radical Polymerization (ATRP) with a Copper(II) Catalyst Concentration in the ppm Range. *Angew. Chem. Int. Ed.* **2018,** 57 (26), 7898-7902.

48. Zhang, W.; He, J.; Lv, C.; Wang, Q.; Pang, X.; Matyjaszewski, K.; Pan, X. Atom Transfer Radical Polymerization Driven by Near-Infrared Light with Recyclable Upconversion Nanoparticles. *Macromolecules* **2020,** 53 (12), 4678-4684.

49. Dolinski, N. D.; Page, Z. A.; Discekici, E. H.; Meis, D.; Lee, I.-H.; Jones, G. R.; Whitfield, R.; Pan, X.; McCarthy, B. G.; Shanmugam, S.; Kottisch, V.; Fors, B. P.; Boyer, C.; Miyake, G. M.; Matyjaszewski, K.; Haddleton, D. M.; de Alaniz, J. R.; Anastasaki, A.; Hawker, C. J. What happens in the dark? Assessing the temporal control of photo-mediated controlled radical polymerizations. *J. Polym. Sci., Part A: Polym. Chem.* **2019,** 57 (3), 268-273.

50. Fantin, M.; Isse, A. A.; Venzo, A.; Gennaro, A.; Matyjaszewski, K. Atom Transfer Radical Polymerization of Methacrylic Acid: A Won Challenge. *J. Am. Chem. Soc.* **2016,** 138 (23), 7216-7219.

51. Li, B.; Yu, B.; Huck, W. T. S.; Liu, W.; Zhou, F. Electrochemically Mediated Atom Transfer Radical Polymerization on Nonconducting Substrates: Controlled Brush Growth through Catalyst Diffusion. *J. Am. Chem. Soc.* **2013,** 135 (5), 1708-1710.

52. Dadashi-Silab, S.; Lorandi, F.; Fantin, M.; Matyjaszewski, K. Redox-switchable atom transfer radical polymerization. *Chem. Commun.* **2019,** 55 (5), 612-615.

Chapter 2.   Temporal Control in Atom Transfer Radical Polymerization

2.1. Preface

As presented in Chapter 1, ATRP in the presence of low ppm catalyst concentrations relies on various reducing stimuli to regenerate the activator L/Cu^I catalyst to drive polymerizations forward. Therefore, these techniques can potentially offer the possibility of modulating the activity of the catalyst and hence the rate of polymerization via redox reactions. This chapter is aimed to provide an in-depth analysis of externally controlled ATRP regarding temporal control. In this chapter, I explored temporal control under SARA, photoinduced, and ARGET ATRP conditions to establish new means for achieving temporal control as well as to elucidate the mechanism of temporal control in copper-catalyzed ATRP systems with regard to the effect of various polymerization components in offering temporal control.

The first section of this chapter presents the possibility of controlling the kinetics of ATRP in the presence or absence of a zerovalent metal such as Cu or Ag wires which act as reducing agents. We envisaged that removal of the metal wire from the polymerization mixture would stop the (re)generation of the Cu catalyst and therefore the rate of polymerization should slow down and eventually stop. A structure-property relationship was established between the activity of the Cu catalysts and their performance in offering temporal control. The effect of the activity of the catalyst was studied in the presence of different ligands that impart a wide range of catalytic activity in ATRP in the presence of Cu.

The second section of this chapter was a collaborative work with the groups of Prof. Craig

_____

Work in this chapter was published in:

1- **S. Dadashi-Silab**, K. Matyjaszewski, Temporal Control in Atom Transfer Radical Polymerization Using Zerovalent Metals, *Macromolecules*, **2018**, *51*, 4250–4258. © 2018 American Chemical Society.

2- **S. Dadashi-Silab**,* I.-H. Lee,* A. Anastasaki, F. Lorandi, B. Narupai, N. D. Dolinski, M. L. Allegrezza, M. Fantin, D. Konkolewicz, C. J. Hawker, K. Matyjaszewski, Investigating Temporal Control in Photoinduced Atom Transfer Radical Polymerization, *Macromolecules*, **2020**, *53*, 5280–5288 *(* denotes equal contribution)*. © 2020 American Chemical Society.

3- **S. Dadashi-Silab**, F. Lorandi, M. Fantin, K. Matyjaszewski, Redox-Switchable Atom Transfer Radical Polymerization, *Chem. Commun.*, **2019**, *55*, 612–615. © 2019 Royal Society of Chemistry.

Hawker, Prof. Athina Anastasaki, and Prof. Dominik Konkolewicz that strived to explore temporal control in photoinduced ATRP systems. In this study, we analyzed the effect of polymerization components including concentration of ligand, solvent and the activity of the catalyst. Importantly, we discovered that temporal control in ATRP depends, among other factors, on the activity of the copper catalysts which can be tuned using different ligands. High activity of the Cu catalyst ensures activators are present at low concentrations and therefore provided superior temporal control over polymerization as the low concentration of the activator can be quickly consumed and polymerization stopped. On the other hand, catalysts with lower activity provide high concentration of the activator form of the catalyst and thus can activate polymerization for a longer time increasing monomer conversion in the dark periods, as compared to more active systems. In addition to extensive polymerization kinetics under intermittent light on/off periods, we used electrochemical analysis and simulations to gain further insights and explain the effect of catalysts and other factors involved in ATRP including various modes of radical termination in achieving temporal control.

Having discovered how under some conditions ATRP can continue upon removal of external stimuli, we envisioned switching the catalyst between on and off states (*i.e.*, activator and deactivator) would enable gaining on-demand temporal control over the kinetics of ATRP. The oxidation state of the Cu catalysts can be controlled by external means by using redox agents as external stimuli. Chemically reducing agents such as ascorbic acid generated L/Cu^I activator by reducing L/Cu^{II}-Br species to start polymerization. Additionally, I developed a new strategy to reversibly switch the Cu catalyst and hence the polymerization off by oxidizing the L/Cu^I activator to L/Cu^{II} by using oxidizing stimuli such as oxygen or a ferrocenium salt. We discovered that oxidation of the activator species to inactive L/Cu^{II} can immediately stop the polymerization. We were able to switch the polymerization back on multiple times by using additional reducing agents to generate L/Cu^I activator. We showed that by switching the Cu catalyst between on and off states using redox agents we could gain on-demand control over kinetics of ATRP in a controlled manner.

I designed and conducted the experiments, collected data, and analyzed the results for the first section of this chapter (temporal control using zerovalent metals) under the guidance of

Professor Matyjaszewski. I thank Dr. Thomas G. Ribelli and Dr. Alan E. Enciso for the synthesis of TPMA^{*3} and TPMA^{NMe2} ligands used in this study.

For the second section, I conducted experiments in photoinduced ATRP under batch conditions, collected the data and analyzed the results. The in situ NMR experiments were designed and conducted by our collaborators In-Hwan Lee, Athina Anastasaki, Benjaporn Narupai, and Neil D. Dolinski at the University of California, Santa Barbara. Dr. Francesca Lorandi conducted electrochemical analysis of the ATRP catalysts. Together with Michael L. Allegrezza and Prof. Dominik Konkolewicz (Miami University) and Dr. Lorandi we performed simulations. I wrote a first draft of the manuscript for publication with input from all authors to revise and edit it. Prof. Matyjaszewski, Professor Hawker, and Professor Anastasaki supervised the project.

I designed and conducted the experiments in the last section of this chapter, collected data, and analyzed the results. All authors contributed in discussion and analysis of the results. The manuscript was written through contribution of all authors. Professor Matyjaszewski supervised the project.

2.2. Temporal Control in Atom Transfer Radical Polymerization Using Zerovalent Metals

2.2.1 Abstract

Polymer chain growth can be controlled in a spatiotemporal manner by external stimuli including chemical, redox, light, electrical current, and mechanical procedures. In this paper, atom transfer radical polymerization (ATRP) was investigated in the presence of zerovalent metals, such as copper or silver wire, as chemical stimuli to assert temporal control over ATRP reactions. The ATRP activator, L/Cu^I complex, was (re)generated, or catalyst was switched 'On', in the presence of the metal wires to start the reaction whereas removing the wire from the solution stopped activator (re)generation. In the absence of the metal zero wires, the residual activator in the solution was consumed by irreversible radical termination processes converting activators to deactivator species – catalyst switched 'Off' – and hence polymerization stopped. However, the nature of the ligand played a crucial role in defining the concentrations of deactivator and activator species, $[L/Cu^{II}]/[L/Cu^I]$, present in the polymerization medium. More active catalysts shifted the ATRP equilibrium towards a higher concentration of L/Cu^{II}, hence lower concentration of activator L/Cu^I. In this case the reaction quickly stopped in the absence of metal wires. On the other hand, lower activity catalysts provided a higher concentration of the L/Cu^I species that took a longer time to be consumed by radical termination processes so that the reactions continued for longer times in the absence of the wires.
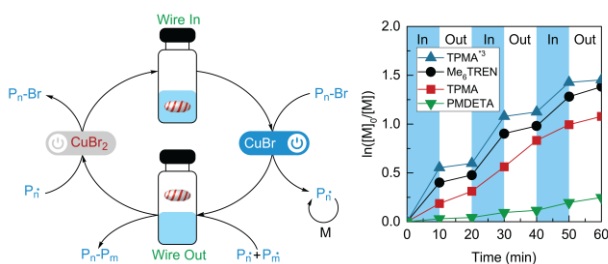
2.2.2 Introduction

In biological processes, allosteric regulation refers to reversible control of the catalytic reactivity of an enzyme through binding molecules to structural sites remote from the enzyme's active center. Allosteric regulation promotes conformational changes in the enzyme structure that alters the catalytic reactivity in a spatially and temporally controlled manner. Inspired by the possibilities offered by nature for controlling a chemical transformation in response to a signal input, chemists have developed strategies based upon switchable catalysis to precisely control

51

the rate, catalytic reactivity and outcome of chemical reactions.[1] External stimuli trigger changes in catalyst properties which in turn results in reversibly switching their activity/selectivity between 'On/Off' states.

External regulation of controlled polymerization reactions is an evolving research area in polymer synthesis.[2, 3] This approach combines the benefits of controlling molecular weight properties, composition, monomer sequence and properties in polymers with additional opportunities to spatially and temporally control the reaction, or sequence of reactions, enabled by external stimuli. Temporal control in a polymerization reaction relies on a dynamic regulation of the polymerization activator or catalyst in the presence of external stimuli to start a reaction, whereas removing the stimuli switches off the polymerization. The polymerization catalyst needs to be efficiently changed between 'On' and 'Off' states quickly for successful temporal control in a reversible manner in the presence/absence of external stimuli. Importantly, multiple 'On/Off' switches should not lead to any deterioration of the catalysts' reactivity. Moreover, control over polymerization should be maintained throughout multiple 'On/Off' periods without resulting in any significant termination processes.

A wide array of external stimuli including allosteric, chemical, electrochemical, photochemical, and mechanochemical control have been developed to provide temporal control over polymerization reactions. For instance, allosteric control over a ring-opening polymerization (ROP) process using a triple-layer catalyst was developed.[4] The presence of chloride anions (Cl$^-$) opened the closed structure of the catalyst exposing a catalytically active aluminum center, which initiated and controlled the ROP of ε-caprolactone. Removing Cl$^-$ anions reversibly closed the catalytic site and, as a result, polymerization was halted. Redox control was utilized to temporally switch the activity of a ROP catalyst by changing the redox properties of ferrocenyl functionalized ligands.[5-9] The catalytic activity of the metal center was switched off by oxidizing the ferrocenyl groups whereas the catalyst with the neutral form of the ferrocene groups was catalytically reactive.

Photochemistry is a convenient approach to induce and control a variety of chemical transformations.[7] Light has been employed in controlling a multitude of polymerization reactions, including atom transfer radical polymerization (ATRP),[9-11] reversible-addition fragmentation chain transfer (RAFT) polymerization,[12, 13] iodine-mediated radical

polymerization,[14, 15] ROP,[13-15] cationic polymerization,[16, 17] and ring-opening metathesis polymerization (ROMP).[18, 19]

Over the past two decades, ATRP has evolved to enable polymerizations to be controlled in the presence of parts per million levels of Cu catalysts with high catalytic efficiency.[17-20] Indeed, recent advances in catalyst design for ATRP systems have been based upon using reagents that (re)generate activator catalyst species starting from an air-stable L/Cu^{II} deactivator complex. For instance, ATRP systems including initiators for continuous activator regeneration (ICAR),[21, 22] activators regenerated by electron transfer (ARGET),[21, 23, 24] supplemental activator and reducing agents (SARA),[25-28] electrical current (*e*ATRP),[29-33] photoirradiation,[31-37] mechanochemical[38, 39] and sonochemical[40, 41] have been developed to (re)generate the L/Cu^{I} activator.

Interestingly, since regeneration of the activator species in ATRP depends on the presence of reducing agents, the rate of the reaction can be reversibly manipulated to gain temporal control over the process with reducing agents acting as external stimuli. For example, ATRP could proceed when ascorbic acid, acting as a chemical stimulus, was fed into the medium whereas the rate of the reaction decreased when feeding ascorbic acid was stopped.[42] Recent advances have allowed for a robust manipulation of reaction rate and temporal control in the presence of photochemical or electrochemical stimuli.

In ATRP reactions mediated by a Cu catalyst, switching the reaction off depends on how fast L/Cu^{I} activators can be removed from (or consumed in) the solution. For example, in *e*ATRP the activator L/Cu^{I} catalyst is generated *in situ* by applying a reducing potential to reduce L/Cu^{II} species and thus initiating polymerization.[33, 43, 44] Applying an oxidizing potential oxidizes activator L/Cu^{I} to L/Cu^{II} in a reversible manner so that the reaction stops. However, in photoinduced ATRP, the activator species is expected to be consumed only by irreversible termination processes after which no more activation is feasible.[33, 45]

In this regard, regulation of the catalytic activity of Cu complexes through, for example, ligand design or selection of the reaction media to modify ATRP equilibrium constant (K_{ATRP}) allows for a successful temporal control over process. In a more active catalytic system, in which the large value for K_{ATRP} shifts the ATRP equilibrium to provide more L/Cu^{II}, the resulting very low concentration of L/Cu^{I} activator is quickly consumed by irreversible radical terminations so the reaction stops. On the other hand, a less active catalyst, with lower K_{ATRP}, provides relatively

high concentrations of L/Cu^I which would require longer times to be consumed by termination processes. It should be noted that in highly active catalytic systems, the very low concentration of L/Cu^I results in minimal radical termination, thus a majority of the chains preserve their end functionality.[46]

In photoATRP reactions catalyzed by either transition-metal or organic photoredox catalysts, the activation of the polymer chain end depends on the photoexcited state of the catalysts. Considering the relatively short life-time of excited state photocatalysts, and hence low concentration of activator, the kinetics of polymerization can be easily manipulated by light stimuli with excellent temporal control achieved by applying or removing light.[37, 47-50]

In this contribution to the field of temporal control, we explore the ability of zerovalent metals such as Cu^0 or Ag^0 as chemical stimuli in gaining temporal control in ATRP reactions. In the presence of Cu^0 or Ag^0 wire, the ATRP catalyst can be switched on by comproportionation and hence reduction of L/Cu^{II} to activator L/Cu^I. Cu^0 also acts directly as a supplemental activator of alkyl halides. Physically removing wires from solution switches off activator (re)generation/supplemental activation, as previously observed experimentally and also explained by computational simulation.[25, 51, 52] Herein, we show that the rate with which the reaction can stop in the absence of the metal zero wire depends on the redox potential of the complexes and nature of ligands used.

2.2.3 Results and Discussion

In supplemental activator and reducing agent atom transfer radical polymerization (SARA ATRP), which uses a Cu^0 wire as both supplemental activator and reducing agent, the Cu^0 wire and L/Cu^{II} comproportionate to form L/Cu^I activators. Scheme 4-(A) shows the overall mechanism of SARA ATRP. Comproportionation increases the concentration of total soluble Cu species in the medium, Scheme 4-(B). Mechanistic studies have shown the necessity of the presence of excess ligand to promote comproportionation and supplemental activation, i.e. polymerization.[25, 53] The heterogeneity of zerovalent metals as reducing agent in ATRP provides an easy reaction set-up as well as reusability of the wires in multiple reactions. The question remained, "can we take advantage of the heterogeneous nature of zerovalent metals as external stimuli in gaining temporal control in ATRP reactions?" Therefore, temporal control was

investigated in ATRP in the presence of Cu^0 or Ag^0 wires. The effect of reducing metal, ligand nature, solvent, and monomer was studied, Scheme 5.
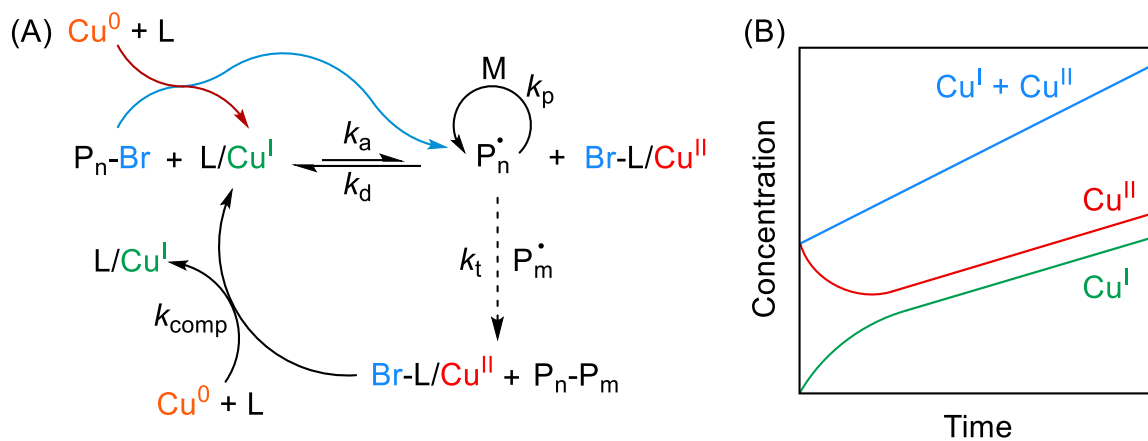
Scheme 4. (A) Mechanism of SARA ATRP, (B) schematic representation of the concentration of Cu species in SARA ATRP.
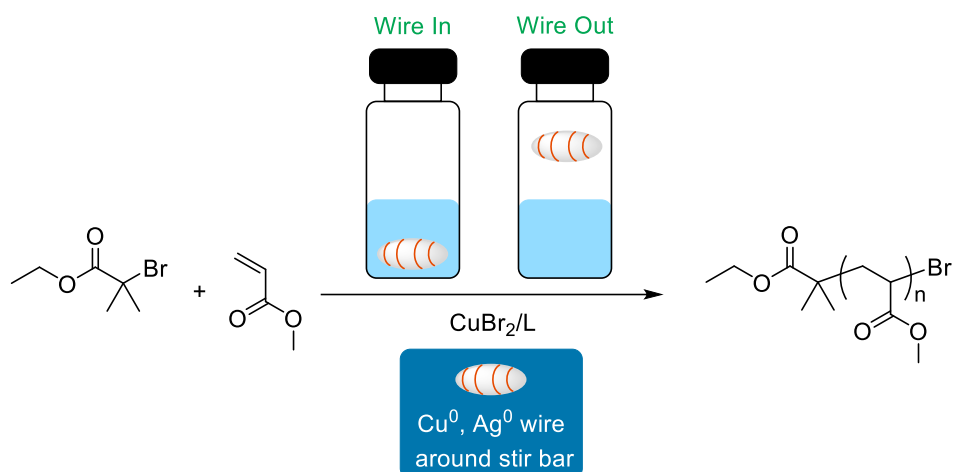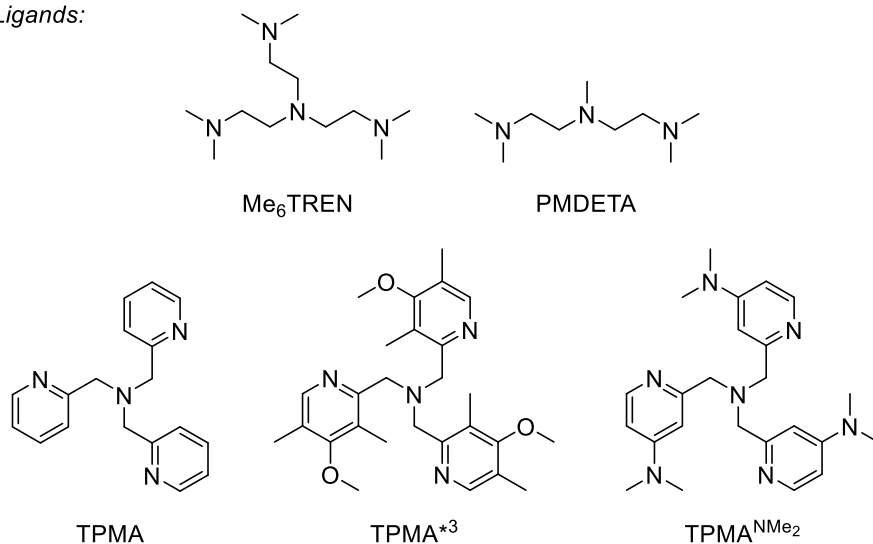
Scheme 5. Schematic representation of temporal control in ATRP using zerovalent metals and structure of the ligands studied.

Temporal Control in SARA ATRP

Effect of CuBr2 and ligand concentration. Temporal control in SARA ATRP of methyl acrylate (MA) was conducted using various initial concentrations of $CuBr_2$. It can be clearly observed that the reaction proceeded mainly when the reducing agent (Cu^0 wire) was inside the solution and significantly slowed down when the wire was lifted from the solution, Figure 3. The rate of the reaction decreased significantly with lower concentrations of $CuBr_2$ in the system resulting in slightly better temporal control. The reactions were well-controlled with molecular weights in agreement with theoretical values and low dispersity $Đ$ exhibiting symmetric size-exclusion chromatography (SEC) traces (Table 1 and Figures S1-S4 in Supporting Information).

Interestingly, in the presence of 25 ppm of CuBr$_2$, a lower rate of the polymerization was observed especially during the second 'wire-in' period and no further reaction was detected after this point, suggesting that there was not enough free ligand available to drive comproportionation and form soluble L/Cu^I complexes or assist in direct supplemental activation. To further prove this assumption, a control experiment was conducted in the absence of excess Me$_6$TREN ligand, i.e., using [CuBr$_2$]/[Me$_6$TREN] = 1/1. No polymerization was observed in this reaction indicating the presence of excess ligand to drive SARA ATRP forward was required.
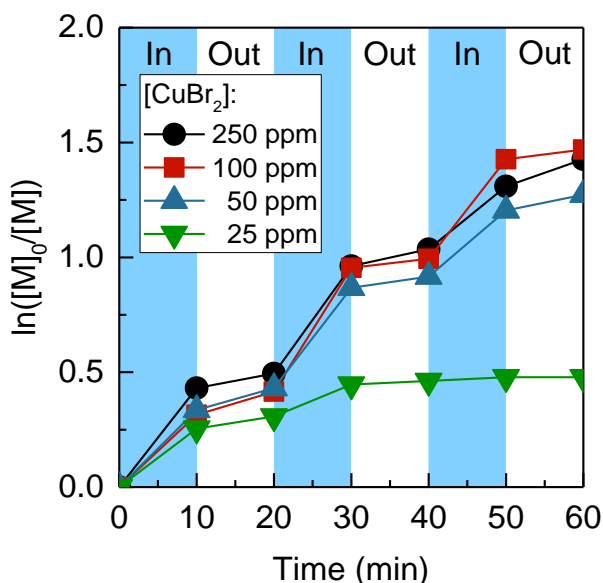
Figure 3. Kinetics of temporal control in SARA ATRP using different ligands under conditions: [MA]/[EBiB]/[CuBr$_2$]/[Me$_6$TREN] = 200/1/x/3x (x: 0.005, 0.01, 0.02, 0.05) in 50 vol. % DMSO at 30 °C; Cu^0 wire length = 5 cm, diameter = 0.5 mm.

Table 1. Polymerization results of temporal control in SARA ATRP of MA with different concentrations of ligand and CuBr$_2$ (kinetic results are shown in Figure 3)[a]

Entry	CuBr$_2$ (ppm)	Time (min)	Conversion (%)	$M_{n,th}$	M_n	Đ
1	250	60	76	13280	13100	1.03
2	100	60	77	13450	13630	1.04
3	50	60	72	12600	12950	1.06
4	25	60	38	6750	7200	1.12

[a] [MA]/[EBiB]/[CuBr$_2$]/[Me$_6$TREN]: 200/1/x/3x (x: 0.05, 0.02, 0.01, or 0.005) in 50 vol. % DMSO, at 30 °C. Cu^0 wire length = 5 cm, diameter = 0.5 mm.

Effect of ligand. The activity of an ATRP catalyst depends on the redox potential of the L/Cu complex. More negative redox potential results in larger K_{ATRP} values, shifting the ATRP equilibrium towards relatively higher [L/Cu^{II}] and lower [L/Cu^{I}]. In regard to temporal control, the rate of the reaction in the absence of Cu^0 wire depends on the concentration and activity of residual L/Cu^{I} catalyst in the reaction medium. As noted above, the reaction would stop once all L/Cu^{I} complex is consumed through radical termination processes. Considering this provision, temporal control in SARA ATRP of MA was investigated in the presence of different ligands including tris[2-(dimethylamino)ethyl]amine (Me$_6$TREN), *N,N,N′,N″,N″-*pentamethyldiethylenetriamine (PMDETA), tris(2-pyridylmethyl)amine (TPMA), and tris((4-methoxy-3,5-dimethylpyridin-2-yl)methyl)amine (TPMA^{*3}).[54] Figure 4 shows the effect of ligand structure on the kinetics of temporal control in SARA ATRP.

Cu complexes with these ligands have different K_{ATRP} values and are expected to exhibit different kinetics in temporal control reactions. PMDETA (Figure 4 and Figure S8) and TPMA (Figure 4) showed a slower rate of polymerization, compared with the other ligands. Moreover, when the wire was lifted out of the solution, the polymerization continued to higher conversions with almost similar rates compared to when the metal wire was in the solution. The reaction proceeding in the 'wire-out' periods could be attributed to the low value of K_{ATRP} for the Cu complexes associated with PMDETA or TPMA ligands. As a result, after removing the wire, the higher residual concentration of the L/Cu^{I} complex persisted for longer times and activate further reactions. In addition, slower reactions indicated lower radical concentration and slower termination. In the presence of active ligands such as Me$_6$TREN or TPMA^{*3}, the overall rate of the reaction was high, and it was significantly reduced when the Cu^0 wire was lifted from the solution. All the polymerizations in the presence of the different ligands were well controlled (Table 2 and Figures S5-S8).
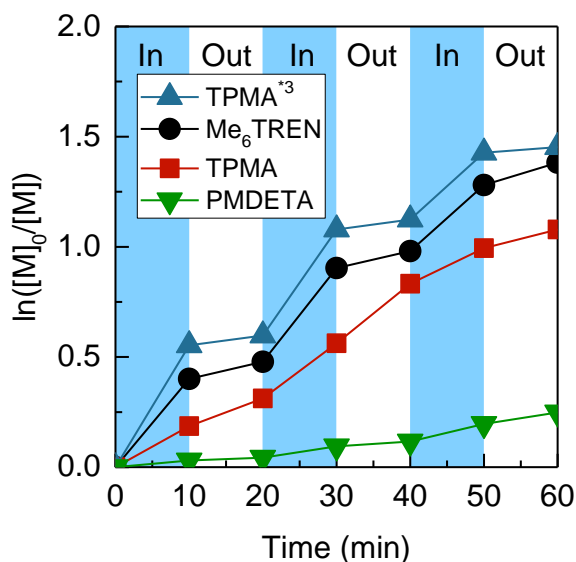
Figure 4. Kinetics of temporal control in SARA ATRP using different ligands under conditions: [MA]/[EBiB]/[CuBr$_2$]/[L] = 200/1/0.05/0.30 (L: TPMA[*3], Me$_6$TREN, TPMA, or PMDETA) in 50 vol. % DMSO at 30 °C; Cu^0 wire length = 5 cm, diameter = 0.5 mm.

Table 2. Polymerization results of temporal control in SARA ATRP of MA with different ligands (kinetic results are shown in Figure 4) [a]

Entry	Ligand	Time (min)	Conversion (%)	$M_{n,th}$	M_n	$Đ$
1	TPMA[*3]	60	76	13300	13600	1.03
2	Me$_6$TREN	60	75	13100	12900	1.04
3	TPMA	60	66	11550	11900	1.07
4	PMDETA	60	22	4000	n.d.	n.d.

[a] [MA]/[EBiB]/[CuBr$_2$]/[L]: 200/1/0.05/0.30 (L: TPMA[*3], Me$_6$TREN, TPMA, or PMDETA) in 50 vol. % DMSO, at 30 °C; Cu^0 wire length: 5 cm, diameter: 0.5 mm.

The effect of ligand was also investigated by following the kinetics of temporal control when the catalyst was lifted out of the solution for longer periods of time. The reactions were conducted using TPMA[*3], Me$_6$TREN, TPMA, and PMDETA, ligands under initial reaction conditions: [MA]/[EBiB]/[CuBr$_2$]/[L] = 200/1/0.02/0.06 in 50 vol. % DMSO. In the presence of TPMA[*3], the reaction resulted in ~23 % monomer conversion when the wire was inserted in the solution for 10 min (Figure 5-A). When the Cu^0 wire was lifted from the reaction media for 40 min, the

reaction stopped completely, without any noticeable conversion achieved in this period. Moreover, reinserting the wire in the solution for 10 min restarted the reaction resulting in ~50 % total monomer conversion after 20 minutes in the presence of Cu^0. Figure 5-B shows the kinetics of the reaction using Me_6TREN in which a 34 % monomer conversion was reached when the wire was inserted in the solution for 10 min. When the Cu^0 wire was lifted out for 40 min the kinetics showed very low additional conversion during the first 10 min, total conversion 38 %, after which the rate appeared to plateau and total monomer conversion was ~40 % after keeping the wire out of the solution for 40 min. Reinserting the wire in the solution for 10 min reinitiated the reaction and resulted in a monomer conversion increasing to ~77 %.
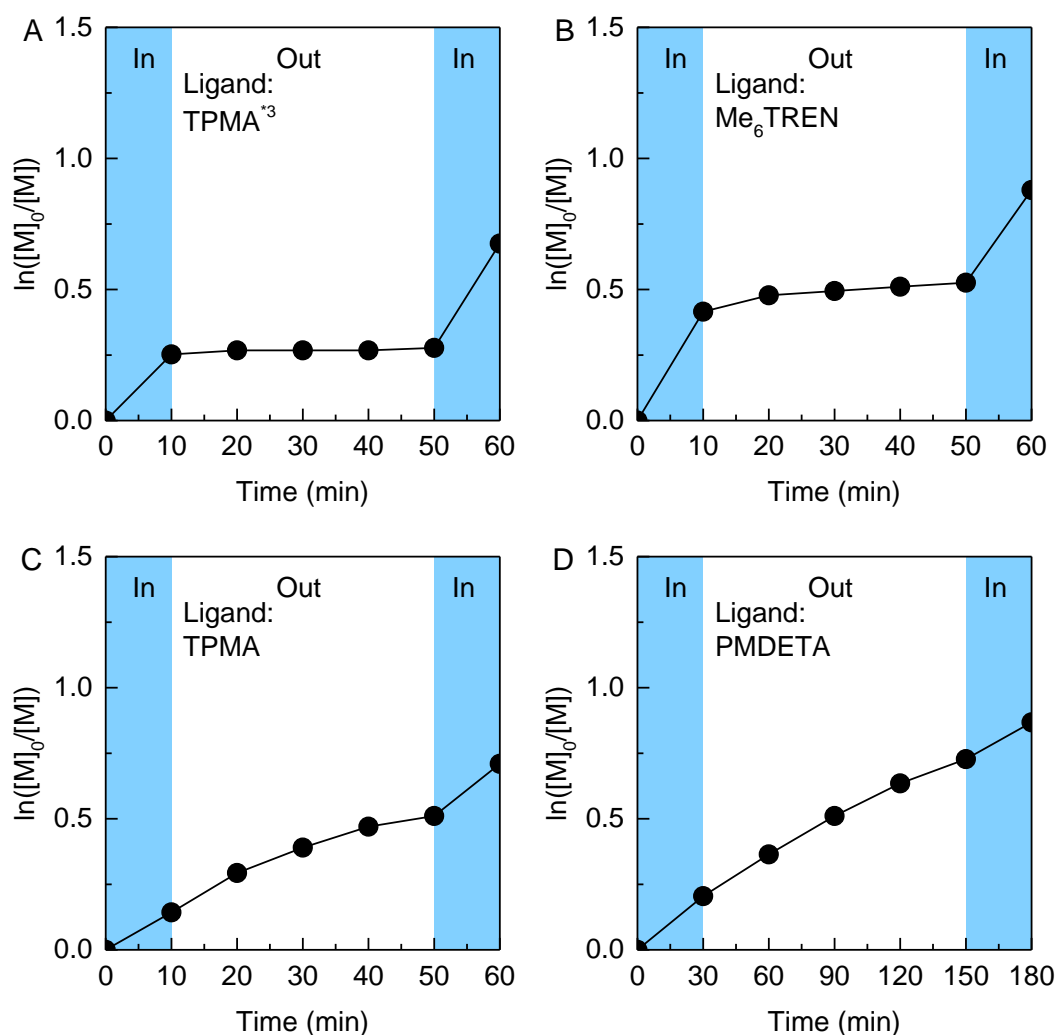
Figure 5. Kinetics of temporal control in SARA ATRP in the presence of Cu^0 wire under conditions: $[MA]/[EBiB]/[CuBr_2]/[L] = 200/1/0.02/0.06$ (L = (A): Me_6TREN, (B):

PMDETA, (C): TPMA, or (D): TPMA^{*3}) in 50 vol. % DMSO, at 30 °C; Cu^0 wire length = 5 cm, diameter = 0.5 mm.

In the presence of TPMA as ligand, the reaction continued to take place for longer times after the wire was lifted from the solution for 40 min, Figure 5-C. The rate of the reaction appeared to decrease slightly, but only towards the end of this period, resulting in a 40% monomer conversion. Reinsertion of the Cu^0 wire restarted polymerization and led to a 51% monomer conversion after an additional 10 min in the presence of the wire.

Similarly, with PMDETA, ~18% monomer conversion was observed when the catalyst was in the solution for 30 min (Figure 5-D). Afterward, the Cu^0 wire catalyst was lifted from the solution for 120 min. Kinetic analysis showed that the reaction continued to higher conversions throughout the wire-out period. The reaction exhibited almost linear semi-logarithmic kinetics regardless of the wire being in or out of the solution. This can be attributed to the low K_{ATRP} value associated with CuBr/PMDETA complex providing a higher concentration of L/Cu^I in the reaction medium. Also, the comproportionation should be largest for this complex. Thus, the remaining CuBr/PMDETA complex continued to activate the polymerization, even after the Cu^0 wire was removed from the solution for longer period of times. It should be mentioned that by removing wire from the solution, the stirring was stopped. Due to the homogeneous nature of these systems, stirring did not have a significant impact on the kinetics of the polymerization during 'wire-out' periods in which the reaction was not stirred. For example, in the case of PMDETA where polymerization did not stop, a linear kinetic was observed which could be indicative of efficient diffusion during 'wire-out' periods without affecting the kinetics under our conditions.

Control experiments were conducted in the absence of Cu^0 to investigate whether ligands alone could contribute to activator regeneration by reducing L/Cu^{II} species during wire-out periods. No monomer conversion was observed with PMDETA even after 50 h. A slow polymerization of MA was achieved with Me$_6$TREN showing an induction period of ~6 h. These results suggest that in temporal control reactions the continuation of the reaction in the absence of Cu^0 wire is predominately related to the presence of L/Cu^I species generated by comproportionation in the presence of the Cu^0 wire.

Effect of solvent. The effect of solvent was investigated in temporal control of SARA ATRP of MA using Me_6TREN as ligand with DMSO and acetonitrile (MeCN) as solvents. Kinetics of the polymerizations are shown in Figure 6. The reaction exhibited moderate temporal control in DMSO, as the polymerization mainly proceeded in the presence of the Cu^0 wire and a slower rate was observed when the wire was removed. In MeCN, the rate of the reaction was generally lower than in DMSO and it showed a better temporal control, as the reaction stopped during the wire-out periods. This may be related to higher equilibrium constants and activation rate constants in DMSO than in MeCN.[55-57] Polymerizations were well-controlled in these solvents, with molecular weight in agreement with theoretical values and low *Đ*'s (Table S2 and Figures S6 and S9).
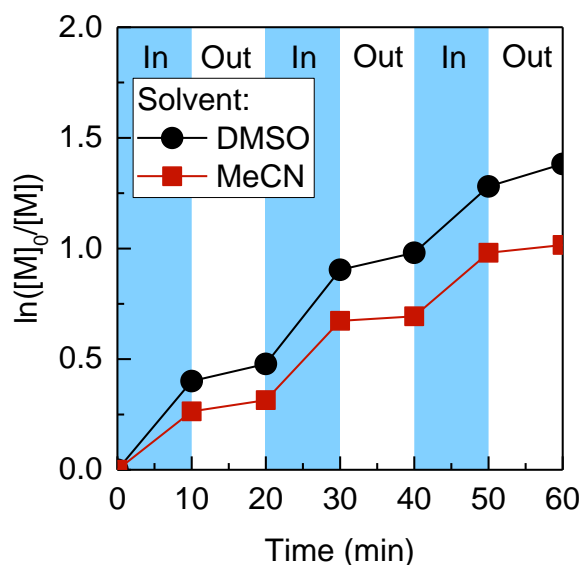
Figure 6. Kinetics of temporal control in SARA ATRP in the presence of Cu^0 wire with various solvents under conditions: $[MA]/[EBiB]/[CuBr_2]/[Me_6TREN]$ = 200/1/0.05/0.30 in 50 vol. % solvent (DMSO or MeCN), at 30 °C; Cu^0 wire length = 5 cm, diameter = 0.5 mm.

Temporal control in SARA ATRP of MMA. Temporal control was attempted in SARA ATRP of methyl methacrylate (MMA) using ethyl α-bromophenylacetate (EBPA) as initiator (Figure 7 and Figure S10). The reaction was started by inserting a Cu^0 wire into the solution resulting in ~9 % monomer conversion after 2 h. The wire was removed from the solution for 2 h and monomer conversion reached ~13 %. Reinserting the Cu^0 wire for a second 2 h resulted in a faster rate

compared to the first 'wire-in' period with monomer conversion reaching 37 %. Noticeably, in the absence of the Cu^0 wire the reaction proceeded to higher monomer conversions at only slightly lower reaction rate than in the presence of Cu^0 wire. This can be attributed to higher activation rate coefficients and larger concentration of soluble Cu species in ATRP of MMA.[58, 59]
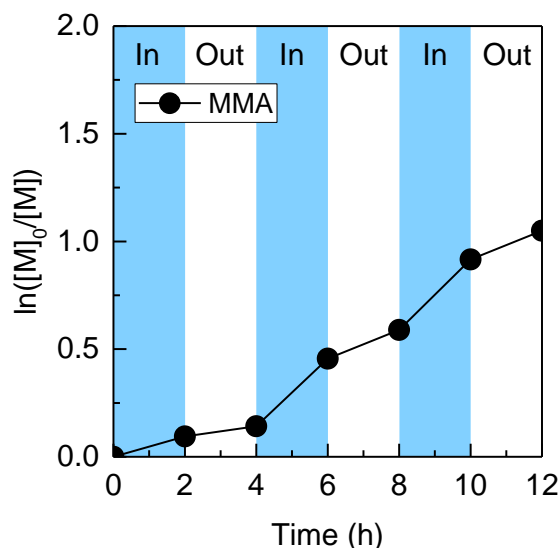
Figure 7.   Kinetics of temporal control in SARA ATRP of MMA in the presence of Cu^0 wire under conditions: $[MMA]/[EBPA]/[CuBr_2]/[Me_6TREN] = 200/1/0.05/0.150$ in 50 vol. % DMSO, at 30 °C; Cu^0 wire length = 5 cm, diameter = 0.5 mm.

Temporal Control in ATRP with Ag^0

In SARA ATRP, supplemental activation and comproportionation result in an increase in the concentration of soluble Cu species in the reaction media. In contrast, using a silver (Ag^0) wire as a reducing agent for $CuBr_2$ (Scheme 6-(A)) does not change the concentration of soluble Cu species (Figure 5-(B)) and consequently was expected to show a better temporal control.[60] For this reason, temporal control was then investigated in the ATRP of MA using Ag wire as a reducing agent.
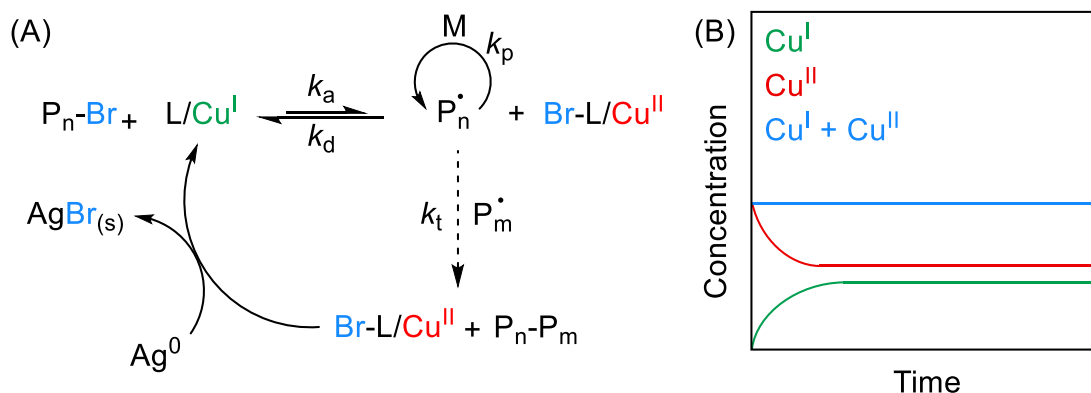
Scheme 6. (A) Mechanism of Ag ATRP and (B) schematic representation of the concentration of Cu species in Ag ATRP.

Figure 8 shows the results of temporal control in Ag ATRP of MA with 250 ppm $CuBr_2$ (with respect to monomer) in the presence of Me_6TREN as a ligand. The reaction started by inserting the Ag^0 wire in the solution (wire-in) at 30 °C. After 20 min, monomer conversion was ~33 %. At this point the Ag^0 wire was lifted out of the solution (wire-out) for 20 min and monomer conversion reached ~35 %. Reinserting the wire in the solution restarted the reaction and resulted in ~51 % monomer conversion after an additional 20 min. The wire could be inserted in or lifted out of the solution to successfully manipulate the kinetics of the polymerization with the reaction proceeding mainly when the Ag^0 wire was in the solution and stopping when it was lifted out. Moreover, the control over the reaction was maintained throughout the 'wire-in' and 'wire-out' processes with molecular weights in agreement with theoretical values and low $Đ$ values (Table S3 and Figures S11 and S12). Decreasing the concentration of $CuBr_2$ from 250 ppm to 100 resulted in a decrease in the overall rate of the reaction, as shown in Figure 8, as well as in a better temporal control as the reaction essentially stopped when the Ag^0 wire was lifted out of the solution.
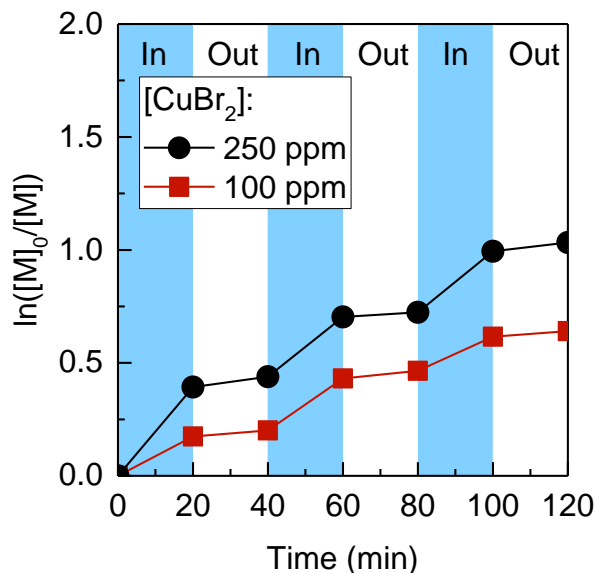
Figure 8. Kinetics of temporal control in Ag ATRP using different concentrations of $CuBr_2$ under conditions: [MA]/[EBiB]/[CuBr$_2$]/[Me$_6$TREN] = 200/1/x/3x (x: 0.02 or 0.05) in 50 vol. % DMSO at 30 °C; Ag^0 wire length = 5 cm, diameter = 2 mm.

 The effect of ligand structure in temporal control in Ag ATRP was also investigated. With an active ligand such as Me$_6$TREN, successful temporal control was achieved by removing the Ag^0 wire. In a similar manner, TPMA^{*3} and tris[(4-dimethylamino-2-pyridyl)methyl]amine (TPMA^{NMe2}) resulted in a successful temporal control with the reaction proceeding in the presence of the Ag^0 wire and stopping while the wire was removed. Interestingly, and unexpectedly, the overall rate of the reaction decreased when using ligands that form more active complexes than Me$_6$TREN, i.e. TPMA^{*3} and TPMA^{NMe2}. Although Cu complex with TPMA^{NMe2} exhibits the highest K_{ATRP} value among the ligands investigated in here,[61] the reaction had the lowest rate of all the ligands examined. This decrease in the rate of the reaction in the presence of more active complexes can be attributed to the more negative redox potential of these complexes. Since Ag^0 wire is a mild reducing agent it cannot generate a sufficient concentration of activator species to provide a high rate of polymerization. Nevertheless, reactions conducted in the presence of the various ligands were well-controlled with molecular weights in agreement with theoretical values and low Đ's (Table 3 and Figures S11, and S13-S14).
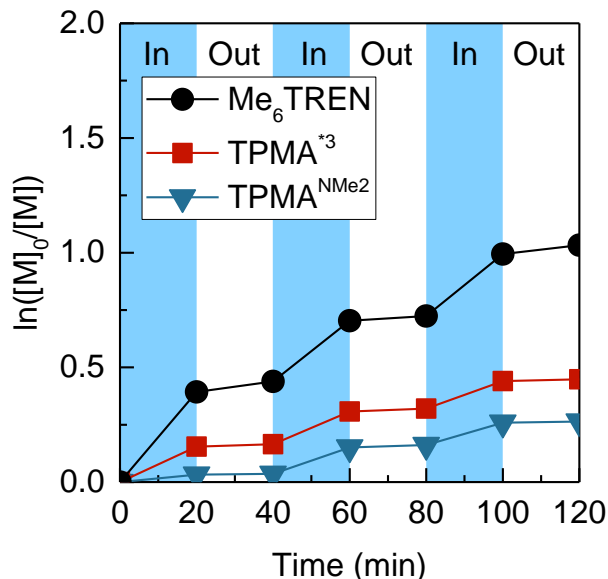
Figure 9. Kinetics of temporal control in Ag ATRP using different ligands under conditions: [MA]/[EBiB]/[CuBr$_2$]/[L] = 200/1/0.05/0.15 (L = Me$_6$TREN, TPMA^{*3} or TPMA^{NMe2} (0.06 equiv.)) in 50 vol. % DMSO at 30 °C; Ag^0 wire length = 5 cm, diameter = 2 mm.

Table 3. Polymerization results of temporal control in Ag ATRP of MA with different ligands (kinetic results are shown in Figure 9) [a]

Entry	Ligand	Time (min)	Conversion (%)	$M_{n,th}$	M_n	Đ
1	Me$_6$TREN	120	64	11200	10900	1.03
2	TPMA*3	120	36	6400	6450	1.09
3 [b]	TPMA^{NMe2}	120	23	4150	4000	1.13

[a] [MA]/[EBiB]/[CuBr$_2$]/[L]: 200/1/0.05/0.15 (L: Me$_6$TREN, TPMA^{*3} or TPMA^{NMe2}) at 30 °C; Ag^0 wire length: 5 cm, diameter: 2 mm. [b] TPMA^{NMe2} was used in 0.06 equiv. Ag^0 wire length = 5 cm, diameter = 2 mm.

2.2.4 Conclusions

We have developed a simple strategy to assert temporal control in ATRP using zerovalent metals such as Cu^0 or Ag^0 wires as activator generators. Inserting a wire in the solution triggers the reaction by (re)generating activator species. Lifting the wire out of the solution stops further

regeneration of the activator catalyst complex and the residual activator is slowly consumed by radical termination processes thereby continuously reducing the rate of polymerization.

As shown throughout this study, once the wire is lifted from the polymerization medium the reaction can exhibit different kinetic behaviors, depending on the concentration and nature of the added catalyst complex. Ideally, the reaction should stop as soon as the wire is lifted out of the polymerization medium. However, this depends on the concentration and activity of the residual L/Cu^I catalyst formed, and remaining in, the system. By tuning the K_{ATRP} equilibrium through selection of various ligands, the concentration of L/Cu^I species can be adjusted. Active ligands such as Me$_6$TREN or TPMA^{*3} in SARA ATRP, with large values for K_{ATRP}, result in shifting the equilibrium towards retaining more L/Cu^{II} in the reaction medium, i.e., generating less L/Cu^I to reach the concentration required for K_{ATRP}. Thus, the reaction stopped soon after lifting the wire. However, in the presence of ligands forming less active catalyst complexes, such as PMDETA or TPMA, polymerization proceeded for longer periods of time after the wire was lifted out. The lower K_{ATRP} values in these systems provides higher concentrations of L/Cu^I catalyst. Therefore, after removing the wire, it takes longer times for the activator to be consumed by radical termination processes and stop the reaction. Contrary to SARA ATRP, where supplemental activation and comproportionation with Cu^0 wire increases concentration of soluble Cu in the reaction, Ag^0 wire acts as only a mild reducing agent, which maintains a constant concentration of soluble Cu species in the polymerization medium. As a result, good temporal control was observed in Ag ATRP compared to SARA ATRP.

2.2.5   Experimental Section and Supporting Information

Materials

Methyl acrylate (MA; Sigma-Aldrich, 99%) and methyl methacrylate (MMA; Sigma-Aldrich, 99%) were passed through a basic alumina column to remove polymerization inhibitor prior to use. Ethyl α-bromoisobutyrate (EBiB; Sigma-Aldrich, 98%), ethyl α-bromophenylacetate (EBPA; Alfa Aesar, 97%), *N,N,N',N'',N''*-pentamethyldiethylenetriamine (PMDETA; Sigma-Aldrich, 98%), dimethyl sulfoxide (DMSO), and acetonitrile (MeCN) were used as received. Tris[2-(dimethylamino)ethyl]amine (Me$_6$TREN) and tris(2-pyridylmethyl)amine (TPMA) were received from Koei Chemical Co., Ltd. (Japan). Tris((4-methoxy-3,5-dimethylpyridin-2-yl)methyl)amine (TPMA^{*3})[62] and tris[(4-dimethylamino-2-pyridyl)methyl]amine (TPMA^{NMe2})[63]

were synthesized according to literature procedures. Copper (Cu^0) wire (diameter 0.5 mm) was immersed in concentrated hydrochloric acid for 20 min, washed with methanol and dried under air. Silver (Ag^0) wire (diameter 2 mm) was placed overnight in a concentrated sodium bicarbonate solution in the presence of aluminum foil pieces.

Instrumentation

[1]H nuclear magnetic resonance (^{1}H NMR) measurements were performed on a Bruker Avance 300 MHz spectrometer. Molecular weight properties of the polymers were determined by size-exclusion chromatography (SEC). The SEC instrument used a Waters 515 pump and a Waters 2414 differential refractometer using PSS columns (SDV 105, 103, and 500 Å) with THF as eluent at 35 °C and a flow rate of 1 mL min^{-1}. Linear poly(methyl methacrylate) standards were used for calibration.

General Procedure for Temporal Control in SARA ATRP of MA

A 20 mL vial equipped with a stir bar was sealed with a rubber septum and subjected to vacuum and backfilled with nitrogen for 5 times. Degassed DMSO (3 mL), degassed MA (3 mL, 33.1 mmol, 200 equiv.), $CuBr_2$ (1.85 mg, 8.27×10^{-6} mol, 0.05 equiv.), Me_6TREN (6.7 µL, 2.48×10^{-5} mol, 0.15 equiv.), and EBiB (24 µL, 0.165 mmol, 1 equiv.) were added into the vial under nitrogen. The vial was degassed for more 5 min and placed in a water bath at 30 °C. The reaction was activated by inserting Cu^0 wire (length 5 cm, diameter 0.5 mm) wire wrapped around a stir bar. Samples were taken periodically for ^{1}H NMR and SEC analyses.

General Procedure for Temporal Control in SARA ATRP of MMA

A 20 mL vial equipped with a stir bar was sealed with a rubber septum and subjected to vacuum and backfilled with nitrogen 5 times. Degassed DMSO (3 mL), degassed MMA (3 mL, 28.2 mmol, 200 equiv.), $CuBr_2$ (1.57 mg, 7.05×10^{-6} mol, 0.05 equiv.), Me_6TREN (5.7 µL, 2.11×10^{-5} mol, 0.15 equiv.), and EBPA (24 .7µL, 0.141 mmol, 1 equiv.) were added into the vial under nitrogen. The vial was degassed for more 5 min and placed in a water bath at 30 °C. The reaction was activated by inserting Cu^0 wire (length 5 cm, diameter 0.5 mm) wire wrapped around a stir bar. Samples were taken periodically for ^{1}H NMR and SEC analyses.

General Procedure for Temporal Control in Ag ATRP of MA

A 20 mL vial equipped with a stir bar was sealed with a rubber septum and subjected to vacuum and backfilled with nitrogen 5 times. Degassed DMSO (3 mL), degassed MA (3 mL, 33.1 mmol, 200 equiv.), CuBr$_2$ (1.85 mg, 8.27×10^{-6} mol, 0.05 equiv.), Me$_6$TREN (6.7 µL, 2.48×10^{-5} mol, 0.15 equiv.), and EBiB (24 µL, 0.165 mmol, 1 equiv.) were added into the vial under nitrogen. The vial was degassed for more 5 min and placed in a water bath at 30 °C. The reaction was activated by inserting Ag^0 wire (length 5 cm, diameter 2.0 mm) wire wrapped around a stir bar to the reaction medium. Samples were taken periodically for ^{1}H NMR and SEC analyses.

POLYMERIZATION RESULTS

Temporal control in SARA ATRP
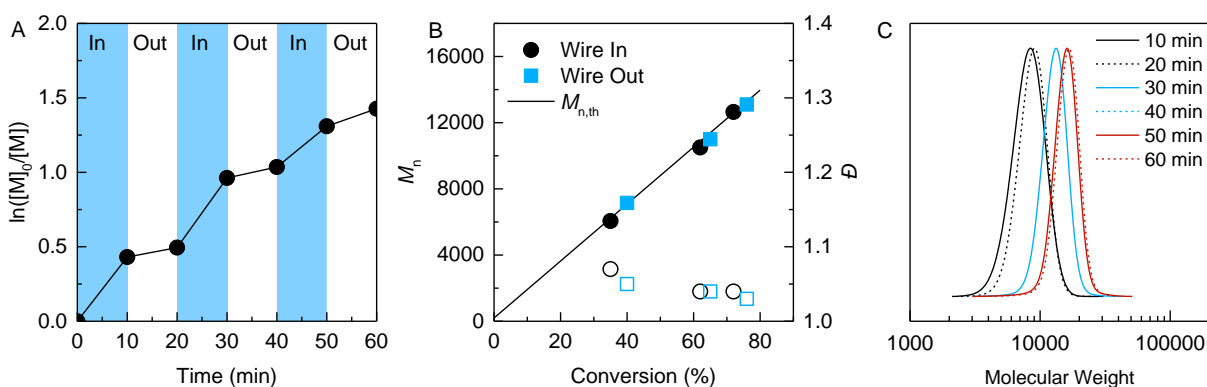
Figure 10. Temporal control in SARA ATRP in the presence of Cu^0 wire under conditions: [MA]/[EBiB]/[CuBr$_2$]/[Me$_6$TREN]: 200/1/0.05/0.15 in 50 vol% DMSO, at 30 °C; Cu^0 wire length: 5 cm, diameter: 0.5 mm. (A) Kinetics of the polymerization. (B) Number-average molecular weight (M_n, solid points) and dispersity (Đ, open points) as a function of monomer conversion. (C) SEC traces, solid lines correspond for 'wire-in' periods and dashed lines correspond for 'wire-out' periods.
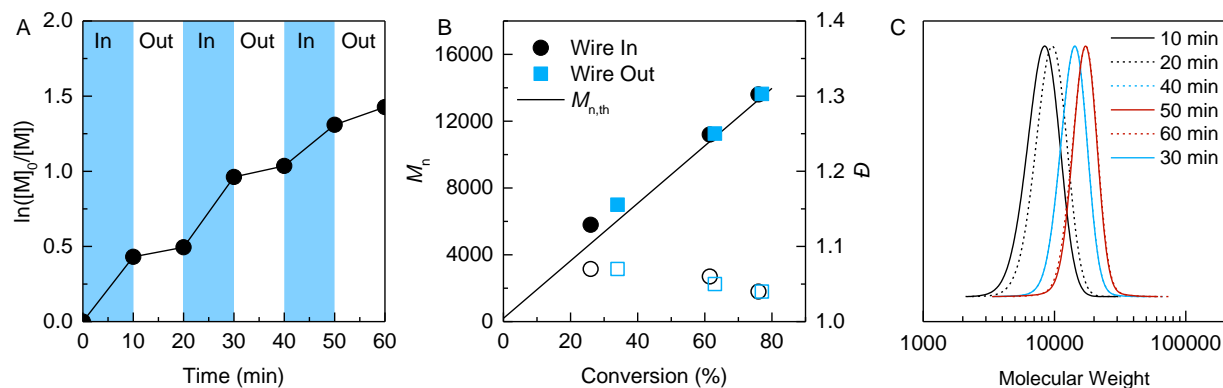
Figure 11. Temporal control in SARA ATRP in the presence of Cu^0 wire under conditions: [MA]/[EBiB]/[CuBr$_2$]/[Me$_6$TREN]: 200/1/0.02/0.06 in 50 vol% DMSO, at 30 °C; Cu^0 wire length: 5 cm, diameter: 0.5 mm. (A) Kinetics of the polymerization. (B) Number-average molecular weight (M_n, solid points) and dispersity (Đ, open points) as a function of monomer conversion. (C) SEC traces, solid lines correspond for 'wire-in' periods and dashed lines correspond for 'wire-out' periods.
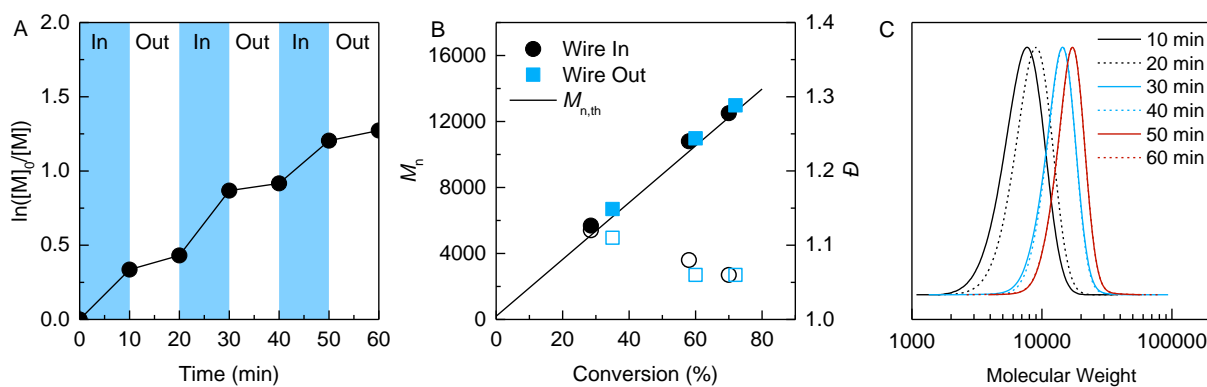
Figure 12. Temporal control in SARA ATRP in the presence of Cu^0 wire under conditions: [MA]/[EBiB]/[CuBr$_2$]/[Me$_6$TREN]: 200/1/0.01/0.03 in 50 vol% DMSO, at 30 °C; Cu^0 wire length: 5 cm, diameter: 0.5 mm. (A) Kinetics of the polymerization. (B) Number-average molecular weight (M_n, solid points) and dispersity (Đ, open points) as a function of monomer conversion. (C) SEC traces, solid lines correspond for 'wire-in' periods and dashed lines correspond for 'wire-out' periods.
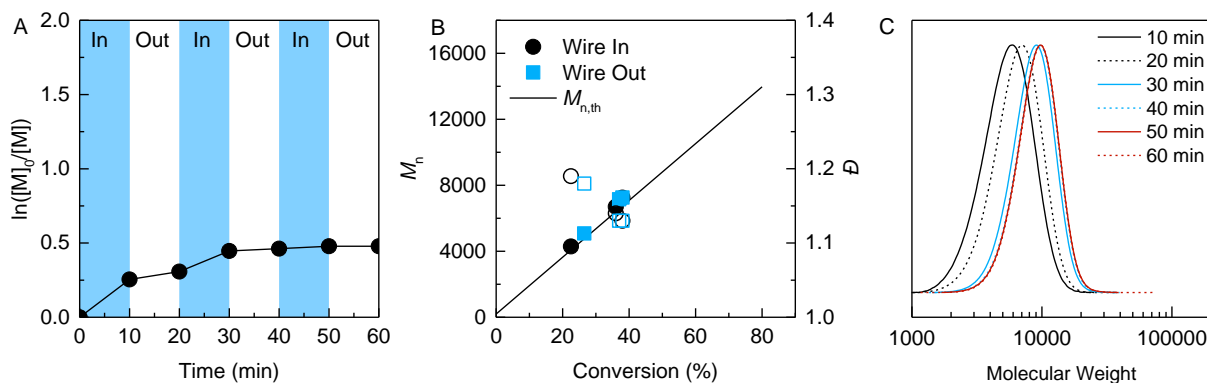
Figure 13. Temporal control in SARA ATRP in the presence of Cu^0 wire under conditions: [MA]/[EBiB]/[CuBr$_2$]/[Me$_6$TREN]: 200/1/0.005/0.015 in 50 vol% DMSO, at 30 °C; Cu^0 wire length: 5 cm, diameter: 0.5 mm. (A) Kinetics of the polymerization. (B) Number-average molecular weight (M_n, solid points) and dispersity ($Đ$, open points) as a function of monomer conversion. (C) SEC traces, solid lines correspond for 'wire-in' periods and dashed lines correspond for 'wire-out' periods.
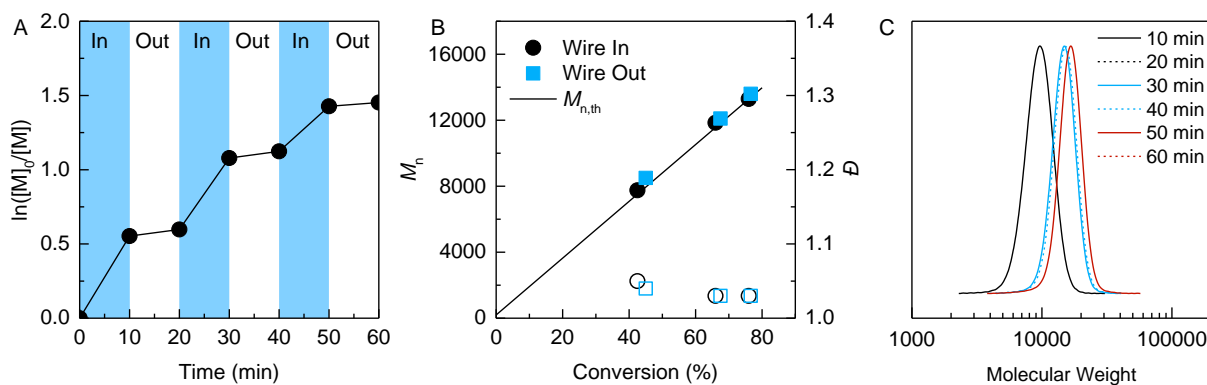
Figure 14. Temporal control in SARA ATRP in the presence of Cu^0 wire with TPMA^{*3} as ligand under conditions: [MA]/[EBiB]/[CuBr$_2$]/[TPMA^{*3}]: 200/1/0.05/0.30 in 50 vol% DMSO at 30 °C; Cu^0 wire length: 5 cm, diameter: 0.5 mm. (A) Kinetics of the polymerization. (B) Number-average molecular weight (M_n, solid points) and dispersity ($Đ$, open points) as a function of monomer conversion. (C) SEC traces, solid lines correspond for 'wire-in' periods and dashed lines correspond for 'wire-out' periods.
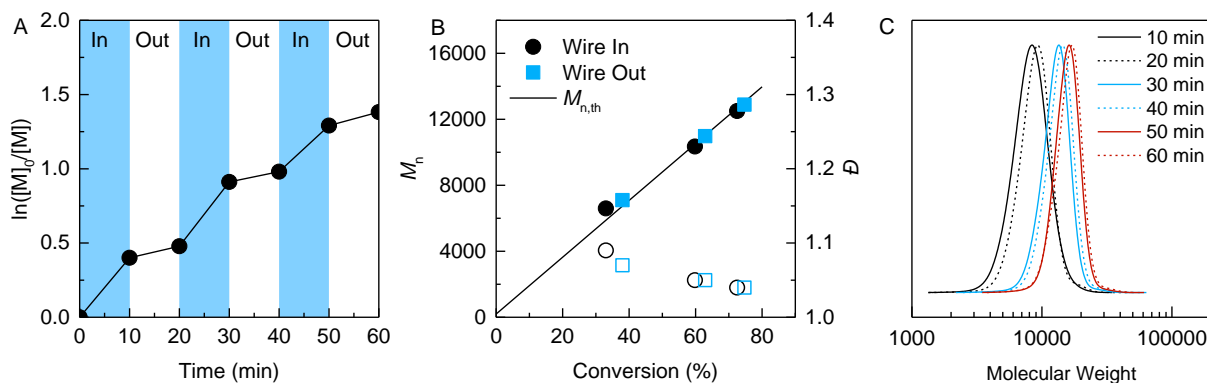
Figure 15. Temporal control in SARA ATRP in the presence of Cu^0 wire with Me_6TREN as ligand under conditions: [MA]/[EBiB]/[CuBr$_2$]/[Me$_6$TREN]: 200/1/0.05/0.30 in 50 vol% DMSO at 30 °C; Cu^0 wire length: 5 cm, diameter: 0.5 mm. (A) Kinetics of the polymerization. (B) Number-average molecular weight (M_n, solid points) and dispersity ($Đ$, open points) as a function of monomer conversion. (C) SEC traces, solid lines correspond for 'wire-in' periods and dashed lines correspond for 'wire-out' periods.
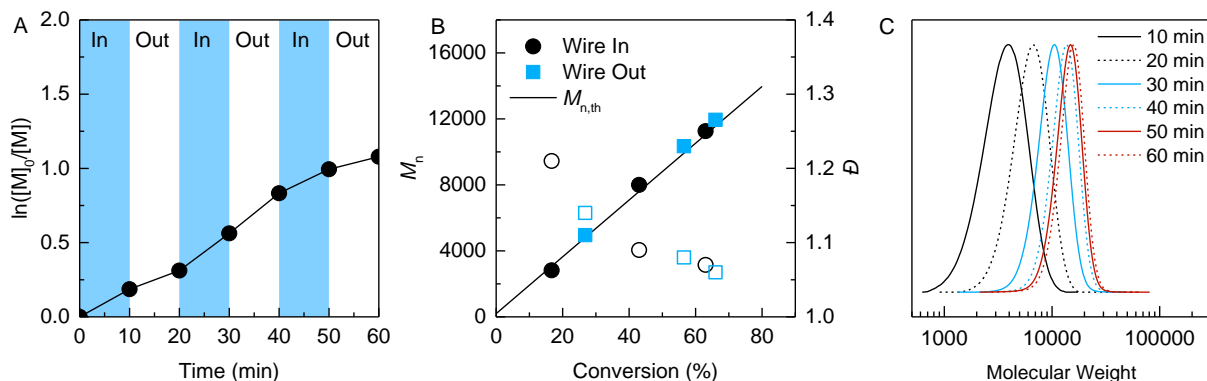
Figure 16. Temporal control in SARA ATRP in the presence of Cu^0 wire with TPMA as ligand under conditions: [MA]/[EBiB]/[CuBr$_2$]/[TPMA]: 200/1/0.05/0.30 in 50 vol% DMSO at 30 °C; Cu^0 wire length: 5 cm, diameter: 0.5 mm. (A) Kinetics of the polymerization. (B) Number-average molecular weight (M_n, solid points) and dispersity ($Đ$, open points) as a function of monomer conversion. (C) SEC traces, solid lines correspond for 'wire-in' periods and dashed lines correspond for 'wire-out' periods.
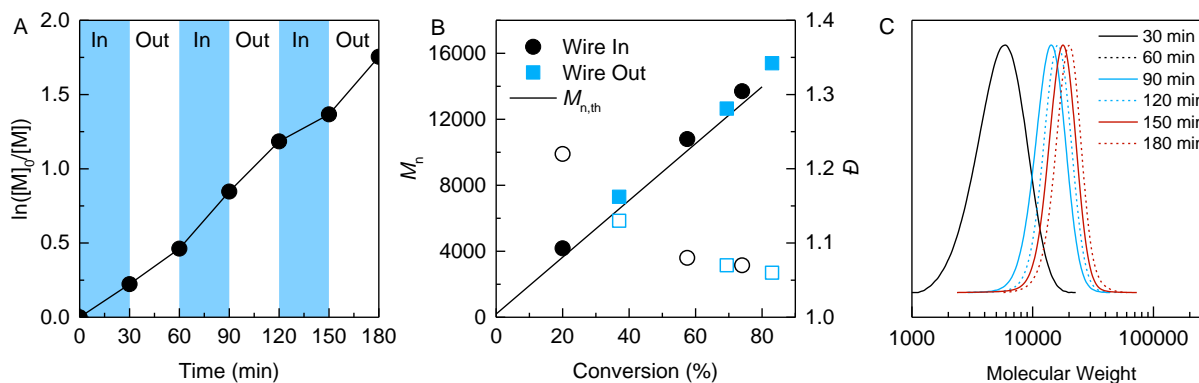
Figure 17. Temporal control in SARA ATRP in the presence of Cu^0 wire with PMDETA as ligand under conditions: [MA]/[EBiB]/[CuBr$_2$]/[PMDETA]: 200/1/0.05/0.30 in 50 vol% DMSO at 30 °C; Cu^0 wire length: 5 cm, diameter: 0.5 mm. (A) Kinetics of the polymerization. (B) Number-average molecular weight (M_n, solid points) and dispersity ($Đ$, open points) as a function of monomer conversion. (C) SEC traces, solid lines correspond for 'wire-in' periods and dashed lines correspond for 'wire-out' periods.

Table 4. Polymerization results of temporal control in SARA ATRP of MA with different ligands by keeping the Cu^0 wire out for longer periods of time (kinetics shown in Figure 3 in the main text) [a]

Entry	Ligand	Time (min)	Conversion (%)	$M_{n,th}$	M_n	$Đ$
1	TPMA[*3]	60	50	8800	9200	1.06
2	Me$_6$TREN	60	59	10350	10900	1.06
3	TPMA	60	51	8950	8750	1.08
4	PMDETA	180	58	10180	11500	1.14

[a] [MA]/[EBiB]/[CuBr$_2$]/[L]: 200/1/0.02/0.06 in 50 vol% DMSO; L: TPMA[*3], Me$_6$TREN, or TPMA, PMDETA, at 30 °C; Cu^0 wire length: 5 cm, diameter: 0.5 mm.

Table 5.   Polymerization results of temporal control in SARA ATRP of MA in different solvents [a]

Entry	Solvent	Time (min)	Conversion (%)	$M_{n,th}$	M_n	$Đ$
1	DMSO	60	75	13100	12900	1.04
2	MeCN	60	64	11250	12300	1.05

[a] Reaction conditions: [MA]/[EBiB]/[CuBr$_2$]/[Me$_6$TREN]: 200/1/0.05/0.30 in 50 vol. % solvent (DMSO or MeCN), at 30 °C; Cu^0 wire length: 5 cm, diameter: 0.5 mm.
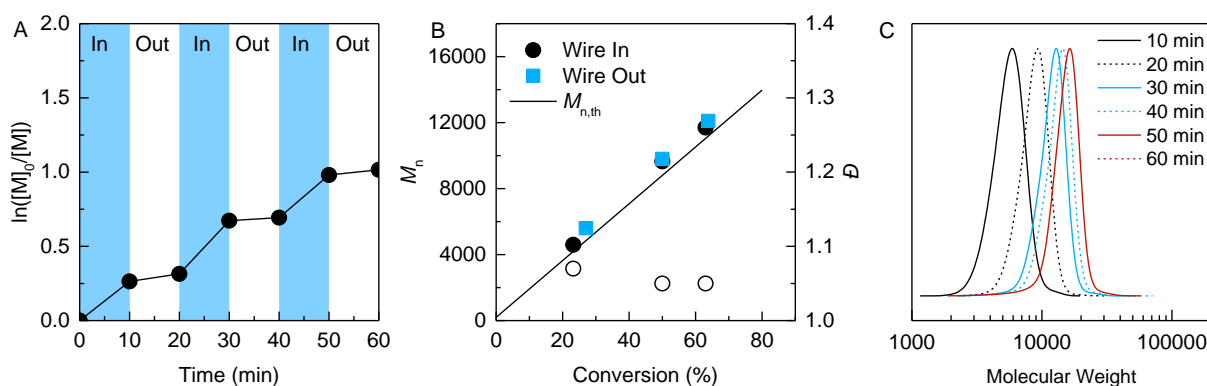
Figure 18.   Temporal control in SARA ATRP in the presence of Cu^0 wire under conditions: [MA]/[EBiB]/[CuBr$_2$]/[Me$_6$TREN]: 200/1/0.05/0.30 in 50 vol% MeCN, at 30 °C; Cu^0 wire length: 5 cm, diameter: 0.5 mm. (A) Kinetics of the polymerization. (B) Number-average molecular weight (M_n, solid points) and dispersity ($Đ$, open points) as a function of monomer conversion. (C) SEC traces, solid lines correspond for 'wire-in' periods and dashed lines correspond for 'wire-out' periods.
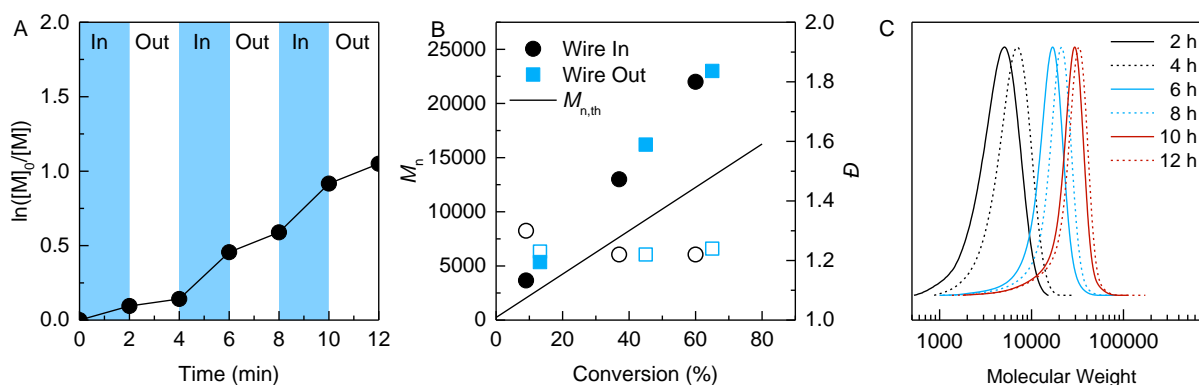
Figure 19. Temporal control in SARA ATRP of MMA in the presence of Cu^0 wire under conditions: [MMA]/[EBPA]/[CuBr$_2$]/[Me$_6$TREN]: 200/1/0.05/0.15 in 50 vol% DMSO, at 30 °C; Cu^0 wire length: 5 cm, diameter: 0.5 mm. (A) Kinetics of the polymerization. (B) Number-average molecular weight (M_n, solid points) and dispersity ($Đ$, open points) as a function of monomer conversion. (C) SEC traces, solid lines correspond for 'wire-in' periods and dashed lines correspond for 'wire-out' periods.

Temporal control in Ag ATRP

Table 6. Polymerization results of temporal control in Ag ATRP of MA with different concentrations of CuBr$_2$ [a]

Entry	CuBr$_2$ (ppm)	Time (min)	Conversion (%)	$M_{n,th}$	M_n	$Đ$
1	250	120	64	11200	10900	1.03
3	100	120	47	8350	8500	1.09

[a] [MA]/[EBiB]/[CuBr$_2$]/[Me$_6$TREN]: 200/1/x/3x (x: 0.02 or 0.05) in 50 vol. % DMSO, at 30 °C; Ag^0 wire length: 5 cm, diameter: 2.0 mm.
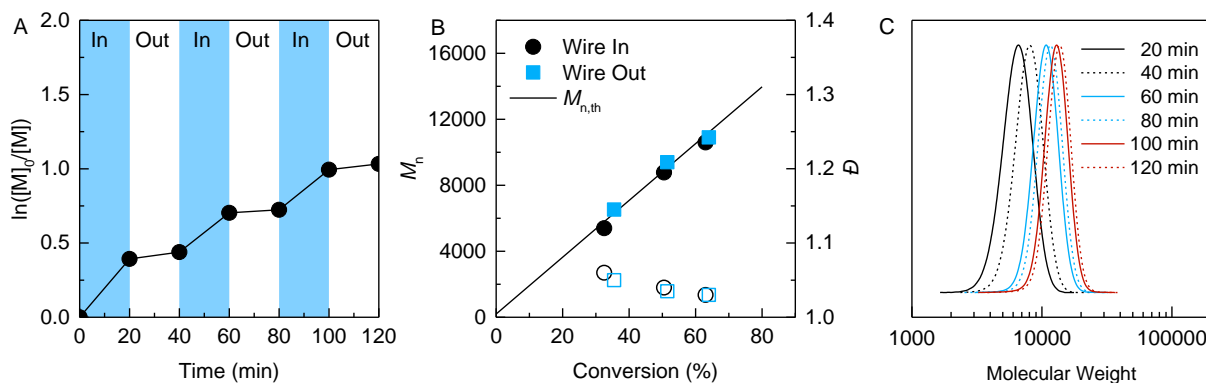
Figure 20. Temporal control in Ag ATRP in the presence of Ag^0 wire under conditions: $[MA]/[EBiB]/[CuBr_2]/[Me_6TREN] = 200/1/0.05/0.15$ in 50 vol% DMSO, at 30 °C; Ag^0 wire length: 5 cm, diameter: 2.0 mm. (A) Kinetics of the polymerization. (B) Number-average molecular weight (M_n, solid points) and dispersity ($Đ$, open points) as a function of monomer conversion. (C) SEC traces, solid lines correspond for 'wire-in' periods and dashed lines correspond for 'wire-out' periods.
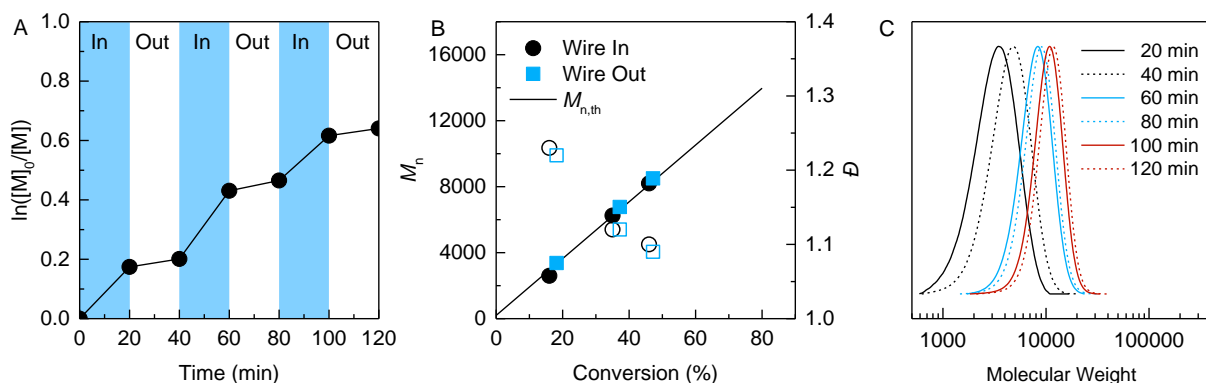
Figure 21. Temporal control in Ag ATRP in the presence of Ag^0 wire under conditions: $[MA]/[EBiB]/[CuBr_2]/[Me_6TREN] = 200/1/0.02/0.06$ in 50 vol% DMSO, at 30 °C; Ag^0 wire length: 5 cm, diameter: 2.0 mm. (A) Kinetics of the polymerization. (B) Number-average molecular weight (M_n, solid points) and dispersity ($Đ$, open points) as a function of monomer conversion. (C) SEC traces, solid lines correspond for 'wire-in' periods and dashed lines correspond for 'wire-out' periods.
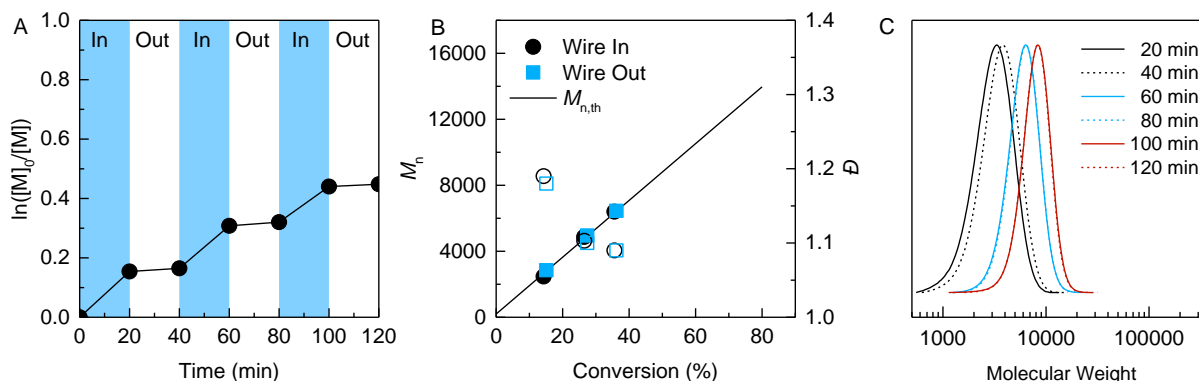
Figure 22. Temporal control in Ag ATRP in the presence of Ag^0 wire under conditions: $[MA]/[EBiB]/[CuBr_2]/[TPMA^{*3}] = 200/1/0.05/0.15$ in 50 vol% DMSO, at 30 °C; Ag^0 wire length = 5 cm, diameter = 2.0 mm. (A) Kinetics of the polymerization. (B) Number-average molecular weight (M_n, solid points) and dispersity ($Đ$, open points) as a function of monomer conversion. (C) SEC traces, solid lines correspond for 'wire-in' periods and dashed lines correspond for 'wire-out' periods.
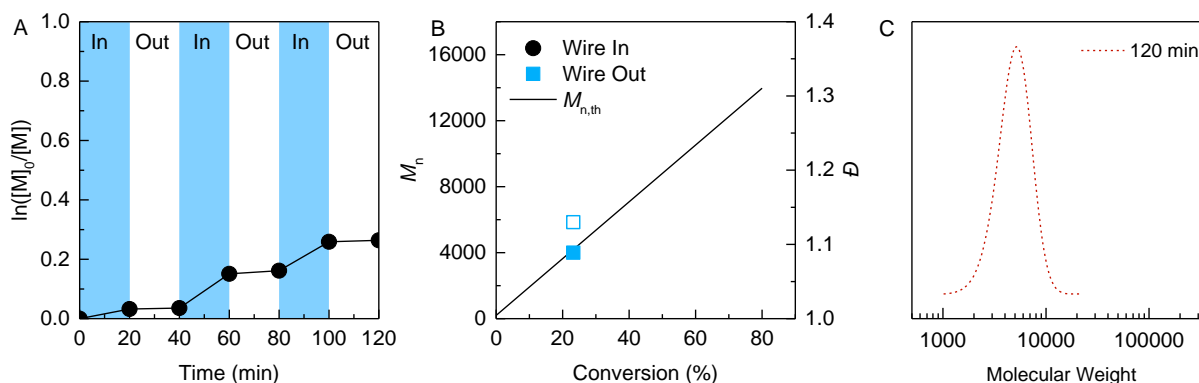
Figure 23. Temporal control in Ag ATRP in the presence of Ag^0 wire under conditions: $[MA]/[EBiB]/[CuBr_2]/[TPMA^{NMe2}] = 200/1/0.05/0.06$ in 50 vol% DMSO, at 30 °C; Ag^0 wire length = 5 cm, diameter = 2.0 mm. (A) Kinetics of the polymerization. (B) Number-average molecular weight (M_n, solid points) and dispersity ($Đ$, open points) as a function of monomer conversion. (C) SEC traces, solid lines correspond for 'wire-in' periods and dashed lines correspond for 'wire-out' periods.

2.2.6 References

1. Blanco, V.; Leigh, D. A.; Marcos, V. Artificial switchable catalysts. *Chem. Soc. Rev.* **2015,** 44 (15), 5341-5370.

2. Leibfarth, F. A.; Mattson, K. M.; Fors, B. P.; Collins, H. A.; Hawker, C. J. External Regulation of Controlled Polymerizations. *Angew. Chem. Int. Ed.* **2013,** 52 (1), 199-210.

3. Teator, A. J.; Lastovickova, D. N.; Bielawski, C. W. Switchable Polymerization Catalysts. *Chem. Rev.* **2016,** 116 (4), 1969-1992.

4. Yoon, H. J.; Kuwabara, J.; Kim, J.-H.; Mirkin, C. A. Allosteric Supramolecular Triple-Layer Catalysts. *Science* **2010,** 330 (6000), 66-69.

5. Gregson, C. K. A.; Gibson, V. C.; Long, N. J.; Marshall, E. L.; Oxford, P. J.; White, A. J. P. Redox Control within Single-Site Polymerization Catalysts. *J. Am. Chem. Soc.* **2006,** 128 (23), 7410-7411.

6. Broderick, E. M.; Guo, N.; Vogel, C. S.; Xu, C.; Sutter, J.; Miller, J. T.; Meyer, K.; Mehrkhodavandi, P.; Diaconescu, P. L. Redox Control of a Ring-Opening Polymerization Catalyst. *J. Am. Chem. Soc.* **2011,** 133 (24), 9278-9281.

7. Broderick, E. M.; Guo, N.; Wu, T.; Vogel, C. S.; Xu, C.; Sutter, J.; Miller, J. T.; Meyer, K.; Cantat, T.; Diaconescu, P. L. Redox control of a polymerization catalyst by changing the oxidation state of the metal center. *Chem. Commun.* **2011,** 47 (35), 9897-9899.

8. Wang, X.; Thevenon, A.; Brosmer, J. L.; Yu, I.; Khan, S. I.; Mehrkhodavandi, P.; Diaconescu, P. L. Redox Control of Group 4 Metal Ring-Opening Polymerization Activity toward l-Lactide and ε-Caprolactone. *J. Am. Chem. Soc.* **2014,** 136 (32), 11264-11267.

9. Biernesser, A. B.; Li, B.; Byers, J. A. Redox-Controlled Polymerization of Lactide Catalyzed by Bis(imino)pyridine Iron Bis(alkoxide) Complexes. *J. Am. Chem. Soc.* **2013,** 135 (44), 16553-16560.

10. Pan, X.; Tasdelen, M. A.; Laun, J.; Junkers, T.; Yagci, Y.; Matyjaszewski, K. Photomediated controlled radical polymerization. *Prog. Polym. Sci.* **2016,** 62, 73-125.

11. Chen, M.; Zhong, M.; Johnson, J. A. Light-Controlled Radical Polymerization: Mechanisms, Methods, and Applications. *Chem. Rev.* **2016,** 116 (17), 10167-10211.

12. Xu, J.; Jung, K.; Atme, A.; Shanmugam, S.; Boyer, C. A Robust and Versatile Photoinduced Living Polymerization of Conjugated and Unconjugated Monomers and Its Oxygen Tolerance. *J. Am. Chem. Soc.* **2014,** 136 (14), 5508-5519.

13. Shanmugam, S.; Xu, J.; Boyer, C. Photocontrolled Living Polymerization Systems with Reversible Deactivations through Electron and Energy Transfer. *Macromol. Rapid Commun.* **2017,** 38 (13), 1700143.

14. Ohtsuki, A.; Goto, A.; Kaji, H. Visible-Light-Induced Reversible Complexation Mediated Living Radical Polymerization of Methacrylates with Organic Catalysts. *Macromolecules* **2013,** 46 (1), 96-102.

15. Ohtsuki, A.; Lei, L.; Tanishima, M.; Goto, A.; Kaji, H. Photocontrolled Organocatalyzed Living Radical Polymerization Feasible over a Wide Range of Wavelengths. *J. Am. Chem. Soc.* **2015,** 137 (16), 5610-5617.

16. Michaudel, Q.; Kottisch, V.; Fors, B. P. Cationic Polymerization: From Photoinitiation to Photocontrol. *Angew. Chem. Int. Ed.* **2017,** 56 (33), 9670-9679.

17. Kottisch, V.; Michaudel, Q.; Fors, B. P. Cationic Polymerization of Vinyl Ethers Controlled by Visible Light. *J. Am. Chem. Soc.* **2016,** 138 (48), 15535-15538.

18. Teator, A. J.; Bielawski, C. W. Remote control grubbs catalysts that modulate ring-opening metathesis polymerizations. *J. Polym. Sci., Part A: Polym. Chem.* **2017,** 55 (18), 2949-2960.

19. Ogawa, K. A.; Goetz, A. E.; Boydston, A. J. Metal-Free Ring-Opening Metathesis Polymerization. *J. Am. Chem. Soc.* **2015,** 137 (4), 1400-1403.

20. Wang, J.-S.; Matyjaszewski, K. Controlled/"living" radical polymerization. atom transfer radical polymerization in the presence of transition-metal complexes. *J. Am. Chem. Soc.* **1995,** 117 (20), 5614-5615.

21. Matyjaszewski, K.; Jakubowski, W.; Min, K.; Tang, W.; Huang, J.; Braunecker, W. A.; Tsarevsky, N. V. Diminishing catalyst concentration in atom transfer radical polymerization with reducing agents. *Proc. Natl. Acad. Sci. U.S.A.* **2006,** 103 (42), 15309-15314.

22. Konkolewicz, D.; Magenau, A. J. D.; Averick, S. E.; Simakova, A.; He, H. K.; Matyjaszewski, K. ICAR ATRP with ppm Cu Catalyst in Water. *Macromolecules* **2012,** 45 (11), 4461-4468.

23. Min, K.; Gao, H. F.; Matyjaszewski, K. Preparation of homopolymers and block copolymers in miniemulsion by ATRP using activators generated by electron transfer (AGET). *J. Am. Chem. Soc.* **2005,** 127 (11), 3825-3830.

24. Jakubowski, W.; Matyjaszewski, K. Activators regenerated by electron transfer for atom-transfer radical polymerization of (meth)acrylates and related block copolymers. *Angew. Chem. Int. Ed.* **2006,** 45 (27), 4482-4486.

25. Konkolewicz, D.; Wang, Y.; Zhong, M. J.; Krys, P.; Isse, A. A.; Gennaro, A.; Matyjaszewski, K. Reversible-Deactivation Radical Polymerization in the Presence of Metallic Copper. A Critical Assessment of the SARA ATRP and SET-LRP Mechanisms. *Macromolecules* **2013,** 46 (22), 8749-8772.

26. Matyjaszewski, K.; Coca, S.; Gaynor, S. G.; Wei, M. L.; Woodworth, B. E. Zerovalent metals in controlled "living" radical polymerization. *Macromolecules* **1997,** 30 (23), 7348-7350.

27. Anastasaki, A.; Nikolaou, V.; Nurumbetov, G.; Wilson, P.; Kempe, K.; Quinn, J. F.; Davis, T. P.; Whittaker, M. R.; Haddleton, D. M. Cu(0)-Mediated Living Radical Polymerization: A Versatile Tool for Materials Synthesis. *Chem. Rev.* **2016,** 116 (3), 835-877.

28. Boyer, C.; Corrigan, N. A.; Jung, K.; Nguyen, D.; Nguyen, T. K.; Adnan, N. N. M.; Oliver, S.; Shanmugam, S.; Yeow, J. Copper-Mediated Living Radical Polymerization (Atom Transfer Radical Polymerization and Copper(0) Mediated Polymerization): From Fundamentals to Bioapplications. *Chem. Rev.* **2016,** 116 (4), 1803-1949.

29. Magenau, A. J. D.; Strandwitz, N. C.; Gennaro, A.; Matyjaszewski, K. Electrochemically Mediated Atom Transfer Radical Polymerization. *Science* **2011,** 332 (6025), 81-84.

30. Li, B.; Yu, B.; Huck, W. T. S.; Zhou, F.; Liu, W. Electrochemically Induced Surface-Initiated Atom-Transfer Radical Polymerization. *Angew. Chem. Int. Ed.* **2012,** 51 (21), 5092-5095.

31. Li, B.; Yu, B.; Huck, W. T. S.; Liu, W.; Zhou, F. Electrochemically Mediated Atom Transfer Radical Polymerization on Nonconducting Substrates: Controlled Brush Growth through Catalyst Diffusion. *J. Am. Chem. Soc.* **2013,** 135 (5), 1708-1710.

32. Shida, N.; Koizumi, Y.; Nishiyama, H.; Tomita, I.; Inagi, S. Electrochemically Mediated Atom Transfer Radical Polymerization from a Substrate Surface Manipulated by Bipolar Electrolysis: Fabrication of Gradient and Patterned Polymer Brushes. *Angew. Chem. Int. Ed.* **2015,** 54 (13), 3922-3926.

33. Chmielarz, P.; Fantin, M.; Park, S.; Isse, A. A.; Gennaro, A.; Magenau, A. J. D.; Sobkowiak, A.; Matyjaszewski, K. Electrochemically mediated atom transfer radical polymerization (eATRP). *Prog. Polym. Sci.* **2017,** 69, 47-78.

34. Mosnáček, J.; Ilčíková, M. Photochemically Mediated Atom Transfer Radical Polymerization of Methyl Methacrylate Using ppm Amounts of Catalyst. *Macromolecules* **2012,** 45 (15), 5859-5865.

35. Konkolewicz, D.; Schröder, K.; Buback, J.; Bernhard, S.; Matyjaszewski, K. Visible Light and Sunlight Photoinduced ATRP with ppm of Cu Catalyst. *ACS Macro Lett.* **2012,** 1 (10), 1219-1223.

36. Anastasaki, A.; Nikolaou, V.; Zhang, Q.; Burns, J.; Samanta, S. R.; Waldron, C.; Haddleton, A. J.; McHale, R.; Fox, D.; Percec, V.; Wilson, P.; Haddleton, D. M. Copper(II)/Tertiary Amine Synergy in Photoinduced Living Radical Polymerization: Accelerated Synthesis of ω-Functional and α,ω-Heterofunctional Poly(acrylates). *J. Am. Chem. Soc.* **2014,** 136 (3), 1141-1149.

37. Ribelli, T. G.; Konkolewicz, D.; Bernhard, S.; Matyjaszewski, K. How are Radicals (Re)Generated in Photochemical ATRP? *J. Am. Chem. Soc.* **2014,** 136 (38), 13303-13312.

38. Dadashi-Silab, S.; Tasdelen, M. A.; Kiskan, B.; Wang, X.; Antonietti, M.; Yagci, Y. Photochemically Mediated Atom Transfer Radical Polymerization Using Polymeric Semiconductor Mesoporous Graphitic Carbon Nitride. *Macromol. Chem. Phys.* **2014,** 215 (7), 675-681.

39. Wang, Z.; Pan, X.; Li, L.; Fantin, M.; Yan, J.; Wang, Z.; Wang, Z.; Xia, H.; Matyjaszewski, K. Enhancing Mechanically Induced ATRP by Promoting Interfacial Electron Transfer from Piezoelectric Nanoparticles to Cu Catalysts. *Macromolecules* **2017,** 50 (20), 7940-7948.

40. Dadashi-Silab, S.; Atilla Tasdelen, M.; Yagci, Y. Photoinitiated atom transfer radical polymerization: Current status and future perspectives. *J. Polym. Sci., Part A: Polym. Chem.* **2014,** 52 (20), 2878-2888.

41. Mohapatra, H.; Kleiman, M.; Esser-Kahn, A. P. Mechanically controlled radical polymerization initiated by ultrasound. *Nat. Chem.* **2017,** 9 (2), 135-139.

42. Wang, Z.; Pan, X.; Yan, J.; Dadashi-Silab, S.; Xie, G.; Zhang, J.; Wang, Z.; Xia, H.; Matyjaszewski, K. Temporal Control in Mechanically Controlled Atom Transfer Radical Polymerization Using Low ppm of Cu Catalyst. *ACS Macro Lett.* **2017,** 6 (5), 546-549.

43. Wang, Z.; Wang, Z.; Pan, X.; Fu, L.; Lathwal, S.; Olszewski, M.; Yan, J.; Enciso, A. E.; Wang, Z.; Xia, H.; Matyjaszewski, K. Ultrasonication-Induced Aqueous Atom Transfer Radical Polymerization. *ACS Macro Lett.* **2018,** 7 (3), 275-280.

44. Simakova, A.; Averick, S. E.; Konkolewicz, D.; Matyjaszewski, K. Aqueous ARGET ATRP. *Macromolecules* **2012,** 45 (16), 6371-6379.

45. Fantin, M.; Isse, A. A.; Venzo, A.; Gennaro, A.; Matyjaszewski, K. Atom Transfer Radical Polymerization of Methacrylic Acid: A Won Challenge. *J. Am. Chem. Soc.* **2016,** 138 (23), 7216-7219.

46. Lorandi, F.; Fantin, M.; Isse, A. A.; Gennaro, A. Electrochemical triggering and control of atom transfer radical polymerization. *Curr. Opin. Electrochem.* **2018,** 8, 1-7.

47. Dadashi-Silab, S.; Pan, X.; Matyjaszewski, K. Photoinduced Iron-Catalyzed Atom Transfer Radical Polymerization with ppm Levels of Iron Catalyst under Blue Light Irradiation. *Macromolecules* **2017,** 50 (20), 7967-7977.

48. Ribelli, T. G.; Fantin, M.; Daran, J.-C.; Augustine, K. F.; Poli, R.; Matyjaszewski, K. Synthesis and Characterization of the Most Active Copper ATRP Catalyst Based on Tris[(4-dimethylaminopyridyl)methyl]amine. *J. Am. Chem. Soc.* **2018,** 140 (4), 1525-1534.

49. Fors, B. P.; Hawker, C. J. Control of a Living Radical Polymerization of Methacrylates by Light. *Angew. Chem. Int. Ed.* **2012,** 51 (35), 8850-8853.

50. Pan, X.; Fang, C.; Fantin, M.; Malhotra, N.; So, W. Y.; Peteanu, L. A.; Isse, A. A.; Gennaro, A.; Liu, P.; Matyjaszewski, K. Mechanism of Photoinduced Metal-Free Atom Transfer Radical Polymerization: Experimental and Computational Studies. *J. Am. Chem. Soc.* **2016,** 138 (7), 2411-2425.

51. Treat, N. J.; Sprafke, H.; Kramer, J. W.; Clark, P. G.; Barton, B. E.; Read de Alaniz, J.; Fors, B. P.; Hawker, C. J. Metal-Free Atom Transfer Radical Polymerization. *J. Am. Chem. Soc.* **2014,** 136 (45), 16096-16101.

52. Dadashi-Silab, S.; Pan, X.; Matyjaszewski, K. Phenyl Benzo[b]phenothiazine as a Visible Light Photoredox Catalyst for Metal-Free Atom Transfer Radical Polymerization. *Chem. Eur. J.* **2017,** 23 (25), 5972-5977.

53. Levere, M. E.; Nguyen, N. H.; Sun, H.-J.; Percec, V. Interrupted SET-LRP of methyl acrylate demonstrates Cu(0) colloidal particles as activating species. *Polym. Chem.* **2013,** 4 (3), 686-694.

54. Konkolewicz, D.; Wang, Y.; Krys, P.; Zhong, M.; Isse, A. A.; Gennaro, A.; Matyjaszewski, K. SARA ATRP or SET-LRP. End of controversy? *Polym. Chem.* **2014,** 5 (15), 4396-4417.

55. Augustine, K. F.; Ribelli, T. G.; Fantin, M.; Krys, P.; Cong, Y.; Matyjaszewski, K. Activation of alkyl halides at the Cu0 surface in SARA ATRP: An assessment of reaction order and surface mechanisms. *J. Polym. Sci., Part A: Polym. Chem.* **2017,** 55 (18), 3048-3057.

56. Peng, C.-H.; Zhong, M.; Wang, Y.; Kwak, Y.; Zhang, Y.; Zhu, W.; Tonge, M.; Buback, J.; Park, S.; Krys, P.; Konkolewicz, D.; Gennaro, A.; Matyjaszewski, K. Reversible-Deactivation Radical Polymerization in the Presence of Metallic Copper. Activation of Alkyl Halides by Cu0. *Macromolecules* **2013,** 46 (10), 3803-3815.

57. Schröder, K.; Mathers, R. T.; Buback, J.; Konkolewicz, D.; Magenau, A. J. D.; Matyjaszewski, K. Substituted Tris(2-pyridylmethyl)amine Ligands for Highly Active ATRP Catalysts. *ACS Macro Lett.* **2012,** 1 (8), 1037-1040.

58. Braunecker, W. A.; Tsarevsky, N. V.; Gennaro, A.; Matyjaszewski, K. Thermodynamic Components of the Atom Transfer Radical Polymerization Equilibrium: Quantifying Solvent Effects. *Macromolecules* **2009,** 42 (17), 6348-6360.

59. Horn, M.; Matyjaszewski, K. Solvent Effects on the Activation Rate Constant in Atom Transfer Radical Polymerization. *Macromolecules* **2013,** 46 (9), 3350-3357.

60. Wang, Y.; Kwak, Y.; Buback, J.; Buback, M.; Matyjaszewski, K. Determination of ATRP Equilibrium Constants under Polymerization Conditions. *ACS Macro Lett.* **2012,** 1 (12), 1367-1370.

61. Tang, W.; Matyjaszewski, K. Effects of Initiator Structure on Activation Rate Constants in ATRP. *Macromolecules* **2007,** 40 (6), 1858-1863.

62. Tang, W.; Kwak, Y.; Braunecker, W.; Tsarevsky, N. V.; Coote, M. L.; Matyjaszewski, K. Understanding Atom Transfer Radical Polymerization: Effect of Ligand and Initiator Structures on the Equilibrium Constants. *J. Am. Chem. Soc.* **2008,** 130 (32), 10702-10713.

63. Williams, V. A.; Ribelli, T. G.; Chmielarz, P.; Park, S.; Matyjaszewski, K. A Silver Bullet: Elemental Silver as an Efficient Reducing Agent for Atom Transfer Radical Polymerization of Acrylates. *J. Am. Chem. Soc.* **2015,** 137 (4), 1428-1431.

2.3. Investigating Temporal Control in Photoinduced Atom Transfer Radical Polymerization

2.3.1 Abstract

External regulation of controlled polymerizations allows for controlling the kinetics of the polymerization and gaining spatial or temporal control over polymer growth. In photoinduced atom transfer radical polymerization (ATRP), light irradiation (re)generates the copper catalyst to switch the polymerization on. However, removing the light does not immediately inactivate the catalyst nor does the rate of polymerization become zero, as chains may grow in the dark due to continued activation by the residual activator catalyst or regeneration of the Cu catalyst in the dark. In this paper, the effect of polymerization components on photoinduced ATRP was investigated to understand the interplay of temporal control and light switching. Kinetics of polymerization were monitored using *in-situ* NMR as well as under conventional batch conditions. The extent of the polymerization in the dark depended on the activity of the Cu catalyst, which was regulated by the nature of the ligand and reaction medium. For highly active catalysts, the equilibrium concentration of the L/Cu^I activator is very low, and it was rapidly depleted by radical termination reactions, yielding temporal control which closely matched the switching of light - on or off. Decreasing the activity of the Cu catalyst increased the equilibrium concentration of the activator, leading to significant chain growth in the dark.
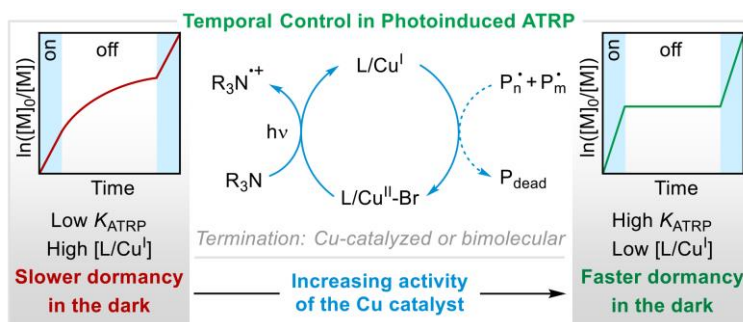
2.3.2 Introduction

Stimuli-responsive catalytic systems can be modulated by external factors such as heat, light or electrochemical potential to alter their properties and function in catalyzing and controlling the rate and selectivity of chemical reactions.[1] In controlled polymerization techniques, external regulation has provided new opportunities to synthesize advanced polymers and expand understanding of underlying mechanisms.[1-3]

Tied to these catalytic systems, photochemistry has been extensively used for chemical transformations.[4] Application of photochemistry in controlled polymerization techniques[5-7] such as atom transfer radical polymerization (ATRP),[8-17] photoinduced electron/energy transfer in reversible addition-fragmentation chain transfer (PET-RAFT),[18-22] cationic,[23, 24] ring-opening,[25] and ring-opening metathesis polymerizations[26] has led to significant advancements in polymer synthesis and enabled spatial and temporal control over polymerization.

ATRP[27, 28] can be efficiently carried out with minute amounts of Cu catalysts, using various activator (re)generation techniques.[29-31] For example, ATRP has been performed using zerovalent metals,[32-36] radical initiators,[37] reducing agents,[38, 39] and photo-,[18, 19, 40-43] electro-,[10, 44-46] and mechano-chemical stimuli.[46-49] A common feature of these ATRP initiating systems is the (re)generation of the activator L/Cu^I species via reduction of the deactivator, L/Cu^{II}-Br, which is used initially and is accumulated throughout polymerization due to unavoidable radical terminations.

The use of external stimuli provides temporal control over ATRP through modulating the oxidation state of the Cu catalyst.[49-51] In the case of photoinduced ATRP, light is used to promote reaction of the L/Cu^{II}-Br deactivator in the excited state with electron donors such as amines.[6] However, upon removal of the external stimulus, the remaining L/Cu^I activator in solution can often lead to further chain growth.[43, 52, 53] In photo-controlled polymerizations, the growth of polymer chains depends on continuous light irradiation, during which chain growth is enabled by photochemical electron or energy transfer reactions by photoexcited state catalysts. Consequently, temporal control can be efficiently achieved upon applying or removing light while maintaining control over polymerization. In Cu-catalyzed photoinduced ATRP, chain ends are activated by L/Cu^I activator in the ground state, and switching light off stops regeneration of the activator catalyst. However, polymer chains may continue further growth in the dark as a result of the presence of residual L/Cu^I activator in solution, which is regulated by the ATRP equilibrium between L/Cu^I and L/Cu^{II}-Br species. The extent of polymerization in the absence of external stimuli depends on the relative concentration of L/Cu^I and L/Cu^{II}-Br, which is determined by the nature of the catalyst/ligand, reaction medium, and (re)generation mechanism.[51, 54, 55] Highly active catalysts shift the ATRP equilibrium toward a low concentration of L/Cu^I whereas with less active catalysts, a higher concentration of L/Cu^I in

solution may continue polymerization without stimuli. Accordingly, temporal control in ATRP using Cu catalysts depends, among other factors, on the activity and concentration of the catalyst.[3, 52, 54, 56, 57]

ATRP is subject to the persistent radical effect, where unavoidable radical termination processes consume the activator and lead to a buildup of the deactivator.[58] As a consequence, the rate of polymerization decreases over time and the consumption of the L/Cu^I activator causes the polymerization to pause. However, use of oxidizing external stimuli offers a more efficient way to pause the polymerization while preserving high chain-end functionality for subsequent re-starting of the polymerization under reducing stimuli. Indeed, switching the oxidation state of the Cu catalyst with external stimuli offers switching polymerization on demand between on and off states.[55, 59]

This paper investigates temporal control in photoinduced ATRP and examines how the nature and activity of the Cu catalyst with different ligands or reaction medium impacts the response of the polymerization to switching the light on/off. Significantly, highly active catalytic systems were shown to enable excellent temporal control through multiple on/off light switches with minimal polymerization observed in the dark periods. In the absence of light, radical termination reactions consume the low concentration of activator present, stopping the polymerization. However, when using catalysts with lower activity, the polymerization continued in the dark due to the presence of a relatively high concentration of the ATRP activator when the light was switched off. Strongly improved temporal control was attained with less active catalytic systems by using oxygen to oxidize the residual L/Cu^I activator.

2.3.3   Results and Discussion

Temporal control in photoinduced ATRP was investigated in the polymerization of methyl acrylate (MA) using *N,N,N',N'',N''*-pentamethyldiethylenetriamine (PMDETA), tris(2-pyridylmethyl)amine (TPMA), and tris[2-(dimethylamino)ethyl]amine (Me₆TREN) ligands (Scheme 7). The choice of the ligand and reaction medium allows for tuning the activity of the Cu catalyst and hence the kinetics of the polymerization.[60] The activity of the Cu catalyst in ATRP increases by changing the ligand from PMDETA to TPMA and to Me₆TREN.[61] Therefore, temporal control in photoinduced ATRP was studied using different ligands and solvents to examine their effect on the polymerization behavior in response to photochemical

switching. To minimize potential experimental errors, real-time optical fiber-coupled ^{1}H NMR monitoring[53] was applied in addition to conventional batch conditions. Specifically, polymerization of MA was performed in an NMR tube equipped with the optical fiber on top of the sample and the reaction was monitored with intermittent on/off cycles (cf. SI).
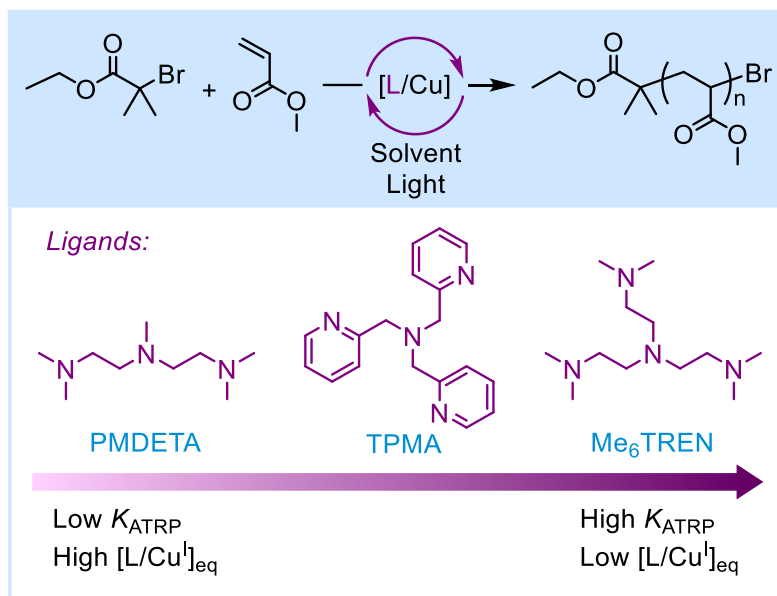
Scheme 7. Photoinduced ATRP in the presence of different ligands promoting different catalytic activity. Ligands: PMDETA, TPMA, and Me$_6$TREN.

To begin temporal control studies, a series of *in-situ* experiments using Me$_6$TREN were carried out under fixed conditions. Polymerization of MA (50 equiv.) was performed with 0.02 equiv. of copper(II) bromide (CuBr$_2$), 0.12 equiv. of Me$_6$TREN, and 1 equiv. of ethyl α-bromoisobutyrate (EBiB) as the initiator in deuterated dimethyl sulfoxide (d$_6$-DMSO) under irradiation with 405 nm LEDs. Kinetic analysis revealed rapid polymerization reaching 63% conversion after 30 min. Then, the light was turned off and the reaction was monitored in the dark for an extended time period. Without light exposure, the rate of polymerization was lower and gradually decreased with time. However, polymerization never ceased, ultimately reaching 93% monomer conversion after 12 h (Figure 24-A). This result strongly suggests that the activator complex, L/Cu^I, continuously drove the polymerization through the dark period. Importantly, similar behavior was observed for the attempted temporal control of MA polymerization under conventional batch conditions. Significant chain growth occurs over an extended period after removal of the light (Figure 24-B, and Figure S1). As a result, it is necessary to identify the contribution of

polymerization components, such as reaction medium, concentration of the Cu catalyst and ligand, on the chain growth in the dark. The ultimate goal is to identify conditions for improving temporal control in photoinduced ATRP.
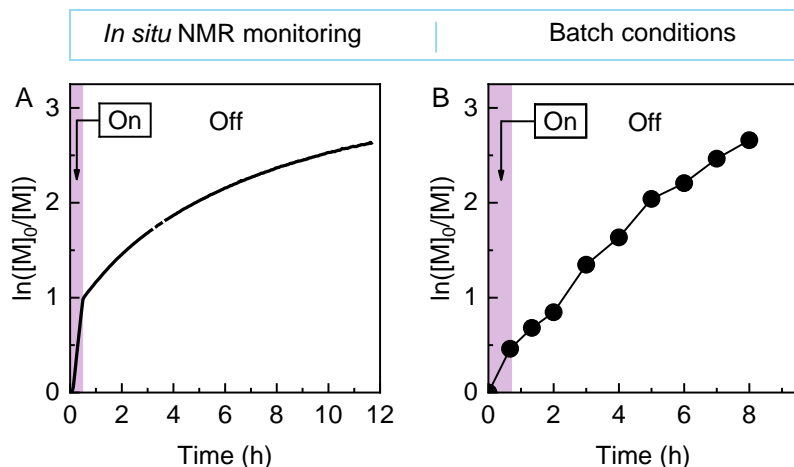
Figure 24. Temporal control in photoinduced ATRP demonstrating continued chain growth in the dark monitored *via* (A) *in situ* NMR monitoring or (B) under conventional batch conditions. Reaction conditions: [MA]/[EBiB]/[CuBr$_2$]/[Me$_6$TREN] = 50/1/0.02/0.12 in DMSO ([MA] = 5.5 M).

Control experiments performed in the dark showed that polymerization of MA could be initiated without light irradiation. For example, under typical conditions with a target DP of 50 using 0.12 equiv. of Me$_6$TREN in DMSO, polymerization of MA reached 92% monomer conversion in 24 h in the dark (no exposure to ambient light). These results suggest that the L/Cu^I activator is generated in the dark in the presence of Me$_6$TREN, which could then act as a reducing agent for L/Cu^{II}-Br and/or as an activator of alkyl halide initiator to generate initiating radicals in the dark. Similar observations were reported for using alkyl amine containing compounds such as PMDETA or 2-(dimethylamino)ethyl methacrylate as reducing agents.[57, 61]

Effect of concentration of the ligand and Cu catalyst on temporal control in photoinduced ATRP.

To investigate the effect of the excess of ligand relative to Cu loading, the concentration of Me$_6$TREN was systematically decreased to reduce the rate of regeneration of L/Cu^I activator, thus suppressing polymerization during the dark period. In the presence of 0.02 equiv. of CuBr$_2$, the amount of Me$_6$TREN was gradually reduced from 0.12 to 0.06 and to 0.04 equiv. (relative to initiator, which corresponds to 6, 3, and 2 times vs. CuBr$_2$), and tested through three on/off

cycles (each on/off period for 30 minutes; Table 7, entries 1-3). Upon decreasing the amount of Me$_6$TREN from 0.12 to 0.06 and to 0.04 equiv., the ratio of the apparent propagation rate constants in the light-off and on periods (k_{off}/k_{on}) for the first cycles gradually decreased from 0.18 to 0.08 to 0.07, respectively (Table 7, entries 1-3), indicating enhanced temporal control in the presence of low concentration of Me$_6$TREN. Importantly, polymerizations reached high monomer conversion (>90%) with number-average molecular weights (M_n) of 4200-5300, and low dispersities ($Đ \sim$ 1.08-1.11), suggesting well-controlled polymerizations under all conditions (Table 7, entries 1-3).

The effect of catalyst loading was then investigated by systematically reducing the concentration of CuBr$_2$ from 0.02 to 0.005 equiv. (with respect to initiator) while keeping the amount of Me$_6$TREN constant at 0.12 equiv. (Table 1, entries 1, 4, and 5). By decreasing the amount of CuBr$_2$ from 0.02 to 0.005 equiv., k_{off} decreased by a factor of ~2, from 18% to 10% of the respective k_{on} (Table 7, entries 1, 4, and 5), indicating improved temporal control. Polymerizations were well-controlled with high monomer conversions (93-95%) and low $Đ$ (1.08-1.27). Accordingly, the polymerization of MA was carried out with reduced concentrations of both CuBr$_2$ and Me$_6$TREN to synergistically achieve low k_{off}/k_{on} values. Polymerization with 0.005 equiv. of CuBr$_2$ and 0.015 equiv. of Me$_6$TREN (4 and 8 times less than the corresponding amounts used under standard conditions) showed excellent temporal control (k_{off}/k_{on} = 0.05 for the first cycle) while maintaining high monomer conversion (87%) and resulting in polymers with low $Đ$ = 1.16 (Table 7, entry 6). Further decreasing the concentration of Me$_6$TREN to 0.01 equiv. resulted in a similar enhancement of temporal control (k_{off}/k_{on} = 0.05 for the first cycle). However, the rate of polymerization decreased (75% conversion after 3 cycles), and the third cycle showed inferior response when irradiation is switched off. Additionally, the resulting polymer showed higher $Đ$ than the case of 0.015 equiv. of Me$_6$TREN (1.26 vs. 1.16; Table 7, entries 6 and 7, and Figure 25). These results indicated that polymerization can be efficiently controlled even with diminished concentrations of the catalyst. Decreasing the concentration of CuBr$_2$ and ligand decreased the equilibrium concentration of L/Cu^I, thereby resulted in enhanced temporal response.

Table 7. Reactivity and on/off control of polymerizations depending on the concentrations of CuBr$_2$ and Me$_6$TREN[a]

Entry	CuBr$_2$ (equiv.)	Me$_6$TREN (equiv.)	Conv. (%)	M_n	$Đ$	k_{off}/k_{on} 1st | 2nd | 3rd
1	0.02	0.12	94	5300	1.08	0.18 | 0.23 | 0.26
2	0.02	0.06	93	4400	1.10	0.08 | 0.09 | 0.08
3	0.02	0.04	91	4200	1.11	0.07 | 0.07 | 0.03
4	0.01	0.12	95	4100	1.15	0.11 | 0.19 | 0.23
5	0.005	0.12	93	3400	1.27	0.10 | 0.18 | 0.22
6	0.005	0.015	87	4100	1.16	0.05 | 0 | 0
7	0.005	0.010	75	3000	1.26	0.05 | 0.02 | 0.12

[a] Reactions were performed under in situ NMR monitoring. Molecular weight properties were obtained using SEC in chloroform with polystyrene standards.
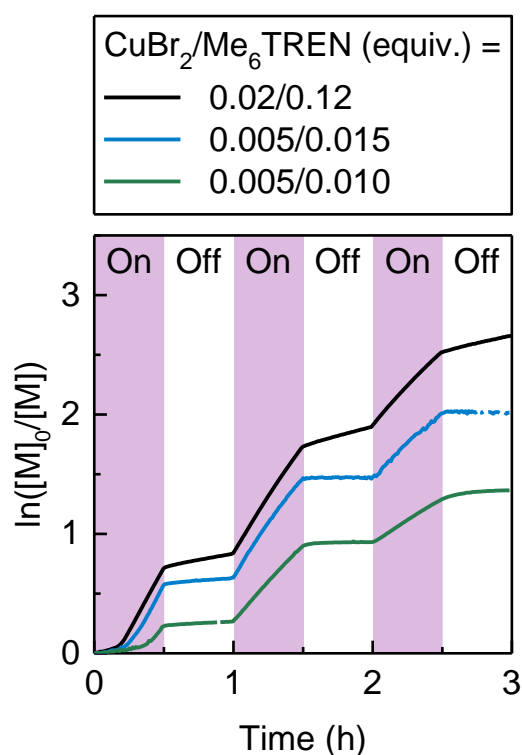
Figure 25. Effect of decreasing concentration of CuBr$_2$ and Me$_6$TREN in kinetics of temporal control in photoinduced ATRP of MA. Reaction conditions: [CuBr$_2$]/[Me$_6$TREN] = 0.02/0.12, 0.005/0.015, or 0.005/0.010 corresponding to Entries 1, 6, and 7 in Table 7, kinetics monitored by in situ NMR.

Effect of solvent on temporal control in photoinduced ATRP.

Based on the optimized reaction conditions in DMSO, two additional deuterated solvents including acetonitrile (CD_3CN) and methanol (MeOD), that show different reactivity in ATRP,[62] were chosen to study the effect of solvent using in situ NMR monitoring. Polymerizations were performed using $CuBr_2$ (0.01 equiv.) and Me_6TREN (0.06 equiv.). The k_{off}/k_{on} values for the first cycles were 0.04 and 0.11 in MeOD and CD_3CN, respectively, demonstrating good temporal control (Figure S2).

Reducing the concentration of $CuBr_2$ to 0.005 equiv. in the presence of 0.015 equiv. of Me_6TREN resulted in enhanced temporal control (k_{off}/k_{on} values down to 0.02 and 0.09 in MeOD and CD_3CN, respectively), without compromising control over the polymerization process (Figure 26). Thus, the stoichiometric adjustment of the catalytic system resulted in enhanced temporal regulation in both solvents, proving a general strategy to improve temporal control in photoinduced ATRP.
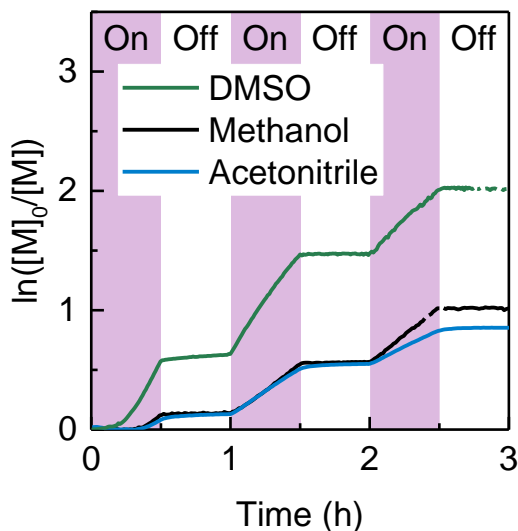
Figure 26. Temporal control of photoinduced ATRP in different solvents followed by in situ NMR monitoring using $CuBr_2$ (0.005 equiv.) and Me_6TREN (0.015 equiv.). k_{off}/k_{on} values of $1^{st}/2^{nd}/3^{rd}$ cycles are 0.02/0.03/0.02 in methanol or 0.09/0.04/0.04 in acetonitrile, respectively.

Similarly, under batch conditions, changing the solvent from DMSO to MeCN or DMF, resulted in limited chain growth in the dark with the rate of the polymerization decreasing over time and

eventually stopping (Figure 27). Re-exposing the solutions to light re-initiated the polymerizations with higher monomer conversions and well-controlled polymerizations being observed (Figure S3). Furthermore, control experiments performed in the dark with a target DP of 50 showed no polymerization in DMF after keeping the reaction in the dark for 90 h. In MeCN, a slow polymerization of MA was observed in the dark with ~ 57% monomer conversion obtained in 90 h, showing an induction period > 24 h. These results suggest that in the presence of tertiary amines as a reducing agent, progression of the polymerization is more pronounced in DMSO than MeCN or DMF due to the higher K_{ATRP} in DMSO.[63]
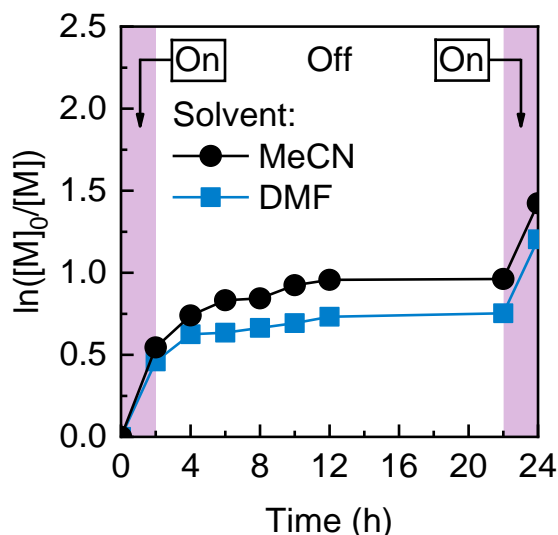
Figure 27. Temporal control in photoinduced ATRP of MA using MeCN and DMF as solvent. Reaction conditions: $[MA]/[EBiB]/[CuBr_2]/[Me_6TREN] = 50/1/0.02/0.12$ in 50 vol% solvent (MeCN or DMF, $[MA] = 5.5$ M), irradiated with violet LEDs ($\lambda_{max} = 394$ nm, 2.6 mW/cm^2), under batch conditions.

Effect of the activity of the Cu catalyst on temporal control in photoinduced ATRP.

The activity of the Cu catalyst in ATRP can also be tuned using different ligands, enabling a dynamic modulation of the molar ratio of the activator and deactivator species. Temporal control in the photoinduced ATRP of MA (target DP = 200) in the presence of 0.02 equiv. of CuBr$_2$ using Me$_6$TREN, TPMA and PMDETA ligands (0.12 equiv.) in DMSO was then examined under conventional batch conditions. Excellent temporal control was achieved in photoinduced

ATRP of MA using Me$_6$TREN as a ligand. As shown in Figure 28-A, temporal control was achieved upon intermittent light on/off periods for 20 min with low monomer conversion being observed during the dark periods. Importantly, no significant chain growth is apparent when the light was removed for a longer time period - 80 min (Figure 28-B). Re-exposing the solutions to light restarted the polymerizations in a controlled manner, yielding polymers with molecular weights in agreement with theoretical values and low dispersities ($Đ < 1.1$, Figure S4).

The higher ATRP activity of the Cu complex with Me$_6$TREN results in a larger ATRP equilibrium constant, K_{ATRP},[64] and increases the ratio of the concentration of L/Cu^{II}-Br deactivator to L/Cu^{I} activator under equilibrium. This higher value of K_{ATRP} results in a lower concentration of L/Cu^{I} during the polymerization.[65] Upon removal of the light, the low concentration of residual L/Cu^{I} was rapidly consumed by radical termination reactions, converting L/Cu^{I} to L/ Cu^{II}-Br and therefore stopping the polymerization.

In contrast, when using TPMA as the ligand in DMSO, the polymerization responded slowly to switching the light off leading to poor temporal control. Figure 28-C shows that the polymerization continued in dark periods with similar rates as under light irradiation. However, as shown in Figure 28-D, when the reaction was kept in the dark for 4 h, chain growth was observed only in the first hour and subsequently the polymerization rate decreased. Re-exposing the solution to light restarted the polymerization in a controlled way (Figures S5 and S6). From these studies it can be concluded that the Cu catalyst with TPMA ligand is less active compared to Me$_6$TREN, therefore the equilibrium concentration of L/Cu^{I} with TPMA was higher, resulting in chain growth during dark periods.
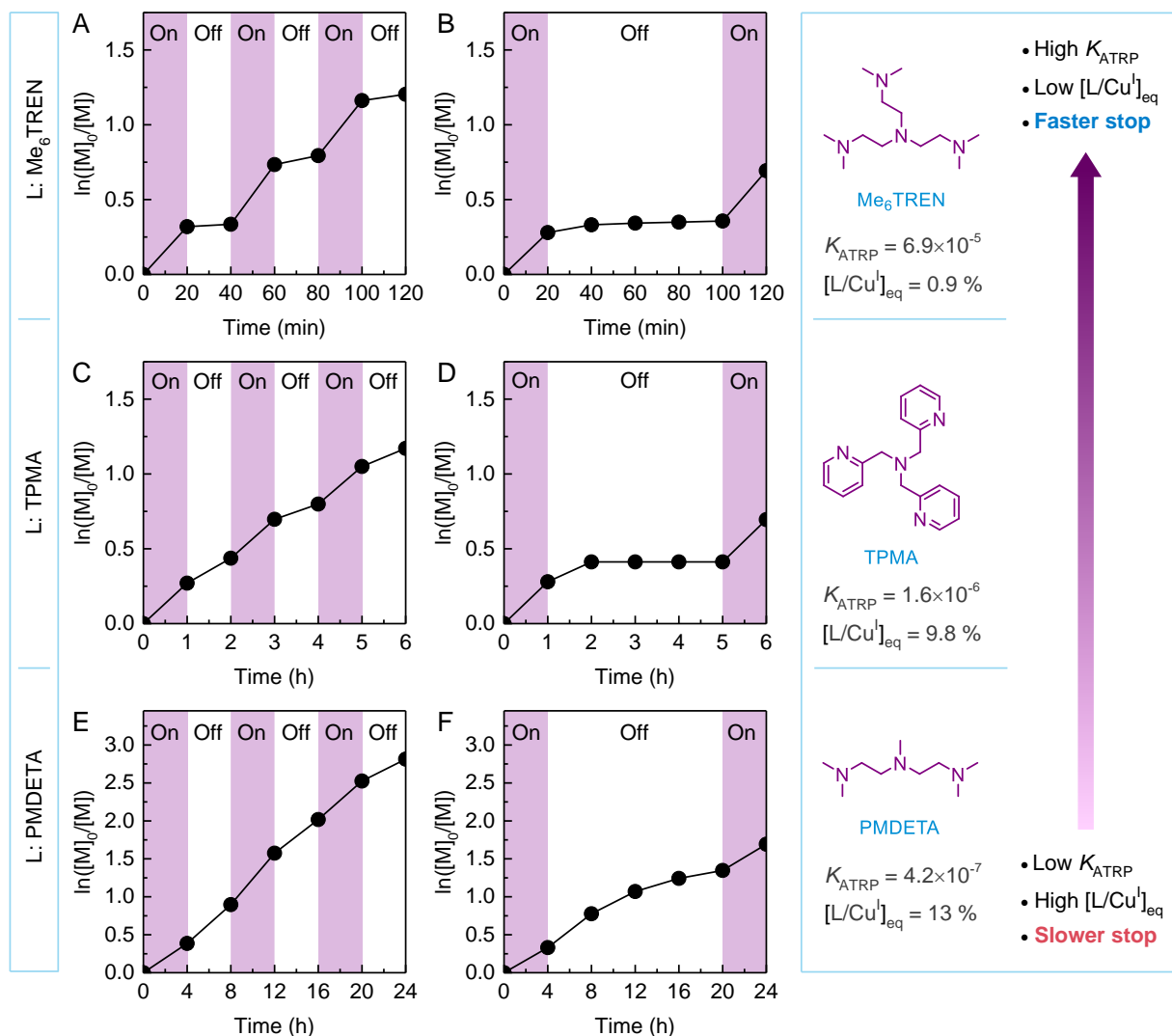
Figure 28. Temporal control in photoinduced ATRP of MA using Me$_6$TREN (A, B), TPMA (C, D), and PMDETA (E, F) ligands demonstrating dependency on the activity of the Cu catalyst as a result of the nature of the ligand. Reaction conditions: [MA]/[EBiB]/[CuBr$_2$]/[L] = 200/1/0.02/0.12 (for TPMA, L = 0.02, triethylamine = 0.4 equiv.) in 50 vol% DMSO ([MA] = 5.5 M). Irradiated with violet LEDs (λ_{max} = 394 nm, 2.6 mW/cm^2) under batch conditions.

Significant chain growth was observed in dark periods when PMDETA was used as the ligand. As presented in Figure 28-E, polymerization with PMDETA showed essentially no response to switching the light off, and a linear kinetics behavior was obtained regardless of the light being on or off. Moreover, significant monomer conversion was observed even when the reaction was kept in the dark for longer periods (Figure 28-F). The polymerization was started by irradiating

the solution with violet LEDs, yielding 27% monomer conversion within 4 h. Afterward, the solution was kept in the dark for 16 h. Interestingly, the polymerization continued during this period reaching 82% monomer conversion. A decrease in the polymerization rate was observed only toward the end of the dark period (Figure 28-F). Importantly, these polymerizations undergoing significant chain growth in the dark were still well-controlled, giving polymers with molecular weights in agreement with theoretical values and low *Đ* of 1.10 (Figures S7 and S8). Analysis of these results show that PMDETA forms a Cu complex with a lower catalytic activity compared to both TPMA and Me$_6$TREN,[65] resulting in a lower rate of polymerization and hence lower concentration of radicals. In addition, the low activity of the catalyst determined a relatively high concentration of L/Cu^I, and therefore, the polymerization continued to high monomer conversions without the need for light-induced activator (re)generation.

Consuming the L/Cu^I catalyst via external stimuli would improve temporal control in the presence of PMDETA ligand. Oxygen was successfully used as an oxidizer to switch the Cu catalyst off and achieve temporal control with PMDETA. The polymerization was started upon light irradiation, giving 22% monomer conversion in 4 h. The light was then switched off, and the solution was bubbled with air for 1 min. The Cu catalyst was switched off upon oxidation with oxygen, and no polymerization was observed in the subsequent dark period. Re-exposing the solution to light restarted the polymerization with the monomer conversion reaching 35% within 4 h (Figure 29). The polymerization then reached high monomer conversion under continuous light irradiation (final conversion = 93%) with SEC analysis revealing narrow, symmetric distribution of molecular weights and low *Đ* (M_n = 15 800, $M_{n,th}$ = 16 200, *Đ* = 1.11), all in agreement with theoretical values and a well-controlled process. This result confirms that excellent temporal control in ATRP can be achieved even in low-activity catalytic systems by applying dual stimuli to switch the polymerization off by oxidation of L/Cu^I. Importantly, introduction of oxygen as an oxidizing agent did not result in loss of control over the polymerization, indicating the tolerance of this system to the presence of small amounts of oxygen due to a very fast reaction of oxygen with L/Cu^I, which is present at a much higher concentration than the radical chain end of the growing polymer chains.
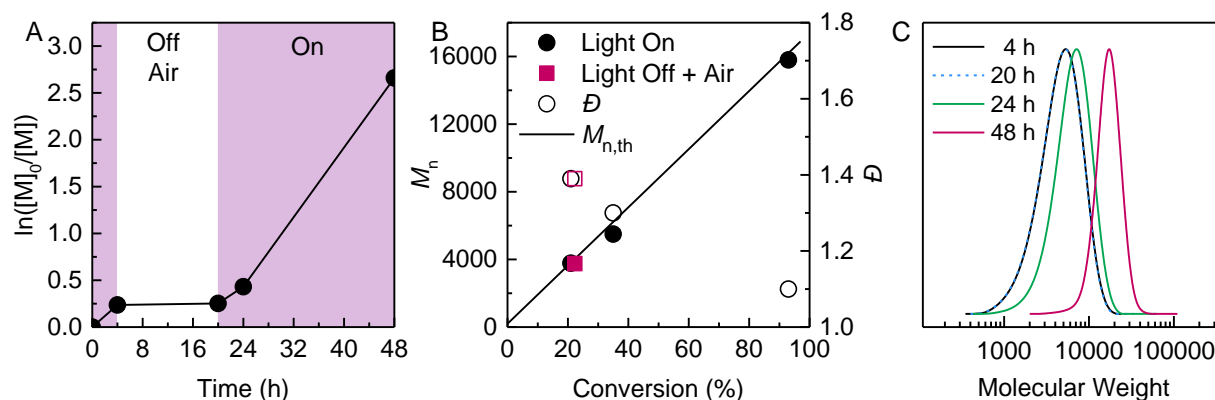
Figure 29. Temporal control in photoinduced ATRP of MA using oxygen as an oxidizing stimulus to stop the polymerization in the dark in the presence of PMDETA. Reaction conditions: [MA]/[EBiB]/[CuBr$_2$]/[PMDETA] = 200/1/0.02/0.12 in 50 vol% DMSO ([MA] = 5.5 M). Irradiation with violet LED's (λ_{max} = 394 nm, 2.6 mW/cm^2) under batch conditions.

Electrochemical analysis of the Cu catalysts used in temporal control.

The concentration of L/Cu^I present at the end of the first light-on period was estimated according to Equation 1. Assuming steady-state conditions, the relative ratio of [L/Cu^I]/[L/Cu^{II}-Br] can be expressed as:

$$\frac{[L/Cu^I]}{[L/Cu^{II} - Br]} = \left(\frac{1}{K_{ATRP}}\right)\left(\frac{[R^\bullet]}{[R - Br]}\right) \qquad \text{Equation 1}$$

In well-controlled radical polymerizations, only a small fraction of chains undergoes radical termination, therefore [R−X] can be assumed equal to its initial concentration, [R−X]$_0$, while [R$^\bullet$] can be calculated from the slope of the semilogarithmic kinetics plot as [R$^\bullet$] = slope/k_p, where k_p is the propagation rate constant. Table 8 shows the values of K_{ATRP}, the rate constants of activation (k_{act}) and deactivation (k_{deact}), and the concentration of radicals and L/Cu^I for the three ligands studied in temporal control experiments. The values of K_{ATRP} and k_{act} in the MA/DMSO mixture were determined by chronoamperometry on a rotating disk electrode, according to previously reported procedures.[56, 66] The k_{deact} values were calculated as k_{act}/K_{ATRP}.

The values presented in Table 7 show that by decreasing the activity of the Cu catalyst and hence the K_{ATRP} value, the concentration of L/Cu^I increases. For example, for Me$_6$TREN as a ligand, ~0.9% of the total catalyst was calculated to be in the L/Cu^I form, whereas for TPMA this value was ~9.8%, and ~13% for PMDETA.

Table 8. Thermodynamic and kinetic parameters of ATRP for various Cu catalysts measured by rotating disk electrode (RDE)[a]

Ligand	$E^{\ominus}_{(L/Cu^{II}-Br)/(L/Cu^I)}$ (V vs. SCE)	K_{ATRP}	k_{act} (M^{-1} s^{-1}) [b]	k_{deact} (M^{-1} s^{-1})	[R$^{\bullet}$] (M)	[L/Cu^I] (mM)	[L/Cu^I] (%)
Me$_6$TREN	-0.297	6.9×10^{-5}	3.8×10^3	5.6×10^7	1.70×10^{-8}	0.0048	0.9
TPMA	-0.159	1.6×10^{-6}	60	3.8×10^7	4.81×10^{-9}	0.0541	9.8
PMDETA	-0.113	4.2×10^{-7}	1.6	3.8×10^6	1.71×10^{-9}	0.0710	13

[a] Conditions: 0.1 M Et$_4$NBF$_4$, T = 25 °C in MA/DMSO (1/1). For determination of K_{ATRP}: [L/Cu^I] = 0.5 mM, [MBP] = 50 mM (for L = Me$_6$TREN, [MBP] = 25 mM), RDE rotation = 2500 rpm. [b] For determination of k_{act}: [L/Cu^I] = 0.5 mM, [MBP] = 0.5 mM (for L = PMDETA, [MBP] = 10 mM), [TEMPO] = 50 mM, RDE rotation = 4000 rpm, k_p = 1.5×10^4 (M^{-1} s^{-1}).[61] MBP: Methyl 2-bromopropionate.

As radical termination reactions consume the L/Cu^I activator to form the L/Cu^{II}-Br deactivator, according to the persistent radical effect, in the absence of light, or any other activator (re)generator, the consumption of the activator by terminations leads the polymerization to slow down and ultimately stop.[67] Considering the concentration of L/Cu^I activators in Table 8, the extent of radical termination needed to consume all L/Cu^I was estimated for the different catalysts. For example, in the presence of Me$_6$TREN, 0.88% of the total Cu catalyst was calculated to be present as L/Cu^I. With the initial concentration of the catalyst being 2 mol% of [RX]$_0$, termination of only 0.017% of chains would lead to the consumption of all residual L/Cu^I. Similarly, in the presence of TPMA and PMDETA ligands, all residual L/Cu^I could be consumed upon termination of 0.19% and 0.25% of the total chains, respectively. These results agree with the experimental observation that highly active catalysts show a quicker response to switching the light off, therefore offering better temporal control, because less termination was required to consume L/Cu^I. Importantly, in each case the chains terminating during the dark periods were a tiny fraction of the living chains.

In the ATRP of acrylate monomers, radical termination reactions can occur through different pathways including conventional radical termination and catalyzed radical termination (CRT) reactions.[66, 68] As presented in Figure 30-A (pink lines), conventional radical termination involves a bimolecular reaction of radicals consuming one molecule of L/Cu^I activator per each terminating radical. In addition, radicals can terminate through the CRT mechanism (blue lines, Figure 30-A). CRT involves the reaction of L/Cu^I with a propagating radical to form an organometallic intermediate, $L/P_n\text{-}Cu^{II}$. Although the exact mechanism of CRT is still under investigation, it has been proposed that the interaction between a propagating chain and the paramagnetic organometallic species leads to terminated chains and regeneration of L/Cu^I.[60] In the overall mass balance of ATRP and CRT, one molecule of L/Cu^I is consumed per each terminating radical.
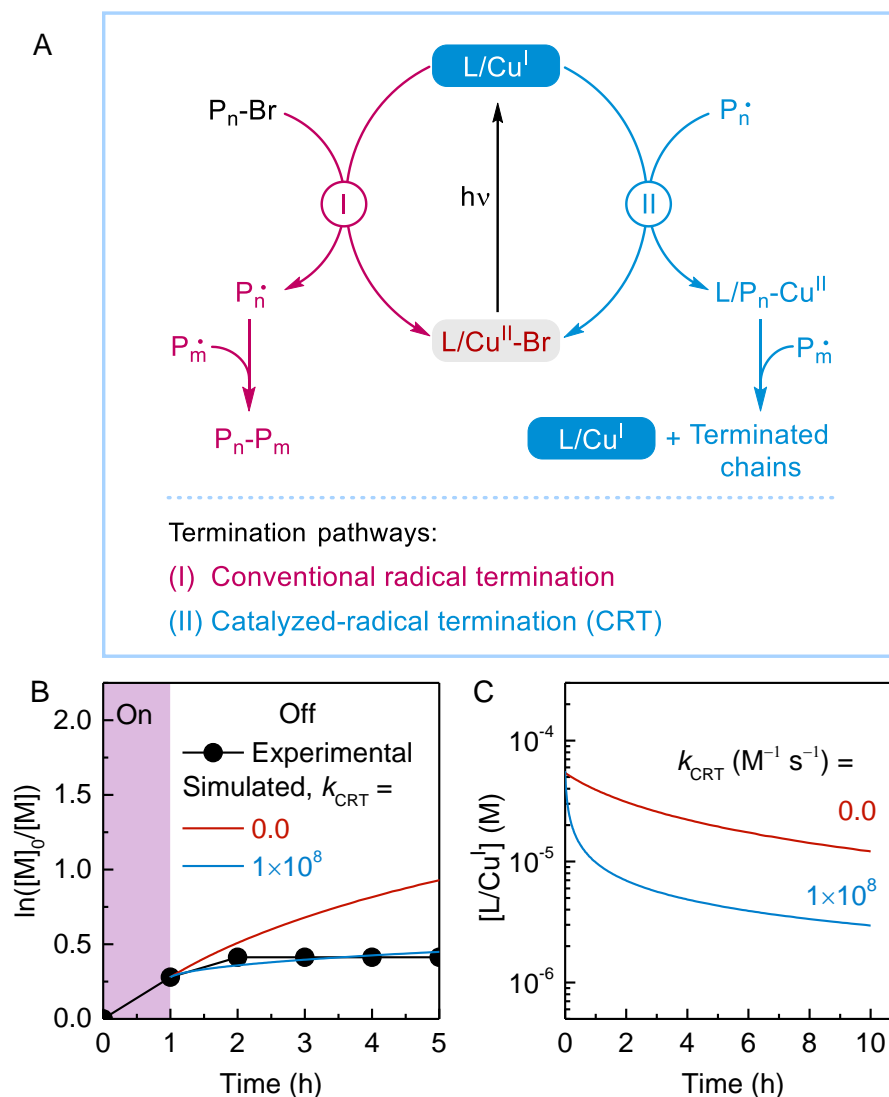
Figure 30. (A) Termination of radicals in ATRP: (I) Pink lines represent conventional radical termination and (II) blue lines represent catalyzed-radical termination (CRT). For each radical terminated, one molecule of L/Cu$^{\mathrm{I}}$ is converted to L/Cu$^{\mathrm{II}}$-Br. (B) Overlay of experimental (shown in black) and simulated kinetics results in the dark periods for the polymerization with L = TPMA, considering only bimolecular radical termination (shown in red) or bimolecular radical termination and CRT (shown in blue). (C) Evolution of [L/Cu$^{\mathrm{I}}$] where L = TPMA in the dark (no activator regeneration) as simulated by PREDICI considering only bimolecular radical termination (shown in red) or bimolecular radical termination and CRT (in blue). Initial reaction conditions: [MA]/[EBiB]/[CuBr$_2$]/[TPMA] = 200/1/0.02/0.12 in 50 vol% DMSO ([MA] = 5.5 M).

Simulations using PREDICI software[69] were therefore performed to quantify the behavior of the polymerization systems in the dark, when no activator (re)generation occurs. In addition, simulations were based on TPMA as the ligand due to the available data on the formation of TPMA/P_n-Cu^{II} intermediates,[57] according to the model shown in Scheme S1. Interestingly, simulations involving only the conventional radical termination pathway showed a slow consumption of TPMA/Cu^{I} resulting in increasing monomer conversion in the dark (Figure 30-B, blue line). However, a more accurate agreement with experimental data was obtained when including both conventional radical termination and CRT pathways in the simulations. CRT promoted a more rapid consumption of L/Cu^{I}, thus favoring a faster decrease in the rate of polymerization. The best agreement between experimental and simulated data was obtained with a rate constant of CRT $k_{CRT} = 10^8$ M^{-1} s^{-1}. This value is higher than recently measured for the Cu/TPMA system in dry DMSO,[70] suggesting additional termination pathways can contribute in this polymerization system, arising from the presence of residual water or other impurities.[71]

2.3.4 Conclusions

Temporal control in photoinduced ATRP processes was investigated to understand the fundamental behavior of ATRP systems in the dark. Conditions were identified for improved temporal control over photoinduced ATRP by studying the effect of reaction components including catalyst, ligand, and solvent. The activity of the catalyst regulates the molar ratio between L/Cu^{I} activator and L/Cu^{II}-Br deactivator, resulting in a decrease in the concentration of L/Cu^{I} as the activity of the catalyst increases. These design parameters allowed excellent temporal control was achieved with Me$_6$TREN, which forms a highly active Cu catalyst, whereas chain growth in the dark was observed in the presence of TPMA or PMDETA ligands. It is noted that these catalyst systems with lower activity compared to Me$_6$TREN. The results of temporal control in photoinduced ATRP illustrate the importance of tuning the activity of the Cu catalyst by modifying the concentration and nature of the ligand and the reaction medium to achieve enhanced temporal control in Cu-catalyzed ATRP. The findings of this work provide a general guideline for understanding how Cu-based catalytic systems behave in externally controlled ATRP and designing better catalysts for gaining efficient temporal control over polymerizations.

2.3.5 Experimental Section and Supporting Information

Materials

Methyl acrylate (MA; Sigma-Aldrich, 99%) was passed through a basic alumina column to remove polymerization inhibitor prior to use. Ethyl α-bromoisobutyrate (EBiB; Sigma-Aldrich, 98%), tris(2-pyridylmethyl)amine (TPMA; AmBeed), N,N,N',N'',N''-pentamethyldiethylenetriamine (PMDETA; Sigma-Aldrich, 98%), triethylamine (TEA), dimethyl sulfoxide (DMSO), N,N-dimethylformamide (DMF), and 2,2,6,6-tetramethyl-1-piperidinyloxy (TEMPO; TCI Chemicals, 98%) were used as received. Tris[2-(dimethylamino)ethyl]amine (Me$_6$TREN) was received from Koei Chemical Co., Ltd. (Japan). Tetraethylammonium tetrafluoroborate (Et$_4$NBF$_4$; Alfa Aesar, 99%), used as supporting electrolyte for electrochemical measurements, was recrystallized from ethanol and dried in a vacuum oven at 70 °C for 24 h. A stock solution of Cu^I was prepared in anhydrous CH$_3$CN (Sigma-Aldrich, 98%) by comproportionation between copper(II) trifluoromethanesulfonate (Cu^{II}(OTf)$_2$; Alfa Aesar, 99%) and a Cu wire, previously activated by washing in MeOH/HCl (3/1 vol) and rinsed with water and acetone. The exact concentration of Cu^I(OTf) was determined by spectrophotometric titration, using 2,9-dimethyl-1,10-phenanthroline as a specific ligand ($\varepsilon = 8458$ M^{-1} cm^{-1}) in a 3-fold excess with respect to the metal.

Instrumentation

^{1}H nuclear magnetic resonance (^{1}H NMR) measurements were performed on a Bruker Avance™ III 500 MHz spectrometer. Molecular weight properties of the polymers were determined by size-exclusion chromatography (SEC). The SEC instrument used a Waters 515 pump and a Waters 2414 differential refractometer using PSS columns (SDV 10^5, 10^3, and 500 Å) with THF as eluent at 35 °C and a flow rate of 1 mL min^{-1}. Linear poly(methyl methacrylate) standards were used for calibration.

The electrochemical measurements of ATRP parameters were conducted in a 6-neck electrochemical cell, connected to an Autolab PGSTAT100N potentiostat/galvanostat, run by a PC with NOVA 2.1 software (Metrohm USA). The cell was equipped with a three-electrode system. The counter electrode was a Platinum foil, the reference electrode was an home-made an Ag|AgI|(0.1 M n-Bu$_4$NI in DMF), whereas the working electrode was a glassy carbon tip (Metrohm, 3 mm dia.). The latter was cleaned before each experiment with a 0.25 mm diamond paste and ultrasonically rinsed with ethanol for 5 min. The ferrocenium/ferrocene redox couple

was used as internal standard to convert all potentials to the aqueous saturated calomel electrode (SCE).

General procedure for temporal control in photoinduced ATRP of MA via in situ NMR monitoring

To a 1-dram glass vial equipped with stir bar, $CuBr_2$ (1 mg, 0.0044 mmol, 0.02 equiv.), Me_6TREN (7 µL, 0.027 mmol, 0.12 equiv.) and DMSO-d_6 (2 ml) were added sequentially. MA was placed in another 1-dram glass vial. The vials were then degassed by purging with argon for 10 minutes. Under argon atmosphere, MA (1 mL, 11.1 mmol, 50 equiv.) was taken and added to the vial containing other reagents. Lastly, EBiB (33 µL, 0.22 mmol, 1 equiv.) was added to the vial, using a stock solution. The 0.35-0.40 mL of reaction mixture was then transferred to an NMR tube under argon atmosphere in the dark. The optical fiber and teflon insert were placed into the NMR tube such that the fiber was ca. 2 mm above the solution. All NMR measurements were performed as an array and a LabVIEW program connected to a T-cube LED driver was used to automate 'on'/'off' times of a 405 nm LED.

General procedure for temporal control in photoinduced ATRP of MA under batch conditions

A 20-mL vial equipped with a stir bar was sealed with a rubber septum, and subjected to vacuum and backfilled with nitrogen for 5 times. DMSO and MA were degassed with nitrogen in separate vials for at least 45 min. DMSO (5 mL), MA (5 mL, 55.5 mmol, 200 equiv.), $CuBr_2$ (1.24 mg, 5.55 µmol, 0.02 equiv.), Me_6TREN (9 µL, 33.3 µmol, 0.12 equiv.), and EBiB (40 µL, 0.27 mmol, 1 equiv.) were added into the vial under nitrogen. The vial was degassed with nitrogen for 2 min more and was irradiated under violet LEDs to start the polymerization. Samples were taken periodically for ^1H NMR and SEC analyses.

General procedure for determination of K_{ATRP} and k_{act} by rotating disk electrode:

The three electrodes and a magnetic stirring bar were put in the electrochemical cell. Et_4NBF_4 supporting electrolyte (0.326 g, 0.1 M) and 15 mL of DMSO/MA 1/1 mixture were inserted into

the cell. Then, the desired amount of ligand was added. TEMPO was also added in the experiments for determining the rate constant of ATRP activation, k_{act}. After degassing the solution for ca. 15 min, cyclic voltammetry (CV) was run to check for impurities and verify the absence of oxygen. The RDE rotation was set at 2500 rpm for the determination of the equilibrium constant K_{ATRP}, or 4000 rpm for measuring k_{act}. A constant potential, E_{app}, was applied, and the resulting current was recorded. E_{app} values were selected such as to follow the oxidation of L/Cu^I under mass transfer control in a potential range where no other process occurred. The required amount of Cu^I was withdrawn with a syringe from the stock solution, under inert atmosphere, and injected into the cell. The initiator was injected into the cell a few seconds after injecting Cu^I. After the measurements, a CV was recorded to verify the presence of L/Br-Cu^{II} complexes and determining their reduction potentials. A 50-fold excess of initiator relative to Cu^I was typically used for determination of K_{ATRP}. For determination of k_{act} with PMDETA as a ligand, a 10-fold excess of initiator was used due to the lower activity of the catalyst. Moreover, when PMDETA was used as a ligand, the initiator was injected before Cu^I to avoid any issues due to the complexation of L/Cu^I by MA.[72] The values of K_{ATRP} and k_{act} were obtained from the decay of the current with time, according to previous reports.[72, 73]

Polymerization results:
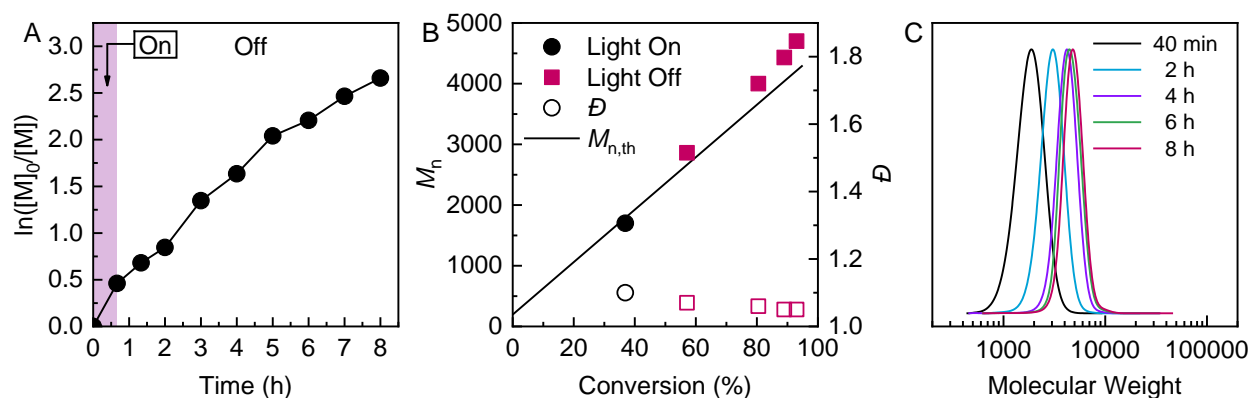
Figure 31. Temporal control in photoATRP of MA under violet LEDs. Reaction conditions: $[MA]/[EBiB]/[CuBr_2]/[Me6TREN] = 50/1/0.02/0.12$ in 50 vol% DMSO ($[MA]$ = 5.5 M), irradiated under violet LEDs (λ_{max} = 394 nm, 2.6 mW/cm^2) for 40 min. (A) Kinetics of the polymerization, (B) number-average molecular weight (M_n, solid points) and dispersity ($Đ$, open points) as a function of monomer conversion. (C) SEC traces. Obtained under batch conditions.
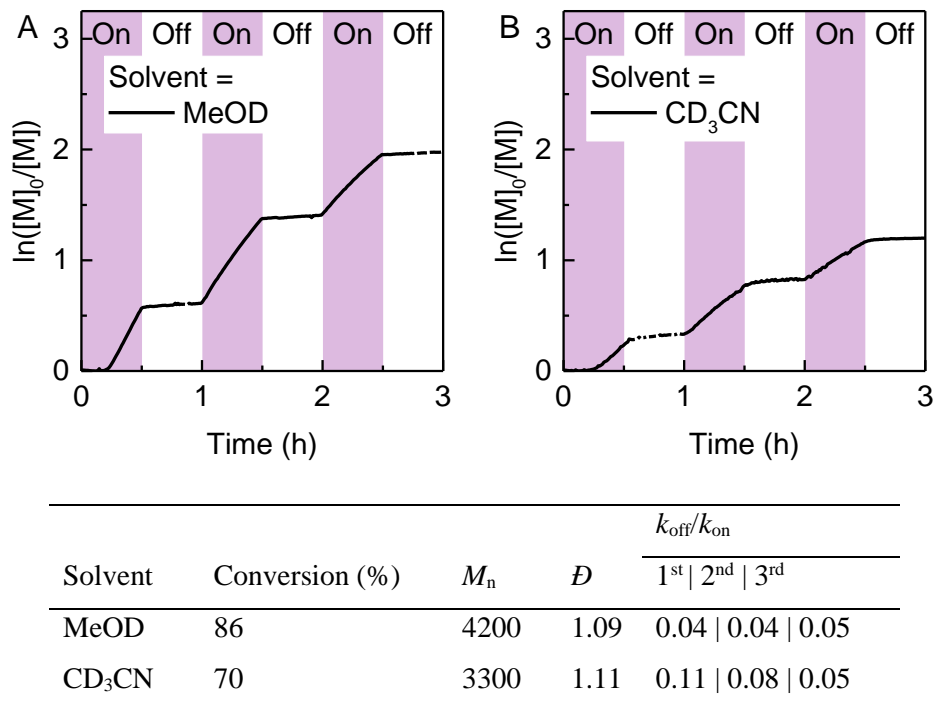
Figure 32. Temporal control achieved in (a) MeOD and (b) CD_3CN. Reaction conditions: $[MA]/[EBiB]/[CuBr_2]/[Me_6TREN] = 50/1/0.01/0.06$. Obtained via in situ NMR monitoring.

Solvent	Conversion (%)	M_n	Đ	k_{off}/k_{on} 1st | 2nd | 3rd
MeOD	86	4200	1.09	0.04 | 0.04 | 0.05
CD_3CN	70	3300	1.11	0.11 | 0.08 | 0.05
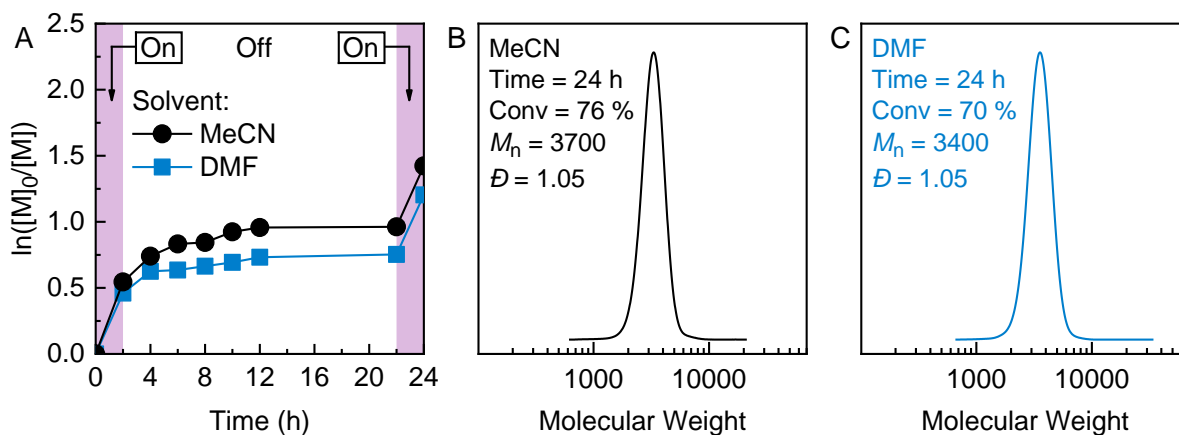
Figure 33. Results of temporal control experiments performed in MeCN of DMF. Reaction conditions: $[MA]/[EBiB]/[CuBr_2]/[Me_6TREN] = 50/1/0.02/0.12$ in 50 vol% solvent (MeCN or DMF, $[MA] = 5.5$ M), irradiated under violet LEDs ($\lambda_{max} = 394$ nm, 2.6 mW/cm^2). Obtained under batch conditions.
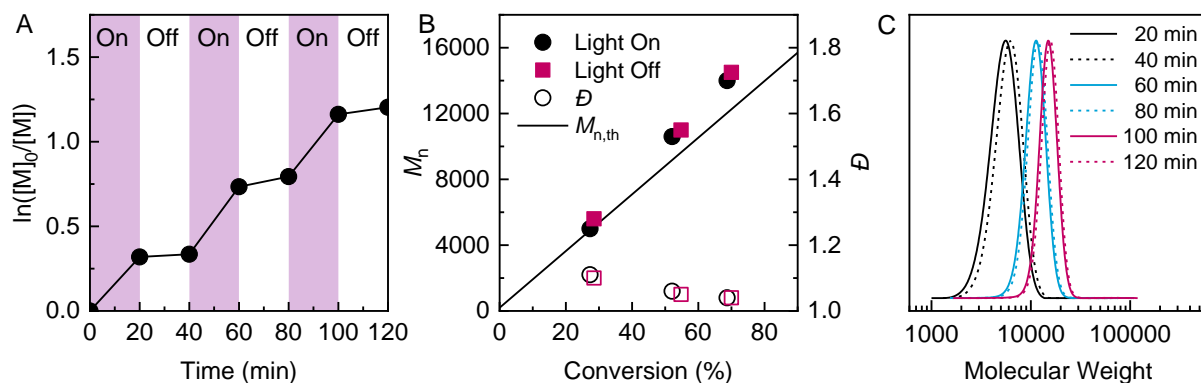
Figure 34. Temporal control in photoATRP of MA under violet LEDs. Reaction conditions: [MA]/[EBiB]/[CuBr$_2$]/[Me$_6$TREN] = 200/1/0.02/0.12 in 50 vol% DMSO ([MA] = 5.5 M), irradiated under violet LEDs (λ_{max} = 394 nm, 2.6 mW/cm^2). (A) Kinetics of the polymerization, (B) number-average molecular weight (M_n, solid points) and dispersity ($Đ$, open points) as a function of monomer conversion. (C) SEC traces; solid lines correspond for light on and dashed lines correspond for light off periods. Obtained under batch conditions.
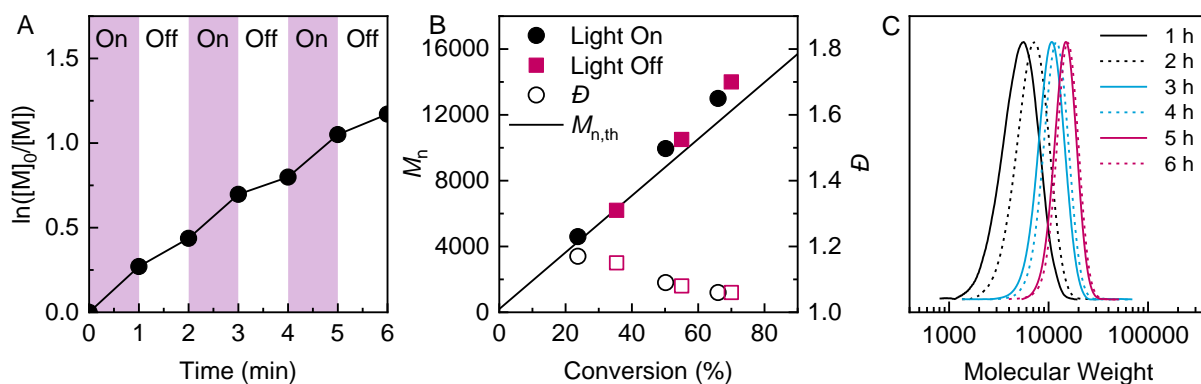
Figure 35. Temporal control in photoATRP of MA using TPMA. Reaction conditions: [MA]/[EBiB]/[CuBr$_2$]/[TPMA]/[TEA] = 200/1/0.02/0.02/0.4 in 50 vol% DMSO ([MA] = 5.5 M), irradiated under violet LEDs (λ_{max} = 394 nm, 2.6 mW/cm^2). (A) Kinetics of the polymerization, (B) number-average molecular weight (M_n, solid points) and dispersity ($Đ$, open points) as a function of monomer conversion. (C) SEC traces; solid lines correspond for light on and dashed lines correspond for light off periods. Obtained under batch conditions.
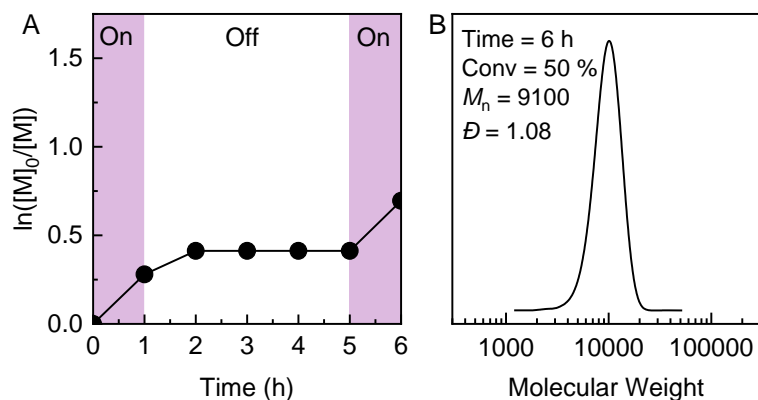
Figure 36. Temporal control in photoATRP of MA using TPMA. Reaction conditions: [MA]/[EBiB]/[CuBr$_2$]/[TPMA]/[TEA] = 200/1/0.02/0.02/0.4 in 50 vol% DMSO ([MA] = 5.5 M), irradiated under violet LEDs (λ_{max} = 394 nm, 2.6 mW/cm^2). (A) Kinetics of the polymerization and (B) SEC traces. Obtained under batch conditions.
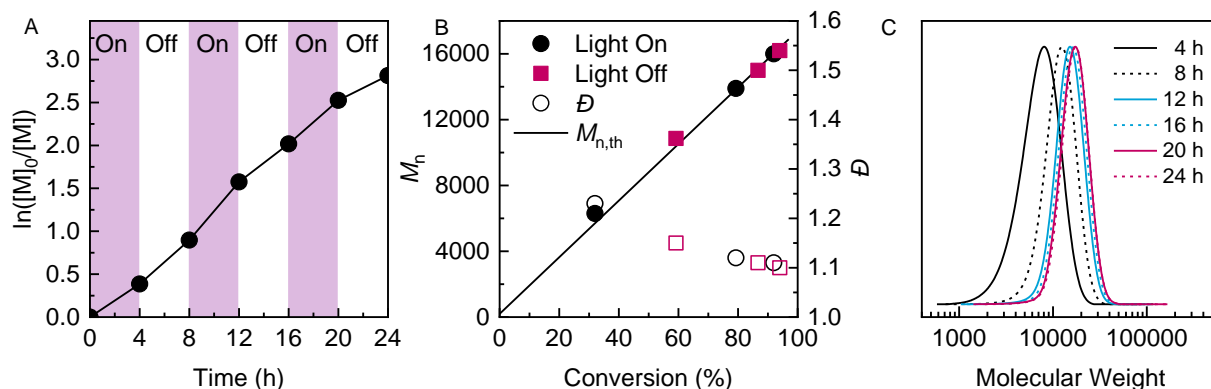
Figure 37. Temporal control in photoATRP of MA using PMDETA. Reaction conditions: [MA]/[EBiB]/[CuBr$_2$]/[PMDETA] = 200/1/0.02/0.12 in 50 vol% DMSO ([MA] = 5.5 M), irradiated under violet LEDs (λ_{max} = 394 nm, 2.6 mW/cm^2). (A) Kinetics of the polymerization, (B) number-average molecular weight (M_n, solid points) and dispersity ($Đ$, open points) as a function of monomer conversion. (C) SEC traces; solid lines correspond for light on and dashed lines correspond for light off periods. Obtained under batch conditions.

107
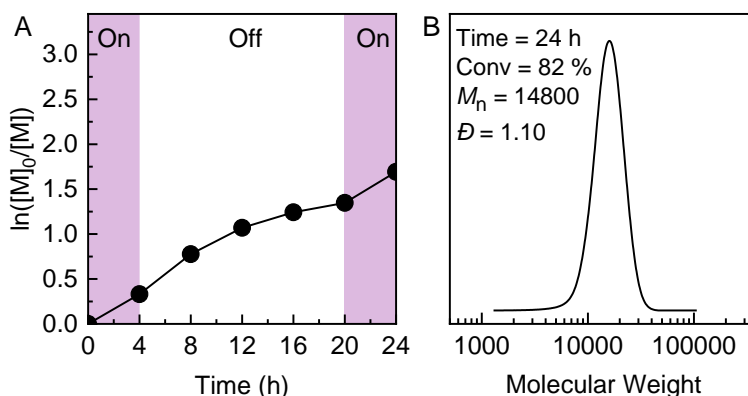
Figure 38. Temporal control in photoATRP of MA using PMDETA. Reaction conditions: [MA]/[EBiB]/[CuBr$_2$]/[PMDETA] = 200/1/0.02/0.12 in 50 vol% DMSO, irradiated under violet LEDs (λ_{max} = 394 nm, 2.6 mW/cm^2). (A) Kinetics of the polymerization and (B) SEC traces. Obtained under batch conditions.

PREDICI simulations:

Simulations using PREDICI software were conducted to simulate how polymerization would behave in temporal control experiments upon removal of light. The model is presented in Scheme S1, and the rate constant values for the reactions below were adopted from literature reports[66, 67, 74] or measured in this work.

	Reactions	Rate constants	Reference
Activation:	P$_n$-Br + L/Cu^I $\xrightarrow{k_{act}}$ P$_n^\bullet$ + L/Br-Cu^{II}	k_{act} = 60 M^{-1} s^{-1}	This work
Deactivation:	P$_n^\bullet$ + L/Br-Cu^{II} $\xrightarrow{k_{deact}}$ P$_n$-Br + L/Cu^I	k_{deact} = 3.8 × 10^7 M^{-1} s^{-1}	This work
Propagation:	P$_n^\bullet$ + M $\xrightarrow{k_p}$ P$_{n+1}^\bullet$	k_p = 1.5 × 10^4 M^{-1} s^{-1}	Ref. 4
OMRP eq.:	P$_n^\bullet$ + L/Cu^I $\underset{k_{diss}}{\overset{k_{ass}}{\rightleftharpoons}}$ P$_n$-L/Cu^{II}	k_{ass} = 5.8 × 10^8 M^{-1} s^{-1} k_{diss} = 6.4 × 10^2 s^{-1}	Ref. 5
CRT:	P$_m^\bullet$ + P$_n$-L/Cu^{II} $\xrightarrow{k_{CRT}}$ P$_{dead}$ + L/Cu^I	k_{CRT} = 1.0 × 10^8 M^{-1} s^{-1}	This work
Radical term:	P$_n^\bullet$ + P$_m^\bullet$ $\xrightarrow{k_t}$ P$_n$-P$_m$	k_t = 2.4 × 10^8 M^{-1} s^{-1}	Ref. 6

108

Scheme 8. PREDICI model for simulating ATRP in the dark in the presence of TPMA ligand. The values of k_{act} and k_{deact} were measured by electrochemistry as explained above, k_{CRT} value was estimated to fit the experimental data.
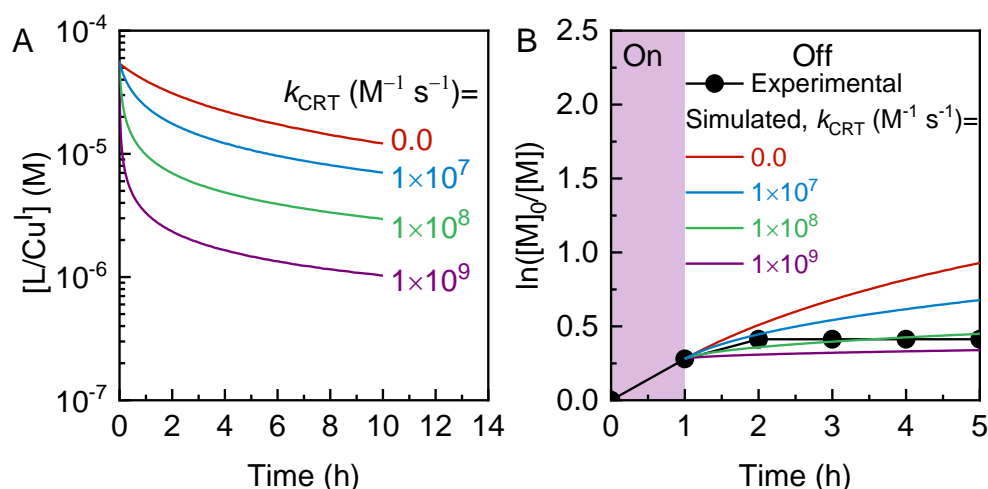
Figure 39. Results of PREDICI simulations. (A) Evolution of $[L/Cu^I]$ where L = TPMA in the dark (no activator regeneration) as simulated by PREDICI considering only bimolecular radical termination (shown in red) or bimolecular radical termination and CRT (shown in blue, green, or purple). (B) Overlay of experimental (shown in black) and simulated kinetics results in the dark periods considering only bimolecular radical termination (shown in red) or bimolecular radical termination and CRT (shown in blue, green, or purple). Initial reaction conditions: [MA]/[EBiB]/[CuBr$_2$]/[TPMA] = 200/1/0.02/0.12 in 50 vol% DMSO.

2.3.6   References

1. Blanco, V.; Leigh, D. A.; Marcos, V. Artificial switchable catalysts. *Chem. Soc. Rev.* **2015,** 44 (15), 5341-5370.

2. Schröder, K.; Mathers, R. T.; Buback, J.; Konkolewicz, D.; Magenau, A. J. D.; Matyjaszewski, K. Substituted Tris(2-pyridylmethyl)amine Ligands for Highly Active ATRP Catalysts. *ACS Macro Lett.* **2012,** 1 (8), 1037-1040.

3. Ribelli, T. G.; Fantin, M.; Daran, J.-C.; Augustine, K. F.; Poli, R.; Matyjaszewski, K. Synthesis and Characterization of the Most Active Copper ATRP Catalyst Based on Tris[(4-dimethylaminopyridyl)methyl]amine. *J. Am. Chem. Soc.* **2018,** 140 (4), 1525-1534.

4. Leibfarth, F. A.; Mattson, K. M.; Fors, B. P.; Collins, H. A.; Hawker, C. J. External Regulation of Controlled Polymerizations. *Angew. Chem. Int. Ed.* **2013,** 52 (1), 199-210.

5. Teator, A. J.; Lastovickova, D. N.; Bielawski, C. W. Switchable Polymerization Catalysts. *Chem. Rev.* **2016,** 116 (4), 1969-1992.

6. Pan, X.; Fantin, M.; Yuan, F.; Matyjaszewski, K. Externally controlled atom transfer radical polymerization. *Chem. Soc. Rev.* **2018,** 47 (14), 5457-5490.

7. Stephenson, C.; Yoon, T.; MacMillan, D. W. C., *Visible Light Photocatalysis in Organic Chemistry*. Wiley‑VCH: 2018.

8. Chen, M.; Zhong, M.; Johnson, J. A. Light-Controlled Radical Polymerization: Mechanisms, Methods, and Applications. *Chem. Rev.* **2016,** 116 (17), 10167-10211.

9. Dadashi-Silab, S.; Doran, S.; Yagci, Y. Photoinduced Electron Transfer Reactions for Macromolecular Syntheses. *Chem. Rev.* **2016,** 116 (17), 10212-10275.

10. Pan, X.; Tasdelen, M. A.; Laun, J.; Junkers, T.; Yagci, Y.; Matyjaszewski, K. Photomediated controlled radical polymerization. *Prog. Polym. Sci.* **2016,** 62, 73-125.

11. Discekici, E. H.; Anastasaki, A.; Read de Alaniz, J.; Hawker, C. J. Evolution and Future Directions of Metal-Free Atom Transfer Radical Polymerization. *Macromolecules* **2018,** 51 (19), 7421-7434.

12. Anastasaki, A.; Nikolaou, V.; Zhang, Q.; Burns, J.; Samanta, S. R.; Waldron, C.; Haddleton, A. J.; McHale, R.; Fox, D.; Percec, V.; Wilson, P.; Haddleton, D. M. Copper(II)/Tertiary Amine Synergy in Photoinduced Living Radical Polymerization: Accelerated Synthesis of ω-Functional and α,ω-Heterofunctional Poly(acrylates). *J. Am. Chem. Soc.* **2014,** 136 (3), 1141-1149.

13. Theriot, J. C.; McCarthy, B. G.; Lim, C.-H.; Miyake, G. M. Organocatalyzed Atom Transfer Radical Polymerization: Perspectives on Catalyst Design and Performance. *Macromol. Rapid Commun.* **2017,** 38 (13), 1700040.

14. Dadashi-Silab, S.; Pan, X.; Matyjaszewski, K. Photoinduced Iron-Catalyzed Atom Transfer Radical Polymerization with ppm Levels of Iron Catalyst under Blue Light Irradiation. *Macromolecules* **2017,** 50 (20), 7967-7977.

15. Kütahya, C.; Schmitz, C.; Strehmel, V.; Yagci, Y.; Strehmel, B. Near-Infrared Sensitized Photoinduced Atom-Transfer Radical Polymerization (ATRP) with a Copper(II) Catalyst Concentration in the ppm Range. *Angew. Chem. Int. Ed.* **2018,** 57 (26), 7898-7902.

16. Treat, N. J.; Sprafke, H.; Kramer, J. W.; Clark, P. G.; Barton, B. E.; Read de Alaniz, J.; Fors, B. P.; Hawker, C. J. Metal-Free Atom Transfer Radical Polymerization. *J. Am. Chem. Soc.* **2014,** 136 (45), 16096-16101.

17. Anastasaki, A.; Oschmann, B.; Willenbacher, J.; Melker, A.; Van Son, M. H. C.; Truong, N. P.; Schulze, M. W.; Discekici, E. H.; McGrath, A. J.; Davis, T. P.; Bates, C. M.; Hawker, C. J. One-Pot Synthesis of ABCDE Multiblock Copolymers with Hydrophobic, Hydrophilic, and Semi-Fluorinated Segments. *Angew. Chem. Int. Ed.* **2017,** 56 (46), 14483-14487.

18. Konkolewicz, D.; Schröder, K.; Buback, J.; Bernhard, S.; Matyjaszewski, K. Visible Light and Sunlight Photoinduced ATRP with ppm of Cu Catalyst. *ACS Macro Lett.* **2012,** 1 (10), 1219-1223.

19. Mosnáček, J.; Ilčíková, M. Photochemically Mediated Atom Transfer Radical Polymerization of Methyl Methacrylate Using ppm Amounts of Catalyst. *Macromolecules* **2012,** 45 (15), 5859-5865.

20. Cole, J. P.; Federico, C. R.; Lim, C.-H.; Miyake, G. M. Photoinduced Organocatalyzed Atom Transfer Radical Polymerization Using Low ppm Catalyst Loading. *Macromolecules* **2019,** 52 (2), 747-754.

21. Xu, J.; Jung, K.; Atme, A.; Shanmugam, S.; Boyer, C. A Robust and Versatile Photoinduced Living Polymerization of Conjugated and Unconjugated Monomers and Its Oxygen Tolerance. *J. Am. Chem. Soc.* **2014,** 136 (14), 5508-5519.

22. Corrigan, N.; Shanmugam, S.; Xu, J.; Boyer, C. Photocatalysis in organic and polymer synthesis. *Chem. Soc. Rev.* **2016,** 45 (22), 6165-6212.

23. Corrigan, N.; Yeow, J.; Judzewitsch, P.; Xu, J.; Boyer, C. Seeing the Light: Advancing Materials Chemistry through Photopolymerization. *Angew. Chem. Int. Ed.* **2019,** 58 (16), 5170-5189.

24. Stache, E. E.; Kottisch, V.; Fors, B. P. Photocontrolled Radical Polymerization from Hydridic C–H Bonds. *J. Am. Chem. Soc.* **2020,** 142 (10), 4581-4585.

25. Jiang, K.; Han, S.; Ma, M.; Zhang, L.; Zhao, Y.; Chen, M. Photoorganocatalyzed Reversible-Deactivation Alternating Copolymerization of Chlorotrifluoroethylene and Vinyl

Ethers under Ambient Conditions: Facile Access to Main-Chain Fluorinated Copolymers. *J. Am. Chem. Soc.* **2020,** 142 (15), 7108-7115.

26. Michaudel, Q.; Kottisch, V.; Fors, B. P. Cationic Polymerization: From Photoinitiation to Photocontrol. *Angew. Chem. Int. Ed.* **2017,** 56 (33), 9670-9679.

27. Kottisch, V.; Supej, M. J.; Fors, B. P. Enhancing Temporal Control and Enabling Chain-End Modification in Photoregulated Cationic Polymerizations by Using Iridium-Based Catalysts. *Angew. Chem. Int. Ed.* **2018,** 57 (27), 8260-8264.

28. Fu, C.; Xu, J.; Boyer, C. Photoacid-mediated ring opening polymerization driven by visible light. *Chem. Commun.* **2016,** 52 (44), 7126-7129.

29. Ogawa, K. A.; Goetz, A. E.; Boydston, A. J. Metal-Free Ring-Opening Metathesis Polymerization. *J. Am. Chem. Soc.* **2015,** 137 (4), 1400-1403.

30. Wang, J.-S.; Matyjaszewski, K. Controlled/"living" radical polymerization. atom transfer radical polymerization in the presence of transition-metal complexes. *J. Am. Chem. Soc.* **1995,** 117 (20), 5614-5615.

31. Matyjaszewski, K.; Xia, J. Atom Transfer Radical Polymerization. *Chem. Rev.* **2001,** 101 (9), 2921-2990.

32. Matyjaszewski, K.; Jakubowski, W.; Min, K.; Tang, W.; Huang, J.; Braunecker, W. A.; Tsarevsky, N. V. Diminishing catalyst concentration in atom transfer radical polymerization with reducing agents. *Proc. Natl. Acad. Sci. U.S.A.* **2006,** 103 (42), 15309-15314.

33. Matyjaszewski, K. Atom Transfer Radical Polymerization (ATRP): Current Status and Future Perspectives. *Macromolecules* **2012,** 45 (10), 4015-4039.

34. Matyjaszewski, K.; Tsarevsky, N. V. Macromolecular Engineering by Atom Transfer Radical Polymerization. *J. Am. Chem. Soc.* **2014,** 136 (18), 6513-6533.

35. Matyjaszewski, K.; Coca, S.; Gaynor, S. G.; Wei, M.; Woodworth, B. E. Zerovalent Metals in Controlled/"Living" Radical Polymerization. *Macromolecules* **1997,** 30 (23), 7348-7350.

36. Matyjaszewski, K.; Tsarevsky, N. V.; Braunecker, W. A.; Dong, H.; Huang, J.; Jakubowski, W.; Kwak, Y.; Nicolay, R.; Tang, W.; Yoon, J. A. Role of Cu0 in Controlled/"Living" Radical Polymerization. *Macromolecules* **2007,** 40 (22), 7795-7806.

37. Konkolewicz, D.; Wang, Y.; Zhong, M.; Krys, P.; Isse, A. A.; Gennaro, A.; Matyjaszewski, K. Reversible-Deactivation Radical Polymerization in the Presence of Metallic Copper. A

Critical Assessment of the SARA ATRP and SET-LRP Mechanisms. *Macromolecules* **2013,** 46 (22), 8749-8772.

38. Jakubowski, W.; Matyjaszewski, K. Activators Regenerated by Electron Transfer for Atom-Transfer Radical Polymerization of (Meth)acrylates and Related Block Copolymers. *Angew. Chem. Int. Ed.* **2006,** 45 (27), 4482-4486.

39. Lorandi, F.; Fantin, M.; Isse, A. A.; Gennaro, A. RDRP in the presence of Cu0: The fate of Cu(I) proves the inconsistency of SET-LRP mechanism. *Polymer* **2015,** 72, 238-245.

40. Konkolewicz, D.; Magenau, A. J. D.; Averick, S. E.; Simakova, A.; He, H.; Matyjaszewski, K. ICAR ATRP with ppm Cu Catalyst in Water. *Macromolecules* **2012,** 45 (11), 4461-4468.

41. Costa, J. R. C.; Góis, J. R.; De Bon, F.; Serra, A. C.; Guliashvili, T.; Isse, A. A.; Gennaro, A.; Coelho, J. F. J. Addressing the role of triphenylphosphine in copper catalyzed ATRP. *Polym. Chem.* **2018,** 9 (44), 5348-5358.

42. Tasdelen, M. A.; Uygun, M.; Yagci, Y. Photoinduced Controlled Radical Polymerization. *Macromol. Rapid Commun.* **2011,** 32 (1), 58-62.

43. Ribelli, T. G.; Konkolewicz, D.; Bernhard, S.; Matyjaszewski, K. How are Radicals (Re)Generated in Photochemical ATRP? *J. Am. Chem. Soc.* **2014,** 136 (38), 13303-13312.

44. Dadashi-Silab, S.; Atilla Tasdelen, M.; Yagci, Y. Photoinitiated atom transfer radical polymerization: Current status and future perspectives. *J. Polym. Sci., Part A: Polym. Chem.* **2014,** 52 (20), 2878-2888.

45. Rolland, M.; Whitfield, R.; Messmer, D.; Parkatzidis, K.; Truong, N. P.; Anastasaki, A. Effect of Polymerization Components on Oxygen-Tolerant Photo-ATRP. *ACS Macro Lett.* **2019,** 8 (12), 1546-1551.

46. Li, B.; Yu, B.; Huck, W. T. S.; Liu, W.; Zhou, F. Electrochemically Mediated Atom Transfer Radical Polymerization on Nonconducting Substrates: Controlled Brush Growth through Catalyst Diffusion. *J. Am. Chem. Soc.* **2013,** 135 (5), 1708-1710.

47. Chmielarz, P.; Fantin, M.; Park, S.; Isse, A. A.; Gennaro, A.; Magenau, A. J. D.; Sobkowiak, A.; Matyjaszewski, K. Electrochemically mediated atom transfer radical polymerization (eATRP). *Prog. Polym. Sci.* **2017,** 69, 47-78.

48. Lorandi, F.; Fantin, M.; Isse, A. A.; Gennaro, A. Electrochemical triggering and control of atom transfer radical polymerization. *Curr. Opin. Electrochem.* **2018,** 8, 1-7.

49. Zhou, Y.-N.; Li, J.-J.; Ljubic, D.; Luo, Z.-H.; Zhu, S. Mechanically Mediated Atom Transfer Radical Polymerization: Exploring Its Potential at High Conversions. *Macromolecules* **2018,** 51 (17), 6911-6921.

50. Wang, Z.; Pan, X.; Yan, J.; Dadashi-Silab, S.; Xie, G.; Zhang, J.; Wang, Z.; Xia, H.; Matyjaszewski, K. Temporal Control in Mechanically Controlled Atom Transfer Radical Polymerization Using Low ppm of Cu Catalyst. *ACS Macro Lett.* **2017,** 6 (5), 546-549.

51. Wang, Z.; Lorandi, F.; Fantin, M.; Wang, Z.; Yan, J.; Wang, Z.; Xia, H.; Matyjaszewski, K. Atom Transfer Radical Polymerization Enabled by Sonochemically Labile Cu-carbonate Species. *ACS Macro Lett.* **2019,** 8, 161-165.

52. Dadashi-Silab, S.; Matyjaszewski, K. Temporal Control in Atom Transfer Radical Polymerization Using Zerovalent Metals. *Macromolecules* **2018,** 51 (11), 4250-4258.

53. Dadashi-Silab, S.; Lorandi, F.; Fantin, M.; Matyjaszewski, K. Redox-switchable atom transfer radical polymerization. *Chem. Commun.* **2019,** 55 (5), 612-615.

54. Dolinski, N. D.; Page, Z. A.; Discekici, E. H.; Meis, D.; Lee, I.-H.; Jones, G. R.; Whitfield, R.; Pan, X.; McCarthy, B. G.; Shanmugam, S.; Kottisch, V.; Fors, B. P.; Boyer, C.; Miyake, G. M.; Matyjaszewski, K.; Haddleton, D. M.; de Alaniz, J. R.; Anastasaki, A.; Hawker, C. J. What happens in the dark? Assessing the temporal control of photo-mediated controlled radical polymerizations. *J. Polym. Sci., Part A: Polym. Chem.* **2019,** 57 (3), 268-273.

55. Dadashi-Silab, S.; Matyjaszewski, K. Iron-Catalyzed Atom Transfer Radical Polymerization of Semifluorinated Methacrylates. *ACS Macro Lett.* **2019,** 8 (9), 1110-1114.

56. Krys, P.; Matyjaszewski, K. Kinetics of Atom Transfer Radical Polymerization. *Eur. Polym. J.* **2017,** 89, 482-523.

57. Ribelli, T. G.; Lorandi, F.; Fantin, M.; Matyjaszewski, K. Atom Transfer Radical Polymerization: Billion Times More Active Catalysts and New Initiation Systems. *Macromol. Rapid Commun.* **2019,** 40 (1), 1800616.

58. Whitfield, R.; Parkatzidis, K.; Rolland, M.; Truong, N. P.; Anastasaki, A. Tuning Dispersity by Photoinduced Atom Transfer Radical Polymerisation: Monomodal Distributions with ppm Copper Concentration. *Angew. Chem. Int. Ed.* **2019,** 58 (38), 13323-13328.

59. Lorandi, F.; Matyjaszewski, K. Why Do We Need More Active ATRP Catalysts? *Isr. J. Chem.* **2020,** 60, 108-123.

60. Fischer, H. The Persistent Radical Effect: A Principle for Selective Radical Reactions and Living Radical Polymerizations. *Chem. Rev.* **2001,** 101 (12), 3581-3610.

61. Fantin, M.; Isse, A. A.; Bortolamei, N.; Matyjaszewski, K.; Gennaro, A. Electrochemical approaches to the determination of rate constants for the activation step in atom transfer radical polymerization. *Electrochim. Acta* **2016,** 222, 393-401.

62. Dolinski, N. D.; Page, Z. A.; Eisenreich, F.; Niu, J.; Hecht, S.; Read de Alaniz, J.; Hawker, C. J. A Versatile Approach for In Situ Monitoring of Photoswitches and Photopolymerizations. *ChemPhotoChem* **2017,** 1 (4), 125-131.

63. Dong, H.; Matyjaszewski, K. ARGET ATRP of 2-(Dimethylamino)ethyl Methacrylate as an Intrinsic Reducing Agent. *Macromolecules* **2008,** 41 (19), 6868-6870.

64. Kwak, Y.; Matyjaszewski, K. ARGET ATRP of methyl methacrylate in the presence of nitrogen-based ligands as reducing agents. *Polym. Int.* **2009,** 58 (3), 242-247.

65. Braunecker, W. A.; Tsarevsky, N. V.; Gennaro, A.; Matyjaszewski, K. Thermodynamic Components of the Atom Transfer Radical Polymerization Equilibrium: Quantifying Solvent Effects. *Macromolecules* **2009,** 42 (17), 6348-6360.

66. Lorandi, F.; Fantin, M.; Isse, A. A.; Gennaro, A.; Matyjaszewski, K. New protocol to determine the equilibrium constant of atom transfer radical polymerization. *Electrochim. Acta* **2018,** 260, 648-655.

67. Isse, A. A.; Bortolamei, N.; De Paoli, P.; Gennaro, A. On the mechanism of activation of copper-catalyzed atom transfer radical polymerization. *Electrochim. Acta* **2013,** 110, 655-662.

68. Buback, M.; Kurz, C. H.; Schmaltz, C. Pressure dependence of propagation rate coefficients in free-radical homopolymerizations of methyl acrylate and dodecyl acrylate. *Macromol. Chem. Phys.* **1998,** 199 (8), 1721-1727.

69. Ribelli, T. G.; Augustine, K. F.; Fantin, M.; Krys, P.; Poli, R.; Matyjaszewski, K. Disproportionation or Combination? The Termination of Acrylate Radicals in ATRP. *Macromolecules* **2017,** 50 (20), 7920-7929.

70. Ribelli, T. G.; Wahidur Rahaman, S. M.; Daran, J.-C.; Krys, P.; Matyjaszewski, K.; Poli, R. Effect of Ligand Structure on the CuII–R OMRP Dormant Species and Its Consequences for Catalytic Radical Termination in ATRP. *Macromolecules* **2016,** 49 (20), 7749-7757.

71. Wulkow, M. Computer Aided Modeling of Polymer Reaction Engineering—The Status of Predici, I-Simulation. *Macromolecular Reaction Engineering* **2008,** 2 (6), 461-494.

72. Fantin, M.; Lorandi, F.; Ribelli, T. G.; Szczepaniak, G.; Enciso, A. E.; Fliedel, C.; Thevenin, L.; Isse, A. A.; Poli, R.; Matyjaszewski, K. Impact of Organometallic Intermediates on Copper-Catalyzed Atom Transfer Radical Polymerization. *Macromolecules* **2019,** 52 (11), 4079-4090.

73. Thevenin, L.; Fliedel, C.; Fantin, M.; Ribelli, T. G.; Matyjaszewski, K.; Poli, R. Reductive Termination of Cyanoisopropyl Radicals by Copper(I) Complexes and Proton Donors: Organometallic Intermediates or Coupled Proton–Electron Transfer? *Inorg. Chem.* **2019,** 58 (9), 6445-6457.

74. Braunecker, W. A.; Tsarevsky, N. V.; Pintauer, T.; Gil, R. R.; Matyjaszewski, K. Quantifying Vinyl Monomer Coordination to CuI in Solution and the Effect of Coordination on Monomer Reactivity in Radical Copolymerization. *Macromolecules* **2005,** 38 (10), 4081-4088.

2.4. Redox-Switchable Atom Transfer Radical Polymerization

2.4.1 Abstract

Temporal control in atom transfer radical polymerization (ATRP) relies on modulating the oxidation state of a copper catalyst, as polymer chains are activated by L/Cu^I and deactivated by L/Cu^{II}. Regeneration of L/Cu^I activator has been achieved by applying a multitude of external stimuli. However, switching the Cu catalyst off by oxidizing to L/Cu^{II} through external chemical stimuli has not yet been investigated. A redox switchable ATRP was developed in which an oxidizing agent was used to oxidize L/Cu^I activator to L/Cu^{II}, thus halting the polymerization. A ferrocenium salt or oxygen were used to switch off the Cu catalyst, whereas ascorbic acid was used to switch the catalyst on by (re)generating L/Cu^I. The redox switches efficiently modulated the oxidation state of the catalyst without sacrificing control over polymerization.
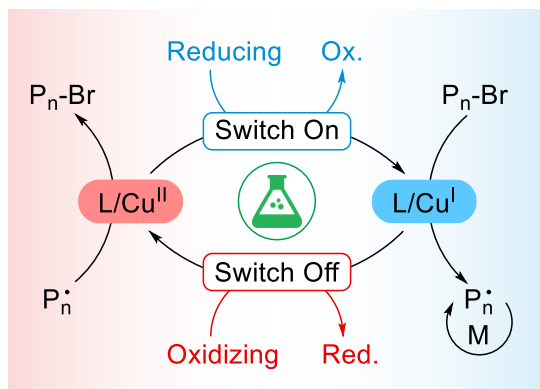
2.4.2 Introduction

Catalysts' activity can be efficiently tuned by external stimuli, altering their redox properties or steric environment. Redox-switchable catalysis can provide chemo-, regio- and stereochemical and temporal control over reactions, thus being a fundamental tool in catalysis and supramolecular chemistry.[1-3] The most explored strategy consists of designing ligands that incorporate redox-active groups,[4] particularly ferrocenyl units.[5-7] Alternatively, the oxidation state of a catalyst center can be directly modulated to alter its activity.[8-10]

Controlled polymerization techniques have recently been advanced by applying external stimuli for triggering polymerization processes.[4, 11, 12] The use of external stimuli allows polymerizations to be controlled in a spatiotemporal manner, providing a great opportunity for synthesis of advanced polymers with pre-determined, tunable properties.

A great deal of research has been devoted to regulating various polymerization techniques by external control. Most widely studied stimuli include photochemistry,[11, 13-20] electrochemistry,[15, 21, 22] mechanical,[23] chemical,[24, 25] and redox control.[12, 23, 26-32] These stimuli reversibly affect the redox properties of the catalyst, thus allowing control over polymerization rate or mechanism.

Atom transfer radical polymerization (ATRP) has become a common technique to prepare well-defined polymers.[33-38] Recent advances in ATRP have focused on (re)generation of the activator form of the catalyst through external means. Using external stimuli for activator (re)generation elicits spatiotemporal control over ATRP processes.[39]

In Cu-catalyzed ATRP, temporal control depends on the concentration of L/Cu^I activator, as well as how fast it can be consumed or removed from the reaction media. In the absence of stimuli, L/Cu^I is mainly consumed by irreversible radical terminations. Each termination event causes the accumulation of two molecules of L/Cu^{II} deactivator. Subsequently, polymerization stops in the absence of activator regeneration. In this regard, the ATRP equilibrium and the ratio of $[L/Cu^{II}]/[L/Cu^I]$ depend on the activity of the catalyst.[40] Therefore, for highly active catalytic systems, the large ATRP equilibrium constant results in a very low L/Cu^I concentration, and thus the reaction stops rapidly. Conversely, for less active systems, the presence of high concentration of activator species enables the polymerization to continue for longer, until all the catalyst is converted to L/Cu^{II}.[40]

The majority of ATRP reactions regulated by external stimuli relies on using the stimuli to switch the reaction on by reducing L/Cu^{II} to L/Cu^I.[14] However, oxidation of L/Cu^I to L/Cu^{II}, which would lead to on-demand switching of ATRP between on/off states, has not been widely studied. Electrochemically mediated ATRP uniquely enables both the reduction and oxidation of the Cu catalyst *via* alternate application of reducing and oxidizing current or potential.[14, 40-42]

Indeed, the ATRP equilibrium—maintained via a redox process using a Cu catalyst—provides the possibility of on-demand switching of the polymerization by affecting the oxidation state of the catalyst. This behavior allows for efficient temporal control over chain growth to be attained in ATRP, which would not be accessible in other conventional or controlled radical polymerization techniques.

In this paper, a chemically controlled ATRP was developed in which the activity of the Cu catalyst was tuned via redox processes. As in activators regenerated by electron transfer (ARGET) ATRP, ascorbic acid (AscAcid) was used as a reducing agent to (re)generate the L/Cu^I activator and switch the reaction on.[43] Ferrocenium hexafluorophosphate ($FcPF_6$) or oxygen were used as oxidizing agents to oxidize L/Cu^I to L/Cu^{II}, and therefore turn the reaction off (Scheme 9).
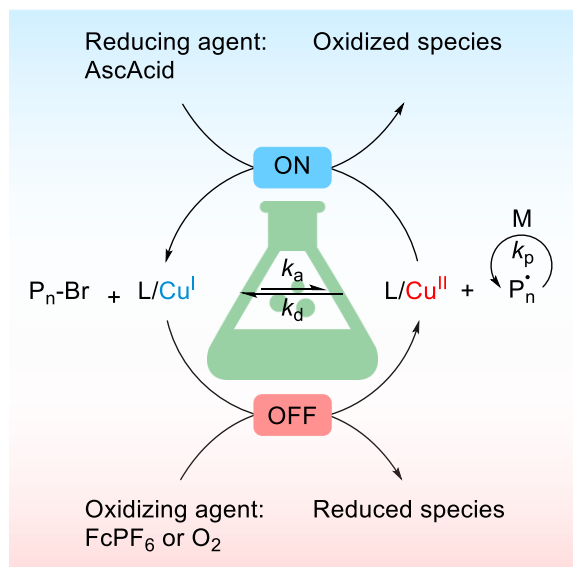
Scheme 9. Redox-switchable ATRP by using AscAcid as reducing agent and FcPF6 or oxygen as oxidizing agents.

2.4.3   Results and Discussion

ARGET ATRP of methyl acrylate (MA) was conducted in *N,N*-dimethylformamide (DMF) using $CuBr_2/Me_6TREN$ as a catalyst (Me_6TREN: tris[2-(dimethylamino)ethyl]amine). AscAcid was added initially to start the polymerization. Monomer conversion reached 56% in 6 h, with the rate of the polymerization decreasing over time (Figure 40). Size exclusion chromatography (SEC) analysis showed the final polymer with a low dispersity ($Đ = 1.10$), and molecular weight (MW) matching theoretical value ($M_{n,th} = 9850$, $M_n = 10100$). The activator L/Cu^I was switched off by oxidizing to L/Cu^{II} using $FcPF_6$ as an oxidizing agent. ARGET ATRP of MA was conducted under similar initial conditions, with ~30% monomer conversion reached within 1 h. Afterward, $FcPF_6$ (10 mol% with respect to Cu) was added. Kinetic results showed a significant decrease in the rate of the reaction, which continued to only ~39 % monomer conversion, and then stopped (Figure 1). Indeed, it was previously determined that the standard reduction

potential of CuBr$_2$/Me$_6$TREN in DMF is $E^{\ominus}_{[(L/Cu^{II})/(L/Cu^{I})]} = -0.32$ V *vs.* saturated calomel electrode (SCE),[44] whereas $E^{\ominus}_{(Fc^+/Fc)} = 0.48$ V *vs.* SCE was measured for the redox couple of ferrocenium/ferrocene in DMF.[42] Therefore, ferrocenium is a suitable oxidant for the Cu catalyst. In addition, AscAcid is oxidized by reacting with both L/Cu^{II} and FcPF$_6$.[45] However, the small increase in monomer conversion suggested that residual AscAcid further regenerated the L/Cu^I activator, and continued the polymerization. Importantly, SEC analysis showed a polymer with a monomodal, symmetric MW distribution ($M_{n,th} = 6950$, $M_n = 7050$ and $Ð = 1.12$). Interestingly, when the amount of FcPF$_6$ was increased to 50 mol% with respect to Cu, the reaction was instantaneously and completely stopped. In this case, the FcPF$_6$ salt oxidized all the L/Cu^I and residual AscAcid, so that no monomer conversion was observed.
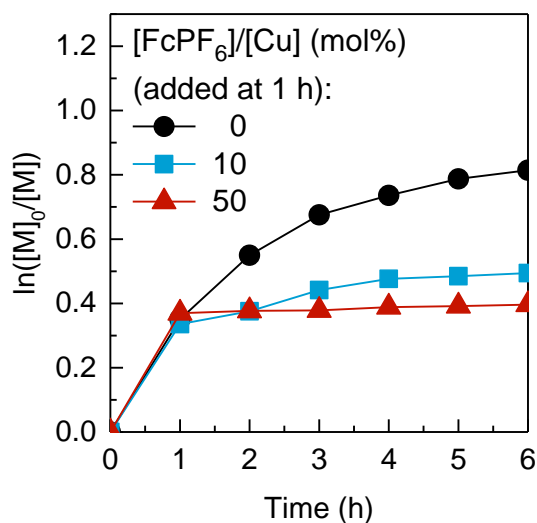
Figure 40. Redox control in ATRP by using AscAcid and FcPF$_6$ as redox agents. Reaction conditions: [MA]/[EBiB]/[CuBr$_2$]/[Me$_6$TREN]/[AscAcid] = 200/1/0.04/0.04/0.04 in 50 vol% DMF at 25 °C. AscAcid added initially. FcPF$_6$ (10 or 50 mol% with respect to Cu) added at 1 h.

Vis-NIR spectroscopy of the Cu catalyst confirmed its successive reduction and oxidation upon sequential addition of AscAcid and FcPF$_6$ (Figure 41). A decrease in the absorption peak of L/Cu^{II} at ~960 nm was observed upon addition of AscAcid, indicating reduction to L/Cu^I. FcPF$_6$ was later added to the solution, and the absorption spectra increased to the initial state. These observations proved that L/Cu^{II} could be successfully reduced to L/Cu^I by addition of AscAcid and oxidized back to L/Cu^{II} in the presence of FcPF$_6$.
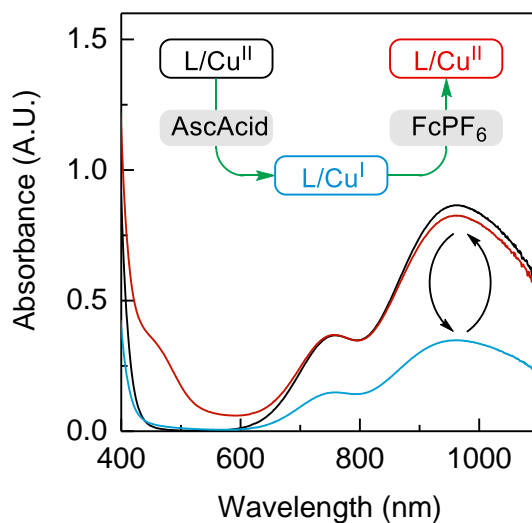
Figure 41. Evolution of the Vis-NIR spectra of Cu catalyst after sequential addition of AscAcid and FcPF$_6$. [CuBr$_2$/Me$_6$TREN] = [AscAcid] = [FcPF$_6$] = 2.22 mM in DMF. FcPF$_6$ was added 30 min after addition of AscAcid.

Having confirmed the efficiency of AscAcid and FcPF$_6$ in switching the redox properties of Cu species, and hence controlling the reaction, temporal control was attempted using these chemical redox switches. AscAcid started the ARGET ATRP of MA with 27% monomer conversion obtained in 1 h. Afterward, FcPF$_6$ (25 mol% with respect to Cu) was added to stop the reaction (Figure 42). Negligible monomer conversion was observed during the 5-h period after the addition of FcPF$_6$, and the reaction stopped (30% conversion at 6 h). A second batch of AscAcid ([AscAcid] = [L/Cu]) was added to switch the reaction on by regenerating L/Cu^I. Monomer conversion reached 48% within 1 h, confirming the preservation of chain-end functionality in the presence of chemical switches.

Importantly, SEC analysis of the polymer showed monomodal, symmetric MW distributions upon successive addition of redox switches. SEC traces showed a clear shift toward higher MWs after the addition of the second batch of AscAcid, indicating a well-controlled process.
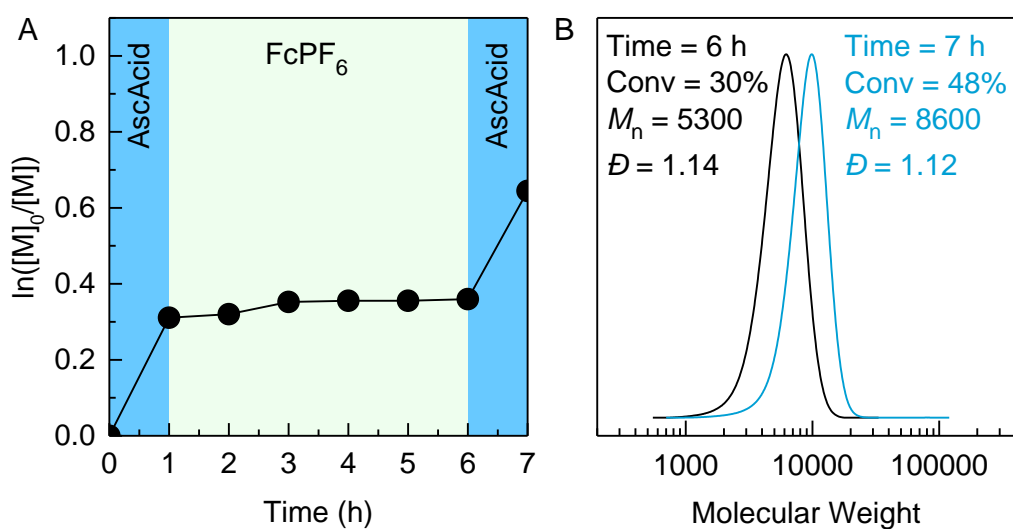
Figure 42. (A) Temporal control of ATRP using AscAcid and $FcPF_6$ as redox switches. (B) SEC traces after addition of $FcPF_6$ and AscAcid. Reaction conditions: $[MA]/[EBiB]/[CuBr_2]/[Me_6TREN]/[AscAcid] = 200/1/0.04/0.04/0.04$ in 50 vol% DMF at 25 °C. AscAcid added at 0 and 6 h. $FcPF_6$ (25 mol% with respect to Cu) added at 1 h.

Oxygen was a simple alternative to $FcPF_6$ as an oxidizing agent for L/Cu^I, efficiently turning the ATRP catalyst off. An ARGET ATRP of MA was conducted under similar conditions using AscAcid, with 37% monomer conversion reached in 1 h (Figure 43). Then, the polymerization solution was bubbled with air for 1 min. No monomer conversion was observed after exposure to oxygen, indicating complete oxidation of all activator and AscAcid. Consequently, the polymerization was successfully switched off. The standard reduction potential of oxygen in DMF was estimated as $E^\ominus_{(O_2/H_2O)} = 1.08$ V *vs.* SCE, therefore oxygen is a stronger oxidizing agent compared to $FcPF_6$.[46] Importantly, the reaction was restarted upon the addition of a second batch of AscAcid ($[AscAcid] = [L/Cu]$) at 6 h. Monomer conversion reached 63% within the following hour. SEC analysis of the polymer revealed a symmetric, mono-modal MW addition of AscAcid. These results indicated that a well- controlled polymerization was achieved in the presence of AscAcid and oxygen as redox switches. The chain-end functionality was preserved throughout the reaction enabling further chain growth in a controlled manner.
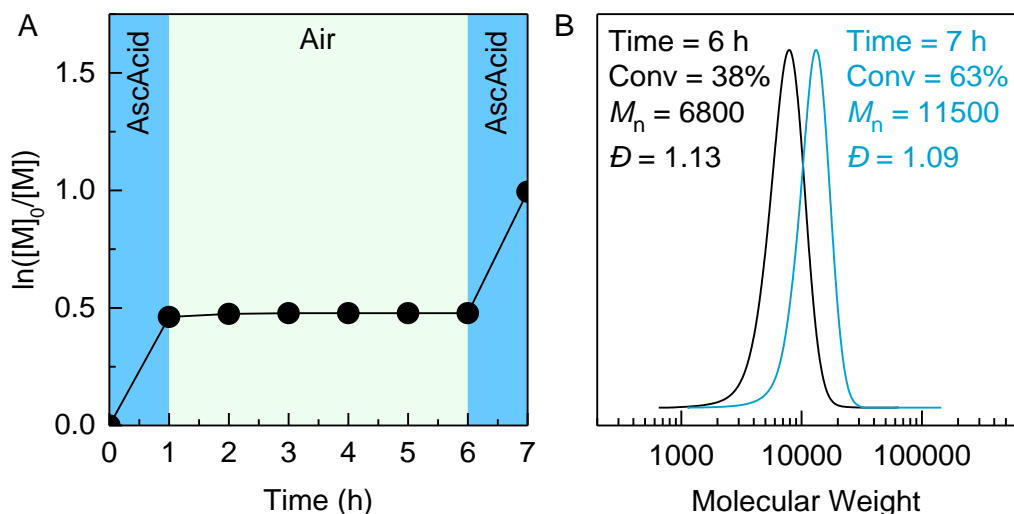
Figure 43. (A) Temporal control of ATRP using AscAcid and oxygen as redox switches. (B) SEC traces after bubbling with air and addition of AscAcid. Reaction conditions: [MA]/[EBiB]/[CuBr$_2$]/[Me$_6$TREN]/[AscAcid] = 200/1/0.04/0.04/0.04 in 50 vol% DMF at 25 °C. AscAcid added at 0 and 6 h. Air bubbled for 1 min at 1 h. Nitrogen bubbled for 2 min at 6 h.

The strength of this system was further confirmed by switching the polymerization for multiple times using AscAcid and oxygen as redox switches (Figure 44 and Figure 48). The reaction was proceeded in the presence of AscAcid, which regenerated the activator. Introducing oxygen stopped the reaction through oxidation of the catalyst. The polymerization was well-controlled upon successive additions of AscAcid and oxygen. It is worth mentioning that in these experiments the amount of oxidizing agents was always relatively low, so as to allow an effective re-starting of the process by adding AscAcid and to limit the contamination of the system.

123
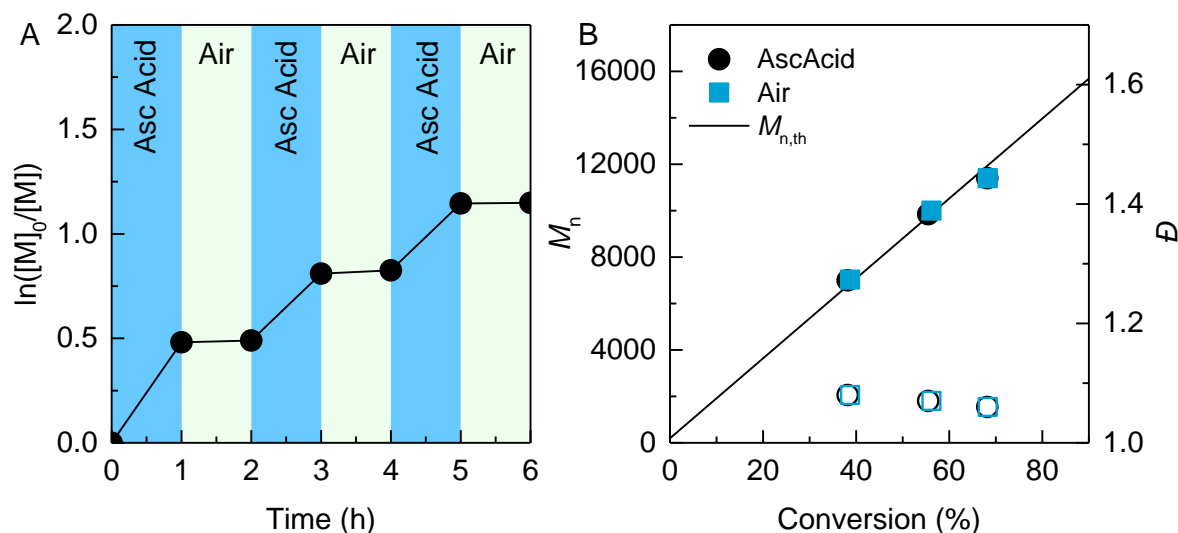
Figure 44. (A) Kinetics of temporal control using AscAcid and oxygen as redox agents. (B) Number-average molecular weight (M_n, solid points) and dispersity ($Đ$, open points) as a function of monomer conversion. Reaction conditions: [MA]/[EBiB]/[CuBr$_2$]/[Me$_6$TREN]/[AscAcid] = 200/1/0.04/0.04/0.04 in 50 vol% DMF at 25 °C. AscAcid added at 0, 2 and 4 h. Air bubbled for 1 min at 1, 3, and 5 h. Nitrogen bubbled for 2 min at 2 and 4 h.

The reduction and oxidation of the Cu catalyst by AscAcid and oxygen was also confirmed by Vis-NIR spectroscopy. The absorption peak of L/Cu^{II} at ~960 nm decreased upon addition of AscAcid indicating reduction to L/Cu^{I}. The solution was bubbled with air and the absorption peak partially increased, suggesting re-oxidation to L/Cu^{II} (Figure 49). Interestingly, further addition of AscAcid resulted in a reduction to L/Cu^{I}. These results supported that the Cu catalyst can be reversibly toggled between L/Cu^{I} and L/Cu^{II} states using redox switches, for multiple times.

2.4.4   Conclusions

In summary, the activity of the Cu catalyst in ATRP was effectively switched on and off using chemical redox switches. AscAcid acted as a reducing agent that turned the reaction on by (re)generating the L/Cu^{I} activator. An oxidizing agent, such as the FcPF$_6$ salt or oxygen, switched off the Cu catalyst by oxidizing it to L/Cu^{II}, thus stopping the reaction. These species efficiently altered the oxidation state of the Cu catalyst enabling perfect temporal control over the polymerization. Importantly, chain-end functionality was preserved in the presence of

oxidizing agents, as further addition of AscAcid restarted the polymerization in a controlled manner.

Future work will focus on investigating temporal control in ATRP regulated by external stimuli to improve the mechanistic understanding of these techniques and broaden their scope. In addition to the chemical stimuli presented in here, new advanced techniques comprised of orthogonal multi-stimuli will be developed to precisely modulate the ATRP catalyst.

2.4.5 Experimental Section and Supporting Information

Materials

Methyl acrylate (MA; Sigma-Aldrich, 99%) was purified by passing through a basic alumina column to remove polymerization inhibitor prior to use. Ethyl α-bromoisobutyrate (EBiB; Sigma-Aldrich, 98%), copper(II) bromide ($CuBr_2$; Sigma-Aldrich, 99%), L-ascorbic acid (AscAcid, Sigma-Aldrich), ferrocenium hexafluorophosphate ($FcPF_6$; Sigma-Aldrich, 97%) and *N,N*-dimethylformamide (DMF; Fisher Chemical) were used as received. Tris[2-(dimethylamino)ethyl]amine (Me_6TREN) was received from Koei Chemical Co., Ltd. (Japan).

Instrumentation

Proton nuclear magnetic resonance (^1H NMR) measurements were performed on a Bruker Advance 500 MHz spectrometer. Number-average molecular weight (M_n) and dispersity ($Đ$) of the polymers were determined by size-exclusion chromatography (SEC). The SEC instrument was equipped with a Waters 515 pump and a Waters 2414 differential refractometer using PSS columns (SDV 10^5, 10^3, and 500 Å) with THF as eluent at 35 °C and a flow rate of 1 mL/min. Linear poly(methyl methacrylate) standards were used for calibration. UV-vis spectra were recorded using Agilent 8453 spectrophotometer.

General ATRP Procedures

ARGET ATRP of MA

A 20 mL vial equipped with a stir bar was sealed with a rubber septum and subjected to vacuum and backfilled with nitrogen for 5 times. MA and DMF were degassed separately for 40 min. DMF (2 mL), MA (2 mL, 22.2 mmol, 200 equiv.), $CuBr_2$ (1.0 mg, 4.4×10^{-6} mol, 0.04 equiv.), Me_6TREN (1.2 µL, 4.4×10^{-6} mol, 0.04 equiv.), and EBiB (16.3 µL, 0.111 mmol, 1 equiv.) were

added into the vial under nitrogen. The vial was placed in a water bath at 25 °C. A degassed solution of AscAcid (50 µL, 88.8 mM in DMF; 0.78 mg, 0.04 equiv.) was added to start the reaction. Samples were taken periodically for ^{1}H NMR and SEC analyses.

Redox Switchable ATRP using AscAcid/FcPF$_6$ as Redox Switches

A 20 mL vial equipped with a stir bar was sealed with a rubber septum and subjected to vacuum and backfilled with nitrogen for 5 times. MA and DMF were degassed separately for 40 min. DMF (2 mL), MA (2 mL, 22.2 mmol, 200 equiv.), CuBr$_2$ (1.0 mg, 4.4×10^{-6} mol, 0.04 equiv.), Me$_6$TREN (1.2 µL, 4.4×10^{-6} mol, 0.04 equiv.), and EBiB (16.3 µL, 0.111 mmol, 1 equiv.) were added into the vial under nitrogen. The vial was placed in a water bath at 25 °C. A degassed solution of AscAcid (50 µL, 88.8 mM in DMF; 0.78 mg, 0.04 equiv.) was added to start the reaction. A degassed solution of FcPF$_6$ (50 µL, 44.4 mM in DMF; 0.735 mg, 2.22×10^{-6} mol) was added to polymerization solution after 1 h. Samples were taken periodically for ^{1}H NMR and SEC analyses.

Redox Switchable ATRP using AscAcid/O$_2$ as Redox Switches

A 2-dram vial equipped with a stir bar was sealed with a rubber septum and subjected to vacuum and backfilled with nitrogen for 5 times. MA and DMF were degassed separately for 40 min. DMF (2 mL), MA (2 mL, 22.2 mmol, 200 equiv.), CuBr$_2$ (1.0 mg, 4.4×10^{-6} mol, 0.04 equiv.), Me$_6$TREN (1.2 µL, 4.4×10^{-6} mol, 0.04 equiv.), and EBiB (16.3 µL, 0.111 mmol, 1 equiv.) were added into the vial under nitrogen. The vial was placed in a water bath at 25 °C. A degassed solution of AscAcid (50 µL, 88.8 mM in DMF; 0.78 mg, 0.04 equiv.) was added to start the reaction. After 1 h, the polymerization solution was bubbled with air for 1 min. The reaction was bubbled with nitrogen for 2 min before adding a second batch of AscAcid (50 µL, 88.8 mM in DMF; 0.78 mg, 0.04 equiv.). Samples were taken periodically for ^{1}H NMR and SEC analyses.

Kinetics and polymerization data:
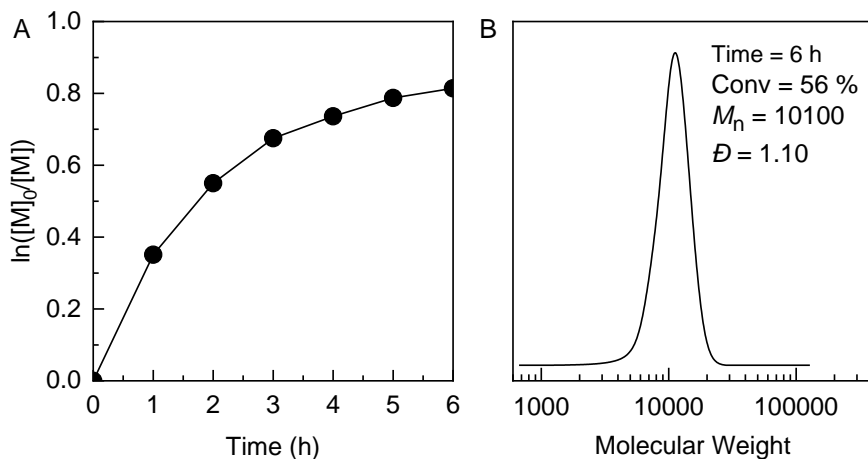
Figure 45. ARGET ATRP of MA using Me$_6$TREN in DMF. Reaction conditions: [MA]/[EBiB]/[CuBr$_2$]/[Me$_6$TREN]/[AscAcid] = 200/1/0.04/0.04/0.04 in 50 vol% DMF at 25 °C. AscAcid added initially.
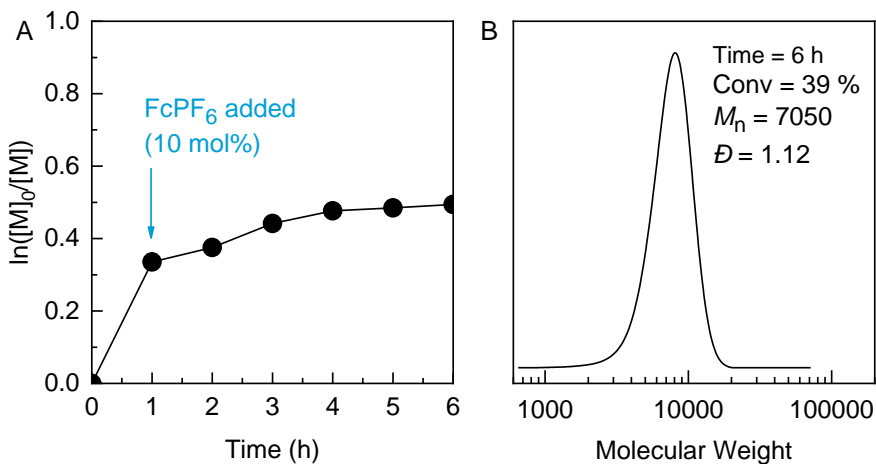
Figure 46. Redox control in ATRP. Reaction conditions: [MA]/[EBiB]/[CuBr$_2$]/[Me$_6$TREN]/ [AscAcid] = 200/1/0.04/0.0/0.04 in 50 vol% DMF at 25 °C. AscAcid added initially. FcPF$_6$ (10 mol% with respect to Cu) added at 1 h.
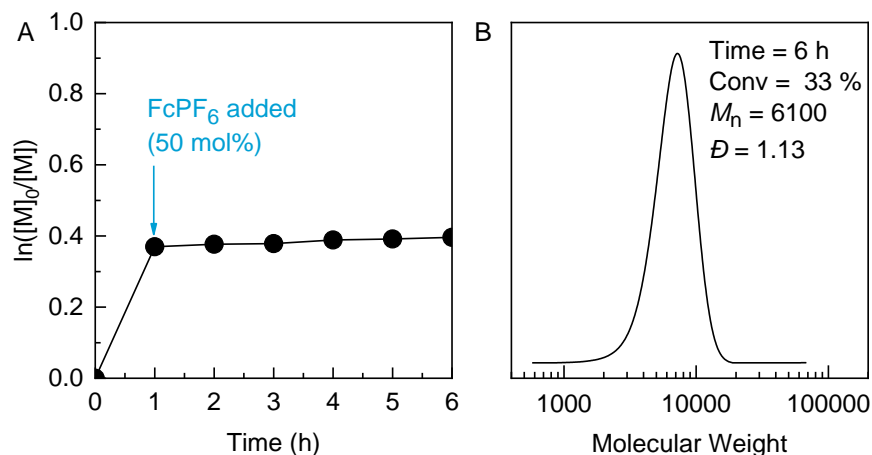
Figure 47. Redox control in ATRP. Reaction conditions: [MA]/[EBiB]/[CuBr$_2$]/[Me$_6$TREN]/[AscAcid] = 200/1/0.04/0.0/0.04 in 50 vol% DMF at 25 °C. AscAcid added initially. FcPF$_6$ (50 mol% with respect to Cu) added at 1 h.
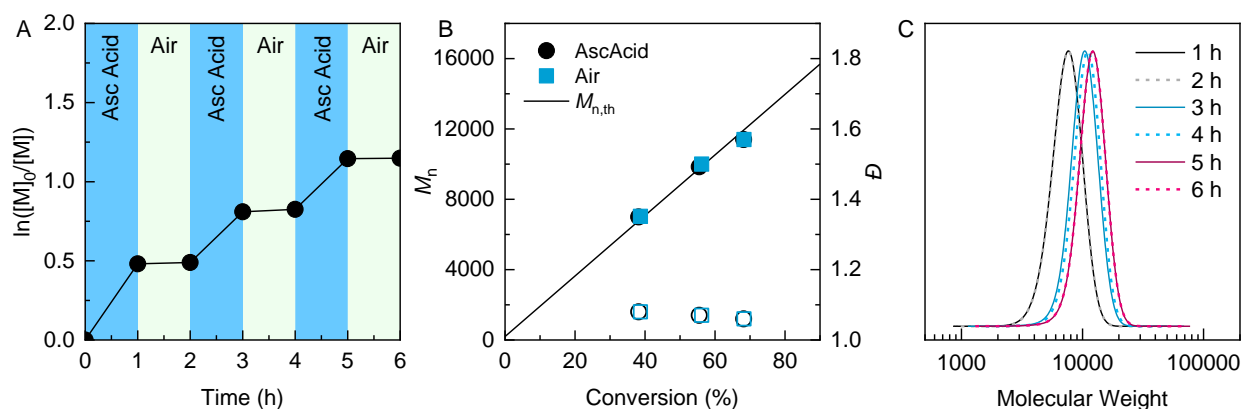
Figure 48. (A) Kinetics of temporal control using AscAcid and oxygen as redox agents. (B) Number-average molecular weight (M_n, solid points) and dispersity ($Đ$, open points) as a function of monomer conversion. (C) SEC traces: solid lines after addition of AscAcid and dashed lines after air bubbling. Reaction conditions: [MA]/[EBiB]/[CuBr$_2$]/[Me$_6$TREN]/[AscAcid] = 200/1/0.04/0.04/0.04 in 50 vol% DMF at 25 °C. AscAcid added at 0, 2 and 4 h. Air bubbled for 1 min at 1, 3, and 5 h. Nitrogen bubbled for 2 min at 2 and 4 h.
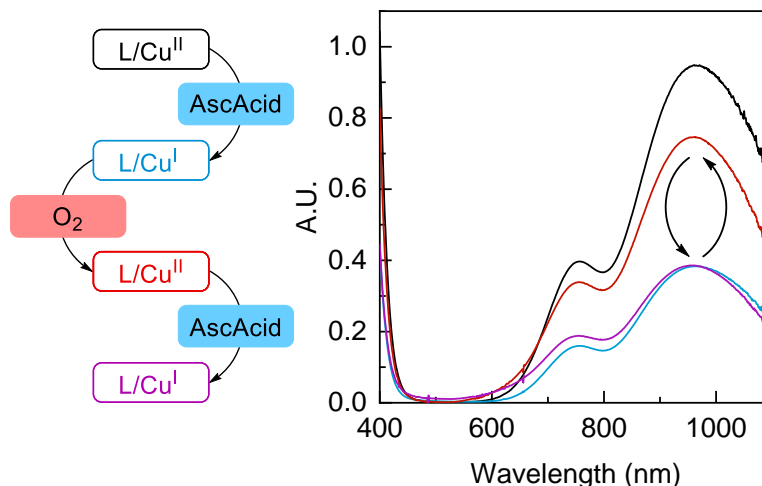
Figure 49. Evolution of the Vis-NIR spectra of Cu catalyst after sequential addition of AscAcid and oxygen. [CuBr$_2$/Me$_6$TREN] = [AscAcid] = 2.22 mM in DMF. Oxygen was introduced by bubbling with air for 1 min.

2.4.6   References

1. Buback, M.; Kurz, C. H.; Schmaltz, C. Pressure dependence of propagation rate coefficients in free-radical homopolymerizations of methyl acrylate and dodecyl acrylate. *Macromol. Chem. Phys.* **1998,** 199 (8), 1721-1727.

2. Fantin, M.; Lorandi, F.; Ribelli, T. G.; Szczepaniak, G.; Enciso, A. E.; Fliedel, C.; Thevenin, L.; Isse, A. A.; Poli, R.; Matyjaszewski, K. Impact of Organometallic Intermediates on Copper-Catalyzed Atom Transfer Radical Polymerization. *Macromolecules* **2019,** 52 (11), 4079-4090.

3. Buback, M.; Kuelpmann, A.; Kurz, C. Termination Kinetics of Methyl Acrylate and Dodecyl Acrylate Free-Radical Homopolymerizations up to High Pressure. *Macromol. Chem. Phys.* **2002,** 203 (8), 1065-1070.

4. Blanco, V.; Leigh, D. A.; Marcos, V. Artificial switchable catalysts. *Chem. Soc. Rev.* **2015,** 44 (15), 5341-5370.

5. Wiester, M. J.; Ulmann, P. A.; Mirkin, C. A. Enzyme Mimics Based Upon Supramolecular Coordination Chemistry. *Angew. Chem. Int. Ed.* **2011,** 50 (1), 114-137.

6. Allgeier, A. M.; Mirkin, C. A. Ligand Design for Electrochemically Controlling Stoichiometric and Catalytic Reactivity of Transition Metals. *Angew. Chem. Int. Ed.* **1998,** 37 (7), 894-908.

7. Singewald, E. T.; Mirkin, C. A.; Stern, C. L. A Redox-Switchable Hemilabile Ligand: Electrochemical Control of the Coordination Environment of a RhI Complex. *Angew. Chem. Int. Ed.* **1995,** 34 (15), 1624-1627.

8. Plenio, H.; Diodone, R. METAL-COMPLEXES OF FERROCENE CRYPTANDS. *J. Organomet. Chem.* **1995,** 492 (1), 73-80.

9. Antonio Togni, T. H., *Ferrocenes: Homogeneous Catalysis, Organic Synthesis, Materials Science*. John Wiley & Sons: 2008.

10. Cheng, H. F.; d'Aquino, A. I.; Barroso-Flores, J.; Mirkin, C. A. A Redox-Switchable, Allosteric Coordination Complex. *J. Am. Chem. Soc.* **2018,** 140 (44), 14590-14594.

11. Teator, A. J.; Lastovickova, D. N.; Bielawski, C. W. Switchable Polymerization Catalysts. *Chem. Rev.* **2016,** 116 (4), 1969-1992.

12. Chen, C. Redox-Controlled Polymerization and Copolymerization. *ACS Cat.* **2018,** 8 (6), 5506-5514.

13. Leibfarth, F. A.; Mattson, K. M.; Fors, B. P.; Collins, H. A.; Hawker, C. J. External Regulation of Controlled Polymerizations. *Angew. Chem. Int. Ed.* **2013,** 52 (1), 199-210.

14. Pan, X.; Fantin, M.; Yuan, F.; Matyjaszewski, K. Externally controlled atom transfer radical polymerization. *Chem. Soc. Rev.* **2018,** 47 (14), 5457-5490.

15. Dadashi-Silab, S.; Doran, S.; Yagci, Y. Photoinduced Electron Transfer Reactions for Macromolecular Syntheses. *Chem. Rev.* **2016,** 116 (17), 10212-10275.

16. Konkolewicz, D.; Schröder, K.; Buback, J.; Bernhard, S.; Matyjaszewski, K. Visible Light and Sunlight Photoinduced ATRP with ppm of Cu Catalyst. *ACS Macro Lett.* **2012,** 1 (10), 1219-1223.

17. Pan, X.; Tasdelen, M. A.; Laun, J.; Junkers, T.; Yagci, Y.; Matyjaszewski, K. Photomediated controlled radical polymerization. *Prog. Polym. Sci.* **2016,** 62, 73-125.

18. Fors, B. P.; Hawker, C. J. Control of a Living Radical Polymerization of Methacrylates by Light. *Angew. Chem. Int. Ed.* **2012,** 51 (35), 8850-8853.

19. Chen, M.; Zhong, M.; Johnson, J. A. Light-Controlled Radical Polymerization: Mechanisms, Methods, and Applications. *Chem. Rev.* **2016,** 116 (17), 10167-10211.

20. Kottisch, V.; Supej, M. J.; Fors, B. P. Enhancing Temporal Control and Enabling Chain-End Modification in Photoregulated Cationic Polymerizations by Using Iridium-Based Catalysts. *Angew. Chem. Int. Ed.* **2018,** 57 (27), 8260-8264.

21. Corrigan, N.; Shanmugam, S.; Xu, J.; Boyer, C. Photocatalysis in organic and polymer synthesis. *Chem. Soc. Rev.* **2016,** 45 (22), 6165-6212.

22. Dadashi-Silab, S.; Pan, X.; Matyjaszewski, K. Photoinduced Iron-Catalyzed Atom Transfer Radical Polymerization with ppm Levels of Iron Catalyst under Blue Light Irradiation. *Macromolecules* **2017,** 50 (20), 7967-7977.

23. Wang, Z.; Pan, X.; Yan, J.; Dadashi-Silab, S.; Xie, G.; Zhang, J.; Wang, Z.; Xia, H.; Matyjaszewski, K. Temporal Control in Mechanically Controlled Atom Transfer Radical Polymerization Using Low ppm of Cu Catalyst. *ACS Macro Lett.* **2017,** 6 (5), 546-549.

24. Peterson, B. M.; Lin, S.; Fors, B. P. Electrochemically Controlled Cationic Polymerization of Vinyl Ethers. *J. Am. Chem. Soc.* **2018,** 140 (6), 2076-2079.

25. Qi, M.; Dong, Q.; Wang, D.; Byers, J. A. Electrochemically Switchable Ring-Opening Polymerization of Lactide and Cyclohexene Oxide. *J. Am. Chem. Soc.* **2018,** 140 (17), 5686-5690.

26. Yoon, H. J.; Kuwabara, J.; Kim, J.-H.; Mirkin, C. A. Allosteric Supramolecular Triple-Layer Catalysts. *Science* **2010,** 330 (6000), 66-69.

27. Peterson, B. M.; Kottisch, V.; Supej, M. J.; Fors, B. P. On Demand Switching of Polymerization Mechanism and Monomer Selectivity with Orthogonal Stimuli. *ACS Central Science* **2018,** 4 (9), 1228-1234.

28. Gregson, C. K. A.; Gibson, V. C.; Long, N. J.; Marshall, E. L.; Oxford, P. J.; White, A. J. P. Redox Control within Single-Site Polymerization Catalysts. *J. Am. Chem. Soc.* **2006,** 128 (23), 7410-7411.

29. Broderick, E. M.; Guo, N.; Wu, T.; Vogel, C. S.; Xu, C.; Sutter, J.; Miller, J. T.; Meyer, K.; Cantat, T.; Diaconescu, P. L. Redox control of a polymerization catalyst by changing the oxidation state of the metal center. *Chem. Commun.* **2011,** 47 (35), 9897-9899.

30. Broderick, E. M.; Guo, N.; Vogel, C. S.; Xu, C.; Sutter, J.; Miller, J. T.; Meyer, K.; Mehrkhodavandi, P.; Diaconescu, P. L. Redox Control of a Ring-Opening Polymerization Catalyst. *J. Am. Chem. Soc.* **2011,** 133 (24), 9278-9281.

31. Biernesser, A. B.; Li, B.; Byers, J. A. Redox-Controlled Polymerization of Lactide Catalyzed by Bis(imino)pyridine Iron Bis(alkoxide) Complexes. *J. Am. Chem. Soc.* **2013,** 135 (44), 16553-16560.

32. Wang, X.; Thevenon, A.; Brosmer, J. L.; Yu, I.; Khan, S. I.; Mehrkhodavandi, P.; Diaconescu, P. L. Redox Control of Group 4 Metal Ring-Opening Polymerization Activity toward l-Lactide and ε-Caprolactone. *J. Am. Chem. Soc.* **2014,** 136 (32), 11264-11267.

33. Brown, L. A.; Rhinehart, J. L.; Long, B. K. Effects of Ferrocenyl Proximity and Monomer Presence during Oxidation for the Redox-Switchable Polymerization of l-Lactide. *ACS Cat.* **2015,** 5 (10), 6057-6060.

34. Biernesser, A. B.; Delle Chiaie, K. R.; Curley, J. B.; Byers, J. A. Block Copolymerization of Lactide and an Epoxide Facilitated by a Redox Switchable Iron-Based Catalyst. *Angew. Chem. Int. Ed.* **2016,** 55 (17), 5251-5254.

35. Lastovickova, D. N.; Shao, H.; Lu, G.; Liu, P.; Bielawski, C. W. A Ring-Opening Metathesis Polymerization Catalyst That Exhibits Redox-Switchable Monomer Selectivities. *Chem. Eur. J.* **2017,** 23 (25), 5994-6000.

36. Wang, J.-S.; Matyjaszewski, K. Controlled/"living" radical polymerization. atom transfer radical polymerization in the presence of transition-metal complexes. *J. Am. Chem. Soc.* **1995,** 117 (20), 5614-5615.

37. Matyjaszewski, K.; Xia, J. Atom Transfer Radical Polymerization. *Chem. Rev.* **2001,** 101 (9), 2921-2990.

38. Matyjaszewski, K. Atom Transfer Radical Polymerization (ATRP): Current Status and Future Perspectives. *Macromolecules* **2012,** 45 (10), 4015-4039.

39. Matyjaszewski, K.; Jakubowski, W.; Min, K.; Tang, W.; Huang, J.; Braunecker, W. A.; Tsarevsky, N. V. Diminishing catalyst concentration in atom transfer radical polymerization with reducing agents. *Proc. Natl. Acad. Sci. U.S.A.* **2006,** 103 (42), 15309-15314.

40. Dadashi-Silab, S.; Matyjaszewski, K. Temporal Control in Atom Transfer Radical Polymerization Using Zerovalent Metals. *Macromolecules* **2018,** 51 (11), 4250-4258.

41. Ribelli, T. G.; Fantin, M.; Daran, J.-C.; Augustine, K. F.; Poli, R.; Matyjaszewski, K. Synthesis and Characterization of the Most Active Copper ATRP Catalyst Based on Tris[(4-dimethylaminopyridyl)methyl]amine. *J. Am. Chem. Soc.* **2018,** 140 (4), 1525-1534.

42. Lorandi, F.; Fantin, M.; Isse, A. A.; Gennaro, A. Electrochemical triggering and control of atom transfer radical polymerization. *Curr. Opin. Electrochem.* **2018,** 8, 1-7.

43. Chmielarz, P.; Fantin, M.; Park, S.; Isse, A. A.; Gennaro, A.; Magenau, A. J. D.; Sobkowiak, A.; Matyjaszewski, K. Electrochemically mediated atom transfer radical polymerization (eATRP). *Prog. Polym. Sci.* **2017,** 69, 47-78.

44. Fantin, M.; Isse, A. A.; Venzo, A.; Gennaro, A.; Matyjaszewski, K. Atom Transfer Radical Polymerization of Methacrylic Acid: A Won Challenge. *J. Am. Chem. Soc.* **2016,** 138 (23), 7216-7219.

45. Simakova, A.; Averick, S. E.; Konkolewicz, D.; Matyjaszewski, K. Aqueous ARGET ATRP. *Macromolecules* **2012,** 45 (16), 6371-6379.

46. Lorandi, F.; Fantin, M.; Isse, A. A.; Gennaro, A.; Matyjaszewski, K. New protocol to determine the equilibrium constant of atom transfer radical polymerization. *Electrochim. Acta* **2018,** 260, 648-655.

Chapter 3.   Dual Photoredox Catalysis in ATRP

3.1. Preface

Despite the advances and development of photoinduced ATRP in synthesis of well-defined polymers, the use of UV light may hamper its application in a wide range of areas. In this chapter, I developed dual photoredox catalytic systems where I used the visible or NIR light in promoting photoinduced ATRP systems. In the first section, I developed a heterogeneous, visible-light active photoredox catalyst comprised of conjugated microporous polymers of phenothiazine (PTZ-CMP) for generation of L/Cu^I activator species for mediating the ATRP process under green or red-light irradiation. I designed the photocatalyst by crosslinking of phenothiazine as a photo-catalytically active core with dimethoxy benzene as a crosslinker under Friedel-Crafts alkylation conditions. A heterogeneous network was generated that featured aromatic crosslinkers that extended conjugation and therefore resulted in shifting the network's absorption profile to longer wavelengths of the visible region.

We designed a dual photocatalytic system where the PTZ-CMP photocatalyst was used to generate L/Cu^I activators through photoinduced electron-hole charge transfer processes, and ppm levels of $CuBr_2$ (as low as 25 ppm) to provide excellent control over polymerization. Crosslinking the PTZ units through aromatic groups provides important features for the network such as being photocatalytically active under visible light (owed to the extended conjugation, as opposed to the monomeric PTZ precursor, which is active under UV light) as well as heterogeneity. The heterogeneous nature of the PTZ-CMP photoredox catalyst enabled easy separation as well as recycling in multiple cycles while retaining its photocatalytic efficiency. The photocatalyst could be recycled for more than six cycles in ATRP affording high photocatalytic efficiency and well-controlled polymers.

I and Professor Matyjaszewski designed the research, and I synthesized the heterogeneous photocatalyst, designed and carried out all the polymerization and control experiments and

———————————————————

UV-vis analyses, collected the data, and prepared the results. The network was characterized via diffuse reflectance UV-vis spectroscopy by Matthew J. DiTucci (PPG Industries), nitrogen sorption measurements by Mingkang Sun, and TEM analysis by Tong Liu. Dr. Francesca Lorandi performed the electrochemical analysis to confirm the photoredox process in the presence of the PTZ-CMP photocatalyst with the Cu complex used in ATRP. All collaborators contributed to the design of experiments, discussion and analysis of the results and preparation of the manuscript. Professor Matyjaszewski directed the research.

3.2. Conjugated Crosslinked Phenothiazines as Green or Red Light Heterogeneous Photocatalysts for Copper-Catalyzed Atom Transfer Radical Polymerization

3.2.1 Abstract

Using the power of light to drive controlled radical polymerizations has provided significant advances in synthesis of well-defined polymers. Photoinduced atom transfer radical polymerization (ATRP) systems often employ UV light to regenerate copper activator species to mediate the polymerization. Taking full advantage of long-wavelength visible light for ATRP would require developing appropriate photocatalytic systems that engage in photoinduced electron transfer processes with the ATRP components to generate activating species. Herein, we developed conjugated microporous polymers (CMP) as heterogeneous photocatalysts to exploit the power of visible light in promoting copper-catalyzed ATRP. The photocatalyst was designed by crosslinking phenothiazine (PTZ) as a photoactive core in the presence of dimethoxybenzene as a crosslinker via the Friedel-Crafts reaction. The resulting PTZ-CMP network showed photoactivity in the visible region due to the ex-tended conjugation throughout the network because of the aromatic groups connecting the PTZ units. Therefore, photoinduced copper-catalyzed ATRP was performed with CMPs that re-generated activator species under green or red light irradiation to start the ATRP process. This resulted in efficient polymerization of acrylate and methacrylate monomers with high conversion and well-controlled molecular weight. The heterogeneous nature of the photocatalyst enabled easy separation and efficient reusability in subsequent polymerizations.
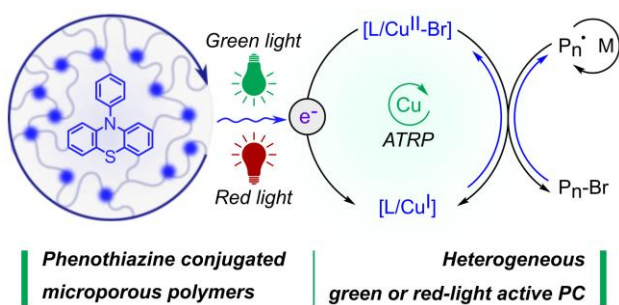
3.2.2 Introduction

Photochemistry is a powerful technique in synthesis of well-defined polymers that offers spatiotemporal control over the growth of polymer chains and fabrication of advanced polymer materials. A multitude of photocatalytic or photosensitization approaches have been developed to

convert the energy of light to promote new chemical reactivities that mediate controlled synthesis of well-defined polymers.[1-6] One possibility for conducting photoinduced polymerizations is *via* direct activation of polymer chains by electron/energy transfer from the excited state photocatalysts, which can also mediate the deactivation and control the polymerization process. For example, organo-catalyzed atom transfer radical polymerization (ATRP)[7, 8] or photoinduced electron/energy transfer radical or cationic reversible addition–fragmentation chain transfer (RAFT) polymerization systems[9, 10] employ photocatalysts to mediate the activation/deactivation of polymer chains. Alternatively, dual catalytic systems use a catalyst to control the polymerization process in the ground state which can be activated by photoinduced electron/energy transfer reactions in the presence of a photocatalyst. We envisioned that use of visible-light-active photocatalysts for activating Cu complexes that offer excellent control in ATRP[11, 12] would open new possibilities for modulating the catalytic reactivity and the polymerization process.

Although visible or near-infrared (NIR) light-active catalytic systems have been successfully applied in RAFT polymerizations,[13-18] the power of visible light in activating ATRP has not been fully explored. In photoinduced ATRP systems, UV light is used to generate L/Cu^I activator to start the polymerization.[19-24] Excitation of the Cu catalysts under UV light followed by a reductive quenching process in the presence of electron donors is suggested as a main pathway for generation of L/Cu^I activators. However, the use of UV light may not be desirable for special applications considering its high energy and low depth of penetration.

Using visible or NIR light in ATRP requires developing suitable photocatalysts or photosensitizers for generation of activating species. Under such dual catalytic systems, photoreduction of the L/Cu^{II}-Br catalyst via electron transfer events from the excited state photocatalyst generates L/Cu^I activator species to start the ATRP process.[25-27] Furthermore, activation of the chain ends by the excited state photocatalyst can provide additional pathways for generation of initiating radicals where control over polymerization can be achieved by the Cu catalysts. Recently, sensitization of the Cu catalyst by up-conversion nanoparticles that absorb NIR light and emit UV light for the excitation of the Cu catalyst has been reported in ATRP.[28] Visible or NIR light active photocatalysts have diverse structures and photophysical properties

(are colorful), but the presence of photoactive species may lead to potentially undesired side reactions.

Moreover, removal of these soluble compounds can often be challenging. Therefore, developing heterogeneous systems would offer the possibility of easy purification of the final product as well as the photocatalyst recycling. Immobilization of photocatalysts onto a heterogeneous support or a gel network was employed to design heterogeneous photocatalytic systems for controlled radical polymerization techniques.[29-34] In contrast, using photocatalysts as building blocks for construction of frameworks or polymeric networks offers the additional opportunity for tuning the photophysical and structural properties of the heterogeneous photocatalysts.[35-39] For example, synthesis of the catalyst network by crosslinking of a photo-catalytically active compound using linkages that extend conjugation throughout the network would alter the absorption profile of the network to longer wavelengths. Therefore, photocatalysis can be performed under longer wavelengths using conjugated microporous polymers (CMP) as photocatalysts.[40, 41]

In this paper, we developed a dual catalyst system comprising a CMP of phenothiazine (PTZ-CMP) as a heterogeneous photocatalyst and a Cu catalyst for mediating ATRP under green light irradiation. Phenothiazines have been previously used as homogeneous photocatalysts for organo-catalyzed ATRP to mediate the activation and deactivation processes during polymerization.[42-46] However, many PTZ compounds show photocatalytic activity under UV light and can provide moderate control over polymerization of a limited range of monomers such as methacrylates. Herein, we show that PTZ can be modified to form heterogeneous photocatalysts for ATRP of several acrylate and methacrylate monomers mediated by Cu complexes. The CMPs showed photocatalytic activity under green light irradiation. Crosslinking the PTZ units through aromatic linkages imparted extended conjugation within the network and therefore visible light activity. The ATRP activator species was generated by photoinduced redox reactions enabled by the heterogeneous photocatalyst to yield well-controlled polymerizations mediated by the ppm amounts of ATRP catalysts. Importantly, the heterogeneous nature of the photocatalyst provided easy separation and excellent reusability in further polymerizations without any decrease of photocatalytic efficiency.

3.2.3 Results and Discussion

Synthesis and characterization of the photocatalyst. Conjugated microporous polymers were synthesized using a Friedel-Crafts alkylation reaction between 10-phenylphenothiazine (Ph-PTZ) as a photocatalyst unit and dimethoxybenzene (DMB) as a crosslinker in the presence of iron(III) chloride to form a hypercrosslinked network (Figure 50-A and Figure 57).[47-49] In addition to yielding a heterogeneous photocatalyst, crosslinking through aromatic units provided extended conjugation throughout the network, therefore shifting its absorption profile to longer wavelengths. Solid-state diffuse reflectance UV-Vis spectra of PTZ-CMP showed absorption in the visible region extending to > 600 nm, which overlaps with the emission spectra of the green LEDs used for polymerization (520 nm) (Figure 50-B) The band gap energy of the photocatalyst was calculated to be $E_g = 2.23$ eV corresponding to ~556 nm (Figure 50-C). Nitrogen sorption isotherms shown in Figure 1-D revealed that the resulting PTZ-CMP possessed a high Brunauer–Emmett–Teller (BET) surface area of 526 m^2/g with an estimated pore size of 32.8 Å (Figure 58). The nitrogen adsorption-desorption isotherm showed a hysteresis loop at low relative pressures suggesting adsorption into mesopores.[50] Scanning electron microscopy (SEM) analysis revealed photocatalyst particles with micrometer dimensions and fused, mixed morphology (Figure 50-E andFigure 59).
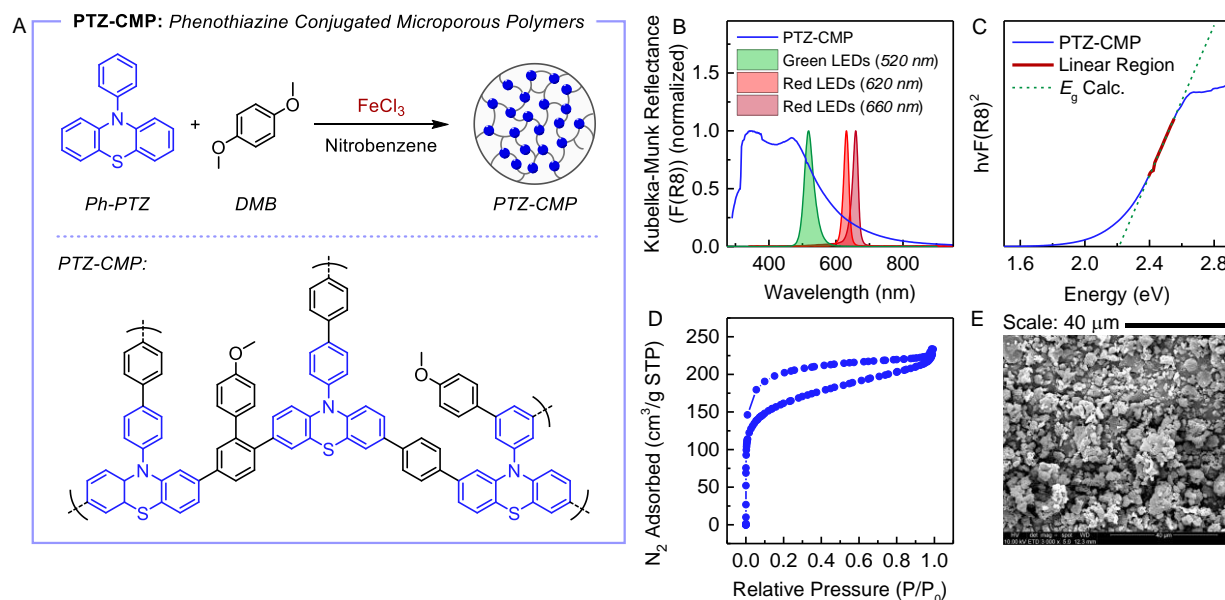
Figure 50. (A) Synthesis of phenothiazine-based conjugated microporous polymers (PTZ-CMP) by Friedel-Crafts alkylation between Ph-PTZ (1 equiv.) and

dimethoxybenzene (DMB, 8 equiv.) as a crosslinker in the presence of FeCl$_3$ (24 equiv.) in nitrobenzene. The reaction was heated at 80 °C for 4 h and then the temperature was increased to 120 °C for 20 h. Bottom-left: an idealized, representative structure of the crosslinked network. (B) UV-Vis diffuse reflectance spectra of the photocatalyst overlaid with the emission spectra of the light sources. (C) Tauc plot of transformed Kubelka-Munk reflectance as a function of the energy for PTZ-CMP. (D) Nitrogen sorption isotherms of BET surface area analysis of the PTZ-CMP polymers. (E) SEM image of the photocatalyst.

Cu-catalyzed ATRP using PTZ-CMP as a photocatalyst. The viability of the synthesized CMPs as a photocatalyst for ATRP was examined in activating Cu-catalyzed ATRP under green light irradiation (Scheme 10). Excitation of the PTZ-CMP photocatalyst results in separation of electron-hole charge carriers that can generate activating species upon reacting with the Cu catalyst and electron donors, respectively. The ATRP activator, L/Cu^I, can be generated by an electron transfer from the photocatalyst reducing L/Cu^{II}-Br to L/Cu^I. Furthermore, transfer of holes to amine electron donors (D) forms amine radical cation (D$^{\bullet+}$) species while also regenerating the initial ground state PTZ-CMP photocatalyst. Deprotonation of the amine radical cation may further proceed to generate α-aminoalkyl radicals (D$^{\bullet}$) that can reduce L/Cu^{II}-Br and generate the activator L/Cu^I catalyst.[51] Therefore, activating/initiating species can be formed through different pathways in the presence of the photocatalyst to start the ATRP process.
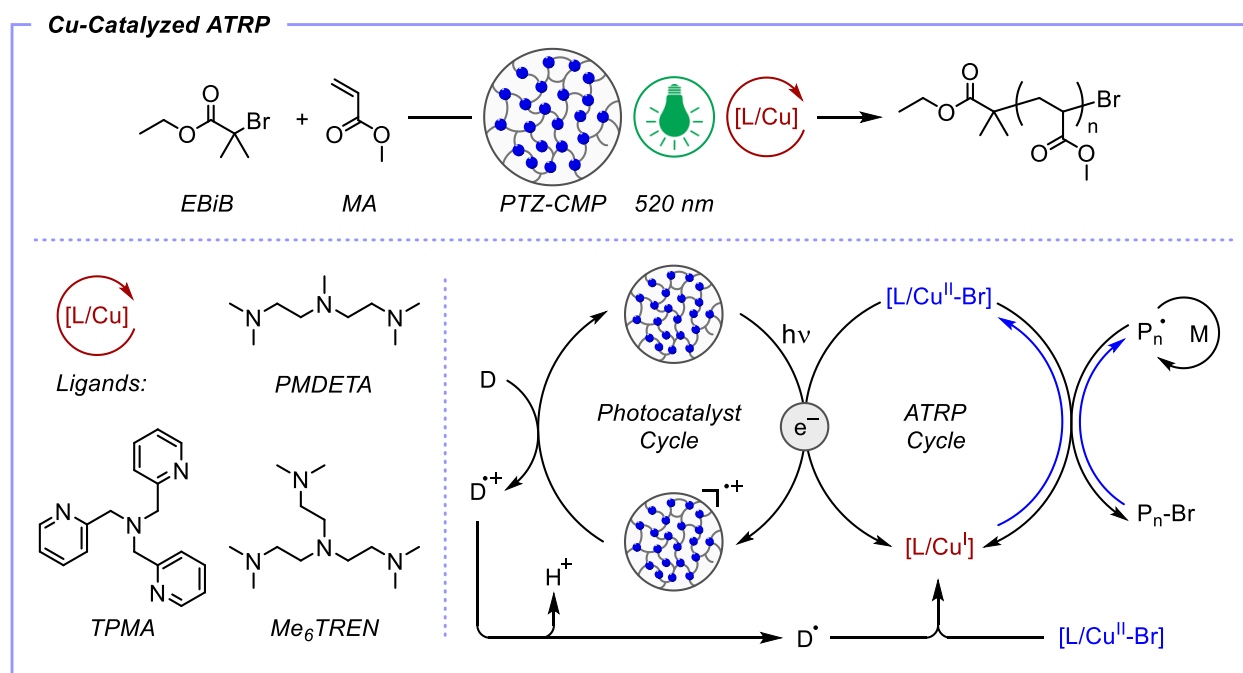
Scheme 10. Photoinduced copper-catalyzed ATRP in the presence of PTZ-CMP as a heterogeneous photocatalyst used to generate the L/Cu^I activator catalyst under green light irradiation in the presence of amine electron donors (D). Bottom left: structure of the ligands *N,N,N',N'',N''*-pentamethyldiethylenetriamine (PMDETA), tris(2-pyridylmethyl)amine (TPMA), and tris[2-(dimethylamino)ethyl]amine (Me$_6$TREN). Bottom-right: proposed mechanism for generation of ATRP activators via photoredox reactions in the presence of CMP-PTZ.

Generation of L/Cu^I activator was confirmed by electrochemical analysis of the catalytic system. A solution of $CuBr_2$ with PMDETA was irradiated under green light in the presence of the PTZ-CMP photocatalyst. Linear sweep voltammetry of the Cu catalyst showed increasing currents as a function of irradiation time. This increase in the current at positive potentials corresponds to generation of Cu^I during the photoreduction process (Figure 51-A). Kinetics of the photoreduction of $L/CuBr_2$ showed a linear semi-logarithmic behavior with a reduction rate constant (k_{red}) of 4.11×10^{-5} s^{-1} (Figure 51- B).
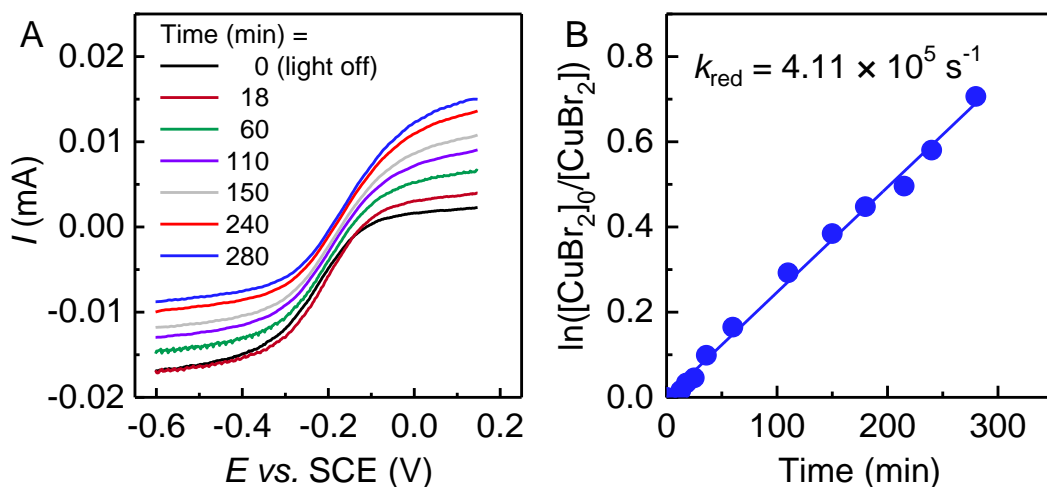
Figure 51. Photoreduction of the Cu catalyst monitored by linear sweep voltammetry (LSV) of CuBr2 with PMDETA showing the generation of CuI species by photoreduction in the presence of PTZ-CMP (2 mg/mL) under green light irradiation (520 nm, 9 mW/cm2) ([CuBr2] = 1.1 mM, PMDETA/CuBr2 = 5 in DMSO). The spectra were recorded on a rotating disk electrode (RDE) with a GC working electrode at v = 0.01 V/s and ω = 2500 rpm.

Polymerization of methyl acrylate (MA) was initially conducted using $CuBr_2$/PMDETA as the ATRP catalyst in dimethyl sulfoxide (DMSO) solvent in the presence of PTZ-CMP as the

photocatalyst under green light irradiation, with ethyl α-bromoisobutyrate (EBiB, 1 equiv.) as the initiator (Scheme 10 and Table 9). An excess of amine electron donor (PMDETA) was needed to start the polymerization. No monomer conversion was observed without excess of electron donor (i.e., $CuBr_2$/PMDETA = 1/1). However, increasing concentration of the ligand from 1 to 3, 5, and 7 equiv. (with respect to $CuBr_2$) resulted in increasing monomer conversion to near-quantitative values, yielding well-defined polymers with low dispersity ($Đ < 1.1$) and controlled molecular weights (Entries 1-4, Table 9). The concentration of PTZ-CMP could be decreased from 2 to 1 and 0.5 mg/mL (corresponding to 0.4, 0.2, and 0.1 wt% with respect to the monomer, respectively) while still providing efficient and well-controlled polymerization of MA with near-quantitative monomer conversions and polymers with low dispersities in all cases (Entries 5 and 6, Table 9) and narrow, monomodal molecular weight distributions (Figure S5). Importantly, no monomer conversion was obtained in the absence of PTZ-CMP or in the dark, signifying the importance of the photocatalyst for (re)generation of the activator species under green light irradiation (Entries 7 and 8, Table 9).

To demonstrate the versatility of this system for a wider range of ATRP catalysts, polymerization of MA was successfully performed in the presence of TPMA and Me_6TREN ligands, in solvents including DMSO, *N,N*-dimethylformamide (DMF) or acetonitrile (MeCN). For example, in the presence of TPMA ligand, polymerization of MA reached 94% conversion within 18 h, yielding polymers with controlled molecular weights (M_n = 17900, $Đ$ = 1.08; Entry 9, Table 9). A control experiment in the absence of the PTZ-CMP photocatalyst or in the dark showed no monomer conversion proving the critical role of the photocatalyst in activating the ATRP process (Entry 10, Table 9). Additionally, control experiments using Me_6TREN in the absence of PTZ-CMP showed no monomer conversion in DMF or MeCN under green light irradiation, indicating that no background reaction generated L/Cu^I activator to start the polymerization. However, polymerizations were successful in the presence of PTZ-CMP under green light irradiation reaching high monomer conversions and yielding polymers with low dispersity values ($Đ < 1.1$) and controlled molecular weights (Entries 11-14, Table 9). Size exclusion chromatography (SEC) analysis of the resultant polymers showed narrow, monomodal molecular weight distributions (Figure S6).

A control experiment performed using a CMP composed of only the dimethoxybenzene crosslinker (DMB-CMP) (without PTZ) proved the importance of the PTZ as a photocatalyst that allowed ATRP under green light. Although ATRP of MA using PTZ-CMP afforded full monomer conversions, DMB-CMP resulted in 48% conversion (M_n = 7100, $Đ$ = 1.06) after 18 h irradiated under green light. The conjugated nature of the DMB-CMP network may be responsible for initiating polymerization under green light.

Table 9. Results of ATRP of MA using PTZ-CMP photocatalyst in the presence of different ligands under green light irradiation [a]

Entry	Ligand	CuBr$_2$/L	PTZ-CMP (mg/mL)	Solvent	Conv. (%)	$M_{n,th}$	M_n	Đ
1	PMDETA	1/1	2	DMSO	0	-	-	-
2	PMDETA	1/3	2	DMSO	50	8700	8300	1.09
3	PMDETA	1/5	2	DMSO	98	17100	18600	1.08
4	PMDETA	1/7	2	DMSO	99	17300	18500	1.09
5	PMDETA	1/5	1	DMSO	98	17100	16700	1.10
6	PMDETA	1/5	0.5	DMSO	98	17100	17800	1.09
7	PMDETA	1/5	2 – in dark	DMSO	0	-	-	-
8	PMDETA	1/5	0	DMSO	0	-	-	-
9 b	TPMA	1/5 c	2	DMSO	94	16500	17900	1.08
10 b	TPMA	1/5 c	0 – in dark	DMSO	0	-	-	-
11 b	Me$_6$TREN	1/5	2	DMF	98	17100	18300	1.08
12 b	Me$_6$TREN	1/5	0	DMF	0	-	-	-
13 b	Me$_6$TREN	1/5	2	MeCN	94	16400	18000	1.07
14 b	Me$_6$TREN	1/5	0	MeCN	0	-	-	-

[a] Reaction conditions: [MA]/[EBiB]/[CuBr$_2$]/[L] = 200/1/0.04/x (L = PMDETA, TPMA, or Me$_6$TREN; x = 1, 3, 5, or 7; c triethanolamine (0.6 equiv. relative to EBiB) was used as the electron donor in the presence of TPMA) in different solvents (50 vol%) under green light irradiation (520 nm, 9 mW/cm^2) for 24 h. b Polymerizations run for 18 h.

ATRP under red light. The efficiency of the PTZ-CMP system was also studied in promoting ATRP under red light irradiation. Polymerization of MA was first conducted using PTZ-CMP under red light irradiation with PMDETA ligand in DMSO (Table 11 and Figure 62). The polymerizations were triggered to high conversions (84%) and well-controlled molecular weight properties only under strong red lights (660 nm, ~ 40 mW/cm^2). Using red LEDs with relatively low light intensity (630 nm, 4 mW/cm^2) did not provide monomer conversion after 24 h.

Similar results were obtained in the presence of Me$_6$TREN where no polymerization of MA was observed under the weak red LEDs (630 nm, 4 mW/cm^2). Using the red lamps with high intensity (660 nm, ~ 40 mW/cm^2), polymerization of MA gave 40% conversion with well-

controlled molecular weight and low dispersity. Importantly, with Me$_6$TREN ligand no monomer conversion was observed in the absence of the photocatalyst, indicating no generation of the L/Cu^I activator was realized under the red light.

Kinetics and temporal control of polymerization. Kinetics of the ATRP of MA in the presence of PMDETA ligand showed a short induction period < 2 h, after which the polymerization progressed with the apparent rate constant of k_p = 0.21 h^{-1}, similar to that observed in the presence of Me$_6$TREN ligand (k_p = 0.22 h^{-1}) (Figure 52-A). Molecular weights of the polymers increased as a function of monomer conversion in line with theoretical values, confirming high initiator efficiency and well-controlled polymerizations with low dispersity values (Figure 64Figure 52-B and Figure 64Figure 63).

Moreover, the polymerizations showed temporal control behavior in response to switching the light on/off. Polymerizations proceeded in the presence of light irradiation. Only negligible monomer conversion was observed after light was switched off due to the presence of small amounts of residual L/Cu^I activator, which could continue activation of the polymer chains (Figure 52-C).[52, 53] However, the L/Cu^I activator can be consumed via radical termination to convert to the deactivator L/Cu^{II}-Br. Consequently, polymerization stopped when the reaction was kept in the dark for consecutive 12 h (after initial 4 h of irradiation, Figure 52-D). The resulting polymers showed well-controlled properties through temporal control of the polymerization (Figure 64).
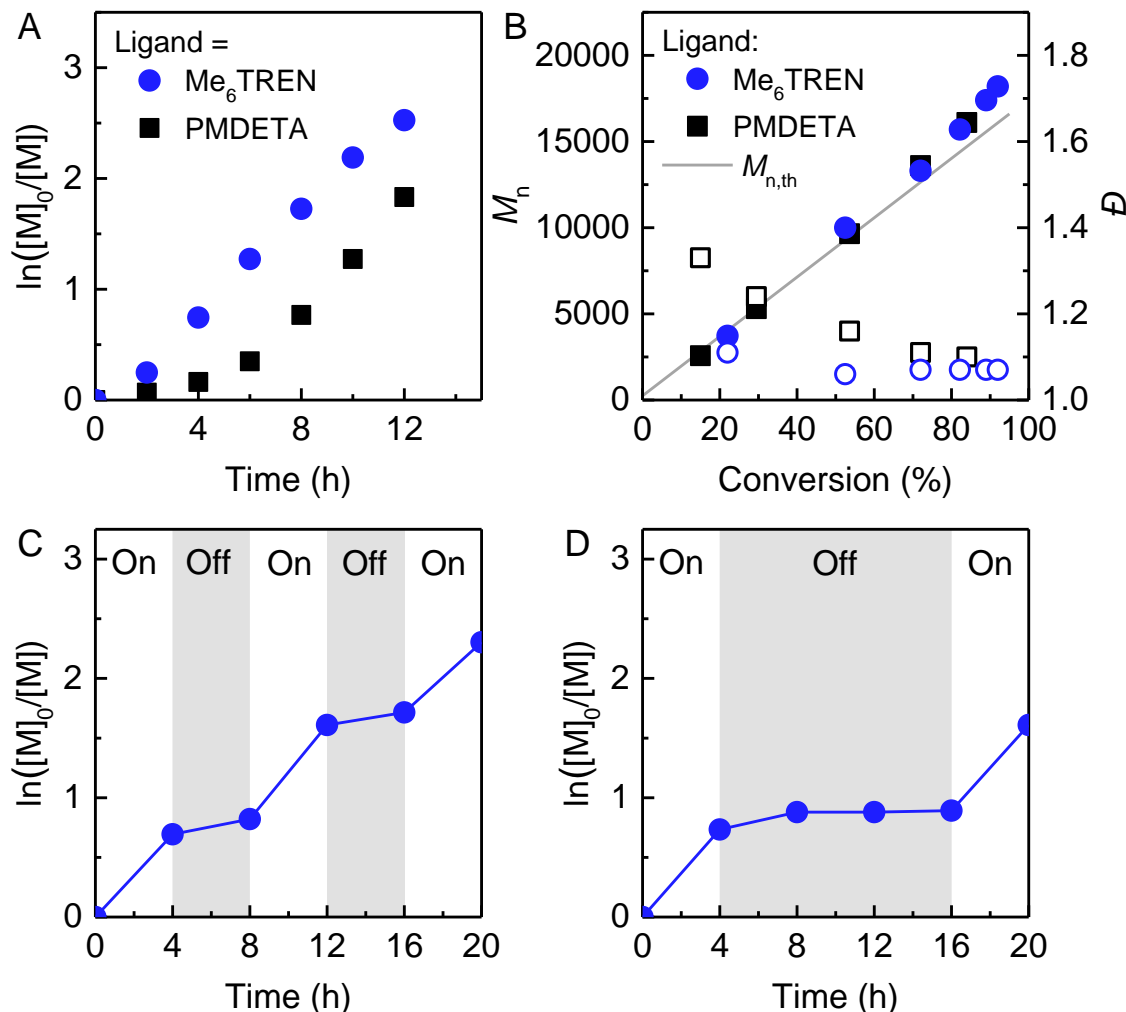
Figure 52. (A) Kinetics and (B) evolution of molecular weight (M_n, filled points) and dispersity ($Đ$, empty points) of the polymers as a function of monomer conversion in the ATRP of MA using PTZ-CMP photocatalyst with PMDETA or Me$_6$TREN ligands. (C) and (D) Temporal control in ATRP of MA upon intermittent switching green light on/off in the presence of Me$_6$TREN ligand. Reaction conditions: [MA]/[EBiB]/[CuBr$_2$]/[L] = 200/1/0.04/0.2, L = PMDETA or Me$_6$TREN in 50 vol% DMSO or MeCN, respectively, irradiated under green light LEDs (520 nm, 9 mW/cm^2).

Effect of the Cu catalyst. Control experiments conducted in the absence of the Cu catalysts showed its importance in providing controlled polymerizations. No conversion of MA was observed in the presence of only monomer or monomer with the EBiB initiator (both run in the

absence of $CuBr_2$ and PMDETA), indicating that under these conditions the excited state photocatalyst was unable to generate initiating radicals from the monomer/initiator (Entries 1 and 2, Table 12). However, in the presence of PMDETA (without additional CuBr2), fast and uncontrolled polymerization of MA was observed under free radical polymerization conditions because of the formation of initiating radicals from PMDETA (Entry 3, Table 12). Conversely, polymerizations were successful and controlled only in the presence of both excess electron donor and the Cu catalyst to facilitate photocatalysis and control the growth of polymer chains (Entries 4 and 5, Table 12). These results indicate the importance of all polymerization components, including the photocatalyst, electron-donors, and the Cu catalyst in initiating and affording well-controlled ATRP under green light.

To further examine the effect of the Cu catalyst, ATRP of MA was performed by decreasing concentration of $CuBr_2$ (Table 10). In the presence of 0.005 equiv. (with respect to initiator or 25 ppm with respect to monomer) of initially added $CuBr_2$ with 0.2 equiv. of PMDETA, fast polymerization of MA was observed that gave 94% monomer conversion in < 4 h showing a high dispersity of 2.06 (Entry 1, Table 10). Increasing concentration of $CuBr_2$ resulted in a decrease in the rate of polymerization but afforded well-controlled polymers with low dispersity values. For example, in the presence of 0.01 or 0.02 equiv. (50 or 100 ppm, respectively) of $CuBr_2$, the resultant polymers showed moderate dispersity of 1.34 and 1.13, respectively (Entries 2 and 3, Table 10). Further increasing the catalyst concentration to 200 ppm provided even better control with a lower dispersity of 1.08 (Entry 4, Table 10). SEC traces of the resulting polymers showed monomodal distribution of molecular weights, broadened as the concentration of the $CuBr_2$/PMDETA catalyst was decreased from 200 to 25 ppm (Figure 65).

Table 10. Polymerization of MA synthesized using heterogeneous PTZ-CMP photocatalyst in the presence of low concentrations of the Cu catalyst [a]

Entry	CuBr$_2$ (equiv.)	Ligand	Solvent	Time (h)	Conv. (%)	$M_{n,th}$	M_n	Đ
1	0.005	PMDETA	DMSO	4	94	16400	20200	2.06
2	0.01	PMDETA	DMSO	4	89	15800	17600	1.34
3	0.02	PMDETA	DMSO	24	99	17300	18600	1.13
4	0.04	PMDETA	DMSO	24	98	17100	18600	1.08
5	0.005	Me$_6$TREN	MeCN	18	98	17100	20700	1.11
6	0.01	Me$_6$TREN	MeCN	18	97	17000	18800	1.09
7	0.02	Me$_6$TREN	MeCN	18	97	17000	20300	1.08
8	0.04	Me$_6$TREN	MeCN	18	94	16400	18000	1.07

[a] Reaction conditions: [MA]/[EBiB]/[CuBr$_2$]/[L] = 200/1/x/0.2 (L = PMDETA or Me$_6$TREN and x = 0.04, 0.02, 0.01, and 0.005 equiv. with respect to initiator corresponding to 200, 100, 50, and 25 ppm with respect to monomer) in 50 vol% solvent under green light irradiation (520 nm, 9 mW/cm^2).

Because of the low activity of the Cu catalyst in the presence of PMDETA, not enough L/Cu^{II}-Br deactivator is present to ensure efficient deactivation of polymer chains at low catalyst concentrations.[54, 55] However, increasing the activity of the Cu catalyst by changing the ligand from PMDETA to Me$_6$TREN results in a higher concentration of the deactivator at the ATR. Therefore, well-controlled polymerizations can be achieved even at lower ppm concentration of the Cu catalyst. For example, good control over the polymerization of MA was achieved with 25 ppm of CuBr$_2$/Me$_6$TREN yielding a PMA with low dispersity of 1.11 (Entries 5-8, Table 10).

Heterogeneous and visible-light photocatalytic activity of PTZ-CMP. The conjugated nature of the heterogeneous network was important for enabling photocatalysis under green light irradiation for activating Cu-catalyzed ATRP. Additional control experiments conducted using the filtrates of the dispersion of PTZ-CMP in various solvents proved the heterogeneous nature of the photocatalytic process and the importance of the conjugated network to enable photocatalysis under green light irradiation. To confirm this feature, a dispersion of PTZ-CMP in solvents such as DMSO, DMF, or MeCN (2 mg/mL of PTZ-CMP) was stirred for 24 h and then filtered through syringe filters to remove the heterogeneous parts. The transparent filtrate

solutions were analyzed by UV-Vis spectroscopy that showed absorption in the UV region < 400 nm (Figure S11). These absorption peaks may be due to the presence of monomeric/oligomeric photocatalyst units that can dissolve in the solvents. The soluble parts were estimated to account for about < 0.5 wt.% of the total network. Moreover, the filtrates were used as solvents to examine the activity of the species dissolved from the network in ATRP under green light irradiation in the presence of Cu catalysts with PMDETA or Me_6TREN ligands. However, no polymerization of MA was observed after 24 h of irradiation in all solutions and regardless of the ligand. These results indicate that the small amount of soluble parts present in the filtrates did not promote photocatalysis to start the ATRP process (Table 13). Considering the very low concentration of the soluble parts and their absorption in the UV region, the conjugated nature of the heterogeneous photocatalyst sheets was essential for inducing photocatalysis under green light irradiation and well-controlled polymerizations.

The heterogeneous CMP photocatalysts were synthesized using Ph-PTZ, which shows absorption profile below 400 nm in the monomeric form. To further confirm the important role of the CMPs as visible light active photocatalysts, ATRP of MA was attempted using the monomeric Ph-PTZ photocatalyst under green light irradiation. However, no polymerization of MA was observed in the presence of $CuBr_2$ and PMDETA, indicating lack of photocatalytic activity of Ph-PTZ under green light irradiation as it absorbs in the UV region (Figure 67). Therefore, the conjugated nature of the catalyst is key for altering the photophysical properties of the photocatalyst to extend its absorption profile to longer wavelengths. As a result of this photocatalytic activity under green light irradiation, CMPs can be used to generate activating species for ATRP.

Reusability. An important feature of the heterogeneous PTZ- CMP photocatalyst was the ability to be easily separated from the reaction mixture and reused in multiple ATRP cycles while retaining its high photocatalytic efficiency. Recycling the PTZ-CMP photocatalyst enabled successive ATRP of MA conducted in the presence of $CuBr_2$/Me_6TREN catalyst in MeCN. After each polymerization cycle, the photocatalyst was separated by centrifugation and washed with MeCN multiple times and dried before using in the next cycle. Near-quantitative monomer conversions and polymers with well-controlled molecular weights and low dispersity values

were obtained over six cycles with no decrease in the photocatalyst's performance (Figure 53 and Figure 68).
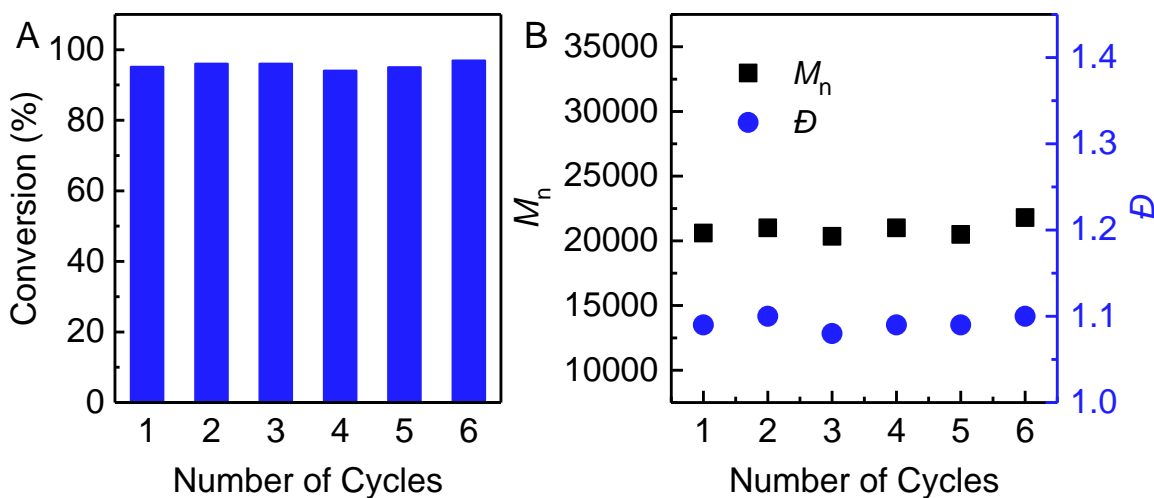
Figure 53. Recycling PTZ-CMP as a photocatalyst in ATRP of MA showing retention of photocatalytic activity over multiple cycles. (A) Monomer conversion and (B) molecular weight (M_n, squares) and dispersity (Đ, circles) of the resulting polymers in recycling experiments. Reaction conditions: [MA]/[EBiB]/[CuBr$_2$]/ [Me$_6$TREN] = 200/1/0.04/0.2 in MeCN (50 vol%) under green light irradiation (520 nm, 9 mW/cm^2), PTZ-CMP = 2 mg/mL.

Monomer scope and copolymerization. Polymerization of a variety of acrylate monomers was successfully initiated and controlled in the presence of PTZ-CMP and CuBr$_2$/Me$_6$TREN as the catalyst under green light irradiation. Monomers such as n-butyl acrylate (BA), (2-methoxyethyl) acrylate (MEA), and 2,2,2-trifluoroethyl acrylate (TFEA) were polymerized to high conversions, yielding polymers with controlled molecular weight and dispersity values < 1.1 (Figure 54-A). Furthermore, chain extension experiments revealed high chain end fidelity of the resulting polymers to enable synthesis of diblock copolymers. A poly(*n*-butyl acrylate) (PBA) macroinitiator was initially synthesized with controlled molecular weight and low dispersity of 1.08 (M_n = 7400, monomer conversion > 90%). The second monomer, MEA, was added in situ to generate the second block. SEC traces of the block copolymer showed a clear shift of the molecular weight distribution to higher values (M_n = 29100 and Đ = 1.11), indicating high retention of chain end fidelity of the polymers (Figure 54-B).
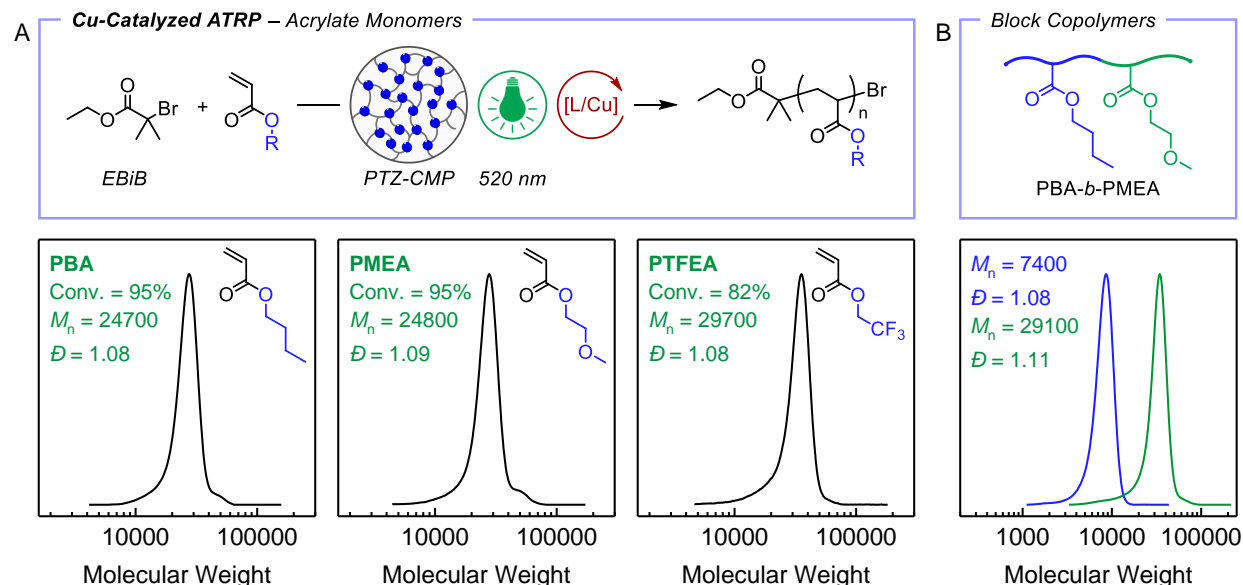
Figure 54. (A) Results of ATRP of acrylate monomers (BA, MEA, and TFEA) and (B) *in situ* block copolymerization experiments using PTZ-CMP photocatalyst. Reaction conditions: $[M]/[EBiB]/[CuBr_2]/[Me_6TREN] = 200/1/0.04/0.2$ in MeCN (50 vol%) under green light irradiation (520 nm, 9 mW/cm^2), PTZ-CMP = 2 mg/mL. (B) SEC traces of PBA macroinitiator (in blue) and PBA-*b*-PMEA block copolymer (in green) upon *in situ* chain extension showing high chain-end fidelity and successful chain extension.

Additionally, polymerization of methyl methacrylate (MMA) was conducted in the presence and absence of the Cu catalyst to study whether PTZ-CMP has similar effects on control of the ATRP of a methacrylate monomer (Figure 6). In the presence of CuBr$_2$/PMDETA and ethyl α-bromophenylacetate (EBPA) as the initiator, ATRP of MMA afforded polymers with controlled molecular weights and low dispersity values (Figure 55-A and B and Figure 69). The rate of the polymerization increased as the concentration of the electron donor (excess PMDETA) was increased (Figure 55-A). However, no monomer conversion was observed in the absence of the Cu catalyst and the ligand. These results indicate that under low energy green light irradiation, the PTZ-CMP acted as a photo-catalyst to selectively reduce L/Cu^{II}-Br as opposed to activation of the EBPA initiator, which has a more negative reduction potential than the Cu catalyst. Therefore, no supplemental activation was feasible with the heterogeneous photocatalyst when irradiated under green light. Using a Cu catalyst that can engage with the photo-catalyst to

generate activating/deactivating species can afford well-controlled polymerization of methacrylate monomers with high efficiency.
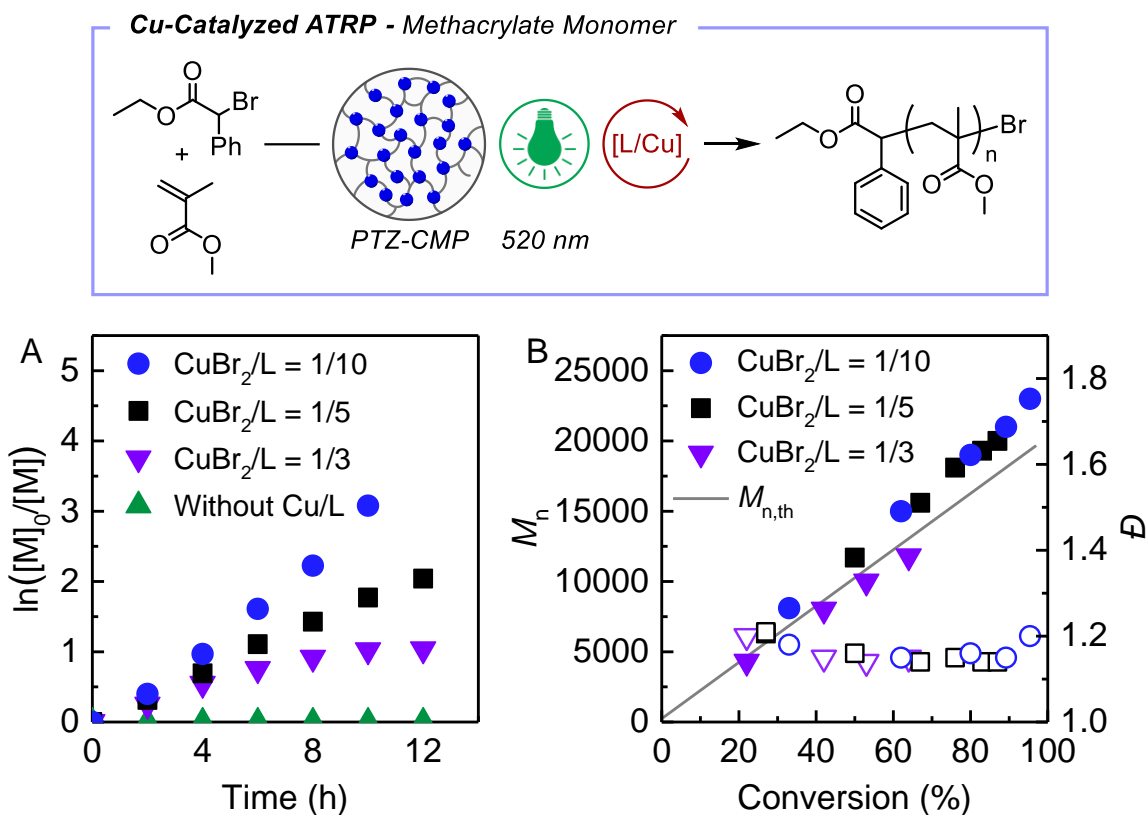
Figure 55. ATRP of methyl methacrylate (MMA) using PTZ-CMP as a photocatalyst in the presence or absence of the Cu catalyst using different concentrations of excess PMDETA ligand as electron donor: (A) kinetics of polymerization and (B) molecular weight (M_n, solid points) and dispersity ($Đ$, empty points) of the resulting polymers as a function of monomer conversion. Reaction conditions: [MMA]/[EBPA]/[CuBr$_2$]/[PMDETA] = 200/1/0.04/x (x = 0.12, 0.2, or 0.4) in DMSO (50 vol%) under green light irradiation (520 nm, 9 mW/cm^2), PTZ-CMP = 2 mg/mL.

3.2.4 Conclusions

In summary, we developed conjugated microporous polymers of phenothiazine as a heterogeneous photocatalyst to activate Cu-catalyzed ATRP under green light irradiation. The conjugated nature of the heterogeneous photocatalyst enabled photocatalysis under green or red-light irradiation. The activator species for ATRP was generated by photoredox reactions of the photocatalyst with the Cu complexes and electron donors. The use of a Cu catalyst enabled

control-ling polymerizations of acrylate and methacrylate monomers with high efficiency to yield near-quantitative monomer conversions and polymers with controlled molecular weights and low dispersity values. The heterogeneous nature of the photocatalyst allowed easy separation and reuse in multiple cycles with retention of high photocatalytic efficiency. As presented in this paper, designing new photocatalytic systems to promote ATRP under visible or NIR light irradiation provides new opportunities in advancing photoinduced ATRP systems. Regarding heterogeneous photocatalysis, developing strategies to further control the physical, structural, and photochemical properties of the photocatalyst networks would enable efficient photocatalysis applicable for a wide range of controlled polymerization systems.

3.2.5   Experimental Section and Supporting Information

Materials

Phenothiazine (PTZ; Sigma-Aldrich, 98%), bromobenzene (TCI, 99%), RuPhos (2-dcyclohexylphosphino-2',6'-diisopropoxybiphenyl; Sigma-Aldrich, 95%), RuPhos Pd G2 (chloro(2-dicyclohexylphosphino-2',6'-diisopropoxy-1,1'-biphenyl)[2-(2'-amino-1,1'-biphenyl)] palladium(II); Sigma-Aldrich) were used as received. Methyl acrylate (MA; Sigma-Aldrich, 99%), *n*-butyl acrylate (BA; Acros Organics, 99%), (2-methoxyethyl) acrylate (MEA; TCI, > 98.0), 2,2,2-trifluoroethyl acrylate (TFEA; TCI, >98.0), and methyl methacrylate (MMA, Sigma-Aldrich, 99%) were passed through a column of basic alumina to remove polymerization inhibitor prior to use. Ethyl α-bromoisobutyrate (EBiB; Sigma-Aldrich, 98%), ethyl α-bromophenylacetate (EBPA; Sigma-Aldrich, 97%), *N,N,N',N'',N''*-pentamethyldiethylenetriamine (PMDETA; Sigma-Aldrich, 98%), tris(2-pyridylmethyl)amine (TPMA; AmBeed), copper(II) bromide (CuBr$_2$; Sigma-Aldrich, 99%), iron(III) chloride (FeCl$_3$, anhydrous; Sigma-Aldrich, 97%), dimethyl sulfoxide (DMSO), *N,N*-dimethylformamide (DMF), and acetonitrile (MeCN), dioxane (anhydrous), and nitrobenzene were used as received. Tris[2-(dimethylamino)ethyl]amine (Me$_6$TREN) was received from Koei Chemical Co., Ltd. (Japan).

Instrumentation

^{1}H nuclear magnetic resonance (^{1}H NMR) measurements were performed on a Bruker Avance™ III 500 MHz spectrometer. Molecular weight properties of the polymers were determined by size-exclusion chromatography (SEC). The SEC instrument was equipped with a Waters 515

pump and a Waters 2414 differential refractometer using PSS columns (SDV 10^5, 10^3, and 500 Å) with THF as eluent at 35 °C and a flow rate of 1 mL min^{-1}. Linear poly(methyl methacrylate) standards were used for calibration.

Nitrogen sorption was conducted using a Nava 3200e porosity and surface analyzer. The samples were heated in vacuum at 120 °C overnight (16 h) prior to N_2 sorption analysis in 77 K. The Brunauer-Emmett-Teller (BET) method was used to determine the surface area. The pore size distribution was calculated using the Barrett-Joyner-Halenda (BJH) method.

Scanning electron microscope (SEM) was performed for microstructural investigation and conducted on a Quanta 600 FEG instrument. Samples for SEM characterization were prepared by distributing the photocatalyst powder onto electrical tape substrate.

The electrochemical analysis was performed in a 7-neck electrochemical cell, equipped with a 3-electrode system, and connected to an Autolab PGSTAT302N potentiostat/galvanostat (Metrohm) run by a PC with NOVA 2.0 software. The 3-electrode system composed of: i) a Pt foil counter electrode; ii) a saturated calomel electrode (SCE) as reference electrode; iii) a glassy carbon (GC) disk tip (3 mm dia., Metrohm), connected to a rotating disk electrode (RDE) system, as working electrode. Before each experiment, the GC disk was cleaned by polishing with a 0.25-μm diamond paste, followed by ultrasonic rinsing in ethanol for 5 min. The electrochemical cell was placed at the center of a green LED photoreactor. The analyses were performed under inert atmosphere (N_2). An initial cyclic voltammetry of the sole PTZ-CMP photocatalyst in DMSO as solvent and 0.1 M Et_4NBF_4 as supporting electrolyte was recorded. No signal corresponding to redox processes involving the photocatalysts could be observed in the electrochemical window. Subsequently, $CuBr_2$ and PMDETA (L/Cu = 6) were added into the system and an initial linear sweep voltammetry (LSV) was recorded. Then, the light was turned on consecutive LSVs were recorded to monitor the evolution in the currents corresponding to the Cu complex.

Diffuse reflectance UV-Vis-NIR spectra were acquired using a Perkin Elmer Lambda 950 spectrophotometer with 150 mm integration sphere and specular port removed. $BaSO_4$ (Bafine BF-20, KOWA American Corp.) was pressed into an 8 mm depth, 2.5 cm diameter powder plate and used as the 100 %R reference in all measurements. Neat PTZ-CMP was prepared over the $BaSO_4$ surface in triplicate with increasing mass from 10, 20, and 30 mg to evaluate and ensure onset of a pseudo-infinite medium for reflectance. Spectra were transformed to Kubelka-Munk,

F(R_{inf}), values and used in generation of Tauc plots (resulting in $(hvF(R_{inf}))^{1/n}$ vs. hv and assuming the PTZ-CMP electronic transition is *direct allowed*, $n = \frac{1}{2}$). Inflection points at ~2.4 eV were identified *via* first derivatives and used to define the onset of linearity. Fitting this linear region to evaluate intersection of the abscissa for each spectrum resulted in an average band gap energy, $E_g = 2.23$ +/- 0.02 eV (~556 nm).

Polymerizations were irradiated under green ($\lambda_{max} = 520$ nm, 9 mW/cm^2) and red ($\lambda_{max} = 630$ nm, 4 mW/cm^2) LEDs purchased from aspectLED or red LED lamps (powerPAR, $\lambda_{max} = 660$ nm, 40 mW/cm^2). The LED strips were mounted inside a glass container (diameter = 9 cm, height = 7 cm) and a cooling fan was used during polymerization to maintain the reactions at room temperature.

Synthetic procedures

Synthesis of Ph-PTZ

Phenothiazine (5 g, 25 mmol, 1 equiv.), RuPhos (467.5 mg, 4 mol%), RuPhos Pd G2 (777 mg, 4 mol%), and KtBuO (5.62 g, 2 equiv.) were charged into a Schlenk flask equipped with a stirrer bar. The flask was subject to vacuum and backfilling with nitrogen for 5 times. Anhydrous dioxane (20 mL) was added to the reaction and the flask was placed in an oil bath at 110 °C overnight. The reaction was cooled to room temperature, diluted with dichloromethane, and washed with water and brine and dried over sodium sulfate. The content was further purified by column chromatography (EtOAc/hexanes = 5/95) to yield 4.9 g of the product in 75% yield. ^{1}H NMR (500 MHz, CDCl$_3$) δ: 7.62 (t, 2H), 7.49 (t, 1H), 7.41 (d, 2H), 7.03 (d, 2H), 6.87-6.80 (m, 4H), 6.21 (d, 2 H) ppm (Figure S15).

Synthesis of PTZ-CMP

Ph-PTZ (200 mg, 0.72 mmol, 1 equiv.), dimethoxybenzene (800 mg, 5.76 mmol, 8 equiv.), and FeCl$_3$ (2.8 g, 17.28 mmol, 24 equiv.) were charged into a Schlenk flask followed by addition of nitrobenzene under nitrogen atmosphere. The flask was placed in an oil bath and was heated at 80 °C for 4 h after which the temperature was increased to 120 °C to allow complete formation of the network for 20 h. After the reaction, the precipitate was extensively washed with acetone, THF, and methanol until the filtrate became clear. The network was further washed by stirring the dispersion in DMSO, DMF, and MeCN multiple times overnight. Finally, the network was

filtered and allowed to dry under vacuum to yield ~470 mg of the PTZ-CMP in dark brown color.

General procedure for photoinduced ATRP using PTZ-CMP

The photocatalyst PTZ-CMP (1-4 mg) was added to a 2-dram reaction vial. The vial equipped with a magnet bar was sealed with a rubber septum and subjected to vacuum and backfilled with nitrogen for 5 times. In separate vials, DMSO and MA were degassed with nitrogen for 30 min. Under nitrogen atmosphere, DMSO (1 mL), and a stock solution of $CuBr_2$ (0.5 mg, 2.2 µmol, 0.04 equiv.), and PMDETA (2.3 µL, 11 µmol, 0.2 equiv.) in DMSO (50 µL) was added followed by the addition of MA (1 mL, 11.1 mmol, 200 equiv.) and EBiB (8.14 µL, 55.5 µmol, 1 equiv.) under nitrogen. The vial was degassed further with nitrogen for 2 min and was then irradiated under green LEDs to start the polymerization. Samples were taken periodically and analyzed by ^{1}H NMR and SEC to determine the monomer conversion and molecular weight properties, respectively.

Procedure for photoinduced ATRP of MMA using PTZ-CMP

The photocatalyst PTZ-CMP (8 mg) was added to a 2-dram reaction vial. The vial equipped with a magnet bar was sealed with a rubber septum and subjected to vacuum and backfilled with nitrogen for 5 times. In separate vials, DMSO and MMA were degassed with nitrogen for 30 min. Under nitrogen atmosphere, DMSO (2 mL), and a stock solution of $CuBr_2$ (0.84 mg, 3.7 µmol, 0.04 equiv.), and PMDETA (3.92 µL, 18.8 µmol, 0.2 equiv.) in DMSO (50 µL) was added followed by the addition of MMA (2 mL, 18.8 mmol, 200 equiv.) and EBPA (16.4 µL, 94 µmol, 1 equiv.) under nitrogen. The vial was degassed further with nitrogen for 2 min and was then irradiated under green LEDs to start the polymerization. Samples were taken periodically and analyzed by ^{1}H NMR and SEC to determine the monomer conversion and molecular weight properties, respectively.

Procedure for recycling the PTZ-CMP photocatalyst

The photocatalyst PTZ-CMP (4 mg) was added to a 2-dram reaction vial. The vial equipped with a magnet bar was sealed with a rubber septum and subjected to vacuum and backfilled with nitrogen for 5 times. In separate vials, MeCN and MA were degassed with nitrogen for 30 min. Under nitrogen atmosphere, MeCN (1 mL), and a stock solution of $CuBr_2$ (0.5 mg, 2.2 µmol,

0.04 equiv.), and Me$_6$TREN (3 µL, 11 µmol, 0.2 equiv.) in MeCN (50 µL) was added followed by the addition of MA (1 mL, 11.1 mmol, 200 equiv.) and EBiB (8.14 µL, 55.5 µmol, 1 equiv.) under nitrogen. The vial was degassed further with nitrogen for 2 min and was then irradiated under green LEDs to start the polymerization. After 18 h, samples were analyzed by ^{1}H NMR and SEC to determine the monomer conversion and molecular weight properties, respectively. The mixture was diluted by adding 8 mL of MeCN and the photocatalyst was separated by centrifugation. The photocatalyst was thoroughly washed with MeCN and separated by centrifugation for 5 times and dried before use in the next cycle. A fresh solution of CuBr$_2$/Me$_6$TREN was used in each cycle.
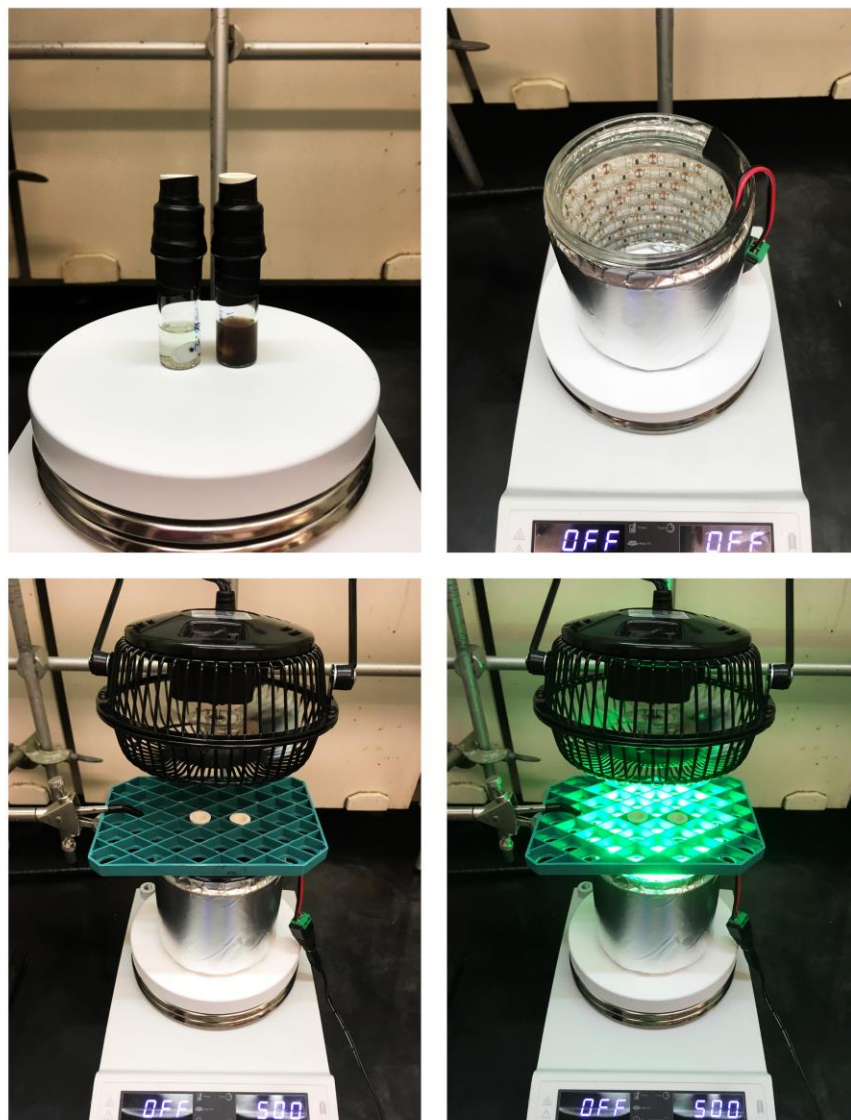
Figure 56. Photoreactor setup used in polymerization reactions. Top-left: pictures of polymerization reactions with (right vial) and without (left vial) the PTZ-CMP photocatalyst. Top-right: picture of the photoreactor with green LED strips installed inside a glass container. Bottom: reaction vials irradiated under green the green light with a colling fan placed on top to maintain the reaction at room temperature.
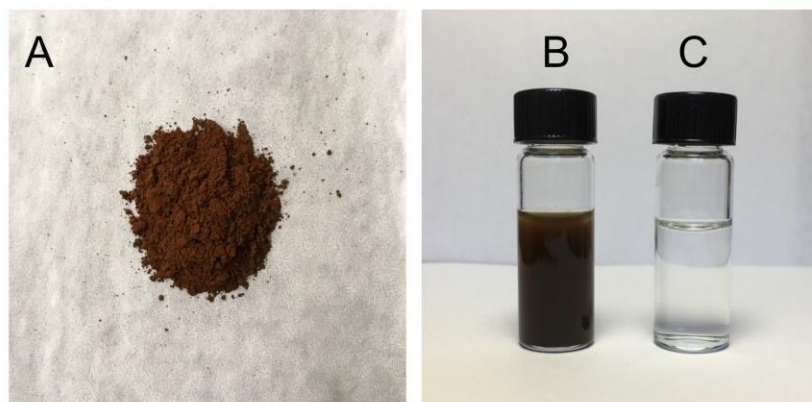
Figure 57. Images of PTZ-CMP in (A) powder form, (B) dispersed in MeCN, and (C) after filtration of the dispersion in MeCN through syringe filters.
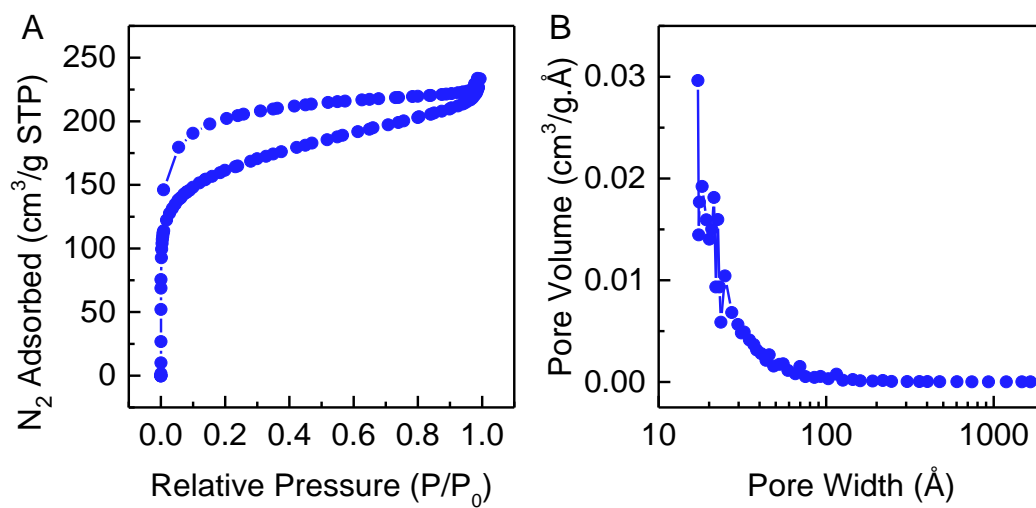
Figure 58. Nitrogen sorption isotherms of BET surface area analysis of the PTZ-CMP polymers and (C) corresponding pore size distribution.
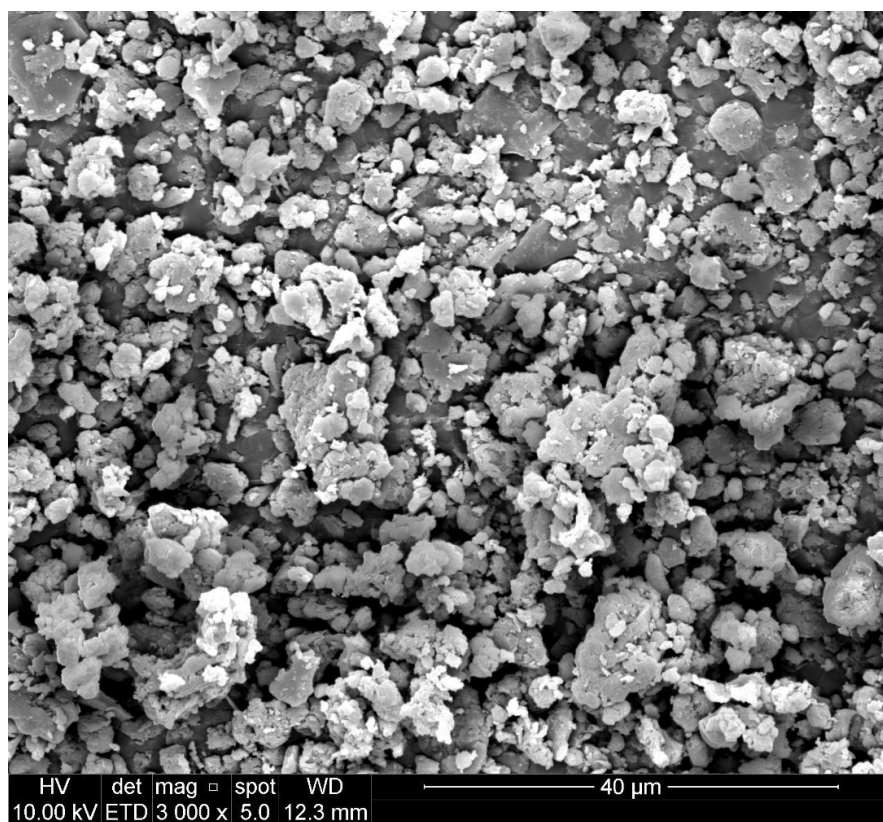
Figure 59. SEM image of the PTZ-CMP photocatalyst.
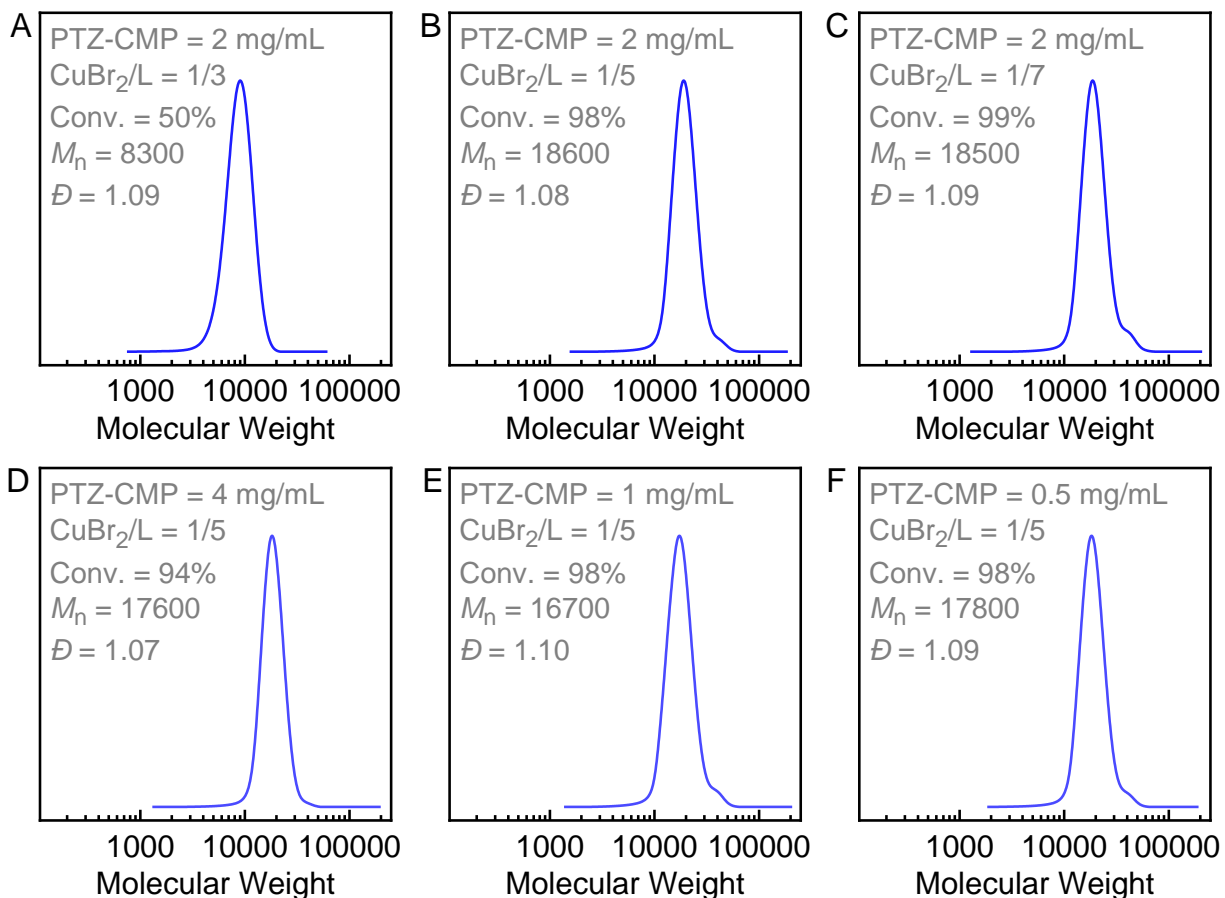
Figure 60. SEC traces of PMA synthesized using PTZ-CMP as a heterogeneous photocatalyst showing the effect of increasing concentration of the excess ligand or the photocatalyst. Conditions: [MA]/[EBiB]/[CuBr$_2$]/[PMDETA] = 200/1/0.04/x (x = 0.12, 0.20, or 0.28) in DMSO (50 vol%), PTZ-CMP = 0.5, 2, or 4 mg/mL irradiated under green light for 24 h.
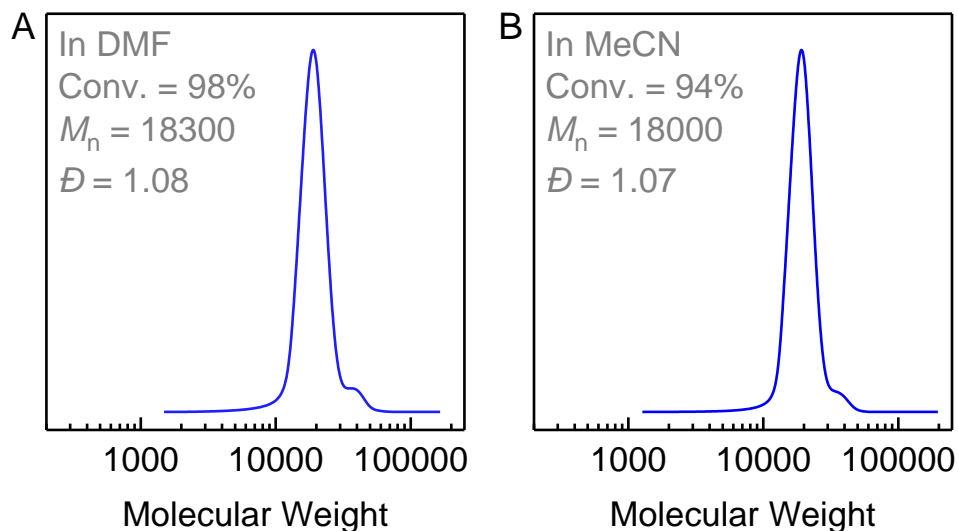
Figure 61. SEC traces of PMA synthesized using PTZ-CMP as a heterogeneous photocatalyst in DMF or MeCN. Reaction conditions: $[MA]/[EBiB]/[CuBr_2]/[Me_6TREN] = 200/1/0.04/0.2$ in DMF or MeCN (50 vol%), PTZ-CMP = 2 mg/mL irradiated under green light for 24 h.

ATRP under red light:

Table 11. Polymerization of MA using heterogeneous PTZ-CMP photocatalyst under red light irradiation [a]

Entry	Light source	Ligand	PTZ-CMP (mg/mL)	Conv. (%)	$M_{n,th}$	M_n	Đ
1	630 nm – 4 mW/cm^2	PMDETA	2	0	-	-	-
2		PMDETA	4	0	-	-	-
3		Me$_6$TREN	0	0	-	-	-
4		Me$_6$TREN	2	0	-	-	-
5	660 nm – 40 mW/cm^2	PMDETA	0	17	3200	3900	1.18
6		PMDETA	2	84	14700	16000	1.07
7		Me$_6$TREN	0	0	-	-	-
8		Me$_6$TREN	2	40	7000	6600	1.07

[a] Reaction conditions: $[MA]/[EBiB]/[CuBr_2]/[L] = 200/1/0.04/0.2$ in 50 vol% solvent (DMSO or MeCN used with PMDETA or Me$_6$TREN ligands, respectively) under red light irradiation (630 nm, 4 mW/cm^2 or 660 nm, 40 mW/cm^2) for 24 h, PTZ-CMP = 2 or 4 mg/mL.
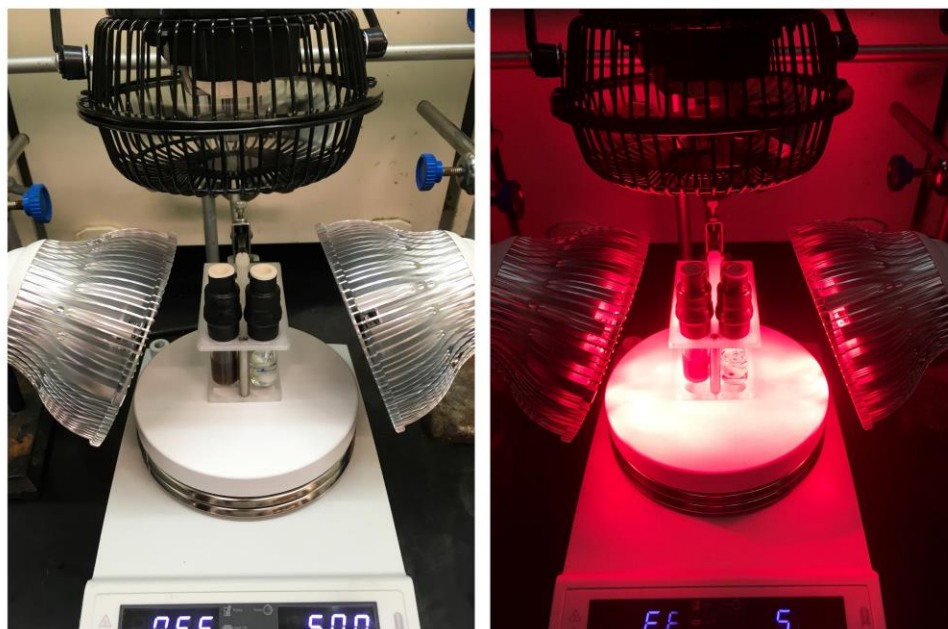
Figure 62. Setup used for polymerizations conducted under red LED lamps (660 nm, 40 mW/cm^2). Reaction vials show ATRP experiments performed in the presence (left vial) or absence (right vial) of the PTZ-CMP photocatalyst in MeCN.

Kinetics and temporal control:
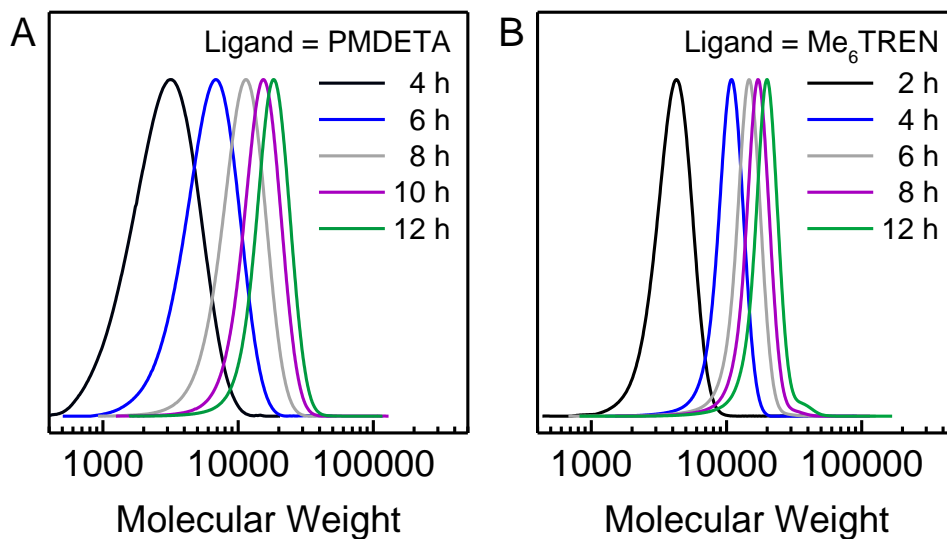
Figure 63. Evolution of GPC traces of PMA synthesized by ATRP using PTZ-CMP photocatalyst in the presence of (A) PMDETA or (B) Me$_6$TREN ligands. Reaction conditions: [MA]/[EBiB]/[CuBr$_2$]/[L] = 200/1/0.04/0.2, L = PMDETA or Me$_6$TREN in 50 vol% DMSO or MeCN, respectively, irradiated under green light LEDs.
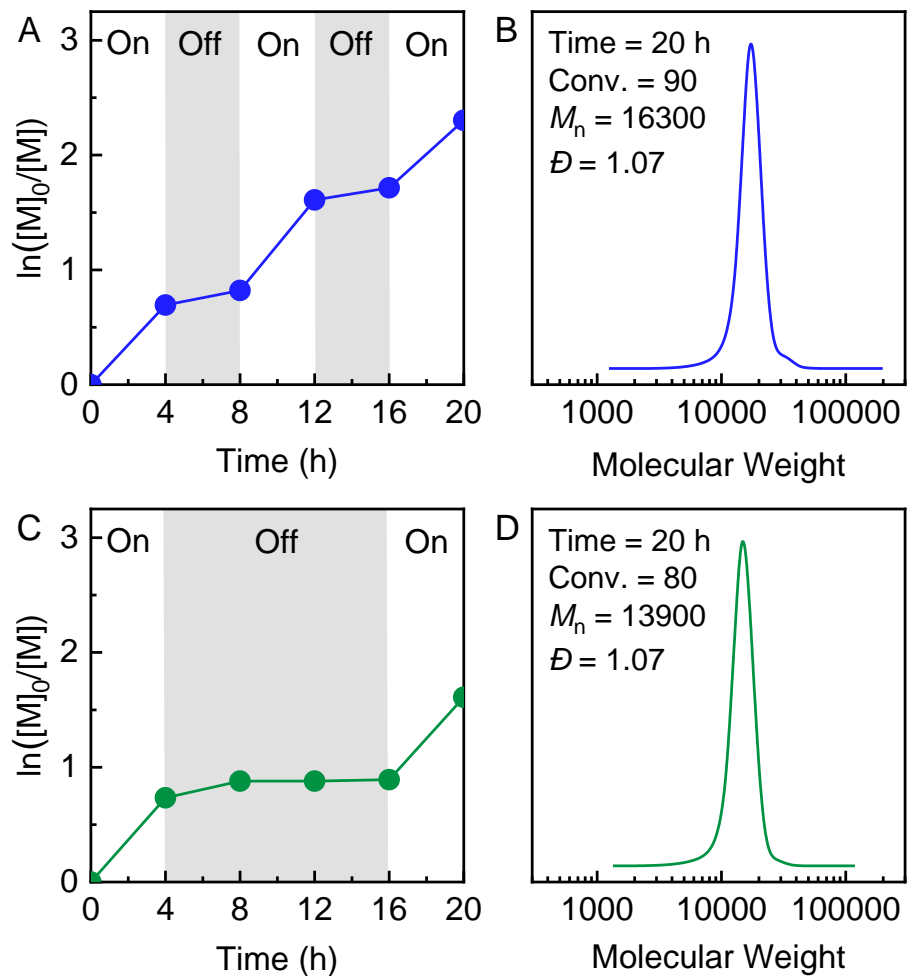
Figure 64. (A) and (C) Kinetics of temporal control in ATRP of MA and (B) and (D) corresponding GPC traces of the resulting polymers after intermittent light on/off periods. Reaction conditions: [MA]/[EBiB]/[CuBr$_2$]/[Me$_6$TREN] = 200/1/0.04/0.2 in MeCN (50 vol%), PTZ-CMP = 2 mg/mL irradiated under green light LEDs.

Effect of the Cu catalyst:

Table 12. Results of control experiments in polymerization of MA using PTZ-CMP as a heterogeneous photocatalyst in the absence of the Cu catalyst [a]

Entry	[EBiB]/[CuBr$_2$]/[PMDETA]	Time (h)	Conv. (%)	$M_{n,th}$	M_n	$Đ$
1	0/0/0	24	0	-	-	-
2	1/0/0	24	0	-	-	-
3	0/0/0.2	3	12	-	650000	1.91
4	1/0.04/0.04	24	0	-	-	-
5	1/0.04/0.2	24	98	17100	18600	1.08

[a] Reaction conditions: [MA] = 200 equiv. in DMSO (50 vol%) under green light irradiation (520 nm, 9 mW/cm^2) for 24 h, PTZ-CMP = 2 mg/mL.
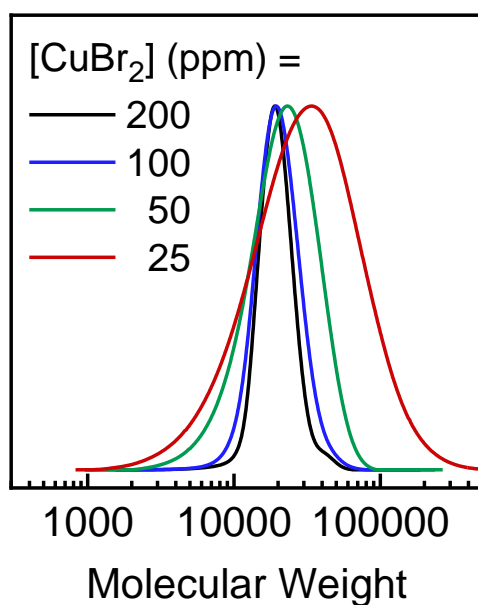
Figure 65. SEC traces of PMA synthesized in the presence of decreasing concentration of the Cu catalyst with PMDETA ligand. Reaction conditions: [MA]/[EBiB]/[CuBr$_2$]/[PMDETA] = 200/1/x/0.2 (x = 0.04, 0.02, 0.01, and 0.005 equiv. with respect to initiator corresponding to 200, 100, 50, and 25 ppm with respect to monomer) in DMSO (50 vol%) under green light irradiation (520 nm, 9 mW/cm^2).
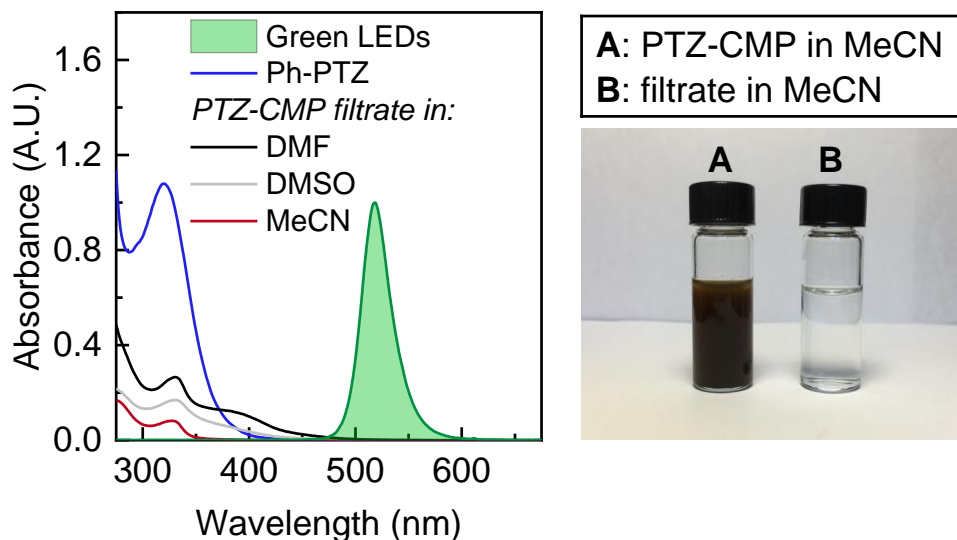
Figure 66. UV-vis spectra of Ph-PTZ and the filtrate of PTZ-CMP dispersed in DMSO, DMF, or MeCN filtered through syringe filters. The UV-vis spectra of the filtrates show absorption in the UV region corresponding to monomeric/oligomeric PTZ photocatalysts dissolved in the solutions that have no overlap with the emission spectra of the LEDs. [Ph-PTZ] = 0.2 mM (0.055 mg/mL in DMSO), [PTZ-CMP] = 2 mg/mL stirred for 24 h. Right: (A) pictures of a dispersion of PTZ-CMP in MeCN and (B) after filtration through syringe filters (0.45 µm) showing complete removal of the heterogeneous photocatalyst.

By comparing the absorbance of the filtrates (maximum at ~330 nm) with that of Ph-PTZ (0.02 mM, maximum at 320 nm), the concentration of the soluble parts in the PTZ-CMP (2 mg/mL) for each solvent can be estimated as following:

[Ph-PTZ] = 0.2 mM (0.055 mg/mL)

Abs at 320 nm = 1.09

PTZ-CMP filtrate in DMSO:

Abs at 330 nm = 0.17

$[PTZ]_{soluble} = (0.17/1.09) \times (0.055 \text{ mg/mL}) = 0.008 \text{ mg/mL}$

$[PTZ]_{soluble}/[PTZ-HCP]_{total} = (0.008 \text{ mg/mL})/(2 \text{ mg/mL}) \times 100 = 0.4\%$

Similarly, the concentration of the soluble parts in MeCN and DMF can be calculated as 0.2 and 0.6% of the total network, respectively.

Table 13. Control experiments using filtrates of PTZ-CMP in different solvents showing no polymerization occurring in the presence of the small amounts of the soluble parts dissolved form PTZ-CMP [a]

Entry	Ligand	Solvent [b]	Conversion (%)	$M_{n,th}$	M_n	Đ
1	PMDETA	DMSO	0	-	-	-
2	Me$_6$TREN	DMF	0	-	-	-
3	Me$_6$TREN	MeCN	0	-	-	-

[a] Reaction conditions: [MA]/[EBiB]/[CuBr$_2$]/[L] = 200/1/0.04/0.2 (solvent 50 vol%) under green light irradiation (520 nm, 9 mW/cm^2) for 24 h. [b] PTZ-CMP was stirred in each solvent (2 mg/mL) for 24 h and was filtered off using syringe filters to remove the heterogeneous parts, leaving transparent solutions which were used as solvents for ATRP.
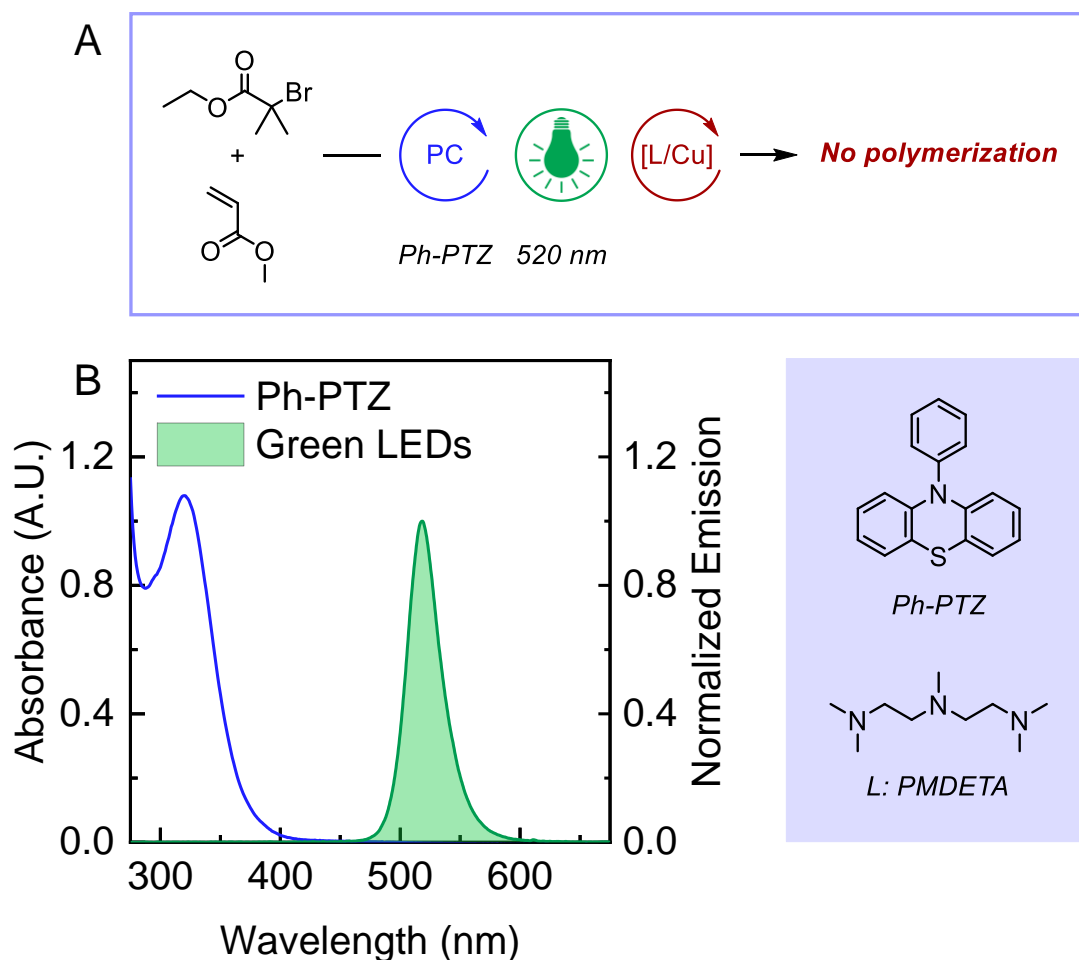
Figure 67. (A) Control experiment in the presence of Ph-PTZ as a photocatalyst that resulted in no polymerization of MA under green light irradiation. (B) UV-vis spectra of Ph-PTZ showing absorbance in the UV region <400 nm with no overlap with the emission spectra of the green LEDs ([Ph-PTZ] = 0.02 mM in DMSO). Reaction conditions: [MA]/[EBiB]/[CuBr$_2$]/[PMDETA] = 200/1/0.04/0.12 in DMSO (50 vol%), Ph-PTZ = 5 or 10 mg/mL (18 or 36 mM, respectively), irradiated under green light (520 nm, 9 mW/cm^2) for 24 h.

Recycling experiments:
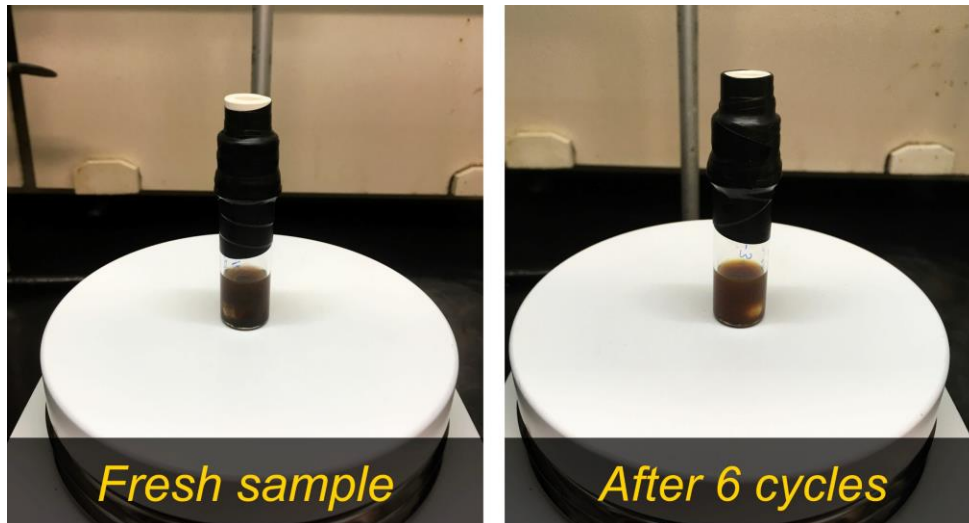
Figure 68. Photographs of the polymerization solution before (fresh) and after recycling experiments (6 cycles).

ATRP of MMA:
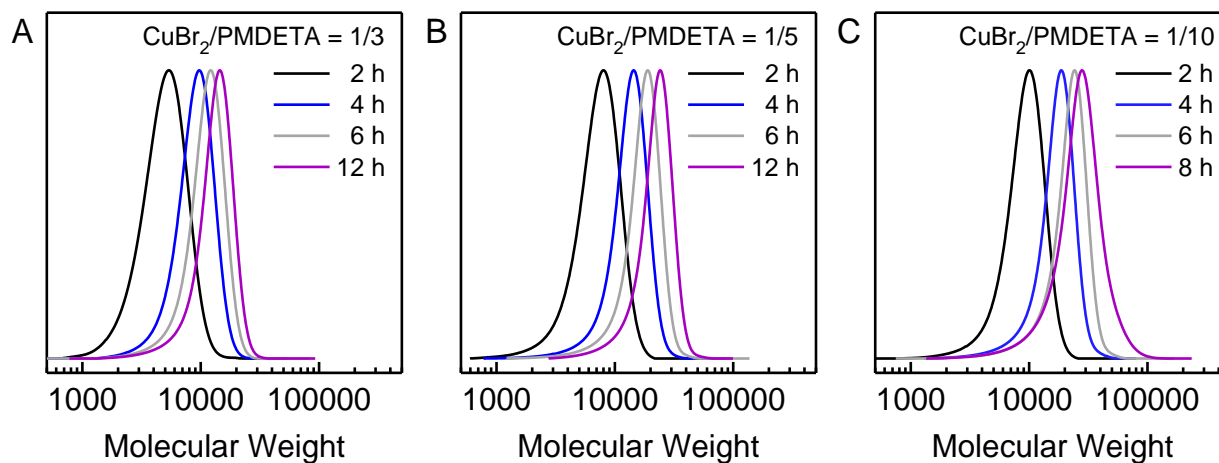
Figure 69. SEC traces for PMMA synthesized using PTZ-CMP as a photocatalyst in the presence of different concentrations of excess PMDETA as electron donor. Reaction conditions: $[MMA]/[EBPA]/[CuBr_2]/[PMDETA] = 200/1/0.04/x$ (x = 0.12, 0.2, and 0.4) in DMSO (50 vol%) under green light irradiation (520 nm, 9 mW/cm^2), PTZ-CMP = 2 mg/mL.
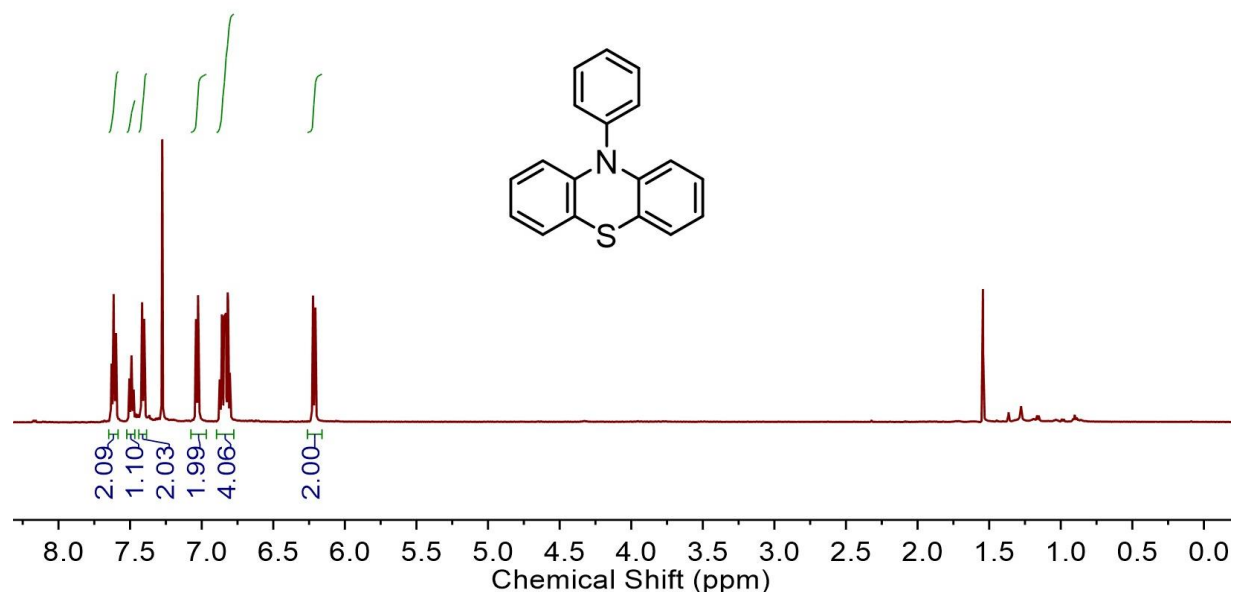
Figure 70. ^{1}H NMR spectra of Ph-PTZ recorded in deuterated chloroform.

3.2.6   References

1.   Falciola, L.; Gennaro, A.; Isse, A. A.; Mussini, P. R.; Rossi, M. The solvent effect in the electrocatalytic reduction of organic bromides on silver. *J. Electroanal. Chem.* **2006,** 593 (1), 47-56.

2.   Cox, B. G.; Jedral, W.; Palou, J. Oxidation of ascorbic acid by copper(II) and the ferrocenium ion in acetonitrile–water mixtures. *J. Chem. Soc., Dalton Trans.* **1988,** (3), 733-740.

3.   Pegis, M. L.; Roberts, J. A. S.; Wasylenko, D. J.; Mader, E. A.; Appel, A. M.; Mayer, J. M. Standard Reduction Potentials for Oxygen and Carbon Dioxide Couples in Acetonitrile and N,N-Dimethylformamide. *Inorg. Chem.* **2015,** 54 (24), 11883-11888.

4.   Chen, M.; Zhong, M.; Johnson, J. A. Light-Controlled Radical Polymerization: Mechanisms, Methods, and Applications. *Chem. Rev.* **2016,** 116 (17), 10167-10211.

5.   Dadashi-Silab, S.; Doran, S.; Yagci, Y. Photoinduced Electron Transfer Reactions for Macromolecular Syntheses. *Chem. Rev.* **2016,** 116 (17), 10212-10275.

6.   Pan, X.; Tasdelen, M. A.; Laun, J.; Junkers, T.; Yagci, Y.; Matyjaszewski, K. Photomediated controlled radical polymerization. *Prog. Polym. Sci.* **2016,** 62, 73-125.

7. Doerr, A. M.; Burroughs, J. M.; Gitter, S. R.; Yang, X.; Boydston, A. J.; Long, B. K. Advances in Polymerizations Modulated by External Stimuli. *ACS Cat.* **2020,** 10 (24), 14457-14515.

8. Parkatzidis, K.; Wang, H. S.; Truong, N. P.; Anastasaki, A. Recent Developments and Future Challenges in Controlled Radical Polymerization: A 2020 Update. *Chem* **2020,** 6 (7), 1575-1588.

9. Corrigan, N.; Jung, K.; Moad, G.; Hawker, C. J.; Matyjaszewski, K.; Boyer, C. Reversible-deactivation radical polymerization (Controlled/living radical polymerization): From discovery to materials design and applications. *Prog. Polym. Sci.* **2020,** 111, 101311.

10. Discekici, E. H.; Anastasaki, A.; Read de Alaniz, J.; Hawker, C. J. Evolution and Future Directions of Metal-Free Atom Transfer Radical Polymerization. *Macromolecules* **2018,** 51 (19), 7421-7434.

11. Theriot, J. C.; McCarthy, B. G.; Lim, C.-H.; Miyake, G. M. Organocatalyzed Atom Transfer Radical Polymerization: Perspectives on Catalyst Design and Performance. *Macromol. Rapid Commun.* **2017,** 38 (13), 1700040.

12. Kottisch, V.; Michaudel, Q.; Fors, B. P. Cationic Polymerization of Vinyl Ethers Controlled by Visible Light. *J. Am. Chem. Soc.* **2016,** 138 (48), 15535-15538.

13. Xu, J.; Jung, K.; Atme, A.; Shanmugam, S.; Boyer, C. A Robust and Versatile Photoinduced Living Polymerization of Conjugated and Unconjugated Monomers and Its Oxygen Tolerance. *J. Am. Chem. Soc.* **2014,** 136 (14), 5508-5519.

14. Matyjaszewski, K. Atom Transfer Radical Polymerization (ATRP): Current Status and Future Perspectives. *Macromolecules* **2012,** 45 (10), 4015-4039.

15. Wang, J.-S.; Matyjaszewski, K. Controlled/"living" radical polymerization. atom transfer radical polymerization in the presence of transition-metal complexes. *J. Am. Chem. Soc.* **1995,** 117 (20), 5614-5615.

16. Wu, Z.; Jung, K.; Boyer, C. Effective Utilization of NIR Wavelengths for Photo-Controlled Polymerization: Penetration Through Thick Barriers and Parallel Solar Syntheses. *Angew. Chem. Int. Ed.* **2020,** 59 (5), 2013-2017.

17. Stache, E. E.; Kottisch, V.; Fors, B. P. Photocontrolled Radical Polymerization from Hydridic C–H Bonds. *J. Am. Chem. Soc.* **2020,** 142 (10), 4581-4585.

18. Shanmugam, S.; Xu, J.; Boyer, C. Light-Regulated Polymerization under Near-Infrared/Far-Red Irradiation Catalyzed by Bacteriochlorophyll a. *Angew. Chem. Int. Ed.* **2016,** 55 (3), 1036-1040.

19. Shanmugam, S.; Xu, J.; Boyer, C. Exploiting Metalloporphyrins for Selective Living Radical Polymerization Tunable over Visible Wavelengths. *J. Am. Chem. Soc.* **2015,** 137 (28), 9174-9185.

20. Jiang, J.; Ye, G.; Lorandi, F.; Liu, Z.; Liu, Y.; Hu, T.; Chen, J.; Lu, Y.; Matyjaszewski, K. Localized Surface Plasmon Resonance Meets Controlled/Living Radical Polymerization: An Adaptable Strategy for Broadband Light-Regulated Macromolecular Synthesis. *Angew. Chem. Int. Ed.* **2019,** 58 (35), 12096-12101.

21. Jiang, K.; Han, S.; Ma, M.; Zhang, L.; Zhao, Y.; Chen, M. Photoorganocatalyzed Reversible-Deactivation Alternating Copolymerization of Chlorotrifluoroethylene and Vinyl Ethers under Ambient Conditions: Facile Access to Main-Chain Fluorinated Copolymers. *J. Am. Chem. Soc.* **2020,** 142 (15), 7108-7115.

22. Anastasaki, A.; Nikolaou, V.; Zhang, Q.; Burns, J.; Samanta, S. R.; Waldron, C.; Haddleton, A. J.; McHale, R.; Fox, D.; Percec, V.; Wilson, P.; Haddleton, D. M. Copper(II)/Tertiary Amine Synergy in Photoinduced Living Radical Polymerization: Accelerated Synthesis of ω-Functional and α,ω-Heterofunctional Poly(acrylates). *J. Am. Chem. Soc.* **2014,** 136 (3), 1141-1149.

23. Ribelli, T. G.; Konkolewicz, D.; Bernhard, S.; Matyjaszewski, K. How are Radicals (Re)Generated in Photochemical ATRP? *J. Am. Chem. Soc.* **2014,** 136 (38), 13303-13312.

24. Discekici, E. H.; Anastasaki, A.; Kaminker, R.; Willenbacher, J.; Truong, N. P.; Fleischmann, C.; Oschmann, B.; Lunn, D. J.; Read de Alaniz, J.; Davis, T. P.; Bates, C. M.; Hawker, C. J. Light-Mediated Atom Transfer Radical Polymerization of Semi-Fluorinated (Meth)acrylates: Facile Access to Functional Materials. *J. Am. Chem. Soc.* **2017,** 139 (16), 5939-5945.

25. Whitfield, R.; Parkatzidis, K.; Rolland, M.; Truong, N. P.; Anastasaki, A. Tuning Dispersity by Photoinduced Atom Transfer Radical Polymerisation: Monomodal Distributions with ppm Copper Concentration. *Angew. Chem. Int. Ed.* **2019,** 58 (38), 13323-13328.

26. Szczepaniak, G.; Łagodzińska, M.; Dadashi-Silab, S.; Gorczyński, A.; Matyjaszewski, K. Fully oxygen-tolerant atom transfer radical polymerization triggered by sodium pyruvate. *Chemical Science* **2020,** 11 (33), 8809-8816.

27. Dadashi-Silab, S.; Lee, I.-H.; Anastasaki, A.; Lorandi, F.; Narupai, B.; Dolinski, N. D.; Allegrezza, M. L.; Fantin, M.; Konkolewicz, D.; Hawker, C. J.; Matyjaszewski, K. Investigating Temporal Control in Photoinduced Atom Transfer Radical Polymerization. *Macromolecules* **2020,** 53 (13), 5280-5288.

28. Kütahya, C.; Schmitz, C.; Strehmel, V.; Yagci, Y.; Strehmel, B. Near-Infrared Sensitized Photoinduced Atom-Transfer Radical Polymerization (ATRP) with a Copper(II) Catalyst Concentration in the ppm Range. *Angew. Chem. Int. Ed.* **2018,** 57 (26), 7898-7902.

29. Kütahya, C.; Meckbach, N.; Strehmel, V.; Gutmann, J. S.; Strehmel, B. NIR Light-Induced ATRP for Synthesis of Block Copolymers Comprising UV-Absorbing Moieties. *Chem. Eur. J.* **2020,** 26 (46), 10444-10451.

30. Kütahya, C.; Zhai, Y.; Li, S.; Liu, S.; Li, J.; Strehmel, V.; Chen, Z.; Strehmel, B. Distinct Sustainable Carbon Nanodots Enable Free Radical Photopolymerization, Photo-ATRP and Photo-CuAAC Chemistry. *Angew. Chem. Int. Ed.* **2021,** 60 (19), 10983-10991.

31. Zhang, W.; He, J.; Lv, C.; Wang, Q.; Pang, X.; Matyjaszewski, K.; Pan, X. Atom Transfer Radical Polymerization Driven by Near-Infrared Light with Recyclable Upconversion Nanoparticles. *Macromolecules* **2020,** 53 (12), 4678-4684.

32. Li, X.; Zhang, Y. C.; Ye, S.; Zhang, X. R.; Cai, T. Eosin Y functionalized tertiary amine-bearing interpenetrating polymer networks for heterogeneous catalysis of logic-controlled oxygen-tolerant radical polymerization. *Journal of Materials Chemistry A* **2020,** 8 (47), 25363-25370.

33. Chen, M.; Deng, S.; Gu, Y.; Lin, J.; MacLeod, M. J.; Johnson, J. A. Logic-Controlled Radical Polymerization with Heat and Light: Multiple-Stimuli Switching of Polymer Chain Growth via a Recyclable, Thermally Responsive Gel Photoredox Catalyst. *J. Am. Chem. Soc.* **2017,** 139 (6), 2257-2266.

34. Shanmugam, S.; Xu, S.; Adnan, N. N. M.; Boyer, C. Heterogeneous Photocatalysis as a Means for Improving Recyclability of Organocatalyst in "Living" Radical Polymerization. *Macromolecules* **2018,** 51 (3), 779-790.

35. Chu, Y.; Huang, Z.; Liang, K.; Guo, J.; Boyer, C.; Xu, J. A photocatalyst immobilized on fibrous and porous monolithic cellulose for heterogeneous catalysis of controlled radical polymerization. *Polym. Chem.* **2018,** 9 (13), 1666-1673.

36. Chu, Y.; Corrigan, N.; Wu, C.; Boyer, C.; Xu, J. A Process for Well-Defined Polymer Synthesis through Textile Dyeing Inspired Catalyst Immobilization. *ACS Sustainable Chem. Eng.* **2018,** 6 (11), 15245-15253.

37. An, Z.; Zhu, S.; An, Z. Heterogeneous photocatalytic reversible deactivation radical polymerization. *Polym. Chem.* **2021,** 12 (16), 2357-2373.

38. Dadashi-Silab, S.; Tasdelen, M. A.; Kiskan, B.; Wang, X.; Antonietti, M.; Yagci, Y. Photochemically Mediated Atom Transfer Radical Polymerization Using Polymeric Semiconductor Mesoporous Graphitic Carbon Nitride. *Macromol. Chem. Phys.* **2014,** 215 (7), 675-681.

39. Pachfule, P.; Acharjya, A.; Roeser, J.; Sivasankaran, R. P.; Ye, M.-Y.; Brückner, A.; Schmidt, J.; Thomas, A. Donor–acceptor covalent organic frameworks for visible light induced free radical polymerization. *Chemical Science* **2019,** 10 (36), 8316-8322.

40. Li, X.; Zhang, Y. C.; Zhao, Y.; Zhao, H. P.; Zhang, B.; Cai, T. Xanthene Dye-Functionalized Conjugated Porous Polymers as Robust and Reusable Photocatalysts for Controlled Radical Polymerization. *Macromolecules* **2020,** 53 (5), 1550-1556.

41. Zhang, L.; Shi, X.; Zhang, Z.; Kuchel, R. P.; Namivandi-Zangeneh, R.; Corrigan, N.; Jung, K.; Liang, K.; Boyer, C. Porphyrinic Zirconium Metal–Organic Frameworks (MOFs) as Heterogeneous Photocatalysts for PET-RAFT Polymerization and Stereolithography. *Angew. Chem. Int. Ed.* **2021,** 60 (10), 5489-5496.

42. Lu, Z.; Fu, X.; Yang, H.; Zhao, Y.; Xiao, L.; Hou, L. A covalent organic framework as a photocatalyst for atom transfer radical polymerization under white light irradiation. *Polym. Chem.* **2021,** 12 (2), 183-188.

43. Dadashi-Silab, S.; Bildirir, H.; Dawson, R.; Thomas, A.; Yagci, Y. Microporous Thioxanthone Polymers as Heterogeneous Photoinitiators for Visible Light Induced Free Radical and Cationic Polymerizations. *Macromolecules* **2014,** 47 (14), 4607-4614.

44. Lee, J.-S. M.; Cooper, A. I. Advances in Conjugated Microporous Polymers. *Chem. Rev.* **2020,** 120 (4), 2171-2214.

45. Treat, N. J.; Sprafke, H.; Kramer, J. W.; Clark, P. G.; Barton, B. E.; Read de Alaniz, J.; Fors, B. P.; Hawker, C. J. Metal-Free Atom Transfer Radical Polymerization. *J. Am. Chem. Soc.* **2014,** 136 (45), 16096-16101.

46. Pan, X.; Fang, C.; Fantin, M.; Malhotra, N.; So, W. Y.; Peteanu, L. A.; Isse, A. A.; Gennaro, A.; Liu, P.; Matyjaszewski, K. Mechanism of Photoinduced Metal-Free Atom Transfer Radical Polymerization: Experimental and Computational Studies. *J. Am. Chem. Soc.* **2016,** 138 (7), 2411-2425.

47. Jockusch, S.; Yagci, Y. The active role of excited states of phenothiazines in photoinduced metal free atom transfer radical polymerization: singlet or triplet excited states? *Polym. Chem.* **2016,** 7 (39), 6039-6043.

48. Dadashi-Silab, S.; Pan, X.; Matyjaszewski, K. Phenyl Benzo[b]phenothiazine as a Visible Light Photoredox Catalyst for Metal-Free Atom Transfer Radical Polymerization. *Chem. Eur. J.* **2017,** 23 (25), 5972-5977.

49. Zhao, Y.; Ma, M.; Lin, X.; Chen, M. Photoorganocatalyzed Divergent Reversible-Deactivation Radical Polymerization towards Linear and Branched Fluoropolymers. *Angew. Chem. Int. Ed.* **2020,** 59 (48), 21470-21474.

50. Tan, L.; Li, B.; Yang, X.; Wang, W.; Tan, B. Knitting hypercrosslinked conjugated microporous polymers with external crosslinker. *Polymer* **2015,** 70, 336-342.

51. Tan, L.; Tan, B. Hypercrosslinked porous polymer materials: design, synthesis, and applications. *Chem. Soc. Rev.* **2017,** 46 (11), 3322-3356.

52. Jiang, X.; Liu, Y.; Liu, J.; Fu, X.; Luo, Y.; Lyu, Y. Hypercrosslinked conjugated microporous polymers for carbon capture and energy storage. *New J. Chem.* **2017,** 41 (10), 3915-3919.

53. Kruk, M.; Jaroniec, M. Gas Adsorption Characterization of Ordered Organic−Inorganic Nanocomposite Materials. *Chem. Mater.* **2001,** 13 (10), 3169-3183.

54. Nicholas, A. M. d. P.; Arnold, D. R. Thermochemical parameters for organic radicals and radical ions. Part 1. The estimation of the pKa of radical cations based on thermochemical calculations. *Can. J. Chem.* **1982,** 60 (17), 2165-2179.

55. Dolinski, N. D.; Page, Z. A.; Discekici, E. H.; Meis, D.; Lee, I.-H.; Jones, G. R.; Whitfield, R.; Pan, X.; McCarthy, B. G.; Shanmugam, S.; Kottisch, V.; Fors, B. P.; Boyer, C.; Miyake, G. M.; Matyjaszewski, K.; Haddleton, D. M.; de Alaniz, J. R.; Anastasaki, A.; Hawker, C. J.

What happens in the dark? Assessing the temporal control of photo-mediated controlled radical polymerizations. *J. Polym. Sci., Part A: Polym. Chem.* **2019,** 57 (3), 268-273.

Chapter 4.   Iron-Catalyzed Atom Transfer Radical Polymerization

4.1. Preface

In addition to copper-based ATRP systems presented in previous chapters, iron-based catalysts also provide well-controlled polymerizations and can be of significance, considering iron's abundance and benign properties. In this Chapter, I strived to study iron-based catalytic systems. In the first section of this chapter, I reviewed the fundamentals and developments of iron catalyzed ATRP. Iron-based ATRP catalysts are described according to the nature of the ligand and their effect in affording well-controlled polymerizations. In addition, challenges in regard to designing iron-based ATRP catalytic systems that can perform well in expanding the scope of iron catalysis to a variety of functional monomers, reaction media and synthesis of polymeric materials were discussed.

The second and third sections of this chapter, reported the development of photoinduced iron-catalyzed ATRP with ppm amounts of the iron catalyst under blue light irradiation. We established well-controlled ATRP of a variety of methacrylate monomers including fluorinated and semi-fluorinated monomers, synthesized well-defined homo and block copolymers, and achieved successful polymerization in the presence of residual oxygen without the need for deoxygenation. I designed and carried out all polymerization experiments under the guidance of Professor Matyjaszewski. I thank Dr. Xinagcheng Pan for his guidance and help in this project.

Finally, in the last section of this chapter, I provide an in-depth analysis of iron-catalyzed ATRP with regard to the effect of halogens and reaction medium in polymerization control. By

_____

performing UV-Vis spectroscopic analysis and polymerization experiments, we showed that the strong Fe-Cl bond led to slow deactivation of growing chains which resulted in polymers with large dispersity in the presence of Cl-based initiating systems. In contrast, in Br-based initiating systems, good control over polymerizations was achieved that enabled synthesis of homo and block copolymers with controlled molecular weights and low dispersities (< 1.2).

Moreover, we investigated the effect of reaction medium on polymerization control in the presence of polar (acetonitrile) and non-polar (anisole) solvents. As a non-polar solvent, anisole provided well-controlled polymers with dispersity < 1.2. In contrast, polar solvents such as acetonitrile provided high stability for the anionic iron species that the deactivation rate diminished, and the polymers showed higher dispersities in ATRP of methyl methacrylate.

I designed and carried out UV-vis analysis and polymerization experiments and collected data and prepared results together with Khidong Kim. Professor Matyjaszewski directed the research. All authors contributed to discussion and analysis of the results and in writing the paper.

4.2. Iron Catalysts in Atom Transfer Radical Polymerization

4.2.1 Abstract

Catalysts are essential for mediating a controlled polymerization in atom transfer radical polymerization (ATRP). Copper-based catalysts are widely explored in ATRP and are highly efficient, leading to well-controlled polymerization of a variety of functional monomers. In addition to copper, iron-based complexes offer new opportunities in ATRP catalysis to develop environmentally friendly, less toxic, inexpensive, and abundant catalytic systems. Despite the high efficiency of iron catalysts in controlling polymerization of various monomers including methacrylates and styrene, ATRP of acrylate-based monomers by iron catalysts still remains a challenge. In this paper, we review the fundamentals and recent advances of iron-catalyzed ATRP focusing on development of ligands, catalyst design and techniques used for iron catalysis in ATRP.

4.2.2 Introduction

Reversible deactivation radical polymerization (RDRP) techniques have provided access to advanced polymers with precise control over molecular weight, dispersity, composition, and structure. Typical approaches to control the growth of polymer chains in radical polymerizations include reversible deactivation of propagating radicals or using degenerative transfer processes to exchange radicals with dormant species in the presence of chain transfer agents. For example, atom transfer radical polymerization (ATRP) employs primarily Cu-based catalysts to control the growth of polymer chains via a reversible redox process that involves transfer of halogen atoms to activate dormant species generating initiating radicals and also to deactivate propagating chains.[1-4] In regard to degenerative transfer processes, reversible addition fragmentation chain transfer (RAFT)[3, 5-7] and iodine-mediated[8, 9] polymerizations have been significantly explored in controlled radical polymerizations.

ATRP catalysis has advanced based on developing new catalytic systems with the aim of progressively increasing the activity, efficiency, and selectivity of catalysts through designing ligands, using external stimuli to control the catalytic process, and also decreasing the amount of catalysts needed for achieving a controlled polymerization.[10, 11] For instance, the L/Cu^I activator for ATRP can be generated in situ via reduction of air stable L/Cu^{II}-X using external stimuli. Regeneration of the activator allows use of low concentration of the catalyst and overcoming the

consumption of the activator as a result of radical termination reactions. In addition, an important aspect of using external stimuli is to exert control over the catalytic system to enable spatial and temporal control over the growth of polymer chains.[2, 12, 13]

ATRP catalysis involves generation of radicals via activation of halogen chain ends by L/Cu^I activator and reversible deactivation of propagating radicals by a halogen atom transfer from L/Cu^{II}-X deactivator (X = Br or Cl). While copper-based complexes have been widely explored and used for polymerization of a wide range of vinyl monomers with high efficiency, ATRP catalysis comprises other transition metal-based catalysts[14, 15] such as iron,[13, 15-17] ruthenium,[18] osmium,[19] and iridium[20] complexes as well as organic-based photoredox catalysts.[21-24]

Iron complexes are particularly interesting due to the abundance of iron and its involvement in important biological processes that make iron-based catalytic systems less toxic, inexpensive, and biocompatible. Iron complexes mainly favor one-electron redox chemistry between +2 and +3 oxidation states, suitable for ATRP catalysis. In iron-catalyzed ATRP, L/Fe^{II} species activate dormant halogen chain ends, whereas L/Fe^{III}-X deactivate propagating radicals via a reversible halogen atom transfer process. Interestingly, iron complexes possessing anionic properties (for example those obtained in the presence of halide anions used as the ligand) have often performed well in ATRP reactions, whereas in copper-catalyzed ATRP, the efficient activator L/Cu^I complexes are cationically charged. In addition to atom transfer reactions, iron catalysts (L/Fe^{II}) can also react with the propagating radicals to form organometallic species (P_n-L/Fe^{III}). While the organometallic species can be involved in an organometallic mediated radical polymerization (OMRP) mechanism,[23, 25] termination reactions may also be promoted through catalytic chain transfer (CCT)[26] or catalytic radical termination (CRT) processes involving P_n-L/Fe^{III} species and propagating radicals to yield terminated chains.[27] In copper-catalyzed ATRP, CRT was reported only for the most active catalysts. Nevertheless, due to the low concentration of L/Cu^I present in these highly active systems, the overall contribution of OMRP and CRT processes in the polymerization is not important.[28] However, the contribution of organometallic species and CRT in iron-catalyzed systems may be more significant, leading to termination, especially in the polymerization of acrylate monomers.

In this paper, we review the principles and recent advances in iron-catalyzed ATRP. Iron catalytic systems are presented based on the structure and properties of the ligands and their

effect in polymerization catalysis. Different ATRP initiating systems based on developing activator regeneration techniques are discussed and challenges and opportunities offered by iron complexes in ATRP.

4.2.3   Ligands and Iron Complexes in Iron-Catalyzed ATRP

Ligands play an important role in controlling the efficiency and performance of ATRP catalysts, affecting polymerization control. A variety of different families of ligands have been developed and explored in ATRP with a special focus on understanding the catalysts' behavior in polymerization and underlying mechanisms.

Halide salts

Halide salts with bulky, non-coordinating cations have been used as simple and robust ligands in promoting iron-catalyzed ATRP with high efficiency. Halide salts containing organic onium counter cations, ionic liquids or inorganic based salts can be used.[29-36] Active iron complexes in the presence of halide salts possess overall anionic charge. Disproportionation (or dismutation) of $Fe^{II}Br_2$ forms a catalytically active anionic complex for ATRP and a cationic species,[37] a much less active (or inactive) form of the catalyst, according to eq. 1:

$$3\ Fe^{II}Br_2 \rightarrow Fe^{II} + 2\ [FeBr_3]^- \qquad\qquad (eq.\ 1)$$

In the presence of halide salts, various iron complexes may be generated that may or may not be the active catalyst for ATRP, depending on the nature of the reaction medium and/or the amount of the ligand used. For example, iron complexes with cationic charges are less effective as ATRP catalysts, whereas anionic complexes efficiently catalyze polymerization due to the presence of high electron density around the metal center attained by complexation of anionic species (Scheme 11).[38] Tri-coordinated monoanionic $[Fe^{II}Br_3/L]^-$ (L = solvent or monomer) species was proposed to be the active species for catalyzing ATRP.[39] In the presence of excess bromide salts, dianionic $[Fe^{II}Br_4]^{2-}$ complexes may also be generated, which contain four coordinated bromide anions rendering this species less effective to undergo a halogen abstraction during the activation

of dormant chains. Therefore, the rate of polymerization decreased in the presence of excess amounts of halide salt ligands.[40, 41]

$$[Fe^{II}L_6]^{2+} \xrightarrow[\substack{+L \\ -Br^-}]{\substack{+Br^- \\ -L}} [Fe^{II}BrL_5]^+ \xrightarrow[\substack{+3L \\ -Br^-}]{\substack{+Br^- \\ -3L}} [Fe^{II}Br_2L_2] \xrightarrow[\substack{+L \\ -Br^-}]{\substack{+Br^- \\ -L}} [Fe^{II}Br_3L]^- \xrightarrow[\substack{+L \\ -Br^-}]{\substack{+Br^- \\ -L}} [Fe^{II}Br_4]^{2-}$$
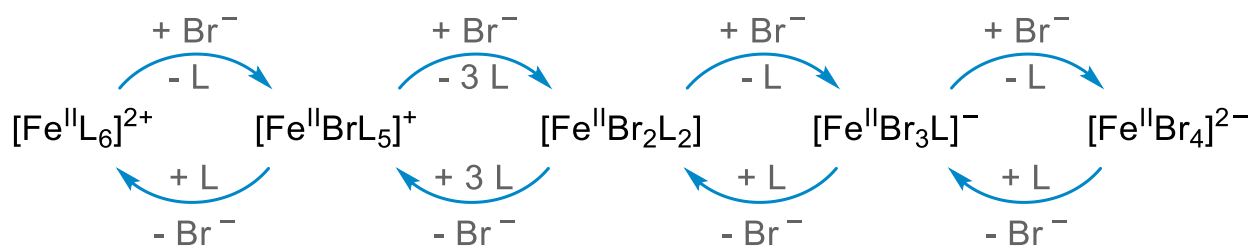
Scheme 11. Iron species in the presence of bromide anions as ligand and solvent (L) generating a number of mononuclear cationic and anionic species in ATRP.[37]

Nitrogen-based ligands

Alkyl amines with mono or multidentate coordinating sites or bipyridine derivatives were used for conducting iron ATRP.[18, 32, 33, 41, 42] A series of Fe^{II} complexes with *N,N,N*-trialkyl-1,4,9-triazacyclononane (TACN) ligands were investigated in ATRP.[43-46] The complexes formed either a mononuclear iron species in the presence of TACN ligands substituted with bulky groups, or trinuclear ionic species with a cationic dinuclear and an anionic mononuclear complex in the presence of less bulky substitution groups to form coordinatively saturated compounds. The mononuclear species performed well in catalyzing ATTP. Interestingly, an iron complex with cyclopentyl-substituted TACN ligand exchanged between mono and dinuclear species, therefore providing efficient catalysis and yielding well-controlled polymers, and also allowing easy purification and reusing the catalyst because of the formation of ionic structures.[47]

Iminopyridine[48, 49] and α-diimine[48, 50, 51] ligands were also developed for iron-based polymerization catalysts. Gibson and coworkers investigated the electronic and steric properties of the iron complexes with diimine ligands that affected the underlying mechanism of polymerization and therefore control over the growth of polymer chains. The electronic properties of the catalyst tuned via different *N*-substitution groups influenced the catalysts' performance and promoted either ATRP of catalytic chain transfer processes.[52] The CCT process was proposed to result from *N*-aryl substitution and involved formation of organometallic species followed by a hydrogen elimination to give low molecular weight terminated polymers. *N*-Alkyl substituted complexes favored ATRP mechanism and therefore yielded well-controlled polymers.

Bis(imino)pyridine ligands were immobilized on a polymer chain to synthesize iron catalysts for controlled polymerization.[53] The bis(imino)pyridine-containing polymer ligand was obtained using an amphiphilic copolymer comprising PEG, dodecyl, and urea/aniline pendant groups that reacted with 2,6-pyridinedicarboxaldehyde to yield self-folded polymers. Iron was immobilized on the polymer ligand and used in controlling polymerization of functional methacrylate monomers. Importantly, the amphiphilic nature of the self-folded polymers with immobilized iron catalyst allowed for easy purification of the products by rinsing with water, as the presence of hydrophilic PEG chains transferred the catalyst to aqueous phase and yielded pure polymethacrylates in the organic phase.

Shaver and co-workers developed amine-bis(phenolate) iron (III) complexes for polymerization of styrene and methacrylate monomers.[29, 54] These iron complexes possess dianionic bisphenolate moieties with fixed and strong multidentate metal-ligand bonds that are less prone to undergo dissociation of the metal center during catalysis. Complexes with electron-withdrawing Cl substitution (especially in the *para* position of the aromatic groups) resulted in well controlled polymerizations, whereas catalysts with alkyl substituted aromatic groups gave uncontrolled results. Polymerizations were performed under reverse ATRP conditions using AIBN as a source of radical initiator and equimolar ratios of the iron complexes. Fast and well-controlled polymerization of styrene and methacrylate monomers was obtained using the amine-bis(phenolate) iron complexes. Both Br and Cl-based catalysts afforded well-controlled results. Control over chain growth was proposed to mainly involve the ATRP pathway as well as minor contribution of the OMRP mechanism. In the absence of ATRP alkyl halide initiators, use of an amine-bis(phenolate) iron (II) complex enabled moderate control over polymerization of methacrylate or styrene monomers via OMRP mechanism.[55-57] A phenolate-bis(pyridyl)amine ligand with monoanionic phenolate group was also used for iron-catalyzed ATRP but showed less efficient control over polymerization compared to the dianionic bisphenolate ligands.[58]

Proteins and enzymes such as horseradish peroxidase, catalase, and hemoglobin that contain iron protoporpyhrine centers were used as naturally occurring, bio-inspired iron catalysts for ATRP.[59-63] Hemin catalyst was also used as a catalyst mimicking the enzymatic catalytic systems. Further modification of the hemin structure was performed by hydrogenation of the vinyl bonds to prevent incorporation of the catalyst in the polymer chains by addition of radicals

to the double bonds. Moreover, the catalyst was functionalized by attaching poly(ethylene glycol) (PEG), imidazole or thioether arms that enabled solubility of the catalyst in aqueous media and therefore performing well-controlled polymerizations in water (Scheme 12).[64-66]
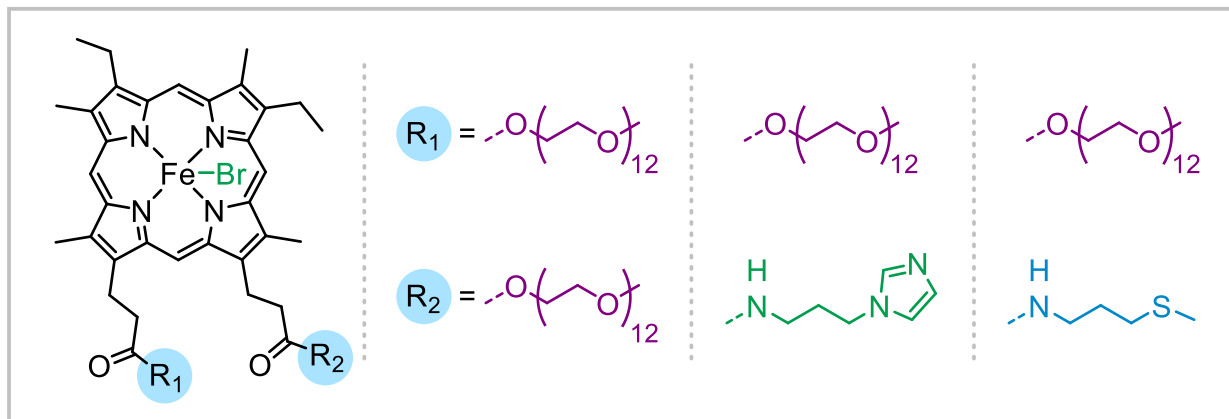
Scheme 12. Iron porphyrin catalysts functionalized with PEG and imidazole or thioether groups used in iron-catalyzed ATRP.

Phosphorus-based ligands

Ligands containing phosphorus such as various alkyl and aryl with mono- or bi-dentate phosphine or phosphite compounds are among the most widely used ligands in iron-catalyzed ATRP.[17, 67-72] The activity of triphenylphosphine ligands in iron-catalyzed ATRP depends on the electronic properties of the ligand, increasing in the presence of electron-donating functionalities.[73] The effect of substitution of electron donating methoxy groups on triphenylphosphine was attributed to an increase in the activity of the iron catalyst in the presence of ligands possessing more electron-donating properties, which is also reported for copper-catalyzed ATRP (Scheme 13).[74, 75] Moreover, the activity of triphenylphosphine compounds as a Lewis base increases by introducing electron donating functional groups leading to stronger reducing agents to generate L/Fe^{II} catalyst.[76] Therefore, the enhanced polymerization can be related to the electron-donating ability of the phosphine-based ligands in ATRP. In addition, similar behavior was observed in photoinduced iron-catalyzed ATRP in the presence of triphenylphosphine ligands where better control over polymerization was achieved in the presence of ligands with more electron donating properties, indicating increased activity of the iron catalyst applied in the ppm levels under blue light irradiation.[77]

The effect of substitution on the phosphine-based ligands in catalyzing ATRP was further explored.[75, 78] In the presence of alkyl substituted phosphines, polymerization of methyl methacrylate was uncontrolled with high dispersity and broad or bimodal molecular weight distributions. Polymerization of MMA with triphenyl phosphine was well-controlled but reached low monomer conversions. Introduction of electron donating groups in the *para* position of triphenylphosphine increased the activity of the resulting iron catalyst showing well-controlled polymerizations with dispersities < 1.2 and yielding high monomer conversions. The iron catalysts were obtained by reacting the phosphine ligands with $FeBr_2$ for 12 h yielding diphosphine iron(II) complexes, followed by addition of monomer and initiator to start the polymerization. As expected, the iron catalyst with chloro-substituted triphenylphosphine having electron withdrawing properties was inefficient in initiating polymerization of MMA. A PEG-substituted triphenylphosphine ligand was effective in controlling polymerization of functional monomers such as hydroxyethyl methacrylate (HEMA). The iron complex with PEG-substituted triphenylphosphine tolerated functional groups due to the bulkiness of the PEG chains, which protected the catalyst center from poisoning by the functional groups. These results further signify the importance of electronic and steric properties of functional groups in designing ligands for achieving a successful and well-controlled polymerization.

In addition, bidentate ligands containing P-P homo[79, 80] and P-N[71, 76] or P-carbonyl[72] hetero chelating sites were reported to perform well in iron-catalyzed ATRP. The presence of a second coordinating site (P or N) increased the catalytic activity and efficiency of the iron complex. Scheme 3 shows examples of phosphorus-containing ligands developed for controlled polymerization in iron-catalyzed ATRP.
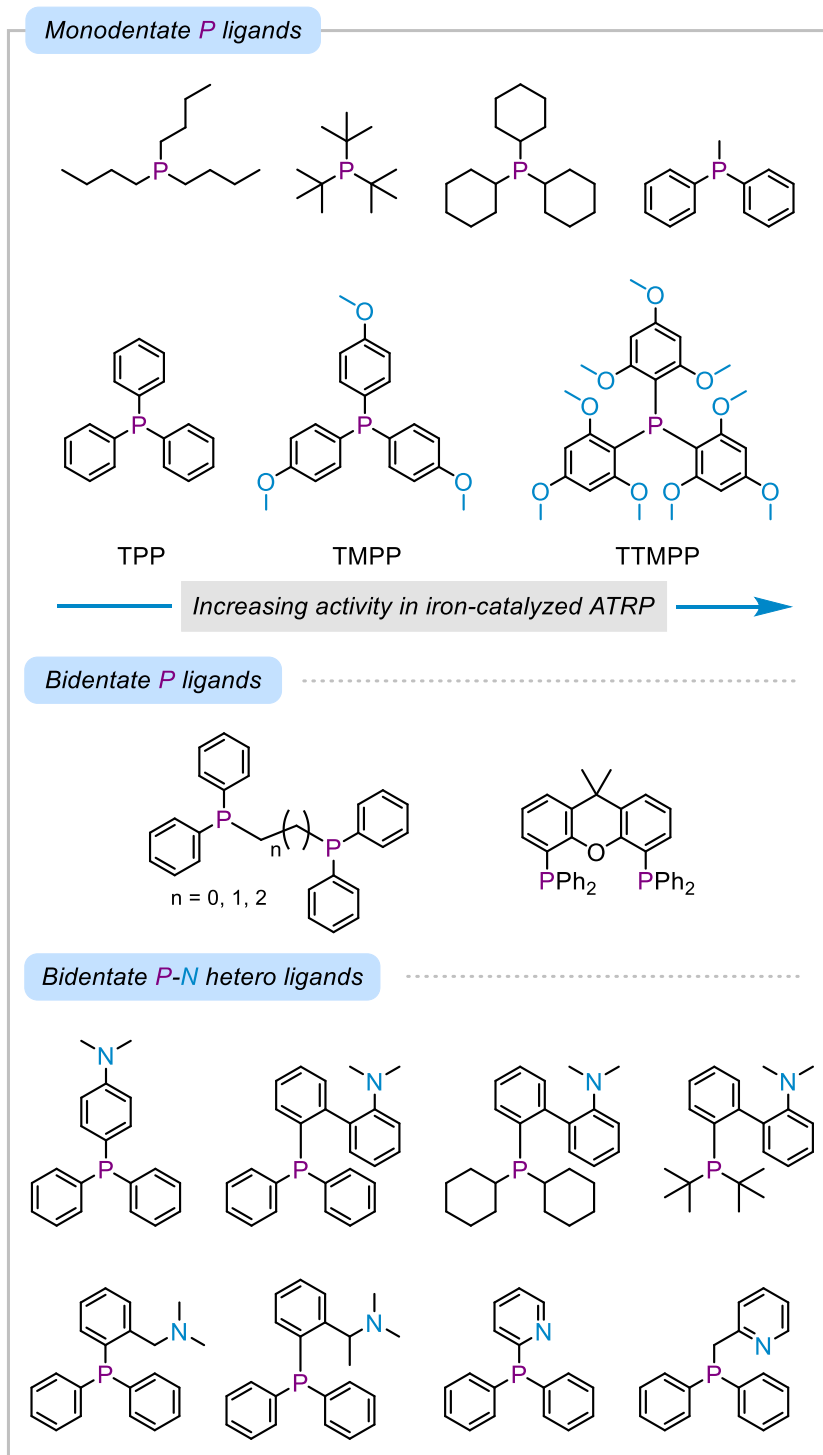
Scheme 13. Examples of mono and bidentate phosphorus-containing ligands used in iron-catalyzed ATRP. Substitution of triphenylphosphine ligands with electron-donating methoxy groups increases the activity of the iron catalyst in ATRP.

Miscellaneous ligands

Iron-catalyzed ATRP can be also successfully performed in the absence of additional ligands with polar solvents that can act as a ligand for stabilizing the iron catalyst.[81] For example, iron-catalyzed ATRP was controlled in the presence of solvents such as acetonitrile, DMF, NMP without the use of other ligands. These solvents resulted in disproportionation of the iron complexes to form inactive cationic species and catalytically active anionic (eq. 1 and Scheme 1).[82, 83]

N-Heterocyclic carbenes (NHC) were used as ligands in iron-catalyzed ATRP.[84] The redox potential of the iron complexes with NHC ligands were more negative than those obtained using halide salts, indicating higher activity of the catalysts with NHC ligands. As a result, control over polymerization was better with Fe/NHC catalysts. Interestingly, polymerizations using Br-based systems resulted in improving polymerization control compared to the Cl-based catalysts. The effect of Br vs Cl initiating systems on control over polymerization may be related to the activity of dormant chain ends regarding the activation process, as well as halidophilicity of the iron catalyst, which influences the deactivation process and hence control over polymerization. More analysis of the Br and Cl-based initiating systems is required to understand the effect of halide nature in the activation and deactivation processes and therefore polymerization control with iron catalysts.

4.2.4 Iron-Catalyzed ATRP Initiating Systems

A common feature of new ATRP initiating systems is the in situ regeneration of the activator catalyst used at ppm amount by applying various reduction processes. Regeneration of the activator species via reduction of the oxidized form of the catalyst (i.e., the deactivator) allows for use of low amounts of the catalyst starting with its more stable oxidized form, and also overcome the problems associated with the consumption of the activator as a result of termination of radicals. These techniques mainly include use of reducing agents as in activators regenerated by electron transfer (ARGET), conventional radical initiators as in initiators for continuous activator regeneration (ICAR), zerovalent metals as in supplemental activator and reducing agent (SARA) systems, or external stimuli such as photo and electrochemical approaches (Scheme 14). These systems are applicable in both copper and iron-based ATRP reactions.[85]
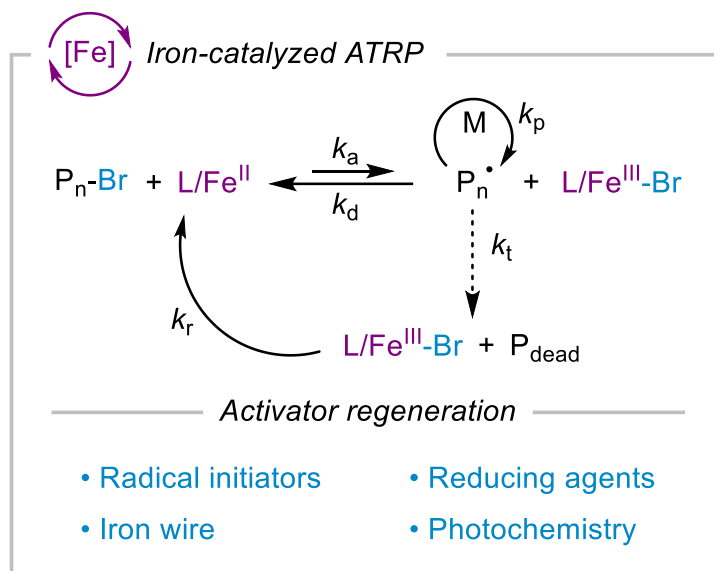
Scheme 14. Iron-catalyzed ATRP initiating systems with activator regeneration techniques developed for generation of L/Fe^{II} activator species via reduction (k_r, rate constant of reduction) of L/Fe^{III}-Br.

ICAR ATRP uses conventional thermal initiators to form radicals that can react with L/Fe^{III}-X to generate the ATRP activator, L/Fe^{II} complexes, and initiate the ATRP process. Generation of radicals from decomposition of the initiator species ensures continuous activator regeneration throughout the reaction and hence results in a steady rate of polymerization and well-controlled polymers.[36, 84, 86, 87]

Reducing agents are used in ARGET ATRP to generate the activator catalyst via electron transfer processes by reducing more stable L/Fe^{III}-X species.[88] Well-controlled ATRP was obtained using phosphorus ligands in the absence of conventional reducing agents. The generation of L/Fe^{II} activator was proposed to occur in the presence of phosphorus ligands that acted as a reducing agent facilitating transfer of bromine radical from L/Fe^{III}-Br to the monomer and therefore generation of both the activator and the ATRP initiator in situ.[86, 89, 90] Decamethylferrocene (FeCp*$_2$) was used as a co-catalyst to improve efficiency of polymerizations catalyzed by iron catalysts.[91] FeCp*$_2$ was proposed to act as a reducing agent for FeBr$_3$ in the presence of TBABr generating FeBr$_2$ activator and the ferrocenium salt with a bromide anion. Indeed, the lower redox potential of decamethylferrocene enabled reduction of

Fe[III] to improve the kinetics of the polymerization whereas use of ferrocene having a higher redox potential than the main iron catalyst showed no effect in the polymerization. Deactivation of growing radicals was improved by contribution of the ferrocenium salt with the bromide anion.

Zerovalent metal species such as iron wire or plates can be used to promote ATRP.[76, 92] Recently, surface-initiated ATRP was investigated under SARA ATRP conditions using iron catalysts and an iron plate that acted as a source of activator (re)generation.[93] This surface functionalization technique was performed under ambient conditions without the need for inert atmosphere, as oxygen was consumed in the presence of iron plate, thereby simplifying the functionalization process. Importantly, the polymerization was conducted in the presence of mammalian cell cultures that showed high viability under polymerization conditions, indicating the potential of iron catalyzed ATRP to be applied under biologically relevant conditions (Scheme 15).
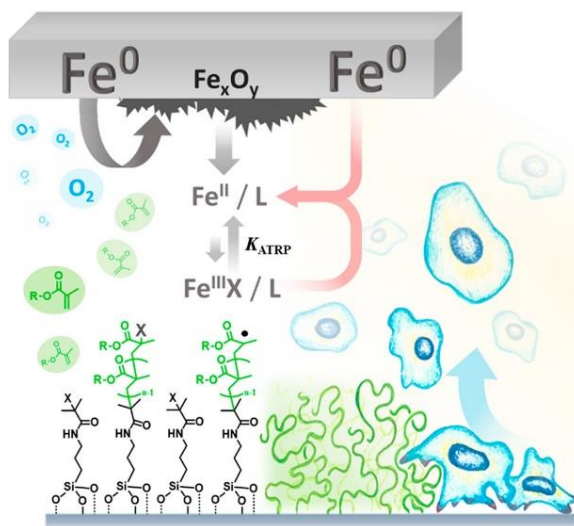
Scheme 15. Iron-catalyzed surface-initiated ATRP using an iron plate to generate L/Fe[II] activators and remove oxygen allowing facile surface functionalization showing high cytocompatibility. Reproduced with permission from Ref [36].

Photochemistry has resulted in great advancements in the field of controlled polymerizations and enabled unique opportunities for synthesis of functional polymeric materials and asserting spatiotemporal control over polymerization.[94-97] Photoinduced iron-catalyzed ATRP was developed for controlled polymerization of methacrylate monomers under light irradiation, which promoted generation of the L/Fe[II] catalyst.[98, 99] The photoreduction of FeBr$_3$ proceeded

through a homolytic cleavage of the Fe-Br bond upon photoexcitation to generate FeBr$_2$ and a Br$^•$ radical. The Br$^•$ radical added to methacrylate monomers and generated new initiating chains. A simplified iron-catalyzed ATRP was reported by using only monomer and FeBr$_3$ catalyst under UV light irradiation without using any conventional alkyl halide ATRP initiators or ligands (Scheme 16).[100] Indeed, polymerizations relied on the formation of initiators in situ via photoreduction of FeBr$_3$ generating Br$^•$ radicals that reacted with methacrylate monomers. Moreover, photoinduced iron-catalyzed ATRP was further improved upon by using ppm amounts of iron catalyst while yielding well-controlled polymers under blue light irradiation.[101]
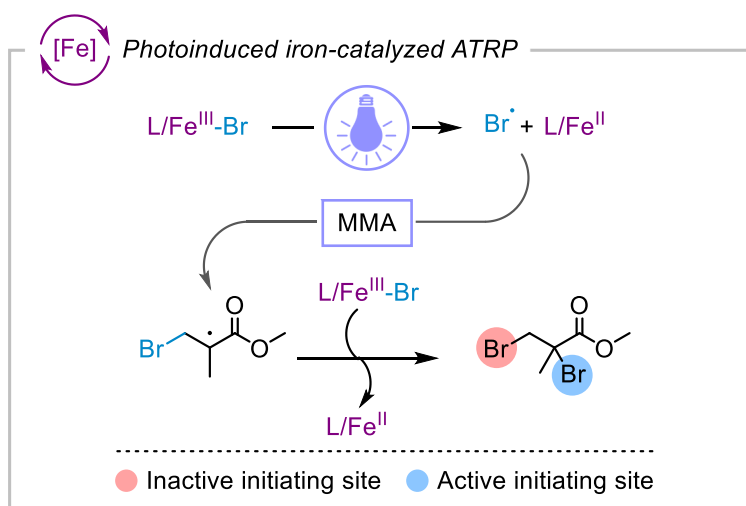
Scheme 16. Photoinduced iron-catalyzed ATRP undergoing a homolytic cleavage of the Fe-Br bond under visible light irradiation to generate the activator L/Fe^{II} and a Br$^•$ radical, which can add to the monomer and initiate new chains.[102, 103] Polymerization can be performed without the need for use of conventional alkyl halide initiators using just the monomer and the catalyst.

Iron-catalyzed ATRP was conducted in the presence of residual oxygen to control polymerizations without performing conventional deoxygenation procedures.[79] For example, polymerization of methyl methacrylate was well-controlled using 10 mol% FeBr$_3$ (with respect to initiator) to give high monomer conversions (> 90%) and well-controlled polymers with low dispersities (< 1.20) under blue light irradiation. Importantly, block copolymers were synthesized with well-controlled properties using photoinduced iron-catalyzed ATRP in the presence of residual oxygen, indicating the potential of this system to simplify the polymerization procedure or apply in areas where no deoxygenation is desired. Although the exact mechanism of

consumption of oxygen was not determined in detail, it is possible that the initiator radicals and/or the iron catalyst would contribute in removing oxygen from the solution to allow a well-controlled polymerization to proceed, as previously shown for photoinduced copper-catalyzed ATRP systems.[101]

Recently, iron-catalyzed ATRP was applied for the polymerization of semi-fluorinated methacrylate monomers controlled under blue light irradiation.[103] The use of iron as a catalyst was advantageous compared to copper-based catalysts, as the use of nitrogen-ligands in these systems promoted undesired transesterification reactions between the fluorinated monomer and protic solvent leading to a loss of control over the polymerization. However, polymerization of fluorinated monomers using iron catalyst was well-controlled in the presence of a variety of fluorinated and non-fluorinated solvents without undergoing side reactions or requiring special solvent systems to control the polymerization. A variety of semi-fluorinated methacrylate monomers were polymerized in a controlled manner using $FeBr_3$/TBABr as the catalyst under blue light irradiation resulting in high monomer conversions and polymers showing low dispersities (< 1.20). Importantly, the use of blue light to trigger polymerization through generation of the $FeBr_2$ activator catalyst enabled gaining temporal control over the growth of polymer chains. The polymerization was initiated under blue light irradiation that generated the activator catalyst. Removal of the light stopped continuous (re)generation of the activator catalyst, continuously consumed as a result of radicals' termination, leading the polymerization to stop in the dark periods. Therefore, by decreasing the concentration of initially added catalyst, better temporal control was achieved as a result of low concentration of the activator, which required less time to be consumed during the light-off periods (Figure 71).[79]
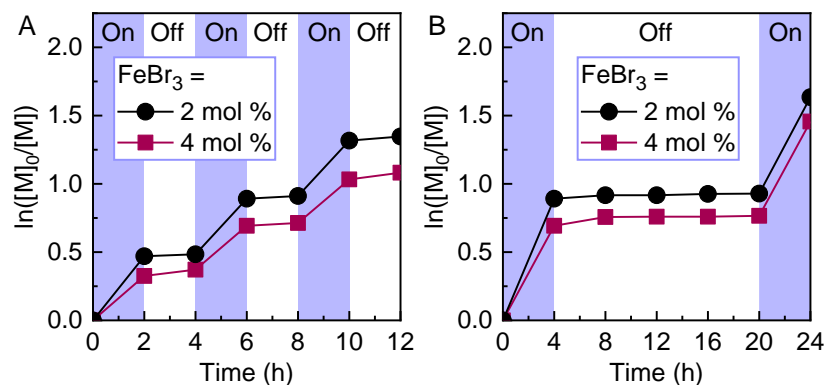
Figure 71. Temporal control in photoinduced iron-catalyzed ATRP of trifluoroethyl methacrylate (TFEMA). Better temporal control was achieved by decreasing the concentration of the iron catalyst from 4 to 2 mol%. Reaction conditions: [TFEMA]/[EBPA]/[FeBr$_3$]/[TBABr] = 50/1/x/2x (x = 0.02 or 0.04) in 50 vol% solvent (trifluoroethanol/anisole = 9/1), irradiated under blue LEDs (465 nm, 12 mW/cm^2). Reproduced with permission from Ref [104].

Photoinduced iron-catalyzed ATRP was attempted in aqueous media using FeBr$_3$ and water-soluble ligands (tetrabutylammonium bromide, tris[2-(2-methoxyethoxy)ethyl]amine, and triphenylphosphine-3,3′,3″-trisulfonic acid trisodium) under UV light irradiation.[39] Polymerizations in water were controlled only in the presence of high concentrations of the iron catalyst as much as 6-10 equiv. with respect to initiator (or 20000-33000 ppm with respect to monomer) giving polymers with dispersities <1.40.

Iron complexes have been used as photocatalysts to enable ATRP under photoredox catalysis conditions.[39, 105] Under visible light irradiation, the catalysts were promoted to the excited state in which the iron catalysts were effective in activating the alkyl halide initiators and generate initiating/propagating radicals. Although these iron complexes were strongly reducing in the photoexcited state (< -2.1 V), they showed very short excited state life-time of < 10 ns, and therefore resulted in moderate control over polymerization.

In photoinduced ATRP, direct photolysis of the Fe-Br bond to generate the activator results in the formation of Br$^•$ radicals, which are also capable of reacting with monomers and initiate polymerization of new chains. As a result, targeting high molecular weight polymers may be not accessible under these conditions, as generation of new initiating species may lead to formation of new low molecular weight chains and higher dispersities. Therefore, developing

photocatalytic processes where (re)generation of the activator is realized via electron or energy transfer events would be advantageous to both expand the applicability of photochemically mediated ATRP to a variety of iron complexes and also achieve well-controlled synthesis of polymers with high molecular weights.

Furthermore, electrochemically-mediated ATRP[106] has not yet been fully investigated in iron-based catalytic systems.[15] Electrochemistry would enable direct use of electrons to generate activator species without contaminating the polymer mixture with side products of the chemical reduction processes, and also better characterize the catalytic processes.

4.2.5   Monomer Scope in Iron-Catalyzed ATRP

Iron-catalyzed ATRP has been successfully applied in well-controlled polymerization of various methacrylate and styrene monomers. However, polymerization of monomers that contain polar functional groups can be challenging under iron-catalyzed conditions as the polar functional groups may interact with catalyst and therefore affect its catalytic efficiency.

ATRP of methacrylic acid (MAA) was controlled using heme catalysts.[107] Direct polymerization of MAA by ATRP was challenging due to termination of chain ends via lactonization. Therefore, direct ATRP of MAA required development of special conditions such as low pH to control the polymerization using a copper catalyst.[108] However, the heme catalyst was effective in controlling the polymerization of MAA to yield well-controlled polymers in aqueous solutions. Importantly, the heme-based catalysts performed well in the presence of acidic groups and in aqueous media, suggesting the potential of these compounds as robust iron based ATRP catalysts.

ATRP of other families of vinyl monomers such as acrylate, (meth)acrylamides, etc., using iron catalysts has been challenging and less efficient. Iron-catalyzed ATRP of acrylates often leads to low monomer conversions, low initiation efficiency and polymers with high dispersities.[108-110] Acrylate-based secondary radicals are more susceptible to undergo formation of organometallic species with the L/Fe^{II} activators than the tertiary methacrylate-based or styrenic radicals. As a result, high degree of the formation of organometallic species and subsequent catalytic radical termination or catalytic chain transfer reactions, result in termination of polymers chains. Furthermore, the lower activity of dormant acrylate chain end compared to the methacrylate chain ends may also contribute for the lower efficiency of control observed in the polymerization

of acrylate monomers using iron catalysts. Considering the high propagation rate constants of acrylate monomers, the deactivation should also be fast enough to provide well-controlled polymerization. The use of iron catalysts that typically have lower activity than copper complexes may not be efficient for promoting fast initiation and activation of the chain ends in polymerization of acrylates.

ATRP of methyl acrylate (MA) using iron catalysts in the presence of halide salts gave low monomer conversions (~ 30%) and polymers with relatively high dispersities (1.3-1.9).[57] Similarly, polymerization of MA using diimine iron complexes was slow and resulted in high dispersity vales (~ 1.5-1.6). Polymerization of butyl acrylate was well-controlled using cyclopentyl-functionalized TACN iron complexes yielding quantitative monomer conversions, and low dispersity values (1.2).[53]

An iodine-based initiating system was developed for the polymerization of acrylate monomers using iron catalysis. Dicarbonylcyclopentadienyliodoiron(II) in conjunction with a metal alkoxide such as $Al(Oi\text{-}Pr)_3$ was used in the presence of an alkyl iodide initiator to control polymerization of acrylate monomers.[32] The nature of the alkyl halide initiator greatly affected control over the polymerization as use of less active Br or Cl chain ends resulted in a loss of control with polymers having high dispersities, whereas I-based initiating system afforded well-controlled polymers with low dispersity (< 1.2). The control was attributed to the synergistic effect of the iron catalyst and the metal alkoxide additive, which enhanced activation of chain ends, as well as using the more active iodine-based initiating system. However, for alkyl iodides, a degenerative transfer is also possible and can provide additional pathway for polymerization control.[32]

Polymerization of vinyl acetate was attempted using iron(II) acetate catalyst and CCl_4 as the initiator.[48] The polymerization mechanism was redox-initiated radical telomerization and not ATRP, resulting in polymers with molecular weights that did not increase with conversion but followed quite precisely $[VOAc]_0/[CCl_4]_0$ ratios due to a C_{tr}~1 for CCl_4. Under OMRP conditions, polymerization of vinyl acetate using iron(II) acetate catalyst showed better controlled results.[111]

4.2.6 Conclusions and Outlook

Iron complexes form an important class of ATRP catalysts that provide efficient and well-controlled polymerization of various functional monomers. There is a great potential to develop biocompatible, less toxic, and inexpensive iron-based catalytic systems for ATRP. Iron catalysts have been mainly applied for well-controlled ATRP of methacrylate and styrene monomers. Despite many successful studies on designing and use of iron catalysts in ATRP, there are still challenges that need to be addressed to take a full advantage of iron catalysis in ATRP. For instance, the use of iron catalysts has been rarely successful for controlling polymerization of acrylates, due to the possibility of formation of organometallic species and subsequent termination events. In addition to developing new iron-based catalytic systems for ATRP and broadening their utility in polymerization of new functional monomers, iron catalysts need to be explored and studied further to better understand their behavior in catalyzing ATRP reactions. For example, establishing structure-reactivity relationships in iron catalysts regarding the activation and deactivation processes would enable a better understanding of iron-catalyzed ATRP and therefore developing more efficient catalytic systems. Establishing computational approaches and high throughput experimentation would enable understanding, designing, and examining efficient iron catalysts for ATRP. Considering the biological relevance of iron compounds, it would be advantageous to develop iron-based catalytic systems, especially those derived or inspired from biological resources, for synthesis of polymer-bioconjugates or other functional polymeric materials by iron-catalyzed ATRP.

4.2.7 References

1. Dadashi-Silab, S.; Lee, I.-H.; Anastasaki, A.; Lorandi, F.; Narupai, B.; Dolinski, N. D.; Allegrezza, M. L.; Fantin, M.; Konkolewicz, D.; Hawker, C. J.; Matyjaszewski, K. Investigating Temporal Control in Photoinduced Atom Transfer Radical Polymerization. *Macromolecules* **2020,** 53 (13), 5280-5288.

2. Ribelli, T. G.; Lorandi, F.; Fantin, M.; Matyjaszewski, K. Atom Transfer Radical Polymerization: Billion Times More Active Catalysts and New Initiation Systems. *Macromol. Rapid Commun.* **2019,** 40 (1), 1800616.

3. Matyjaszewski, K. Atom Transfer Radical Polymerization (ATRP): Current Status and Future Perspectives. *Macromolecules* **2012,** 45 (10), 4015-4039.

4. Wang, J.-S.; Matyjaszewski, K. Controlled/"living" radical polymerization. atom transfer radical polymerization in the presence of transition-metal complexes. *J. Am. Chem. Soc.* **1995,** 117 (20), 5614-5615.

5. Matyjaszewski, K.; Xia, J. Atom Transfer Radical Polymerization. *Chem. Rev.* **2001,** 101 (9), 2921-2990.

6. Matyjaszewski, K.; Tsarevsky, N. V. Macromolecular Engineering by Atom Transfer Radical Polymerization. *J. Am. Chem. Soc.* **2014,** 136 (18), 6513-6533.

7. Perrier, S. 50th Anniversary Perspective: RAFT Polymerization—A User Guide. *Macromolecules* **2017,** 50 (19), 7433-7447.

8. Xu, J.; Jung, K.; Atme, A.; Shanmugam, S.; Boyer, C. A Robust and Versatile Photoinduced Living Polymerization of Conjugated and Unconjugated Monomers and Its Oxygen Tolerance. *J. Am. Chem. Soc.* **2014,** 136 (14), 5508-5519.

9. Moad, G.; Rizzardo, E.; Thang, S. H. Living Radical Polymerization by the RAFT Process – A Third Update. *Aust. J. Chem.* **2012,** 65 (8), 985-1076.

10. Hill, M. R.; Carmean, R. N.; Sumerlin, B. S. Expanding the Scope of RAFT Polymerization: Recent Advances and New Horizons. *Macromolecules* **2015,** 48 (16), 5459-5469.

11. David, G.; Boyer, C.; Tonnar, J.; Ameduri, B.; Lacroix-Desmazes, P.; Boutevin, B. Use of Iodocompounds in Radical Polymerization. *Chem. Rev.* **2006,** 106 (9), 3936-3962.

12. Goto, A.; Ohtsuki, A.; Ohfuji, H.; Tanishima, M.; Kaji, H. Reversible Generation of a Carbon-Centered Radical from Alkyl Iodide Using Organic Salts and Their Application as Organic Catalysts in Living Radical Polymerization. *J. Am. Chem. Soc.* **2013,** 135 (30), 11131-11139.

13. Dadashi-Silab, S.; Lorandi, F.; Fantin, M.; Matyjaszewski, K. Redox-switchable atom transfer radical polymerization. *Chem. Commun.* **2019,** 55 (5), 612-615.

14. Pan, X.; Fantin, M.; Yuan, F.; Matyjaszewski, K. Externally controlled atom transfer radical polymerization. *Chem. Soc. Rev.* **2018,** 47 (14), 5457-5490.

15. Telitel, S.; Dumur, F.; Campolo, D.; Poly, J.; Gigmes, D.; Pierre Fouassier, J.; Lalevée, J. Iron complexes as potential photocatalysts for controlled radical photopolymerizations: A tool for modifications and patterning of surfaces. *J. Polym. Sci., Part A: Polym. Chem.* **2016,** 54 (5), 702-713.

16. di Lena, F.; Matyjaszewski, K. Transition metal catalysts for controlled radical polymerization. *Prog. Polym. Sci.* **2010,** 35 (8), 959-1021.

17. Ando, T.; Kamigaito, M.; Sawamoto, M. Iron(II) Chloride Complex for Living Radical Polymerization of Methyl Methacrylate. *Macromolecules* **1997,** 30 (16), 4507-4510.

18. Matyjaszewski, K.; Wei, M.; Xia, J.; McDermott, N. E. Controlled/"Living" Radical Polymerization of Styrene and Methyl Methacrylate Catalyzed by Iron Complexes. *Macromolecules* **1997,** 30 (26), 8161-8164.

19. Poli, R.; Allan, L. E. N.; Shaver, M. P. Iron-mediated reversible deactivation controlled radical polymerization. *Prog. Polym. Sci.* **2014,** 39 (10), 1827-1845.

20. Xue, Z.; He, D.; Xie, X. Iron-catalyzed atom transfer radical polymerization. *Polym. Chem.* **2015,** 6 (10), 1660-1687.

21. Kato, M.; Kamigaito, M.; Sawamoto, M.; Higashimura, T. Polymerization of Methyl Methacrylate with the Carbon Tetrachloride/Dichlorotris-(triphenylphosphine)ruthenium(II)/Methylaluminum Bis(2,6-di-tert-butylphenoxide) Initiating System: Possibility of Living Radical Polymerization. *Macromolecules* **1995,** 28 (5), 1721-1723.

22. Braunecker, W. A.; Itami, Y.; Matyjaszewski, K. Osmium-Mediated Radical Polymerization. *Macromolecules* **2005,** 38 (23), 9402-9404.

23. Pan, X.; Fang, C.; Fantin, M.; Malhotra, N.; So, W. Y.; Peteanu, L. A.; Isse, A. A.; Gennaro, A.; Liu, P.; Matyjaszewski, K. Mechanism of Photoinduced Metal-Free Atom Transfer Radical Polymerization: Experimental and Computational Studies. *J. Am. Chem. Soc.* **2016,** 138 (7), 2411-2425.

24. Discekici, E. H.; Anastasaki, A.; Read de Alaniz, J.; Hawker, C. J. Evolution and Future Directions of Metal-Free Atom Transfer Radical Polymerization. *Macromolecules* **2018,** 51 (19), 7421-7434.

25. Treat, N. J.; Sprafke, H.; Kramer, J. W.; Clark, P. G.; Barton, B. E.; Read de Alaniz, J.; Fors, B. P.; Hawker, C. J. Metal-Free Atom Transfer Radical Polymerization. *J. Am. Chem. Soc.* **2014,** 136 (45), 16096-16101.

26. Theriot, J. C.; Lim, C.-H.; Yang, H.; Ryan, M. D.; Musgrave, C. B.; Miyake, G. M. Organocatalyzed atom transfer radical polymerization driven by visible light. *Science* **2016,** 352 (6289), 1082-1086.

27. Allan, L. E. N.; Perry, M. R.; Shaver, M. P. Organometallic mediated radical polymerization. *Prog. Polym. Sci.* **2012,** 37 (1), 127-156.

28. Poli, R. New Phenomena in Organometallic-Mediated Radical Polymerization (OMRP) and Perspectives for Control of Less Active Monomers. *Chem. Eur. J.* **2015,** 21 (19), 6988-7001.

29. Shaver, M. P.; Allan, L. E. N.; Rzepa, H. S.; Gibson, V. C. Correlation of Metal Spin State with Catalytic Reactivity: Polymerizations Mediated by α-Diimine–Iron Complexes. *Angew. Chem. Int. Ed.* **2006,** 45 (8), 1241-1244.

30. Lake, B. R. M.; Shaver, M. P., The Interplay of ATRP, OMRP and CCT in Iron-Mediated Controlled Radical Polymerization. In *Controlled Radical Polymerization: Mechanisms*, American Chemical Society: 2015; Vol. 1187, pp 311-326.

31. Fantin, M.; Lorandi, F.; Ribelli, T. G.; Szczepaniak, G.; Enciso, A. E.; Fliedel, C.; Thevenin, L.; Isse, A. A.; Poli, R.; Matyjaszewski, K. Impact of Organometallic Intermediates on Copper-Catalyzed Atom Transfer Radical Polymerization. *Macromolecules* **2019,** 52 (11), 4079-4090.

32. Teodorescu, M.; Gaynor, S. G.; Matyjaszewski, K. Halide Anions as Ligands in Iron-Mediated Atom Transfer Radical Polymerization. *Macromolecules* **2000,** 33 (7), 2335-2339.

33. Wang, Y.; Matyjaszewski, K. ATRP of MMA Catalyzed by FeIIBr2 in the Presence of Triflate Anions. *Macromolecules* **2011,** 44 (6), 1226-1228.

34. Sarbu, T.; Matyjaszewski, K. ATRP of Methyl Methacrylate in the Presence of Ionic Liquids with Ferrous and Cuprous Anions. *Macromol. Chem. Phys.* **2001,** 202 (17), 3379-3391.

35. Ishio, M.; Katsube, M.; Ouchi, M.; Sawamoto, M.; Inoue, Y. Active, Versatile, and Removable Iron Catalysts with Phosphazenium Salts for Living Radical Polymerization of Methacrylates. *Macromolecules* **2009,** 42 (1), 188-193.

36. Wang, Y.; Zhang, Y.; Parker, B.; Matyjaszewski, K. ATRP of MMA with ppm Levels of Iron Catalyst. *Macromolecules* **2011,** 44 (11), 4022-4025.

37. Wang, J.; Han, J.; Xie, X.; Xue, Z.; Fliedel, C.; Poli, R. FeBr2-Catalyzed Bulk ATRP Promoted by Simple Inorganic Salts. *Macromolecules* **2019,** 52 (14), 5366-5376.

38. Wang, J.; Xie, X.; Xue, Z.; Fliedel, C.; Poli, R. Ligand- and solvent-free ATRP of MMA with FeBr3 and inorganic salts. *Polym. Chem.* **2020,** 11 (7), 1375-1385.

39. Dadashi-Silab, S.; Matyjaszewski, K. Iron-Catalyzed Atom Transfer Radical Polymerization of Semifluorinated Methacrylates. *ACS Macro Lett.* **2019,** 8 (9), 1110-1114.

40. Ding, K.; Zannat, F.; Morris, J. C.; Brennessel, W. W.; Holland, P. L. Coordination of N-methylpyrrolidone to iron(II). *J. Organomet. Chem.* **2009,** 694 (26), 4204-4208.

41. Schroeder, H.; Buback, J.; Demeshko, S.; Matyjaszewski, K.; Meyer, F.; Buback, M. Speciation Analysis in Iron-Mediated ATRP Studied via FT-Near-IR and Mössbauer Spectroscopy. *Macromolecules* **2015,** 48 (7), 1981-1990.

42. Matyjaszewski, K.; Coca, S.; Gaynor, S. G.; Wei, M.; Woodworth, B. E. Zerovalent Metals in Controlled/"Living" Radical Polymerization. *Macromolecules* **1997,** 30 (23), 7348-7350.

43. Zhang, H.; Marin, V.; Fijten, M. W. M.; Schubert, U. S. High-throughput experimentation in atom transfer radical polymerization: A general approach toward a directed design and understanding of optimal catalytic systems. *J. Polym. Sci., Part A: Polym. Chem.* **2004,** 42 (8), 1876-1885.

44. Bergenudd, H.; Jonsson, M.; Malmström, E. Investigation of iron complexes in ATRP: Indications of different iron species in normal and reverse ATRP. *J. Mol. Catal. A: Chem.* **2011,** 346 (1), 20-28.

45. Aoshima, H.; Satoh, K.; Umemura, T.; Kamigaito, M. A simple combination of higher-oxidation-state FeX3 and phosphine or amine ligand for living radical polymerization of styrene, methacrylate, and acrylate. *Polym. Chem.* **2013,** 4 (12), 3554-3562.

46. Niibayashi, S.; Hayakawa, H.; Jin, R.-H.; Nagashima, H. Reusable and environmentally friendly ionic trinuclear iron complex catalyst for atom transfer radical polymerization. *Chem. Commun.* **2007,** (18), 1855-1857.

47. Kawamura, M.; Sunada, Y.; Kai, H.; Koike, N.; Hamada, A.; Hayakawa, H.; Jin, R.-H.; Nagashima, H. New Iron(II) Complexes for Atom-Transfer Radical Polymerization: The Ligand Design for Triazacyclononane Results in High Reactivity and Catalyst Performance. *Adv. Synth. Catal.* **2009,** 351 (13), 2086-2090.

48. Nakanishi, S.-i.; Kawamura, M.; Kai, H.; Jin, R.-H.; Sunada, Y.; Nagashima, H. Well-Defined Iron Complexes as Efficient Catalysts for "Green" Atom-Transfer Radical Polymerization of Styrene, Methyl Methacrylate, and Butyl Acrylate with Low Catalyst Loadings and Catalyst Recycling. *Chem. Eur. J.* **2014,** 20 (19), 5802-5814.

49. Nakanishi, S.-i.; Kawamura, M.; Sunada, Y.; Nagashima, H. Atom transfer radical polymerization by solvent-stabilized (Me3TACN)FeX2: a practical access to reusable iron(ii) catalysts. *Polym. Chem.* **2016,** 7 (5), 1037-1048.

50. Gibson, V. C.; O'Reilly, R. K.; Wass, D. F.; White, A. J. P.; Williams, D. J. Iron complexes bearing iminopyridine and aminopyridine ligands as catalysts for atom transfer radical polymerisation. *Dalton Transactions* **2003,** (14), 2824-2830.

51. Göbelt, B.; Matyjaszewski, K. Diimino- and diaminopyridine complexes of CuBr and FeBr2 as catalysts in atom transfer radical polymerization (ATRP). *Macromol. Chem. Phys.* **2000,** 201 (14), 1619-1624.

52. Gibson, V. C.; O'Reilly, R. K.; Reed, W.; Wass, D. F.; White, A. J. P.; Williams, D. J. Four-coordinate iron complexes bearing α-diimine ligands: efficient catalysts for Atom Transfer Radical Polymerisation (ATRP). *Chem. Commun.* **2002,** (17), 1850-1851.

53. O'Reilly, R. K.; Shaver, M. P.; Gibson, V. C.; White, A. J. P. α-Diimine, Diamine, and Diphosphine Iron Catalysts for the Controlled Radical Polymerization of Styrene and Acrylate Monomers. *Macromolecules* **2007,** 40 (21), 7441-7452.

54. Gibson, V. C.; O'Reilly, R. K.; Wass, D. F.; White, A. J. P.; Williams, D. J. Polymerization of Methyl Methacrylate Using Four-Coordinate (α-Diimine)iron Catalysts: Atom Transfer Radical Polymerization vs Catalytic Chain Transfer. *Macromolecules* **2003,** 36 (8), 2591-2593.

55. Azuma, Y.; Terashima, T.; Sawamoto, M. Self-Folding Polymer Iron Catalysts for Living Radical Polymerization. *ACS Macro Lett.* **2017,** 6 (8), 830-835.

56. Allan, L. E. N.; MacDonald, J. P.; Reckling, A. M.; Kozak, C. M.; Shaver, M. P. Controlled Radical Polymerization Mediated by Amine–Bis(phenolate) Iron(III) Complexes. *Macromol. Rapid Commun.* **2012,** 33 (5), 414-418.

57. Allan, L. E. N.; MacDonald, J. P.; Nichol, G. S.; Shaver, M. P. Single Component Iron Catalysts for Atom Transfer and Organometallic Mediated Radical Polymerizations: Mechanistic Studies and Reaction Scope. *Macromolecules* **2014,** 47 (4), 1249-1257.

58. Coward, D. L.; Lake, B. R. M.; Shaver, M. P. Understanding Organometallic-Mediated Radical Polymerization with an Iron(II) Amine–Bis(phenolate). *Organometallics* **2017,** 36 (17), 3322-3328.

59. Schroeder, H.; Lake, B. R. M.; Demeshko, S.; Shaver, M. P.; Buback, M. A Synthetic and Multispectroscopic Speciation Analysis of Controlled Radical Polymerization Mediated by Amine–Bis(phenolate)iron Complexes. *Macromolecules* **2015,** 48 (13), 4329-4338.

60. Poli, R.; Shaver, M. P. Atom Transfer Radical Polymerization (ATRP) and Organometallic Mediated Radical Polymerization (OMRP) of Styrene Mediated by Diaminobis(phenolato)iron(II) Complexes: A DFT Study. *Inorg. Chem.* **2014,** 53 (14), 7580-7590.

61. Nishiura, C.; Williams, V.; Matyjaszewski, K. Iron and copper based catalysts containing anionic phenolate ligands for atom transfer radical polymerization. *Macromolecular Research* **2017,** 25 (6), 504-512.

62. Sigg, S. J.; Seidi, F.; Renggli, K.; Silva, T. B.; Kali, G.; Bruns, N. Horseradish Peroxidase as a Catalyst for Atom Transfer Radical Polymerization. *Macromol. Rapid Commun.* **2011,** 32 (21), 1710-1715.

63. Pollard, J.; Bruns, N., Biocatalytic ATRP. In *Reversible Deactivation Radical Polymerization: Mechanisms and Synthetic Methodologies*, American Chemical Society: 2018; Vol. 1284, pp 379-393.

64. Rodriguez, K. J.; Gajewska, B.; Pollard, J.; Pellizzoni, M. M.; Fodor, C.; Bruns, N. Repurposing Biocatalysts to Control Radical Polymerizations. *ACS Macro Lett.* **2018,** 7 (9), 1111-1119.

65. Ng, Y.-H.; di Lena, F.; Chai, C. L. L. PolyPEGA with predetermined molecular weights from enzyme-mediated radical polymerization in water. *Chem. Commun.* **2011,** 47 (22), 6464-6466.

66. Silva, T. B.; Spulber, M.; Kocik, M. K.; Seidi, F.; Charan, H.; Rother, M.; Sigg, S. J.; Renggli, K.; Kali, G.; Bruns, N. Hemoglobin and Red Blood Cells Catalyze Atom Transfer Radical Polymerization. *Biomacromolecules* **2013,** 14 (8), 2703-2712.

67. Simakova, A.; Mackenzie, M.; Averick, S. E.; Park, S.; Matyjaszewski, K. Bioinspired Iron-Based Catalyst for Atom Transfer Radical Polymerization. *Angew. Chem. Int. Ed.* **2013,** 52 (46), 12148-12151.

68. Fu, L.; Simakova, A.; Park, S.; Wang, Y.; Fantin, M.; Matyjaszewski, K. Axially Ligated Mesohemins as Bio-Mimicking Catalysts for Atom Transfer Radical Polymerization. *Molecules* **2019,** 24 (21), 3969.

69. Smolne, S.; Buback, M.; Demeshko, S.; Matyjaszewski, K.; Meyer, F.; Schroeder, H.; Simakova, A. Kinetics of Fe–Mesohemin–(MPEG500)2-Mediated RDRP in Aqueous Solution. *Macromolecules* **2016,** 49 (21), 8088-8097.

70. Uchiike, C.; Terashima, T.; Ouchi, M.; Ando, T.; Kamigaito, M.; Sawamoto, M. Evolution of Iron Catalysts for Effective Living Radical Polymerization: Design of Phosphine/Halogen Ligands in FeX2(PR3)2. *Macromolecules* **2007,** 40 (24), 8658-8662.

71. Xue, Z.; Linh, N. T. B.; Noh, S. K.; Lyoo, W. S. Phosphorus-Containing Ligands for Iron(III)-Catalyzed Atom Transfer Radical Polymerization. *Angew. Chem. Int. Ed.* **2008,** 47 (34), 6426-6429.

72. Xue, Z.; Oh, H. S.; Noh, S. K.; Lyoo, W. S. Phosphorus Ligands for Iron(III)-Mediated Atom Transfer Radical Polymerization of Methyl Methacrylate. *Macromol. Rapid Commun.* **2008,** 29 (23), 1887-1894.

73. Xue, Z.; Noh, S. K.; Lyoo, W. S. 2-[(Diphenylphosphino)methyl]pyridine as ligand for iron-based atom transfer radical polymerization. *J. Polym. Sci., Part A: Polym. Chem.* **2008,** 46 (9), 2922-2935.

74. Xue, Z.; He, D.; Noh, S. K.; Lyoo, W. S. Iron(III)-Mediated Atom Transfer Radical Polymerization in the Absence of Any Additives. *Macromolecules* **2009,** 42 (8), 2949-2957.

75. Ribelli, T. G.; Fantin, M.; Daran, J.-C.; Augustine, K. F.; Poli, R.; Matyjaszewski, K. Synthesis and Characterization of the Most Active Copper ATRP Catalyst Based on Tris[(4-dimethylaminopyridyl)methyl]amine. *J. Am. Chem. Soc.* **2018,** 140 (4), 1525-1534.

76. Wang, Y.; Kwak, Y.; Matyjaszewski, K. Enhanced Activity of ATRP Fe Catalysts with Phosphines Containing Electron Donating Groups. *Macromolecules* **2012,** 45 (15), 5911-5915.

77. Schröder, K.; Mathers, R. T.; Buback, J.; Konkolewicz, D.; Magenau, A. J. D.; Matyjaszewski, K. Substituted Tris(2-pyridylmethyl)amine Ligands for Highly Active ATRP Catalysts. *ACS Macro Lett.* **2012,** 1 (8), 1037-1040.

78. Schroeder, H.; Matyjaszewski, K.; Buback, M. Kinetics of Fe-Mediated ATRP with Triarylphosphines. *Macromolecules* **2015,** 48 (13), 4431-4437.

79. Dadashi-Silab, S.; Pan, X.; Matyjaszewski, K. Photoinduced Iron-Catalyzed Atom Transfer Radical Polymerization with ppm Levels of Iron Catalyst under Blue Light Irradiation. *Macromolecules* **2017,** 50 (20), 7967-7977.

80. Nishizawa, K.; Ouchi, M.; Sawamoto, M. Phosphine–Ligand Decoration toward Active and Robust Iron Catalysts in LRP. *Macromolecules* **2013,** 46 (9), 3342-3349.

81. Uchiike, C.; Ouchi, M.; Ando, T.; Kamigaito, M.; Sawamoto, M. Evolution of iron catalysts for effective living radical polymerization: P–N chelate ligand for enhancement of catalytic performances. *J. Polym. Sci., Part A: Polym. Chem.* **2008,** 46 (20), 6819-6827.

82. Khan, M. Y.; Zhou, J.; Chen, X.; Khan, A.; Mudassir, H.; Xue, Z.; Lee, S. W.; Noh, S. K. Exploration of highly active bidentate ligands for iron (III)-catalyzed ATRP. *Polymer* **2016,** 90, 309-316.

83. Ishio, M.; Terashima, T.; Ouchi, M.; Sawamoto, M. Carbonyl−Phosphine Heteroligation for Pentamethylcyclopentadienyl (Cp*)−Iron Complexes: Highly Active and Versatile Catalysts for Living Radical Polymerization. *Macromolecules* **2010,** 43 (2), 920-926.

84. Wang, Y.; Matyjaszewski, K. ATRP of MMA in Polar Solvents Catalyzed by FeBr2 without Additional Ligand. *Macromolecules* **2010,** 43 (9), 4003-4005.

85. Eckenhoff, W. T.; Biernesser, A. B.; Pintauer, T. Structural characterization and investigation of iron(III) complexes with nitrogen and phosphorus based ligands in atom transfer radical addition (ATRA). *Inorg. Chim. Acta* **2012,** 382, 84-95.

86. Okada, S.; Park, S.; Matyjaszewski, K. Initiators for Continuous Activator Regeneration Atom Transfer Radical Polymerization of Methyl Methacrylate and Styrene with N-Heterocyclic Carbene as Ligands for Fe-Based Catalysts. *ACS Macro Lett.* **2014,** 3 (9), 944-947.

87. Zhang, L.; Miao, J.; Cheng, Z.; Zhu, X. Iron-Mediated ICAR ATRP of Styrene and Methyl Methacrylate in the Absence of Thermal Radical Initiator. *Macromol. Rapid Commun.* **2010,** 31 (3), 275-280.

88. Zhu, G.; Zhang, L.; Zhang, Z.; Zhu, J.; Tu, Y.; Cheng, Z.; Zhu, X. Iron-Mediated ICAR ATRP of Methyl Methacrylate. *Macromolecules* **2011,** 44 (9), 3233-3239.

89. Mukumoto, K.; Wang, Y.; Matyjaszewski, K. Iron-Based ICAR ATRP of Styrene with ppm Amounts of FeIIIBr3 and 1,1′ -Azobis(cyclohexanecarbonitrile). *ACS Macro Lett.* **2012,** 1 (5), 599-602.

90. Luo, R.; Sen, A. Electron-Transfer-Induced Iron-Based Atom Transfer Radical Polymerization of Styrene Derivatives and Copolymerization of Styrene and Methyl Methacrylate. *Macromolecules* **2008,** 41 (12), 4514-4518.

91. Khan, M. Y.; Chen, X.; Lee, S. W.; Noh, S. K. Development of New Atom Transfer Radical Polymerization System by Iron (III)-Metal Salts Without Using any External Initiator and Reducing Agent. *Macromol. Rapid Commun.* **2013,** 34 (15), 1225-1230.

92. He, D.; Xue, Z.; Khan, M. Y.; Noh, S. K.; Lyoo, W. S. Phosphorus ligands for iron(III)-mediated ATRP of styrene via generation of activators by monomer addition. *J. Polym. Sci., Part A: Polym. Chem.* **2010,** 48 (1), 144-151.

93. Fujimura, K.; Ouchi, M.; Sawamoto, M. Ferrocene Cocatalysis for Iron-Catalyzed Living Radical Polymerization: Active, Robust, and Sustainable System under Concerted Catalysis by Two Iron Complexes. *Macromolecules* **2015,** 48 (13), 4294-4300.

94. Qin, J.; Cheng, Z.; Zhang, L.; Zhang, Z.; Zhu, J.; Zhu, X. A Highly Efficient Iron-Mediated AGET ATRP of Methyl Methacrylate Using Fe(0) Powder as the Reducing Agent. *Macromol. Chem. Phys.* **2011,** 212 (10), 999-1006.

95. Layadi, A.; Kessel, B.; Yan, W.; Romio, M.; Spencer, N. D.; Zenobi-Wong, M.; Matyjaszewski, K.; Benetti, E. M. Oxygen Tolerant and Cytocompatible Iron(0)-Mediated ATRP Enables the Controlled Growth of Polymer Brushes from Mammalian Cell Cultures. *J. Am. Chem. Soc.* **2020,** 142 (6), 3158-3164.

96. Dadashi-Silab, S.; Doran, S.; Yagci, Y. Photoinduced Electron Transfer Reactions for Macromolecular Syntheses. *Chem. Rev.* **2016,** 116 (17), 10212-10275.

97. Pan, X.; Tasdelen, M. A.; Laun, J.; Junkers, T.; Yagci, Y.; Matyjaszewski, K. Photomediated controlled radical polymerization. *Prog. Polym. Sci.* **2016,** 62, 73-125.

98. Chen, M.; Zhong, M.; Johnson, J. A. Light-Controlled Radical Polymerization: Mechanisms, Methods, and Applications. *Chem. Rev.* **2016,** 116 (17), 10167-10211.

99. Corrigan, N.; Shanmugam, S.; Xu, J.; Boyer, C. Photocatalysis in organic and polymer synthesis. *Chem. Soc. Rev.* **2016,** 45 (22), 6165-6212.

100. Dadashi-Silab, S.; Atilla Tasdelen, M.; Yagci, Y. Photoinitiated atom transfer radical polymerization: Current status and future perspectives. *J. Polym. Sci., Part A: Polym. Chem.* **2014,** 52 (20), 2878-2888.

101. Pan, X.; Malhotra, N.; Zhang, J.; Matyjaszewski, K. Photoinduced Fe-Based Atom Transfer Radical Polymerization in the Absence of Additional Ligands, Reducing Agents, and Radical Initiators. *Macromolecules* **2015,** 48 (19), 6948-6954.

102. Zhou, Y.-N.; Guo, J.-K.; Li, J.-J.; Luo, Z.-H. Photoinduced Iron(III)-Mediated Atom Transfer Radical Polymerization with In Situ Generated Initiator: Mechanism and Kinetics Studies. *Industrial & Engineering Chemistry Research* **2016,** 55 (39), 10235-10242.

103. Pan, X.; Malhotra, N.; Dadashi-Silab, S.; Matyjaszewski, K. A Simplified Fe-Based PhotoATRP Using Only Monomers and Solvent. *Macromol. Rapid Commun.* **2017,** 38 (13), 1600651.

104. Rolland, M.; Whitfield, R.; Messmer, D.; Parkatzidis, K.; Truong, N. P.; Anastasaki, A. Effect of Polymerization Components on Oxygen-Tolerant Photo-ATRP. *ACS Macro Lett.* **2019,** 8 (12), 1546-1551.

105. Dadashi-Silab, S.; Matyjaszewski, K. Temporal Control in Atom Transfer Radical Polymerization Using Zerovalent Metals. *Macromolecules* **2018,** 51 (11), 4250-4258.

106. Bian, C.; Zhou, Y.-N.; Guo, J.-K.; Luo, Z.-H. Photoinduced Fe-mediated atom transfer radical polymerization in aqueous media. *Polym. Chem.* **2017,** 8 (47), 7360-7368.

107. Bansal, A.; Kumar, P.; Sharma, C. D.; Ray, S. S.; Jain, S. L. Light-induced controlled free radical polymerization of methacrylates using iron-based photocatalyst in visible light. *J. Polym. Sci., Part A: Polym. Chem.* **2015,** 53 (23), 2739-2746.

108. Fantin, M.; Isse, A. A.; Venzo, A.; Gennaro, A.; Matyjaszewski, K. Atom Transfer Radical Polymerization of Methacrylic Acid: A Won Challenge. *J. Am. Chem. Soc.* **2016,** 138 (23), 7216-7219.

109. Wang, J.; Tian, M.; Li, S.; Wang, R.; Du, F.; Xue, Z. Ligand-free iron-based electrochemically mediated atom transfer radical polymerization of methyl methacrylate. *Polym. Chem.* **2018,** 9 (34), 4386-4394.

110. Fu, L.; Simakova, A.; Fantin, M.; Wang, Y.; Matyjaszewski, K. Direct ATRP of Methacrylic Acid with Iron-Porphyrin Based Catalysts. *ACS Macro Lett.* **2018,** 7 (1), 26-30.

111. Onishi, I.; Baek, K.-Y.; Kotani, Y.; Kamigaito, M.; Sawamoto, M. Iron-catalyzed living radical polymerization of acrylates: Iodide-based initiating systems and block and random copolymerizations. *J. Polym. Sci., Part A: Polym. Chem.* **2002,** 40 (12), 2033-2043.

4.3. Photoinduced Iron-Catalyzed Atom Transfer Radical Polymerization with ppm Levels of Iron Catalyst under Blue Light Irradiation

4.3.1 Abstract

Photoinduced atom transfer radical polymerization (ATRP) has been mainly explored using copper-based catalytic systems. Recently developed iron-catalyzed photochemical ATRP employed high amounts of iron catalysts under high energy UV light irradiation. Herein, a successful photoinduced iron-catalyzed ATRP mediated under blue light irradiation with ppm amounts (100-400 ppm) of iron(III) bromide/tetrabutylammonium bromide as the catalyst is reported. Several methacrylate monomers were polymerized with excellent control providing molecular weight in good agreement with theoretical values and low dispersity ($Đ<1.20$). Near-quantitative monomer conversions (~ 95%) enabled *in situ* chain extension and block copolymerization, indicating high retention of chain-end functionality. Notably, this system can tolerate oxygen, enabling synthesis of well-defined polymers with good chain-end functionality in the presence of air.
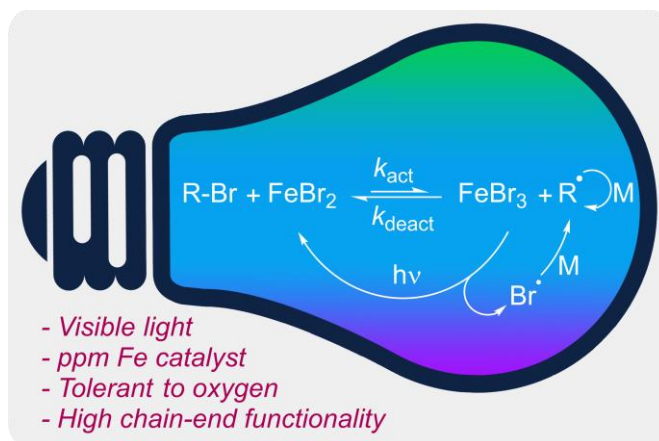
4.3.2 Introduction

The evolution of reversible deactivation radical polymerization (RDRP) techniques has led to the synthesis of well-defined polymers with predetermined molecular weight, incorporated functionality, and complex architecture from a broad range of radically (co)polymerizable monomers. Atom transfer radical polymerization (ATRP),[1-5] reversible addition-fragmentation chain transfer (RAFT),[6] and nitroxide-mediated polymerization (NMP)[4, 7, 8] are the most widely explored RDRP techniques for the controlled synthesis of polymers.

In ATRP, a transition metal catalyst is used to establish and maintain a dynamic equilibrium between dormant and active species resulting in a well-controlled polymerization.[9] Copper complexes (Cu/L) are the most commonly used catalysts in ATRP reactions.[7] Initially, in a procedure known as normal ATRP, large amounts of catalyst was used in order to compensate for irreversible radical termination reactions, that resulted in buildup of the higher oxidation state deactivator catalyst species. Recent developments in ATRP techniques have been directed towards designing new catalytic systems that can minimize catalyst loadings by *in situ* (re)generation of the activator species. For instance, thermal radical initiators can be used to slowly form radicals that react with Cu^{II}/L to regenerate Cu^{I}/L species in a procedure known as initiators for continuous activator regeneration (ICAR) ATRP.[10, 11] Chemical reducing agents are used in activators regenerated by electron transfer (ARGET) ATRP.[12-14] Zerovalent metals can be used in heterogeneous manner in supplemental activator and reducing agents (SARA) ATRP.[12, 13, 15, 16] Applying external stimuli offers the opportunity to mediate and control polymerization in a spatiotemporal manner, in addition to regeneration of the activator catalyst. To that end, the use of electrical current (*e*ATRP),[17-21] light,[22-29] and ultrasound[30, 31] have recently been developed for ATRP. These methods can be employed for activator regeneration under mild conditions while eliminating some side-reactions that could be observed with the use of chemical reducing agents.

Photochemistry has the potential to simplify reaction set up, conduct reactions under mild conditions, and offers spatial and temporal control over the polymerization.[32-37] Photochemical ATRP has been the focus of intense research in recent years using, primarily, Cu^{II}/L complexes. Mechanistically, it was shown that photoinduced electron transfer reactions between the electron-donors and Cu^{II} species results in the activator (re)generation. Recently photoredox catalysis, which is based on utilization of either a transition metal-based photocatalyst[35, 38] or an organo-catalyst[31, 39-43] to drive forward ATRP reactions, has seen a surge in interest for photochemical ATRP. In photoredox ATRP, excitation of the photocatalyst under light generates a highly reducing species that can reduce the alkyl halide initiator to form initiating radicals, which can be deactivated in a photocatalytic cycle to assert control over the polymerization reaction.

Iron (Fe) represents an environmentally benign opportunity to replace Cu catalysts or other precious metal-based complexes in catalyzing ATRP.[41, 44-47] It is one of the most abundant metals on the planet and promotes many biological processes. As such, Fe is of great importance for a wide array of chemical reactions and applications as it provides low toxicity, biocompatibility as well as cost efectivness.[48] A variety of Fe-based catalytic systems have been developed using ligands containing nitrogen[49-51] and phosphorous[52-55] compounds or halide anions.[56-58] Moreover, Fe-catalyzed ATRP can be controlled in the absence of additional ligands with polar solvents acting as complexing ligands.[59] Fe-based photochemical ATRP was shown to initiate and control polymerization of methacrylate monomers under UV light.[60] It was proposed that in the presence of methyl methacrylate (MMA), $FeBr_3$ could be photochemically reduced to the $FeBr_2$ activator species, which in turn also resulted in bromination of the MMA monomer. This process could also proceed in the absence of additional ligands in polar solvents, such as acetonitrile or dimethylformamide, solubilizing the Fe species. The brominated MMA (methyl 2,3-dibromoisobutyrate) formed during the photoreduction of $FeBr_3$ is an alkyl halide species capable of initiating polymerization and this was further taken advantage of in the polymerization of MMA in the absence of ATRP initiators and ligands.[61, 62] Furthermore, iron(III) chloride-mediated systems have been studied.[63] Nitrogen and phosphorous-based ligands were shown to be efficient in photochemical Fe ATRP reactions. However, the majority of photoinduced Fe-catalyzed ATRP systems reported so far have used high concentrations of Fe catalysts under high-energy UV light irradiation.

In this paper, we show that photoinduced Fe-catalyzed ATRP can be conducted in a controlled manner under a wide range of light sources from UV to blue and even to green light LEDs. The versatility of this system allows decreasing the concentration of the Fe catalyst to ppm levels while providing controlled polymerization of several methacrylate monomers. The system was used to form block copolymers *in situ*, which is indicative of the preservation of high chain-end functionality. Furthermore, the polymerization of MMA can be successfully conducted in non-degassed solutions, i.e. in the presence of oxygen.

4.3.3   Results and Discussion

Photoinduced Fe-Catalyzed ATRP: Optimization of Conditions. Originally, photoinduced Fe-catalyzed ATRP occurred in the presence of high catalyst loadings only under relatively high

energy light sources such as UV light. Therefore, we decided to investigate the Fe-based catalysts for ATRP under visible light irradiation while decreasing the catalyst content to ppm levels. Control experiments were performed in a systematic manner to elucidate the influence and contribution of each component involved in the reaction and optimize reaction conditions.

Polymerization of methyl methacrylate (MMA) in anisole was studied using ethyl α-bromophenylacetate (EBPA) as the initiator, $FeBr_3$ as the catalyst, and tetrabutylammonium bromide (TBABr) as the ligand. In the absence of EBPA initiator, with $FeBr_3$/TBABr at 100 ppm with respect to monomer (Entry 1, Table 14), the reaction resulted in <4% monomer conversion after 16 h irradiation under blue light LED irradiation (λ = 450 nm, 4 mW/cm^2) with number average molecular weight (M_n) of 33000 and a relatively high dispersity ($Đ$) of 1.6. EBPA and 100 ppm $FeBr_3$, but without TBABr resulted in no control over the polymerization with molecular weight higher than theoretical value ($M_{n,th}$ = 3950 vs. M_n = 13400) and $Đ$ of 5.15 (Entry 2, Table 14). Moreover, no polymerization was observed after 38 h when the reaction was kept in the dark (Entry 3, Table 14). These results indicated the importance of the initially added ATRP initiator and the ligand in a polymerization using ppm levels of $FeBr_3$ catalyst as well as light source for a successful controlled polymerization.

As shown in entries 4-6, Table 14, reactions proceeded in a well-controlled manner in the presence of 100, 200, and 400 ppm of $FeBr_3$/TBABr under blue light LED irradiation, respectively. The rate of the reaction decreased as the concentration of $FeBr_3$ was increased (see next section for detailed discussion of kinetics results) but high or near-quantitative monomer conversions were achieved with low $Đ$. In a reaction with 1000 ppm $FeBr_3$/TBABr and in the absence of EBPA initiator (Entry 7, Table 14), slightly better control was achieved compared to the 100 ppm $FeBr_3$/TBABr without EBPA (Entry 1, Table 14). As expected, increasing the concentration of $FeBr_3$ to 1000 ppm resulted in a greater decrease in the rate of the reaction, 73% monomer conversion after 16 h irradiation (Entry 8, Table 14).

Moreover, further increasing the concentration of $FeBr_3$ to equimolar ratios with respect to initiator (10000 ppm) resulted in a significant decrease in the rate of the reaction. Although the reaction in the absence of the ligand (Entry 9, Table 14) proceeded slightly faster than those in the presence of TBABr (Entry11, Table 1). However, good control was achieved using TBABr as the ligand in terms of low dispersity ($Đ$ = 1.13 vs. 1.79). The presence of TBABr was

necessary for solubilizing $FeBr_3$ and/or $FeBr_2$ species in a non-polar solvent such as anisole and hence controlling the polymerization process. Polymerization of MMA in the absence of EBPA, using 10000 ppm $FeBr_3$/TBABr, was even slower and it reached only 10% monomer conversion after 96 h irradiation under blue LEDs (Entry 10, Table 14). Finally, in the presence of EBPA initiator with an equimolar ratio of $FeBr_3$, the reaction reached to 40% monomer conversion after 96 h irradiation (Entry 11, Table 14).

Table 14.   Photoinduced Fe-catalyzed ATRP of MMA [a]

Entry	[MMA]/[EBPA]/[FeBr$_3$]/[TBABr]	Time (h)	Conv. (%)	$M_{n,th}$	M_n	Đ
1	100/0/0.01/0.01	16	< 4		33000	1.60
2	100/1/0.01/0	16	37	3950	13400	5.15
3 [b]	100/1/0.01/0.01	38	-	-	-	-
4	100/1/0.01/0.01	10	93	9550	10300	1.32
5	100/1/0.02/0.02	12	92	9450	9400	1.22
6	100/1/0.04/0.04	16	94	9650	10500	1.17
7	100/0/0.1/0.1	16	33		40000	1.43
8	100/1/0.1/0.1	16	73	7550	7700	1.18
9	100/1/1/0	96	75	7750	7100	1.79
10	100/0/1/1	96	10		2750	1.17
11	100/1/1/1	96	40	4250	3200	1.13

[a] Reactions were conducted in 50 vol% anisole, irradiated under blue light LED ($\lambda = 450$ nm, 4 mW/cm^2). Conversions were calculated by ^{1}H NMR. Theoretical molecular weight ($M_{n,th}$) values were calculated based on conversions as: $M_{n,th} = M_{EBPA} + $ [MMA]/[EBPA] $\times$ conversion $\times M_{MMA}$. Number-average molecular weight (M_n) and dispersity (Đ) were obtained by size exclusion chromatography (SEC) in THF based on poly(methyl methacrylate) standards. [b] Reaction was kept in the dark.

Kinetics of Photoinduced Fe-Catalyzed ATRP. After the reaction conditions were optimized, the kinetics of the polymerization of MMA was investigated using 100, 200, and 400 ppm $FeBr_3$/TBABr catalyst. Broad absorption spectra of $FeBr_3$/TBABr allows for controlling the polymerization using light sources with a variety of wavelengths. Different light sources used to initiate reactions, included a UV lamp at $\lambda = 365$ nm (6 mW/cm^2), blue light LEDs at $\lambda = 450$ nm (4 mW/cm^2), and green light LEDs at $\lambda = 520$ nm (2.5 mW/cm^2). Figure 72 shows the kinetics of

the polymerization of MMA under UV light (λ = 365 nm, 6 mW/cm^2) irradiation. Linear semi-logarithmic kinetic plots were observed at various FeBr$_3$/TBABr concentrations with molecular weights increasing as a function of monomer conversion.

The reaction proceeded in a similar fashion using the blue light LEDs with the rate of the reaction decreasing with increasing FeBr$_3$ concentration from 100 to 200 and 400 ppm (Figure 73). Depending on the concentration of the catalyst, reactions reached high or near-quantitative monomer conversions within 10-16 h irradiation under blue light LEDs. In all cases, molecular weights were in good agreement with theoretical values and displayed low *Đ*, in the range of 1.17-1.30. Moreover, the reaction was examined in the presence of excess amounts of TBABr ligand, at a ratio of [FeBr$_3$]/[TBABr] = 1/6. As shown in Figure 74, though not significantly, the rate of the reaction decreased slightly compared to the reaction with an equimolar ratio of the ligand. Nevertheless, in both equimolar and excess ratios of the ligand, reactions proceeded in a well-controlled manner.
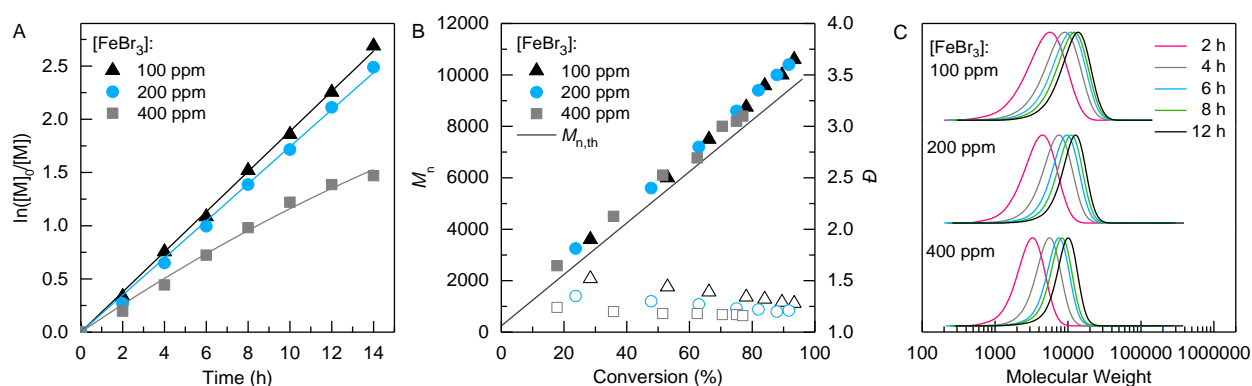
Figure 72. Photoinduced Fe-catalyzed ATRP of MMA under UV light irradiation (λ = 365 nm, 6 mW/cm^2). A: kinetics of the polymerization; B: number-average molecular weight (M_n, solid points) and dispersity (*Đ*, open points) as a function of monomer conversion; and C: SEC traces for the PMMA synthesized with different catalyst loadings. Reaction conditions: [MMA]/[EBPA]/[FeBr$_3$]/[TBABr] = 100/1/x/x in anisole 50 vol% (x = 0.01, 0.02, and 0.04).
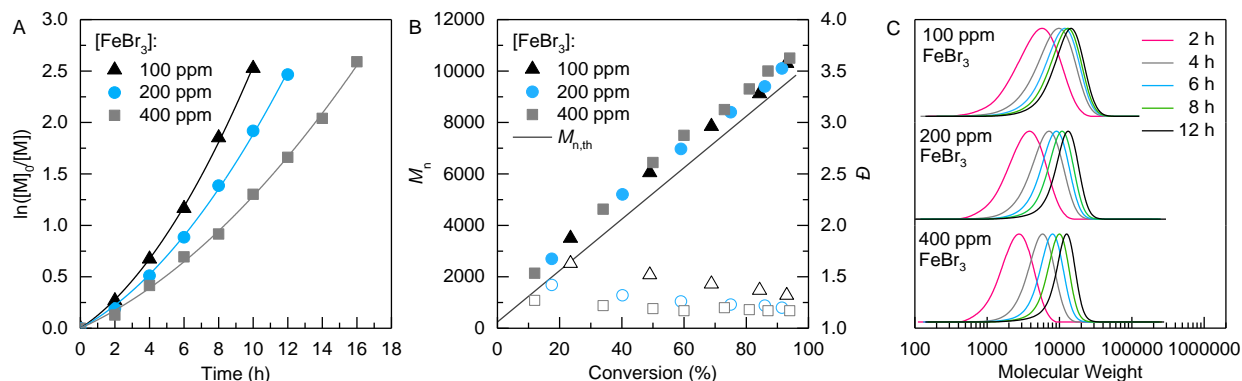
Figure 73. Photoinduced Fe-catalyzed ATRP of MMA under blue light LED irradiation (λ = 450 nm, 4 mW/cm^2). A: kinetics of the polymerization; B: number-average molecular weight (M_n, solid points) and dispersity ($Đ$, open points) as a function of monomer conversion; and C: SEC traces for the PMMA synthesized with different catalyst loadings. Reaction conditions: [MMA]/[EBPA]/[FeBr$_3$]/[TBABr] = 100/1/x/x in anisole 50 vol% (x = 0.01, 0.02, and 0.04).
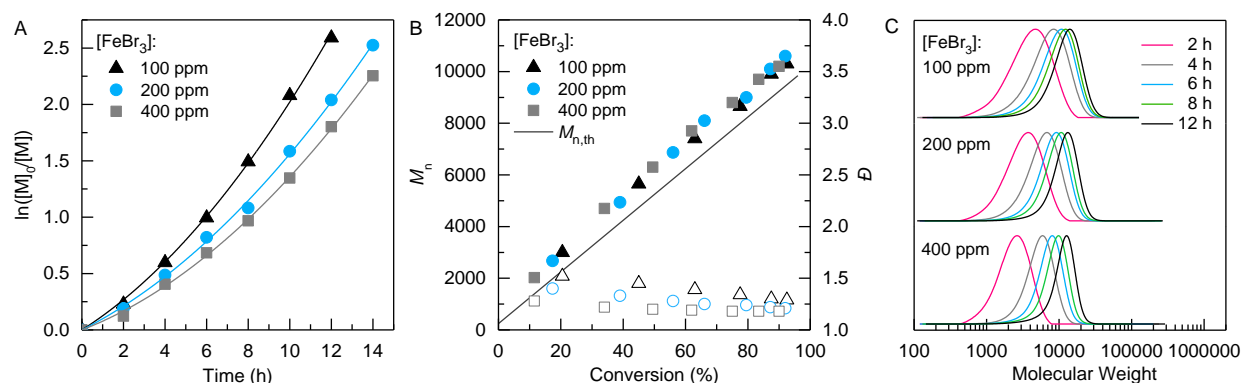
Figure 74. Photoinduced Fe-catalyzed ATRP of MMA under blue light LED irradiation (λ = 450 nm, 4 mW/cm^2) in the presence of excess ligand. A: kinetics of the polymerization; B: number-average molecular weight (M_n, solid points) and dispersity ($Đ$, open points) as a function of monomer conversion; and C: SEC traces for the PMMA synthesized with different catalyst loadings. Reaction conditions: [MMA]/[EBPA]/[FeBr$_3$]/[TBABr] = 100/1/x/6x in anisole 50 vol% (x = 0.01, 0.02, and 0.04).

The kinetics of the polymerization of MMA were also investigated using green light LEDs (λ = 520 nm, 2.5 mW/cm^2). As presented in Figure 75, the rate of the reaction with green LEDs was slower compared to those conducted under blue LEDs. This could be attributed to the fact that the absorption of the catalyst maximized in blue region of the electromagnetic spectrum with a

tailing absorption extending to the green region. The efficiency of green LEDs was not as high in the polymerization of MMA in blue LEDs or under a UV lamp. Monomer conversions were limited to 50-60% whereas in other cases near-quantitative conversions were reached regardless of the $FeBr_3$ ratio, and quite high Đ in the range of 1.30-1.80 were obtained under green light LEDs.
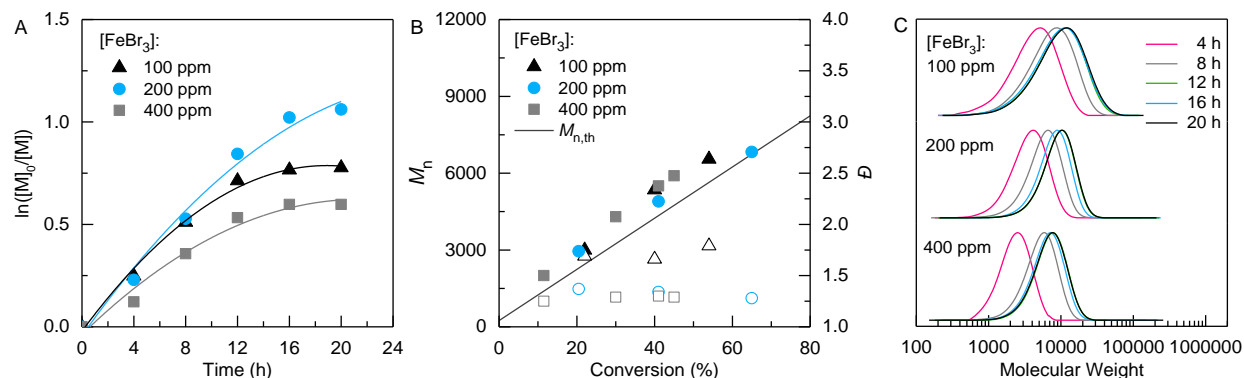
Figure 75. Photoinduced Fe-catalyzed ATRP of MMA under green light LED irradiation (λ = 520 nm, 2.5 mW/cm2). A: kinetics of the polymerization; B: number-average molecular weight (Mn, solid points) and dispersity (Đ, open points) as a function of monomer conversion; and C: SEC traces for the PMMA synthesized with different catalyst loadings. Reaction conditions: $[MMA]/[EBPA]/[FeBr_3]/[TBABr]$ = 100/1/x/x in anisole 50 vol% (x = 0.01, 0.02, and 0.04).

To illustrate the efficiency of the photoinduced Fe-catalyzed ATRP with ppm level catalyst under blue light irradiation, the kinetics of the polymerization of MMA were investigated using an equimolar ratio of $FeBr_3$ with respect to initiator. The results are shown in Figure 760. Due to the high concentration of the deactivator initially present, the reactions proceeded at a much lower rate of polymerization, compared to previous results obtained in the presence of ppm $FeBr_3$ catalyst (Figure 73). An induction period of 16-18 h was observed indicating that in the presence of high amounts of $FeBr_3$, it took a longer time to build up a sufficient concentration of activator $FeBr_2$ species to initiate the reaction. In the absence of TBABr ligand, the reaction with $[MMA]/[EBPA]/[FeBr_3]$ = 100/1/1 was not well-controlled. Monomer conversion reached 80% within 144 h irradiation under blue LEDs with quite high Đ ranging in 1.80-2.08. Including TBABr in the reaction medium resulted in a decrease in the rate of the reaction but a well-controlled polymerization was achieved. However, when reaching higher conversions, a

214

deviation of the molecular weights from theoretical values was observed under these reaction conditions: [MMA]/[EBPA]/[FeBr$_3$]/[TBABr] = 100/1/1/1. This could be attributed to the *in situ* formation of an alkyl halide initiator as a result of the bromination of MMA through photoreduction of FeBr$_3$ over time, as previously reported.[64] Nevertheless, polymerization was well-controlled with *Đ* as low as 1.14. In the absence of EBPA, the reaction was even slower with 10% monomer conversion observed after 144 h irradiation under blue light generating a polymer with low *Đ* (1.14).
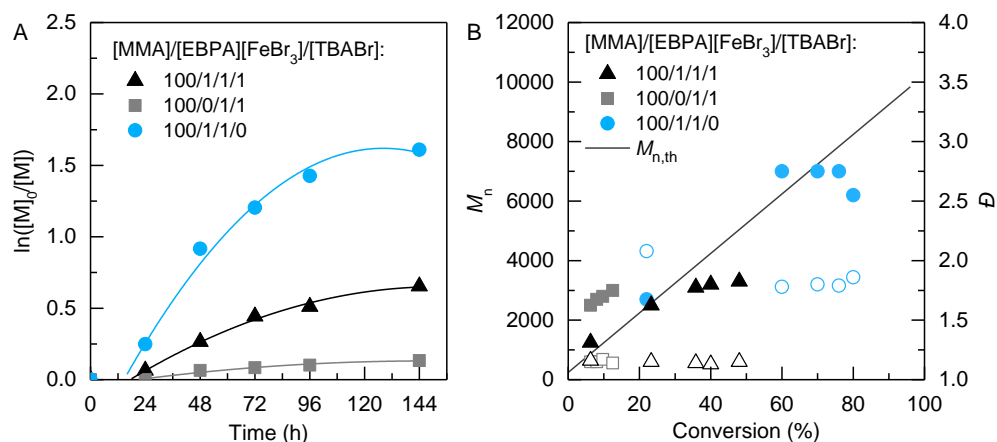
Figure 76. Photoinduced Fe-catalyzed ATRP of MMA under blue LED irradiation (λ = 450 nm, 4 mW/cm^2) using equimolar ratios of FeBr$_3$ catalyst under different conditions. A: kinetics of the polymerization; and B: number-average molecular weight (M_n, solid points) and dispersity (*Đ*, open points) as a function of monomer conversion.

Scope of the Photoinduced Fe-Catalyzed ATRP.

Oxygen Reduction. The presence of oxygen is often detrimental in radical polymerizations as oxygen quenches initiating/growing radicals, generating inactive peroxy radical species. Photochemistry is an efficient approach to overcome oxygen inhibition problems in polymerizations, especially in RDRP techniques.[65] For example, Cu-based photoinduced ATRP can proceed in the presence of oxygen.[63, 65, 66] Oxygen could be consumed by the photochemically generated Cu^I species being oxidized to Cu^{II}, which could then be regenerated by photochemical routes. Furthermore, Boyer and co-workers have advanced oxygen reduction

strategies in PET-RAFT systems wherein singlet oxygen quenchers, such as ascorbic acid, could be used to consume oxygen.[67-69]

The potential of photoinduced Fe-catalyzed ATRP was investigated in non-degassed solutions, i.e. in the presence of residual oxygen. Table 15 compares the results of the polymerization of MMA in degassed and non-degassed solutions using $FeBr_3$/TBABr catalyst under blue LEDs. The reaction employing [MMA]/[EBPA]/[$FeBr_3$]/[TBABr] = 100/1/0.04/0.04 reached 93% monomer conversion in a non-degassed solution. It was well-controlled, forming polymers with molecular weights in agreement with theoretical values and a relatively low $Đ$ of 1.38 (Entry 1, Table 15). In comparison, the reaction was faster in a degassed solution and a lower $Đ$ of 1.17 was achieved (Entry 2, Table 15). Increasing the concentration of $FeBr_3$ to 1000 ppm enhanced the efficiency of the reaction in the presence of oxygen as high conversion was achieved with lower $Đ$ of 1.20 (Entry 3, Table 15). It is worth noting that the reactions conducted in a full, caped vial without empty space on the top were well-controlled. No polymerization was observed when the reaction was conducted in a vial with 40 vol% air, due to continuous diffusion of oxygen to the solution.

To further evaluate the behavior of this system in the presence of oxygen, the kinetics of the polymerization of MMA was investigated. As shown in Figure 77, the reaction conducted in the presence of oxygen (non-degassed solution) proceeded in a slightly lower rate compared to a degassed solution (oxygen-free solution). Nevertheless, in both systems molecular weights increased as a function of monomer conversion in good agreement with theoretical values and polymers with low $Đ$ ranging from 1.17 to 1.25 were obtained. The slower rate of the polymerization in the presence of oxygen could be attributed to the consumption of photochemically reduced $FeBr_2$ in reducing oxygen.

Table 15.   Photoinduced Fe-catalyzed ATRP of MMA in the presence of oxygen [a]

Entry	[MMA]/[EBPA]/[$FeBr_3$]/[TBABr]	Degassed	Time (h)	Conversion (%)	$M_{n,th}$	M_n	$Đ$
1	100/1/0.04/0.04	No	28	93	9550	10000	1.38
2	100/1/0.04/0.04	Yes	16	94	9650	10500	1.17
3	100/1/0.1/0.1	No	36	88	9150	8900	1.20
4	100/1/0.1/0.1	Yes	32	91	9350	8900	1.18

<superscript>a</superscript> Reactions were conducted in 50 vol% anisole, and irradiated under blue light LEDs (λ = 450 nm, 4 mW/cm^2).
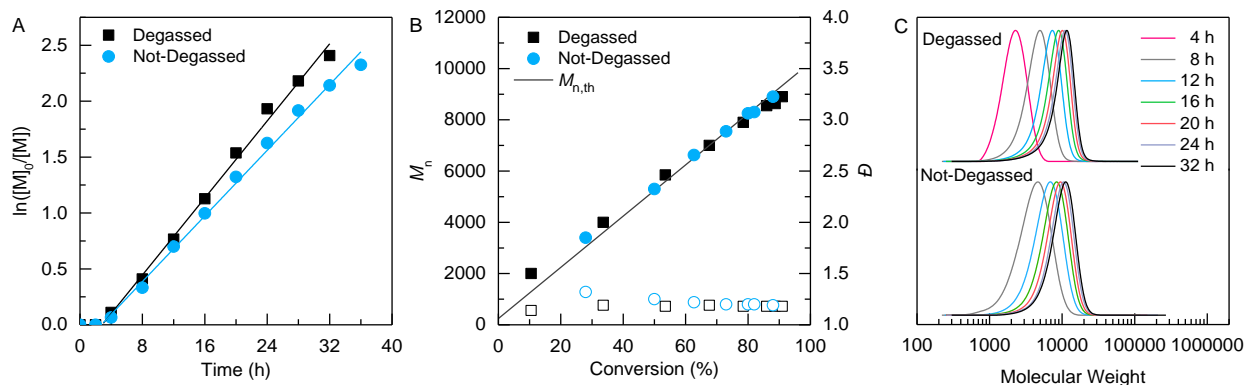
Figure 77. Photoinduced Fe-catalyzed ATRP of MMA under blue LED (λ = 450 nm, 4 mW/cm^2) in degassed and non-degassed solutions. A: kinetics of the polymerization; and B: number-average molecular weight (M_n, solid points) and dispersity ($Đ$, open points) as a function of monomer conversion the PMMA synthesized with different catalyst loading. Reaction conditions: [MMA]/[EBPA]/[FeBr$_3$]/[TBABr] = 100/1/0.1/0.1 in anisole 50 vol%.

Varying Targeted DPs. Photoinduced Fe-catalyzed ATRP was applied to the polymerization of MMA with varying targeted degrees of polymerization (DP). As shown in Table 16 and Figure 78, MMA can be polymerized in a controlled manner with target DPs of 25, 50, 100, and 200. In all cases high monomer conversions (>90%) were reached with molecular weights in agreement with theoretical values while maintaining $Đ$ as low as 1.17-1.25.

Table 16. Polymerization of MMA with varying degrees of polymerization using FeBr$_3$ under blue light LED irradiation ^{a}

Entry	Target DP	Time (h)	Conversion (%)	$M_{n,th}$	M_n	$Đ$
1	25	24	92	2550	2800	1.18
2	50	22	94	5000	5350	1.17
3	100	16	94	9950	10500	1.17
4	200	14	93	18850	18900	1.25

^{a} [MMA]/[EBPA]/[FeBr$_3$]/[TBABr] = x/1/0.04/0.04 (x = 25, 50, 100, 200) in 50 vol% anisole.
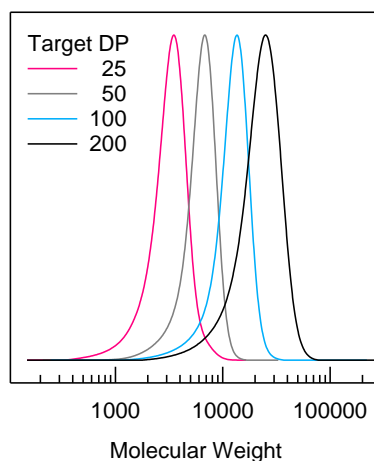
Figure 78. SEC traces for various degrees of polymerization (DP) in the photoinduced Fe-catalyzed ATRP under conditions: [MMA]/[EBPA]/[FeBr3]/[TBABr] = x/1/0.04/0.04 (x = 25, 50, 100, 200) in 50 vol% anisole under blue light irradiation.

Range of Methacrylate Monomers. The scope of the photoinduced Fe-catalyzed ATRP initiated by visible light was explored for a variety of methacrylate monomers. As shown in Figure 79, monomers such as MMA, ethyl methacrylate (EMA), butyl methacrylate (BMA), *tert*-butyl methacrylate (*t*BMA), 2-ethylhexyl methacrylate (EHMA), benzyl methacrylate (BzMA), and di(ethylene glycol) methacrylate (DEGMA) were polymerized using $FeBr_3$/TBABr as the catalyst under blue light LED. Well-controlled polymers were obtained with all monomers tested with low *Đ* values (1.17-1.53) and high or near-quantitative monomer conversions (85-97%).
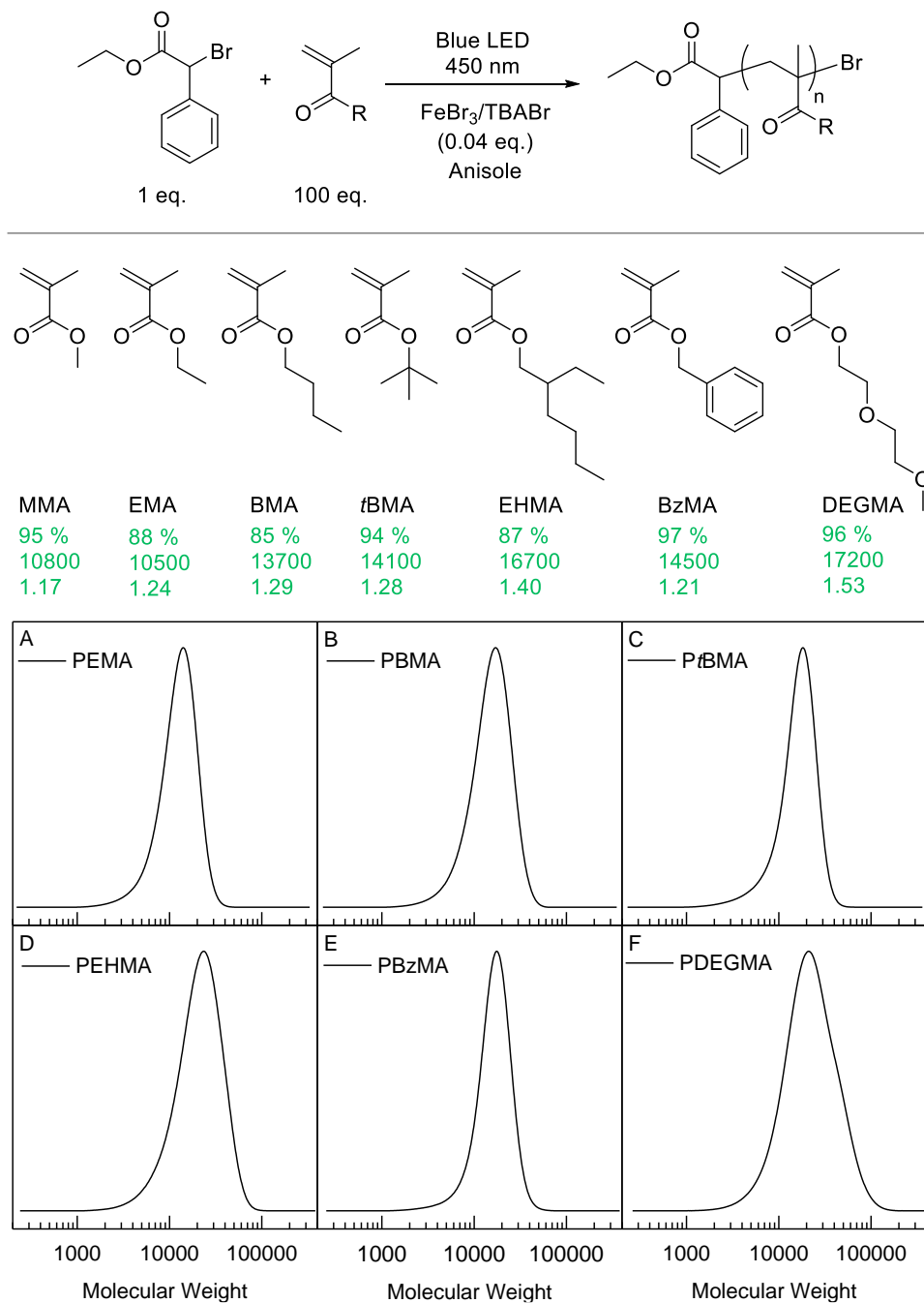
Figure 79. Monomers for the photoinduced Fe-catalyzed ATRP under blue light LED irradiation. Reaction conditions: [M]/[EBPA]/[FeBr$_3$]/[TBABr] = 100/1/0.04/0.04 in 50 vol% anisole, irradiated for 16 h. Numbers shown in green represent monomer conversion, M_n, and $Đ$, respectively from top to bottom.

Ligands. Several ligands, including ionic, phosphine and nitrogen-based ligands, were investigated in the Fe-catalyzed ATRP of MMA under blue light irradiation (Scheme 18 and Table 17). A well-controlled process was observed using TBABr with near-quantitative monomer conversion and low $Đ$ of 1.44. Tetrabutylammonium triflate (TBATfO), which is a relatively weaker coordinating ligand than TBABr, also resulted in a controlled process with 88% monomer conversion and $Đ$ of 1.44. Phosphine ligands including tris(4-methoxyphenyl)phosphine (TMPP) and tris(2,4,6-trimethoxyphenyl)phosphine (TTMPP) showed excellent control in the polymerization of MMA with high or near-quantitative monomer conversion and low $Đ$ of 1.20-1.29 (Entries 3-4, Table 17). However, the nitrogen-based ligands were less efficient for the polymerization of MMA using $FeBr_3$ under blue light irradiation. Limited monomer conversions (<20%) were achieved while generating polymers with relatively high $Đ$ (1.90-1.30)

Chain Extension and Block Copolymerization. Chain-end functionality of the polymers synthesized by the photoinduced Fe-ATRP was confirmed using ^{1}H NMR (Figure 86), by chain extension as well as by block copolymerization. A PMMA macroinitiator was synthesized under conditions [MMA]/[EBPA]/[FeBr$_3$]/[TBABr] = 50/1/0.04/0.04 irradiating under blue light LEDs (conversion >95%, M_n = 5300, $Đ$ = 1.17). The near-quantitative monomer conversion enabled *in situ* chain extension by addition of MMA in the second step without any further purification. Size-exclusion chromatography (SEC) analysis of the polymers presented in Figure 80 showed a clear shift towards higher molecular weights without any detectable shoulder or tailing at lower molecular weights (M_n = 14000, $Đ$ = 1.22). To further demonstrate the versatility of this system, *in situ* chain extension was also examined for a PBzMA polymer obtained by photoinduced Fe-catalyzed ATRP under blue light irradiation. The initial PBzMA macroinitiator (conversion = 97%, M_n = 8200, $Đ$ = 1.18) was successfully chain extended *in situ* with BzMA monomer in photoinduced Fe-catalyzed ATRP to yield P(BzMA-*b*-BzMA) (M_n = 21000, $Đ$ = 1.25) (Figure 80-B).
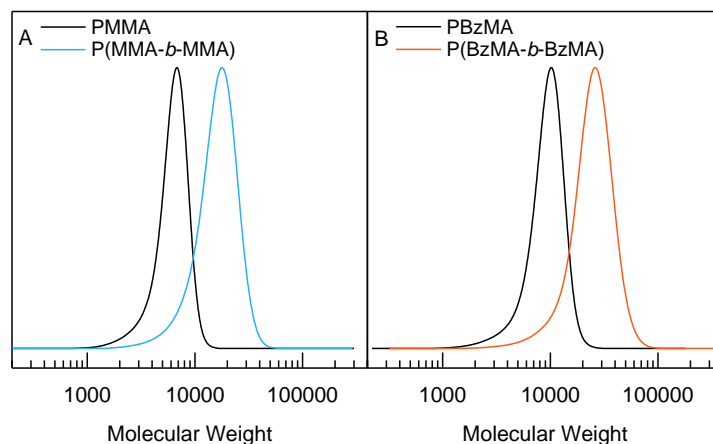
Figure 80. *In situ* chain extension of A: PMMA with MMA and B: PBzMA with BzMA in the photoinduced Fe-catalyzed ATRP under blue light LED irradiation. Reaction conditions for the synthesis of the macroinitiator: $[M]/[EBPA]/[FeBr_3]/[TBABr] =$ 50/1/0.04/0.04 in 50 vol% anisole followed by the second addition of the monomer (100 eq.) and anisole *in situ*.

Chain extension was further investigated in photoinduced Fe-catalyzed ATRP in the presence of oxygen. Initially, a PMMA macroinitiator was synthesized in the presence of oxygen under conditions $[MMA]/[EBPA]/[FeBr_3]/[TBABr] =$ 100/1/0.1/0.1 in 50 vol% anisole under blue LED to yield PMMA with $M_n = 10300$ and $Đ = 1.14$. Chain extension was performed using the above PMMA-Br macroinitiator in photoinduced Fe-catalyzed ATRP in the presence of oxygen under conditions: $[MMA]/[PMMA-Br]/[FeBr_3]/[TBABr] =$ 200/1/0.1/0.1 in 50 vol% anisole. SEC results shown in Figure 81 indicated a successful chain extension of the PMMA to higher molecular weights using photoinduced Fe-catalyzed ATRP in the presence of oxygen ($M_n =$ 28400, $Đ = 1.23$).
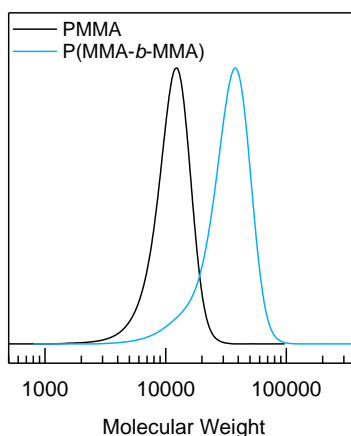
Figure 81. Chain extension of PMMA with MMA in the photoinduced Fe-catalyzed ATRP under blue light irradiation in the presence of oxygen.

Subsequently, *in situ* block copolymerization was also attempted and various block copolymers were synthesized with a PMMA macroinitiator (conversion >95%, M_n = 5300, $Đ$ = 1.17), followed by sequential addition of a degassed solution of the second monomer (100 eq.) in 50 vol% anisole. Monomers including BMA, *t*BMA, EHMA, and BzMA were successfully used in the *in situ* block copolymerization in photoinduced Fe-ATRP. SEC traces showed a shift to higher molecular weights in the block copolymerizations, while copolymers maintained low $Đ$ (1.20-1.30), indicating that high chain-end functionality under blue light LEDs (Figure 82 and Figure 87).
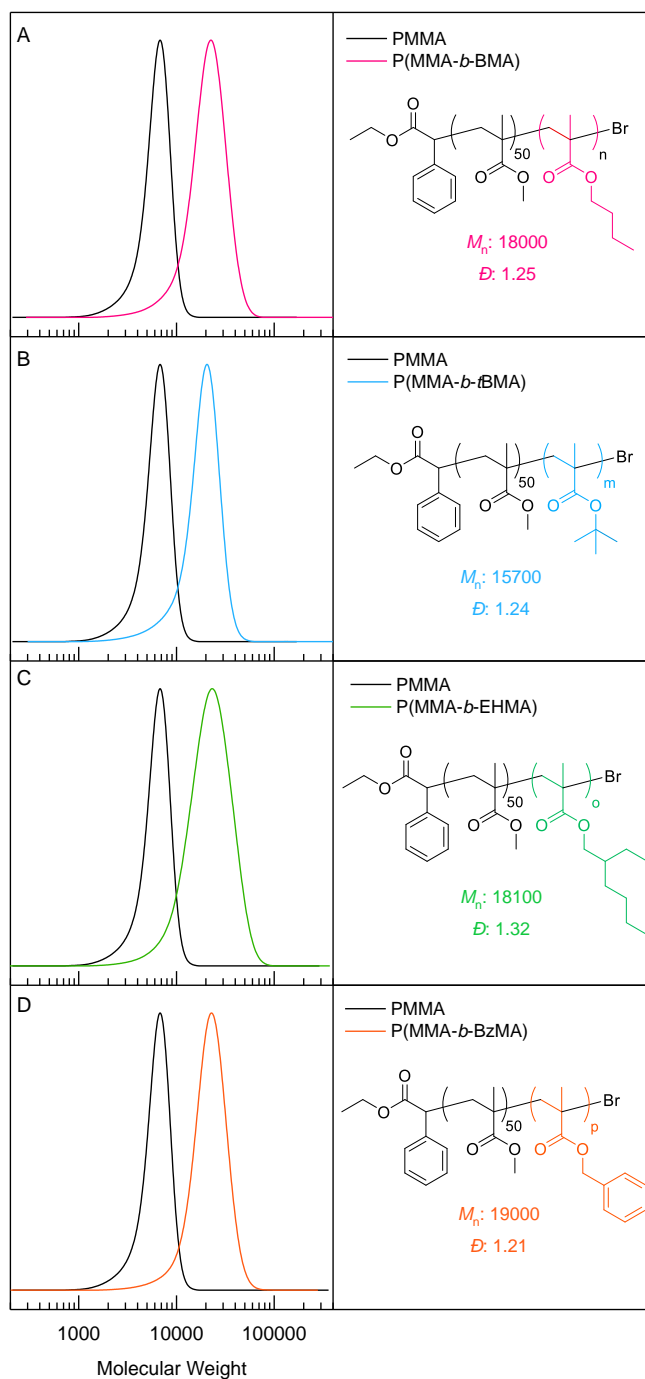
Figure 82. *In situ* block copolymerization of various methacrylate monomers in the photoinduced Fe-catalyzed ATRP under blue light LED irradiation. Reaction conditions for the synthesis of the PMMA macroinitiator: [MMA]/[EBPA]/[FeBr$_3$]/[TBABr] = 50/1/0.04/0.04 in 50 vol% anisole followed by the addition of the second monomer (100 eq.) and anisole *in situ*.

Temporal Control. Temporal control experiments were performed by switching the blue light on/off intermittently. The kinetic results showed the polymerization of MMA in the presence of FeBr$_3$/TBABr proceeding under blue light whereas the rate of the reaction was significantly reduced when the light was turned off. Re-exposing the solution to blue light in the second light-on period restarted the reaction to reach higher conversions. Control was maintained throughout successive on/off periods with molecular weights in agreement with theoretical values and low Đ. As shown in Figure 83, temporal control enabled successful manipulation of the polymerization using FeBr$_3$ catalyst under blue light.
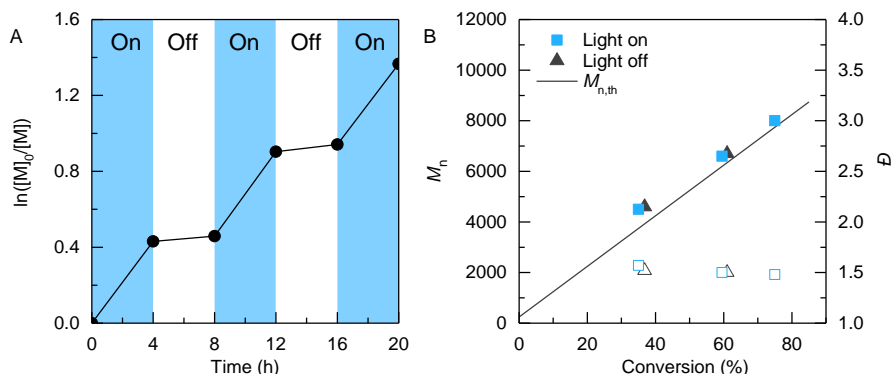
Figure 83. Temporal control of the photoinduced Fe-catalyzed ATRP under blue light LED irradiation. A: kinetics and B: molecular weight and dispersity as a function of monomer conversion. Reaction conditions: [MMA]/[EBPA]/[FeBr$_3$]/[TBABr] = 100/1/0.02/0.02 in 50 vol% anisole.

UV-Vis Spectroscopic Studies and Photoreduction Mechanism. The UV-vis spectra of the polymerization components including FeBr$_3$, TBABr, MMA, and EBPA were recorded and are shown in Figure 84. The FeBr$_3$/TBABr complex exhibits strong, broad absorption from UV up to visible region extending to green light, whereas other components are completely transparent in this region. To better understand the photoreduction mechanism, the UV-vis spectra of the catalytic system were recorded under different conditions. As shown in Figure 85-A, a solution of FeBr$_3$ in anisole showed a reduction in the absorption peak of FeBe$_3$ above 400 nm under blue light LED irradiation. In the presence of MMA, the reduction of the FeBr$_3$ peak was much faster (Figure 85-B). A similar trend was also observed when FeBr$_3$ was complexed with TBABr

ligand with a faster reduction of FeBr$_3$ in the presence of MMA (Figure 85-C vs. D). These results suggest that MMA is involved in the reduction of FeBr$_3$, as previously reported.[70-72]
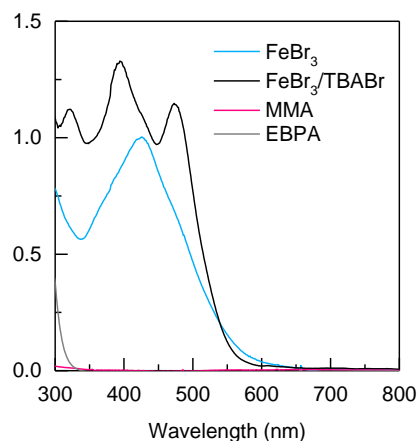
Figure 84. UV-vis spectra of FeBr$_3$, FeBr$_3$/TBABr, MMA, and EBPA in anisole. Concentrations: 0.2 mM.
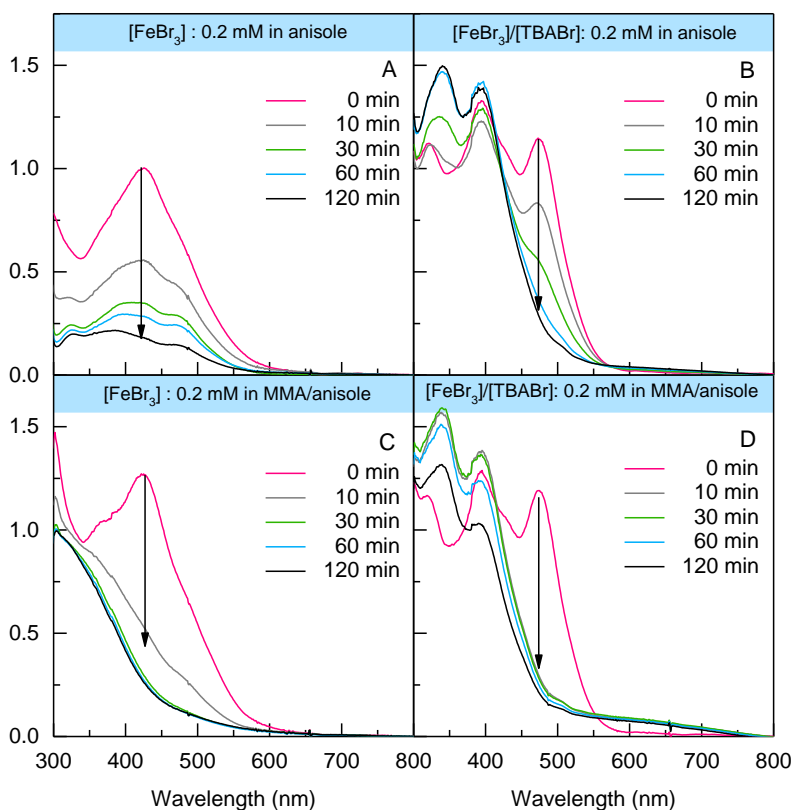
Figure 85. Monitoring the UV-Vis evolution of FeBr$_3$ under blue light LED irradiation as a function of time.

Two possible mechanisms can be considered for the reduction of $FeBr_3$. One pathway involves the homolytic photolysis of an Fe-Br bond under irradiation, yielding $FeBr_2$ and a $Br^{\bullet}$ radical. Another pathway could be MMA-mediated reduction of $FeBr_3$, which in turn forms $FeBr_2$ and an alkyl halide initiator, methyl 2,3-dibromoisobutyrate. To prove whether or not the homolytic Fe-Br bond cleavage was the dominant pathway, a series of control experiments were performed using iron(III)triflate $(Fe(OTf)_3)$ instead of $FeBr_3$, with non-coordinating triflate anions. Control experiments in the presence of $Fe(OTf)_3$ and TBABr ligand indicated 15 % monomer conversion after 24 h irradiation under blue light ($M_n = 11300$, $Đ = 2.70$). However, changing the ligand to TBAOTf or TTMPP in the presence or absence of EBPA initiator gave no monomer conversion during 24 h under blue light. The lack of polymerization in the presence of $Fe(OTf)_3$ and non-Br ligands suggests that homolytic Fe-Br bond photolysis plays an important role in reduction of $FeBr_3$.

Therefore, the plausible mechanism should involve unimolecular Fe-Br cleavage under light, which forms $FeBr_2$ and $Br^{\bullet}$ radical (Scheme 17). While $FeBr_2$ can activate alkyl halide to initiate polymerization, the $Br^{\bullet}$ radical can also add to the monomer and initiate polymerization. The 3-bromoisobuytryl radical thus-formed can then be deactivated by $FeBr_3$ present in the system generating methyl 2,3-dibromoisobutyrate and $FeBr_2$. This should be the reason for the faster reduction of $FeBr_3$ in the presence of MMA, as shown in Figure 85.
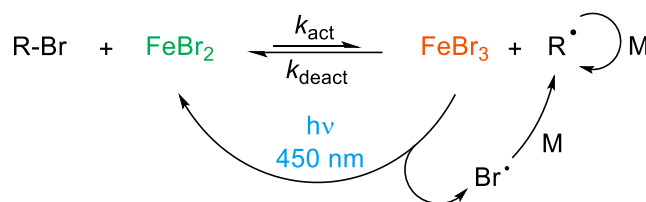
Scheme 17. Proposed mechanism for photoinduced Fe-catalyzed ATRP

4.3.4   Conclusions

Fe-catalyzed ATRP of methacrylate monomers can be promoted with an excellent control under blue LED irradiation. Due to the broad optical absorption of $FeBr_3$ catalyst, wide range of light sources from UV to blue and to green lights can be applied. Well-controlled polymers were synthesized with pre-determined molecular weight and low dispersity. Excellent retention of

chain-end functionality was confirmed by successful formation of block copolymers *in situ*. Furthermore, photocatalytic reduction of oxygen allows for promotion of well-controlled polymerization in the presence of oxygen. The ubiquity and biocompatibility of photocatalytically active Fe species suggest them as promising, inexpensive, green catalysts for ATRP systems.

4.3.5 Experimental Section and Supporting Information

Materials

Methyl methacrylate (MMA; Sigma-Aldrich, 99%), ethyl methacrylate (EMA; Sigma-Aldrich, 99%), butyl methacrylate (BMA; Sigma-Aldrich, 99%), *tert*-butyl methacrylate (*t*BMA; Sigma-Aldrich, 98%), 2-ethylhexyl methacrylate (EHMA; Sigma-Aldrich), benzyl methacrylate (BzMA; Alfa Aesar, 98%), and di(ethylene glycol) methacrylate (DEGMA; TCI, 97%) were passed through a basic alumina column to remove polymerization inhibitors prior to use. Iron(III) bromide (FeBr$_3$; Sigma-Aldrich, 98%), iron(III) trifluoromethanesulfonate (Fe(OTf)$_3$; Sigma-Aldrich, 90%) tetrabutylammonium bromide (TBABr; Sigma-Aldrich, 99%), tetrabutylammonium trifluoromethanesulfonate (TBAOTf); Sigma-Aldrich, 99%), tris(4-methoxyphenyl)phosphine (TMPP; Sigma-Aldrich, 95%) and tris(2,4,6-trimethoxyphenyl)phosphine (TTMPP; Sigma-Aldrich), 4,4′-Dinonyl-2,2′-dipyridyl (dNbpy;), *N,N,N′,N″,N″*-pentamethyldiethylenetriamine (PMDETA; Sigma-Aldrich, 99%), tris[2-(dimethylamino)ethyl]amine (Me$_6$TREN; Alfa Aesar, 99%) and anisole (Acros Organics, 99%) were used as received. Tris(2-pyridylmethyl)amine (TPMA) was synthesized according to literature procedure.

Instrumentation

^{1}H nuclear magnetic resonance (NMR) measurements were performed on a Bruker Avance 300 MHz spectrometer. Molecular weight properties of the polymers were determined by size-exclusion chromatography (SEC). The SEC instrument used a Waters 515 pump and a Waters 2414 differential refractometer using PSS columns (SDV 105, 103, and 500 Å) with THF as eluent at 35 °C and a flow rate of 1 mL min^{-1}. Linear PMMA standards were used for calibration. UV-vis spectra were recorded using Agilent 8453 spectrophotometer. A UV lamp (365 nm, 6. mW/cm^2) was purchased from Melody Susie. Blue light LEDs (5-m strip, λ = 450 nm, 4 mW/cm^2) were purchased from Solid Apollo and wrapped inside a 20-cm cylinder. Green light

LEDs (5-m strip, λ = 520 nm, 2.5 mW/cm^2) were purchased from Super Night and wrapped inside a 20-cm cylinder.

Polymerization Procedures.

General procedure for the photoinduced polymerization of MMA.

In a typical polymerization procedure, FeBr$_3$ (2.2 mg, 7.5 µmol) and TBABr (2.4 mg, 7.5 µmol) were added to a glass vial with a stir bar. The vial was tightly sealed and subjected to vacuum and backfilled with nitrogen at least 5 times. Degassed MMA (2 mL, 18.8 mmol) and 2 mL of degassed anisole were added to the vial before addition of EBPA (32.7 µL, 0.19 mmol) under nitrogen atmosphere. The solution was irradiated under blue light LEDs (450 nm) with a cooling fan placed on the top of the vial. Samples were taken periodically and analyzed by ^{1}H NMR and SEC for monomer conversion and molecular weight properties, respectively.

General procedure for the photoinduced polymerization of MMA in the presence of oxygen.

FeBr$_3$ (2.75 mg, 9.3 mmol), TBABr (3 mg, 9.3 mmol), MMA (1 mL, 9.4 mmol), anisole (1 mL) and EBPA (16.35, 0.094 mmol) were added to a 2-mL glass vial with a stir bar. The vial was irradiated under blue light LEDs without any degassing. Samples were taken periodically and analyzed by ^{1}H NMR and SEC for monomer conversion and molecular weight properties, respectively.

General procedure for in situ chain extension experiments.

In a typical chain extension polymerization, PMMA macroinitiator was initially synthesized as follows: FeBr$_3$ (2.2 mg, 7.5 µmol), TBABr (2.4 mg, 7.5 µmol) were added to a glass vial equipped with a stir bar. The vial was tightly sealed and subjected to vacuum and backfilled with nitrogen at least 5 times. Degassed MMA (1 mL, 9.4 mmol, 50 eq.) and 1 mL of degassed anisole were added to the vial before addition of EBPA (32.7 µL, 0.19 mmol, 1 eq.) under a nitrogen atmosphere. The solution was irradiated under blue light LEDs (450 nm) with a cooling fan placed on the top of the vial. Once the monomer conversion reached ~ 95%, a degassed solution of MMA (2 mL, 18.8 mmol, 100 eq.) and anisole (1 mL) was added to the vial and continued irradiation under blue light LEDs. Samples were taken for ^{1}H NMR and SEC analysis.

Ligands used in the photoinduced Fe-catalyzed ATRP under blue light LED irradiation:
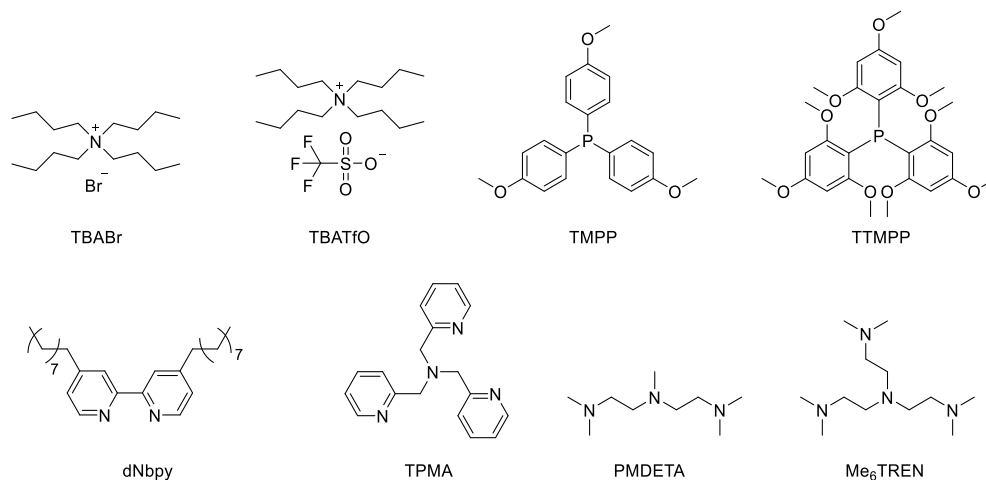
Scheme 18. Chemical structures of ligands used in photoinduced Fe-catalyzed ATRP under blue light LEDs.

Table 17.   Photoinduced Fe-catalyzed ATRP of MMA using various ligands [a]

Entry	Ligand	Time (h)	Conversion (%)	$M_{n,th}$	M_n	Đ
1	TBABr	16	94	9950	10500	1.17
2	TBATfO	18	88	9050	9450	1.44
3	TMPP	24	95	9750	10000	1.29
4	TTMPP	14	75	7750	8300	1.20
5	dNbpy	24	13	1550	6200	2.28
6	TPMA	18	20	2250	60000	2.15
7	PMDETA	24	3	550	6500	1.90
8	Me$_6$TREN	18	31	3350	84000	1.87

[a] [MMA]/[EBPA]/[FeBr$_3$]/[L] = 100/1/0.04/0.04 in 50 vol% anisole, under blue light LED irradiation.
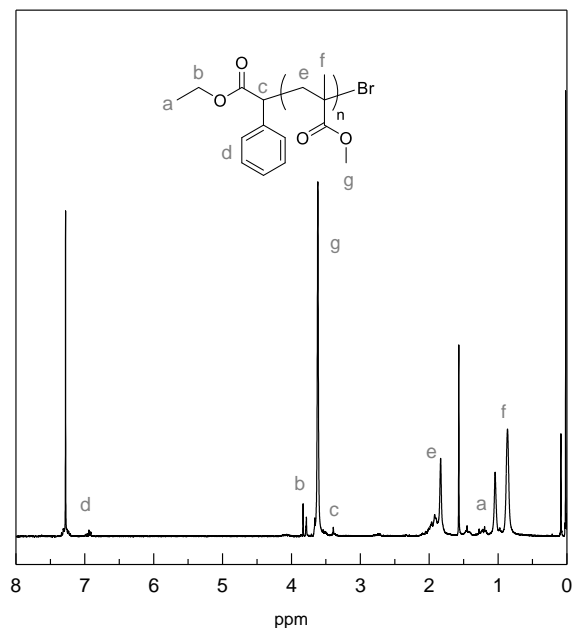
Figure 86. ^{1}H NMR spectra of PMMA synthesized by photoinduced Fe-catalyzed ATRP.
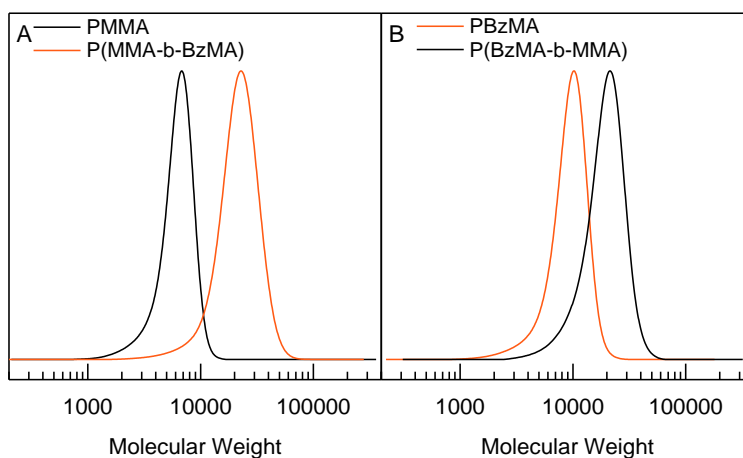
Figure 87. *In situ* block copolymerization of A: PMMA with BzMA and B: PBzMA with MMA in photoinduced Fe-catalyzed ATRP under blue light LED irradiation. Reaction conditions for the synthesis of the PMMA macroinitiator: [MMA]/[EBPA]/[FeBr$_3$]/[TBABr] = 50/1/0.04/0.04 in 50 vol% anisole followed by the addition of the second monomer (100 eq.) and anisole *in situ*.

4.3.6   References

1. Matyjaszewski, K.; Gaynor, S.; Wang, J.-S. Controlled Radical Polymerizations: The Use of Alkyl Iodides in Degenerative Transfer. *Macromolecules* **1995,** 28 (6), 2093-2095.

2. Xia, J.; Paik, H.-j.; Matyjaszewski, K. Polymerization of Vinyl Acetate Promoted by Iron Complexes. *Macromolecules* **1999,** 32 (25), 8310-8314.

3. Xue, Z.; Poli, R. Organometallic mediated radical polymerization of vinyl acetate with Fe(acac)2. *J. Polym. Sci., Part A: Polym. Chem.* **2013,** 51 (16), 3494-3504.

4. Simakova, A.; Averick, S. E.; Konkolewicz, D.; Matyjaszewski, K. Aqueous ARGET ATRP. *Macromolecules* **2012,** 45 (16), 6371-6379.

5. Matyjaszewski, K.; Xia, J. H. Atom transfer radical polymerization. *Chem. Rev.* **2001,** 101 (9), 2921-2990.

6. Kamigaito, M.; Ando, T.; Sawamoto, M. Metal-Catalyzed Living Radical Polymerization. *Chem. Rev.* **2001,** 101 (12), 3689-3746.

7. Nicolas, J.; Guillaneuf, Y.; Lefay, C.; Bertin, D.; Gigmes, D.; Charleux, B. Nitroxide-mediated polymerization. *Prog. Polym. Sci.* **2013,** 38 (1), 63-235.

8. Moad, G.; Rizzardo, E.; Thang, S. H. Living Radical Polymerization by the RAFT Process - A Third Update. *Aust. J. Chem.* **2012,** 65 (8), 985-1076.

9. Hawker, C. J.; Bosman, A. W.; Harth, E. New polymer synthesis by nitroxide mediated living radical polymerizations. *Chem. Rev.* **2001,** 101 (12), 3661-3688.

10. Tebben, L.; Studer, A. Nitroxides: Applications in Synthesis and in Polymer Chemistry. *Angew. Chem. Int. Ed.* **2011,** 50 (22), 5034-5068.

11. Krys, P.; Matyjaszewski, K. Kinetics of Atom Transfer Radical Polymerization. *Eur. Polym. J.* **2017,** 89, 482-523.

12. Min, K.; Gao, H. F.; Matyjaszewski, K. Preparation of homopolymers and block copolymers in miniemulsion by ATRP using activators generated by electron transfer (AGET). *J. Am. Chem. Soc.* **2005,** 127 (11), 3825-3830.

13. Matyjaszewski, K.; Jakubowski, W.; Min, K.; Tang, W.; Huang, J.; Braunecker, W. A.; Tsarevsky, N. V. Diminishing catalyst concentration in atom transfer radical polymerization with reducing agents. *Proc. Natl. Acad. Sci. U.S.A.* **2006,** 103 (42), 15309-15314.

14. Konkolewicz, D.; Magenau, A. J. D.; Averick, S. E.; Simakova, A.; He, H. K.; Matyjaszewski, K. ICAR ATRP with ppm Cu Catalyst in Water. *Macromolecules* **2012,** 45 (11), 4461-4468.

15. Jakubowski, W.; Matyjaszewski, K. Activators regenerated by electron transfer for atom-transfer radical polymerization of (meth)acrylates and related block copolymers. *Angew. Chem. Int. Ed.* **2006,** 45 (27), 4482-4486.

16. Konkolewicz, D.; Wang, Y.; Zhong, M. J.; Krys, P.; Isse, A. A.; Gennaro, A.; Matyjaszewski, K. Reversible-Deactivation Radical Polymerization in the Presence of Metallic Copper. A Critical Assessment of the SARA ATRP and SET-LRP Mechanisms. *Macromolecules* **2013,** 46 (22), 8749-8772.

17. Matyjaszewski, K.; Coca, S.; Gaynor, S. G.; Wei, M. L.; Woodworth, B. E. Zerovalent metals in controlled "living" radical polymerization. *Macromolecules* **1997,** 30 (23), 7348-7350.

18. Anastasaki, A.; Nikolaou, V.; Nurumbetov, G.; Wilson, P.; Kempe, K.; Quinn, J. F.; Davis, T. P.; Whittaker, M. R.; Haddleton, D. M. Cu(0)-Mediated Living Radical Polymerization: A Versatile Tool for Materials Synthesis. *Chem. Rev.* **2016,** 116 (3), 835-877.

19. Boyer, C.; Corrigan, N. A.; Jung, K.; Nguyen, D.; Nguyen, T. K.; Adnan, N. N. M.; Oliver, S.; Shanmugam, S.; Yeow, J. Copper-Mediated Living Radical Polymerization (Atom Transfer Radical Polymerization and Copper(0) Mediated Polymerization): From Fundamentals to Bioapplications. *Chem. Rev.* **2016,** 116 (4), 1803-1949.

20. Magenau, A. J. D.; Strandwitz, N. C.; Gennaro, A.; Matyjaszewski, K. Electrochemically Mediated Atom Transfer Radical Polymerization. *Science* **2011,** 332 (6025), 81-84.

21. Li, B.; Yu, B.; Huck, W. T. S.; Zhou, F.; Liu, W. Electrochemically Induced Surface-Initiated Atom-Transfer Radical Polymerization. *Angew. Chem. Int. Ed.* **2012,** 51 (21), 5092-5095.

22. Li, B.; Yu, B.; Huck, W. T. S.; Liu, W.; Zhou, F. Electrochemically Mediated Atom Transfer Radical Polymerization on Nonconducting Substrates: Controlled Brush Growth through Catalyst Diffusion. *J. Am. Chem. Soc.* **2013,** 135 (5), 1708-1710.

23. Shida, N.; Koizumi, Y.; Nishiyama, H.; Tomita, I.; Inagi, S. Electrochemically Mediated Atom Transfer Radical Polymerization from a Substrate Surface Manipulated by Bipolar

Electrolysis: Fabrication of Gradient and Patterned Polymer Brushes. *Angew. Chem. Int. Ed.* **2015,** 54 (13), 3922-3926.

24. Chmielarz, P.; Fantin, M.; Park, S.; Isse, A. A.; Gennaro, A.; Magenau, A. J. D.; Sobkowiak, A.; Matyjaszewski, K. Electrochemically mediated atom transfer radical polymerization (eATRP). *Prog. Polym. Sci.* **2017,** 69, 47-78.

25. Tasdelen, M. A.; Uygun, M.; Yagci, Y. Photoinduced Controlled Radical Polymerization in Methanol. *Macromol. Chem. Phys.* **2010,** 211 (21), 2271-2275.

26. Anastasaki, A.; Nikolaou, V.; Zhang, Q.; Burns, J.; Samanta, S. R.; Waldron, C.; Haddleton, A. J.; McHale, R.; Fox, D.; Percec, V.; Wilson, P.; Haddleton, D. M. Copper(II)/Tertiary Amine Synergy in Photoinduced Living Radical Polymerization: Accelerated Synthesis of ω-Functional and α,ω-Heterofunctional Poly(acrylates). *J. Am. Chem. Soc.* **2014,** 136 (3), 1141-1149.

27. Mosnáček, J.; Ilčíková, M. Photochemically Mediated Atom Transfer Radical Polymerization of Methyl Methacrylate Using ppm Amounts of Catalyst. *Macromolecules* **2012,** 45 (15), 5859-5865.

28. Konkolewicz, D.; Schröder, K.; Buback, J.; Bernhard, S.; Matyjaszewski, K. Visible Light and Sunlight Photoinduced ATRP with ppm of Cu Catalyst. *ACS Macro Lett.* **2012,** 1 (10), 1219-1223.

29. Ribelli, T. G.; Konkolewicz, D.; Bernhard, S.; Matyjaszewski, K. How are Radicals (Re)Generated in Photochemical ATRP? *J. Am. Chem. Soc.* **2014,** 136 (38), 13303-13312.

30. Dadashi-Silab, S.; Tasdelen, M. A.; Kiskan, B.; Wang, X.; Antonietti, M.; Yagci, Y. Photochemically Mediated Atom Transfer Radical Polymerization Using Polymeric Semiconductor Mesoporous Graphitic Carbon Nitride. *Macromol. Chem. Phys.* **2014,** 215 (7), 675-681.

31. Fors, B. P.; Hawker, C. J. Control of a Living Radical Polymerization of Methacrylates by Light. *Angew. Chem. Int. Ed.* **2012,** 51 (35), 8850-8853.

32. Discekici, E. H.; Anastasaki, A.; Kaminker, R.; Willenbacher, J.; Truong, N. P.; Fleischmann, C.; Oschmann, B.; Lunn, D. J.; Read de Alaniz, J.; Davis, T. P.; Bates, C. M.; Hawker, C. J. Light-Mediated Atom Transfer Radical Polymerization of Semi-Fluorinated (Meth)acrylates: Facile Access to Functional Materials. *J. Am. Chem. Soc.* **2017,** 139 (16), 5939-5945.

33. Mohapatra, H.; Kleiman, M.; Esser-Kahn, A. P. Mechanically controlled radical polymerization initiated by ultrasound. *Nat. Chem.* **2017,** 9 (2), 135-139.

34. Wang, Z.; Pan, X.; Yan, J.; Dadashi-Silab, S.; Xie, G.; Zhang, J.; Wang, Z.; Xia, H.; Matyjaszewski, K. Temporal Control in Mechanically Controlled Atom Transfer Radical Polymerization Using Low ppm of Cu Catalyst. *ACS Macro Lett.* **2017,** 6 (5), 546-549.

35. Corrigan, N.; Shanmugam, S.; Xu, J.; Boyer, C. Photocatalysis in organic and polymer synthesis. *Chem. Soc. Rev.* **2016,** 45 (22), 6165-6212.

36. Chen, M.; Zhong, M. J.; Johnson, J. A. Light-Controlled Radical Polymerization: Mechanisms, Methods, and Applications. *Chem. Rev.* **2016,** 116 (17), 10167-10211.

37. Pan, X.; Tasdelen, M. A.; Laun, J.; Junkers, T.; Yagci, Y.; Matyjaszewski, K. Photomediated controlled radical polymerization. *Prog. Polym. Sci.* **2016,** 62, 73-125.

38. Shanmugam, S.; Xu, J.; Boyer, C. Photocontrolled Living Polymerization Systems with Reversible Deactivations through Electron and Energy Transfer. *Macromol. Rapid Commun.* **2017,** 38 (13), 1700143.

39. Dadashi-Silab, S.; Tasdelen, M. A.; Yagci, Y. Photoinitiated Atom Transfer Radical Polymerization: Current Status and Future Perspectives. *J. Polym. Sci., Part A: Polym. Chem.* **2014,** 52 (20), 2878-2888.

40. Treat, N. J.; Fors, B. P.; Kramer, J. W.; Christianson, M.; Chiu, C.-Y.; Read de Alaniz, J.; Hawker, C. J. Controlled Radical Polymerization of Acrylates Regulated by Visible Light. *ACS Macro Lett.* **2014,** 3 (6), 580-584.

41. Pan, X.; Fang, C.; Fantin, M.; Malhotra, N.; So, W. Y.; Peteanu, L. A.; Isse, A. A.; Gennaro, A.; Liu, P.; Matyjaszewskit, K. Mechanism of Photoinduced Metal-Free Atom Transfer Radical Polymerization: Experimental and Computational Studies. *J. Am. Chem. Soc.* **2016,** 138 (7), 2411-2425.

42. Treat, N. J.; Sprafke, H.; Kramer, J. W.; Clark, P. G.; Barton, B. E.; Read de Alaniz, J.; Fors, B. P.; Hawker, C. J. Metal-Free Atom Transfer Radical Polymerization. *J. Am. Chem. Soc.* **2014,** 136 (45), 16096-16101.

43. Pan, X.; Lamson, M.; Yan, J.; Matyjaszewski, K. Photoinduced Metal-Free Atom Transfer Radical Polymerization of Acrylonitrile. *ACS Macro Lett.* **2015,** 4 (2), 192-196.

44. Theriot, J. C.; Lim, C.-H.; Yang, H.; Ryan, M. D.; Musgrave, C. B.; Miyake, G. M. Organocatalyzed atom transfer radical polymerization driven by visible light. *Science* **2016,** 352 (6289), 1082-1086.

45. Dadashi-Silab, S.; Pan, X.; Matyjaszewski, K. Phenyl Benzo[b]phenothiazine as a Visible Light Photoredox Catalyst for Metal-Free Atom Transfer Radical Polymerization. *Chem. Eur. J.* **2017,** 23 (25), 5972-5977.

46. Matyjaszewski, K.; Wei, M.; Xia, J.; McDermott, N. E. Controlled/"Living" Radical Polymerization of Styrene and Methyl Methacrylate Catalyzed by Iron Complexes. *Macromolecules* **1997,** 30 (26), 8161-8164.

47. Ando, T.; Kamigaito, M.; Sawamoto, M. Iron(II) Chloride Complex for Living Radical Polymerization of Methyl Methacrylate. *Macromolecules* **1997,** 30 (16), 4507-4510.

48. Allan, L. E. N.; MacDonald, J. P.; Nichol, G. S.; Shaver, M. P. Single Component Iron Catalysts for Atom Transfer and Organometallic Mediated Radical Polymerizations: Mechanistic Studies and Reaction Scope. *Macromolecules* **2014,** 47 (4), 1249-1257.

49. Xue, Z.; He, D.; Xie, X. Iron-catalyzed atom transfer radical polymerization. *Polym. Chem.* **2015,** 6 (10), 1660-1687.

50. Poli, R.; Allan, L. E. N.; Shaver, M. P. Iron-mediated reversible deactivation controlled radical polymerization. *Prog. Polym. Sci.* **2014,** 39 (10), 1827-1845.

51. Bauer, I.; Knölker, H.-J. Iron Catalysis in Organic Synthesis. *Chem. Rev.* **2015,** 115 (9), 3170-3387.

52. Niibayashi, S.; Hayakawa, H.; Jin, R.-H.; Nagashima, H. Reusable and environmentally friendly ionic trinuclear iron complex catalyst for atom transfer radical polymerization. *Chem. Commun.* **2007,** (18), 1855-1857.

53. Allan, L. E. N.; MacDonald, J. P.; Reckling, A. M.; Kozak, C. M.; Shaver, M. P. Controlled Radical Polymerization Mediated by Amine–Bis(phenolate) Iron(III) Complexes. *Macromol. Rapid Commun.* **2012,** 33 (5), 414-418.

54. Schroeder, H.; Lake, B. R. M.; Demeshko, S.; Shaver, M. P.; Buback, M. A Synthetic and Multispectroscopic Speciation Analysis of Controlled Radical Polymerization Mediated by Amine–Bis(phenolate)iron Complexes. *Macromolecules* **2015,** 48 (13), 4329-4338.

55. Xue, Z.; Linh, N. T. B.; Noh, S. K.; Lyoo, W. S. Phosphorus-Containing Ligands for Iron(III)-Catalyzed Atom Transfer Radical Polymerization. *Angew. Chem. Int. Ed.* **2008,** 47 (34), 6426-6429.

56. Wang, Y.; Kwak, Y.; Matyjaszewski, K. Enhanced Activity of ATRP Fe Catalysts with Phosphines Containing Electron Donating Groups. *Macromolecules* **2012,** 45 (15), 5911-5915.

57. Nishizawa, K.; Ouchi, M.; Sawamoto, M. Phosphine–Ligand Decoration toward Active and Robust Iron Catalysts in LRP. *Macromolecules* **2013,** 46 (9), 3342-3349.

58. Xue, Z.; Oh, H. S.; Noh, S. K.; Lyoo, W. S. Phosphorus Ligands for Iron(III)-Mediated Atom Transfer Radical Polymerization of Methyl Methacrylate. *Macromol. Rapid Commun.* **2008,** 29 (23), 1887-1894.

59. Teodorescu, M.; Gaynor, S. G.; Matyjaszewski, K. Halide Anions as Ligands in Iron-Mediated Atom Transfer Radical Polymerization. *Macromolecules* **2000,** 33 (7), 2335-2339.

60. Wang, Y.; Matyjaszewski, K. ATRP of MMA Catalyzed by FeIIBr2 in the Presence of Triflate Anions. *Macromolecules* **2011,** 44 (6), 1226-1228.

61. Wang, Y.; Zhang, Y.; Parker, B.; Matyjaszewski, K. ATRP of MMA with ppm Levels of Iron Catalyst. *Macromolecules* **2011,** 44 (11), 4022-4025.

62. Wang, Y.; Matyjaszewski, K. ATRP of MMA in Polar Solvents Catalyzed by FeBr2 without Additional Ligand. *Macromolecules* **2010,** 43 (9), 4003-4005.

63. Pan, X.; Malhotra, N.; Zhang, J.; Matyjaszewski, K. Photoinduced Fe-Based Atom Transfer Radical Polymerization in the Absence of Additional Ligands, Reducing Agents, and Radical Initiators. *Macromolecules* **2015,** 48 (19), 6948-6954.

64. Pan, X.; Malhotra, N.; Dadashi-Silab, S.; Matyjaszewski, K. A Simplified Fe-Based PhotoATRP Using Only Monomers and Solvent. *Macromol. Rapid Commun.* **2017,** 38 (13), 1600651.

65. Ligon, S. C.; Husár, B.; Wutzel, H.; Holman, R.; Liska, R. Strategies to Reduce Oxygen Inhibition in Photoinduced Polymerization. *Chem. Rev.* **2014,** 114 (1), 557-589.

66. Mosnacek, J.; Eckstein-Andicsova, A.; Borska, K. Ligand effect and oxygen tolerance studies in photochemically induced copper mediated reversible deactivation radical polymerization of methyl methacrylate in dimethyl sulfoxide. *Polym. Chem.* **2015,** 6 (13), 2523-2530.

67. Yang, Q.; Lalevée, J.; Poly, J. Development of a Robust Photocatalyzed ATRP Mechanism Exhibiting Good Tolerance to Oxygen and Inhibitors. *Macromolecules* **2016,** 49 (20), 7653-7666.

68. Pan, X.; Lathwal, S.; Mack, S.; Yan, J.; Das, S. R.; Matyjaszewski, K. Automated Synthesis of Well-Defined Polymers and Biohybrids by Atom Transfer Radical Polymerization Using a DNA Synthesizer. *Angew. Chem. Int. Ed.* **2017,** 56 (10), 2740-2743.

69. Borská, K.; Moravčíková, D.; Mosnáček, J. Photochemically Induced ATRP of (Meth)Acrylates in the Presence of Air: The Effect of Light Intensity, Ligand, and Oxygen Concentration. *Macromol. Rapid Commun.* **2017,** 38 (13), 1600639012.

70. Shanmugam, S.; Xu, J.; Boyer, C. Aqueous RAFT Photopolymerization with Oxygen Tolerance. *Macromolecules* **2016,** 49 (24), 9345-9357.

71. Yeow, J.; Chapman, R.; Xu, J.; Boyer, C. Oxygen tolerant photopolymerization for ultralow volumes. *Polym. Chem.* **2017**.

72. Shanmugam, S.; Xu, J.; Boyer, C. Photoinduced Oxygen Reduction for Dark Polymerization. *Macromolecules* **2017,** 50 (5), 1832-1846.

4.4. Iron-Catalyzed Atom Transfer Radical Polymerization of Semi-Fluorinated Methacrylates

4.4.1 Abstract

Fluorinated polymers are an important class of functional materials that exhibit unique properties such as high chemical resistance, thermal stability and low surface energy. Atom transfer radical polymerization (ATRP) of semi-fluorinated monomers catalyzed by copper catalysts often requires development of special conditions to control the polymerization and prevent side reactions such as base-catalyzed transesterification between the fluoro-containing monomers and solvents. In this paper, photoinduced iron-catalyzed ATRP was applied to the polymerization of a variety of semi-fluorinated methacrylate monomers. Polymerizations were initiated by photochemical generation of the Fe catalyst activator under blue light irradiation enabling temporal control over the growth of polymer chains, and were well-controlled in various solvents, including fluorinated and non-fluorinated solvents, without undergoing any side reactions. Moreover, in situ chain extension and block copolymerization experiments demonstrated the preservation of chain end functionality enabling facile synthesis of well-controlled block copolymers.
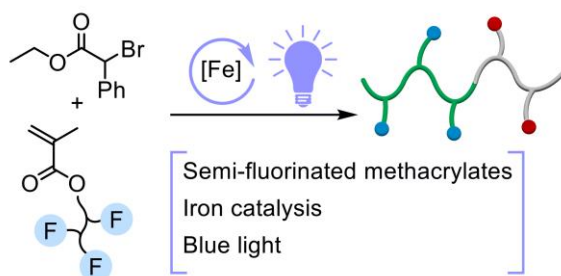
4.4.2 Introduction

Fluorinated polymers possess distinct chemical and physical properties compared to their hydrogenated analogs.[1, 2] These materials are highly hydrophobic in nature, and exhibit excellent chemical and thermal stability and low refractive indices. In particular, the low surface energy of fluorinated materials, imparted by the unique properties of the C-F bond, makes these polymers suitable for a wide range of applications including fabrication of low friction, low adhesion and low energy surfaces and many other areas.[3-5]

Use of reversible deactivation radical polymerization (RDRP) techniques gives access to the synthesis of well-defined, fluorine-containing functional polymeric materials.[6-11] However, atom

transfer radical polymerization (ATRP)[12, 13] of semi-fluorinated monomers has often been challenging and has required development of special reaction conditions to control the polymerization. For example, previous studies have reported that semi-fluorinated ligands[14] or solvents were required to both solubilize the catalytic systems and control the polymerization. Furthermore, a transesterification reaction between the fluorinated monomers and solvents may be promoted in the presence of nitrogen-containing ligands that can also act as a base to catalyze this reaction. Consequently, in the presence of monomers and protic solvents bearing different fluorinated alkyl chains, the transesterification reaction resulted in inhomogeneity along the polymer chains and therefore loss of control over molecular weight.

Conducting polymerizations under acidic conditions was reported to suppress the base-catalyzed transesterification reaction of fluorinated monomers and solvents by the ligand.[15] Moreover, in a recent study, a tertiary fluorinated alcohol was shown to act as a suitable solvent, which in contrast to primary or secondary fluorinated alcohols, did not undergo a transesterification reaction with the monomer.[16] Therefore, photoinduced ATRP of semi-fluorinated monomers was controlled by generation of the activator Cu catalyst under UV light irradiation. However, developing new polymerization platforms that do not require special solvents or reaction conditions and are also operational under mild, environmentally-friendly conditions would be advantageous in many aspects.

In this study, we sought to address this challenge by developing Fe-catalyzed ATRP and also expand its utility to include polymerization of functional monomers including semi-fluorinated methacrylates. Fe-based complexes are a robust and efficient class of ATRP catalysis for polymerization of various monomers with high efficiency.[14, 17-30] Notably, Fe is an abundant metal, has low toxicity, and has important biological and chemical functions that make it suitable for mediating various chemical transformations.[31] In Fe-catalyzed ATRP, control over the growth of polymer chains is established via a redox process between Fe^{II} and X-Fe^{III} (X: Br or Cl) complexes that act as activator and deactivator species, respecitively.[32, 33] Furthermore, the interaction of the propagating radicals with Fe^{II} complexes may contribute to impart control over polymerization through an organometallic-mediated radical polymerization pathway.[34] Recent studies have shown that Fe-catalyzed ATRP can be initiated and controlled by external stimuli

including visible light, and performed in simple catalytic platforms even without the need for use of special ligands or other reagents.[3, 35-38]

In this paper, Fe-catalyzed ATRP was applied to the polymerization of semi-fluorinated methacrylate monomers. Importantly, this Fe-based catalytic system was mediated under blue light irradiation and resulted in controlling the polymerization of different semi-fluorinated monomers in the presence of fluorinated or non-fluorinated solvents (Scheme 19).
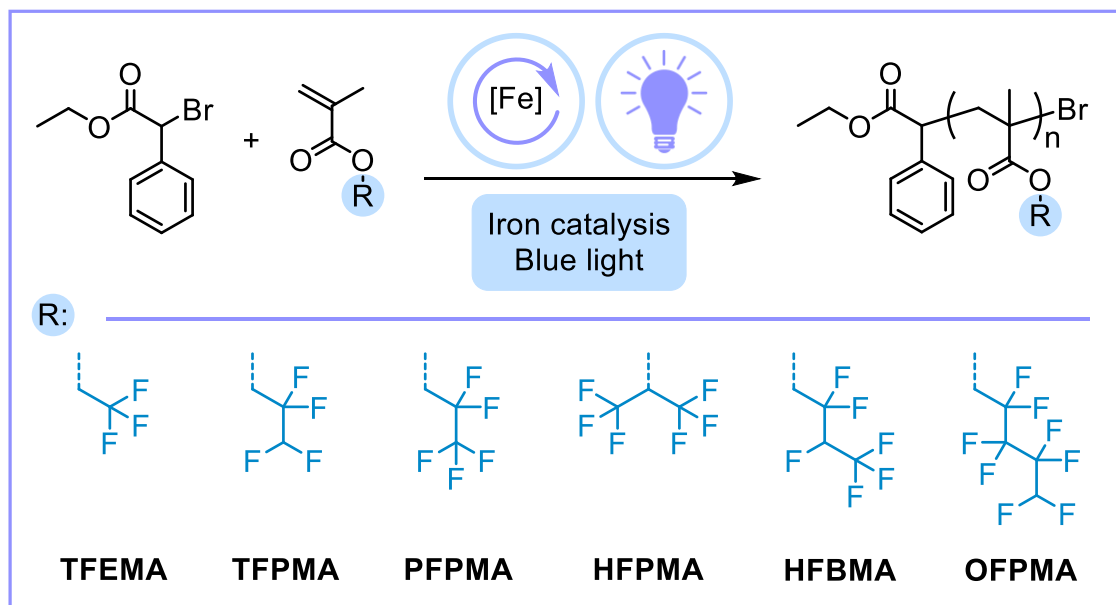
Scheme 19. Polymerization of semi-fluorinated methacrylate monomers by photoinduced Fe-catalyzed ATRP.

4.4.3   Results and Discussion

The efficiency of Fe-catalyzed ATRP was initially demonstrated by the polymerization of 2,2,2-trifluoroethyl methacrylate (TFEMA) in a variety of solvents that resulted in well-controlled polymerizations, Table 18. The polymerizations were conducted using iron(III) bromide (FeBr$_3$) the catalyst in the presence of tetrabutylammonium bromide (TBABr)[1, 39] and irradiated under blue light (465 nm) for 24 h. The generation of FeBr$_2$ activator catalyst was triggered under blue light. The Fe catalyst was only partially soluble in polymerizations run in toluene as a solvent, and that resulted in poor control over the polymerization of TFEMA, Entry 1, Table 18.

Table 18.   Results of Fe-catalyzed ATRP of TFEMA in different solvents [a]

Entry	Solvent	Conv. (%)	$M_{n,th}$	M_n	Đ
1	Toluene	91	7900	6500	2.31
2	DMF	94	8200	11100	1.78
3	Anisole	94	8200	8600	1.17
4	MeCN	92	8000	8300	1.21
5	TFE [b]	90	7800	7900	1.16

[a] Reactions conditions: [TFEMA]/[EBPA]/[FeBr$_3$]/[TBABr] = 50/1/0.04/0.08 in 50 vol% solvent, irradiated under blue light (465 nm, 12 mW/cm^2) for 24 h. [b] 10 vol % anisole was used to dissolve the catalyst (TFE/anisole = 9/1).

In the presence of *N,N*-dimethylformamide (DMF), the polymerization reached high monomer conversion, but showed a relatively high dispersity (Đ) of 1.78, Entry 2, Table 1. However, use of anisole, acetonitrile (MeCN), or 2,2,2-trifluoroethanol (TFE) as solvent resulted in well-controlled polymerizations reaching high monomer conversions (>90%), providing low Đ and molecular weights that were in agreement with theoretical values, Entries 3-5, Table 18.

Synthesis of polymers targeting different degrees of polymerization (DP) were also performed. As shown in Table 19 and Figure 93, polymerization of TFEMA can be controlled while targeting DPs in the 25-400 range reaching high monomer conversion under blue light irradiation. At higher DPs (200 and 400), molecular weights appeared to be lower than theoretical values which might be a result of the formation of new initiating chains due to photoreduction of the FeBr$_3$ species.[40, 41]

Fe-catalyzed ATRP was successful in controlling the polymerization of various semi-fluorinated methacrylates. Monomers containing 3-8 fluorine atoms including TFEMA, tetrafluoropropyl methacrylate (TFPMA), pentafluoropropyl methacrylate (PFPMA), hexafluoroisopropyl methacrylate (HFPMA), hexafluorobutyl methacrylate (HFBMA), and octafluoropentyl methacrylate (OFPMA). The monomers were successfully polymerized by photoinduced Fe-catalyzed ATRP reaching high monomer conversions (>90%) and displaying molecular weights close to theoretical values with low Đ (Figure 88). Size exclusion chromatography (SEC) traces of these polymers presented in Figure S3 show a narrow, monomodal distribution of molecular weights. SEC measurements were performed using THF or DMF as an eluent. Polymers

containing 4 or less fluorine atoms per monomer unit showed positive peak in THF, while polymers with more than 4 fluorine atoms per repeat unit showed negative signals in the SEC measurements in THF or DMF, due to their lower refractive index than the eluent ($n_{THF} = 1.404$, $n_{DMF} = 1.427$). Interestingly, analysis of PHFBMA and POFPMA in DMF SEC gave molecular weights in agreement with the theoretical values, whereas the THF SEC gave molecular weights lower than expected values for these samples. Moreover, polymerization of these monomers was successfully conducted and controlled in different solvents (Table 20).

Monomer	TFEMA	TFPMA	PFPMA	HFPMA	HFBMA	OFPMA
Conv. (%)	90	91	92	70	95	94
$M_{n,th}$	7800	9400	10200	8500	11900	14100
M_n	7900	10000	9900	7700	11400	12800
Đ	1.16	1.17	1.19	1.22	1.16	1.17

Figure 88. Results of Fe-catalyzed ATRP of methacrylate monomers containing different fluoroalkyl groups. Reaction conditions: [M]/[EBPA]/[FeBr$_3$]/[TBABr] = 50/1/0.04/0.08 in 50 vol% solvent (TFE/anisole = 9/1), irradiated under blue LEDs for 24 h.

Chain extension experiments performed upon sequential addition of the monomer demonstrated high chain end functionality obtained in the polymerizations conducted in different solvents. Polymerization of TFEMA was initially performed in the presence of TFE, anisole, or MeCN as solvents. Upon completion of the polymerizations, a second batch of TFEMA monomer in respective solvents was added and the reactions were allowed to continue polymerization under blue light irradiation. SEC results showed a shift toward higher molecular weights indicating a successful chain extension that resulted in well-defined polymer chains with low Đ and monomodal molecular weight distributions in all solvents (Figure 89).

TFE
M_n = 6000 M_n = 13500
$Đ$ = 1.15 $Đ$ = 1.22

Anisole
M_n = 6000 M_n = 13600
$Đ$ = 1.22 $Đ$ = 1.24

MeCN
M_n = 6100 M_n = 14000
$Đ$ = 1.16 $Đ$ = 1.26

A

B

C

1000   10000   100000
Molecular Weight

1000   10000   100000
Molecular Weight

1000   10000   100000
Molecular Weight

Figure 89.   SEC traces of in situ chain extension of PTFEMA in different solvents showing high chain end functionality in Fe-catalyzed photoinduced ATRP. Reactions conditions for the first block: [TFEMA]/[EBPA]/[FeBr$_3$]/[TBABr] = 33/1/0.04/0.08, in 50 vol % solvent irradiated under blue light (465 nm, 12 mW/cm^2) for 24 h. A degassed solution of TFEMA in respective solvents was added and reactions were allowed to run for 24 h under blue light.

Furthermore, in situ block copolymerization experiments were successfully performed upon sequential addition of monomers to synthesize well-defined block copolymers. For example, TFEMA was polymerized to high monomer conversion in TFE solvent (>90%, M_n = 8200, $Đ$ = 1.18) and subsequently a degassed solution of TFPMA in TFE was injected into the reaction. Irradiation of the solution resulted in increasing the molecular weight of the polymer to 22000 with a $Đ$ of 1.33 (Figure 90-A). Similarly, block co-polymerization with butyl methacrylate (BMA) resulted in a well-controlled block copolymer (M_n = 19000, $Đ$ =1.34) containing fluorinated and non-fluorinated segments (Figure 90-B). SEC results showed a shift to higher molecular weights while retaining narrow, monomodal molecular weight distributions as presented in Figure 90.
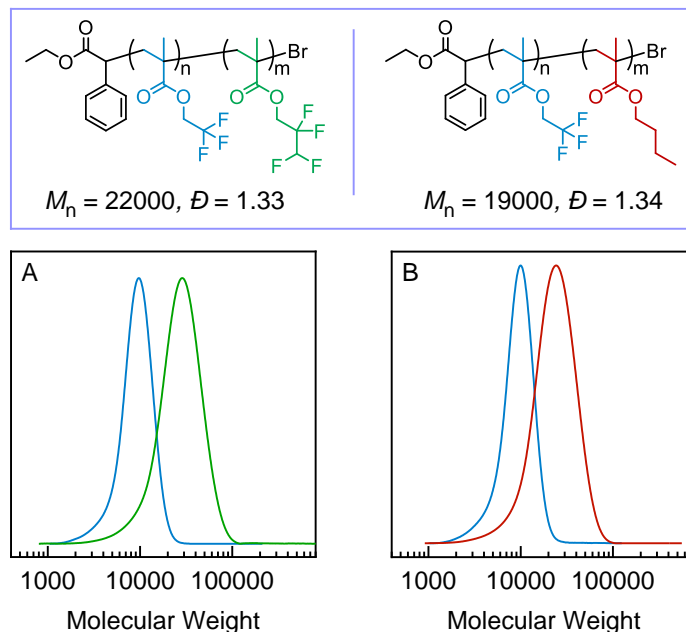
Figure 90. Block copolymers synthesized by in situ chain extension upon sequen-tial addition of monomers in Fe-catalyzed ATRP.

Temporal control was successfully demonstrated in Fe-catalyzed ATRP of TFEMA by switching the light on/off. Irradiation of the reaction under blue light started the polymerization by generation of Fe^{II} activator. Removal of the light significantly decreased the rate of the polymerization with only minimal monomer conversion observed in the dark periods. Therefore, the polymerization was successfully switched between on and off states for multiple times upon applying or removal of the light (Figure 91). Importantly, control over the polymerization was maintained throughout temporal control with molecular weights in agreement with theoretical values and polymers showing low $Đ < 1.2$. Moreover, keeping the polymerization in the dark for longer times showed minimal chain growth only in the early stages and the polymerization stopped afterward (Figure S5). Re-exposing the reaction to light restarted the polymerization as a result of the photochemical generation of Fe^{II} activator catalyst. These observations suggest that Fe^{II} activator was present in very low concentrations that was quickly consumed as a result of radical termination, and consequently polymerizations stopped in the dark.[42] Accordingly, decreasing the concentration of the catalyst from 4 mol % to 2 mol % resulted in perfect temporal control with no monomer conversion in the off periods (Figure 95 and Figure 96).

These results verify a well-controlled polymerization catalyzed by Fe that can be photochemically controlled to mediate the growth of polymer chains in a temporal manner.
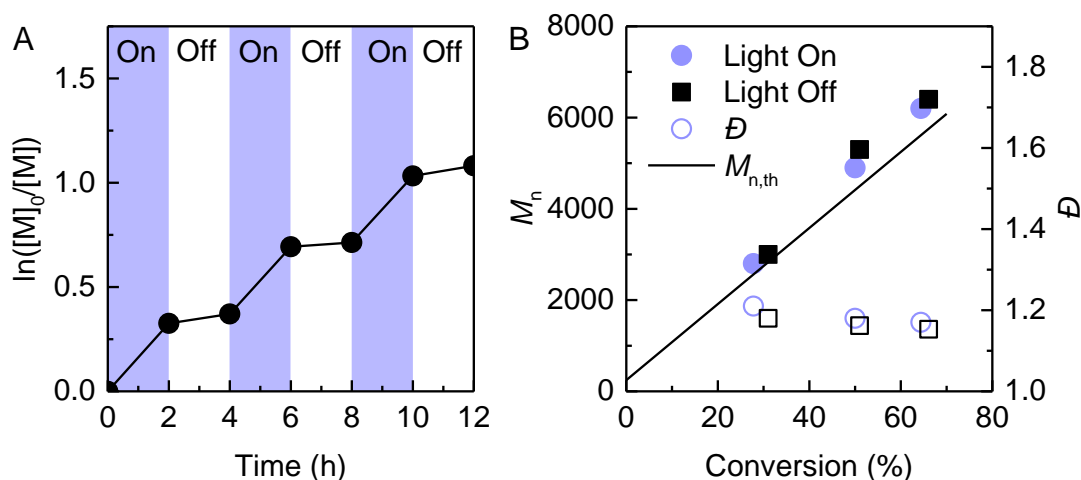
Figure 91. Temporal control in photoinduced Fe-catalyzed ATRP of TFEMA. (A) Kinetics of temporal control and (B) number-average molecular weight (M_n, solid points) and dispersity ($Đ$, open points) as a function of monomer conversion. Reaction conditions: [TFEMA]/[EBPA]/[FeBr$_3$]/[TBABr] = 50/1/0.04/0.08 in 50 vol% solvent (TFE/anisole = 9/1).

The versatility of the Fe-based catalytic system allowed for use of different solvents from fluorinated to non-fluorinated solvents for the polymerization of semi-fluorinated monomers. Importantly, no side reactions were observed when using a semi-fluorinated monomer in the presence of a fluorinated solvent each bearing different fluoroalkyl groups. In Cu-catalyzed ATRP systems, amine-based ligands may induce a base-catalyzed transesterification reaction between the fluorinated monomer and solvent. Therefore, special reaction conditions or special solvents were required to control the polymerization and prevent such side reactions.[1] However, under Fe-catalyzed ATRP conditions, polymerizations were well-controlled in a variety of fluorinated and traditional solvents without undergoing any side reactions. A control experiment using PFPMA monomer and TFE solvent was performed to further demonstrate the lack of side reactions between the monomer and solvent in the presence of FeBr$_3$/TBABr. NMR analysis of the solution showed no change in the respective shifts of the reagents after 24 h, indicating that no transesterification reaction was promoted between the fluorinated monomer and solvent under

Fe-catalyzed ATRP conditions, as presented in Figure 97. Therefore, different semi-fluorinated monomers were successfully polymerized using TFE or other solvents.

4.4.4 Conclusions

In summary, ATRP of semi-fluorinated methacrylate monomers was successfully initiated and controlled by Fe catalysis under visible light irradiation. The versatility of the Fe catalyst allowed the polymerizations to be carried out in a variety of solvents without any side reactions. In situ chain extension and block copolymerization experiments proved the preservation of chain end functionality allowing the synthesis of well-defined block copolymers.

Fe is a ubiquitous and environmentally-friendly catalyst that can be photochemically activate under visible light irradiation and provides a green catalytic approach for catalyzing ATRP processes. Future studies will focus on developing new Fe-based catalysts and study their catalytic efficiency in the polymerization of various functional monomers and architecting polymeric materials.

4.4.5 Experimental Section and Supporting Information

Materials

2,2,2-Trifluoroethyl methacrylate (TFEMA, 98%), 2,2,3,3-tetrafluoropropyl methacrylate (TFPMA, 98%), 2,2,3,3,3-pentafluoropropyl methacrylate (PFPMA, 98%), 1,1,1,3,3,3-hexafluoroisopropyl methacrylate (HFPMA, 98%), 2,2,3,4,4,4-hexafluorobutyl methacrylate (HFBMA, 98%), 1*H*,1*H*,5*H*-octafluoropentyl methacrylate (OFPMA, 98%) were purchased from TCI and purified by passing through a basic alumina column. Ethyl α-bromophenylacetate (EBPA, Sigma-Aldrich, 97%), iron(III) bromide (FeBr$_3$, Alfa Aesar, 98%), tetrabutylammonium bromide (TBABr, Sigma-Aldrich, 98%), 2,2,2-trifluoroethanol (TFE, TCI, 99%), anisol, acetonitrile (MeCN), toluene, and *N*,*N*-dimethylformamide (DMF) were used as received without further purification.

Instrumentation

[1]H nuclear magnetic resonance (^{1}H NMR) measurements were performed on a Bruker Avance™ III 500 MHz spectrometer. Molecular weight properties of the polymers were determined by size-exclusion chromatography (SEC). The SEC instrument used a Waters 515 pump and a Waters 2414 differential refractometer using PSS columns (SDV 10^5, 10^3, and 500 Å) with THF

as eluent at 35 °C and a flow rate of 1 mL min^{-1}. Linear poly(methyl methacrylate) standards were used for calibration. Polymerizations were irradiated under blue LEDs purchased from aspectLED (465 nm, 12 mW/cm^2).

General procedure for Fe-catalyzed ATRP of TFEMA

An 8-ml vial equipped with a stir bar and sealed with a septum rubber was subjected to vacuum and filling with nitrogen for five times. The monomer and solvent were degassed with nitrogen in separate containers for 30 min. A stock solution of FeBr$_3$ and TBABr was prepared in anisole and injected into the solution under nitrogen (100 µL, 56.1 mM; FeBr$_3$ = 1.66 mg, 5.61 µmol; TBABr = 3.62 mg, 11.22 µmol). TFEMA (1 mL, 7.02 mmol), TFE (0.9 mL), and EBPA (24.5 µL, 140 µmol) were added into the vial and the solution was further degassed with nitrogen for ~5 min. The vial was irradiated under blue LEDs for 24 h. Samples were taken analyzed by NMR and SEC techniques.
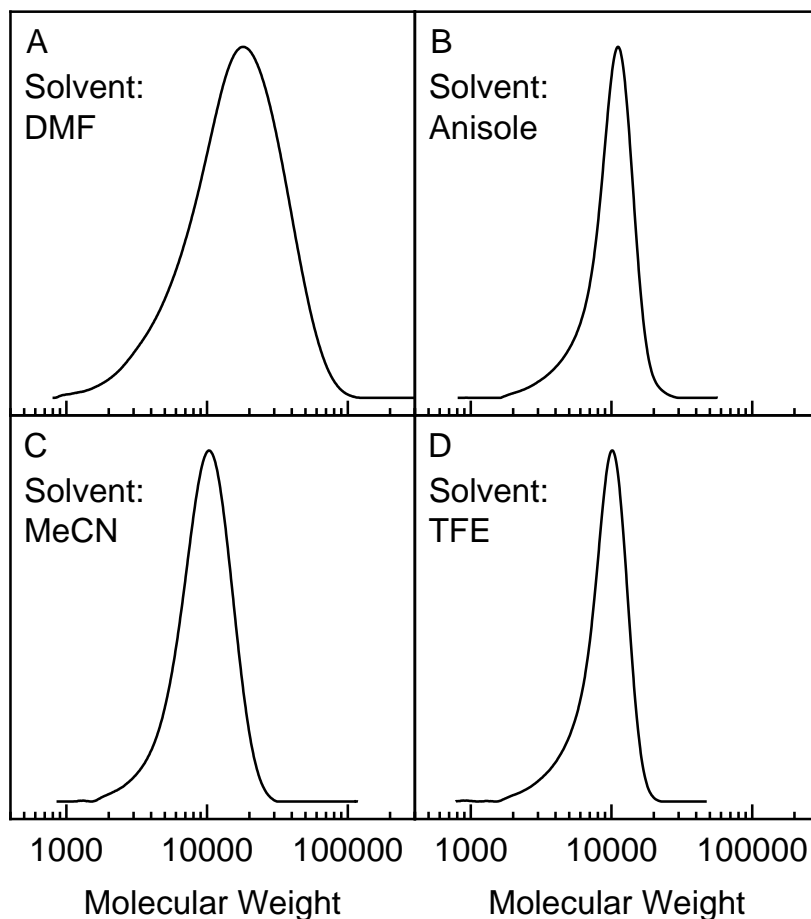
Figure 92. SEC traces of PTFEMA polymerized by Fe-catalyzed ATRP in different solvents. Reaction conditions: [TFEMA]/[EBPA]/[FeBr$_3$]/[TBABr] = 50/1/0.04/0.08 in 50 vol% solvent. Irradiated under blue LEDs (465 nm, 12 mW/cm^2) for 24 h.

Table 19. Results of Fe-catalyzed ATRP of TFEM targeting different DPs [a]

Entry	DP	Conversion (%)	$M_{n,th}$	M_n	Đ
1	25	87	3900	4200	1.14
2	50	90	7800	7900	1.16
3	100	92	15500	14000	1.19
4	200	92	31000	21000	1.30
5	400	90	60000	37000	1.35

[a] [TFEMA]/[EBPA]/[FeBr$_3$]/[TBABr] = 50/x/0.04/0.08 (x = 2, 1, 0.5, 0.25, 0.125 corresponding to DP = 25, 50, 100, 200 and 400, respectively) in 50 vol% solvent (TFE/anisole = 9/1), irradiated under blue LEDs (465 nm, 12 mW/cm^2) for 24 h.
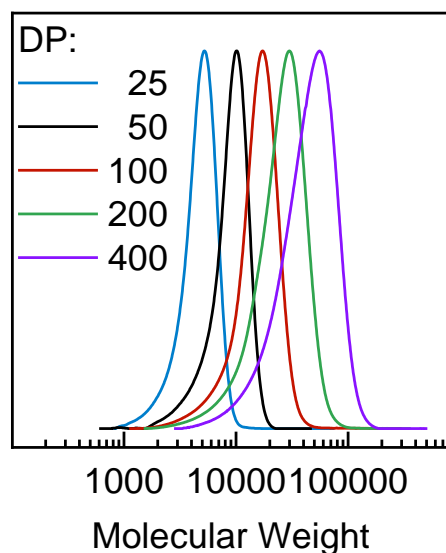
Figure 93. SEC traces of PTFEMA targeting different DPs in Fe-catalyzed ATRP. Reaction conditions: [TFEMA]/[EBPA]/[FeBr$_3$]/[TBABr] = 50/x/0.04/0.08 (x = 2, 1, 0.5, 0.25, 0.125 corresponding to DP = 25, 50, 100, 200 and 400, respectively) in 50 vol% solvent (TFE/anisole = 9/1), irradiated under blue LEDs (465 nm, 12 mW/cm^2) for 24 h.
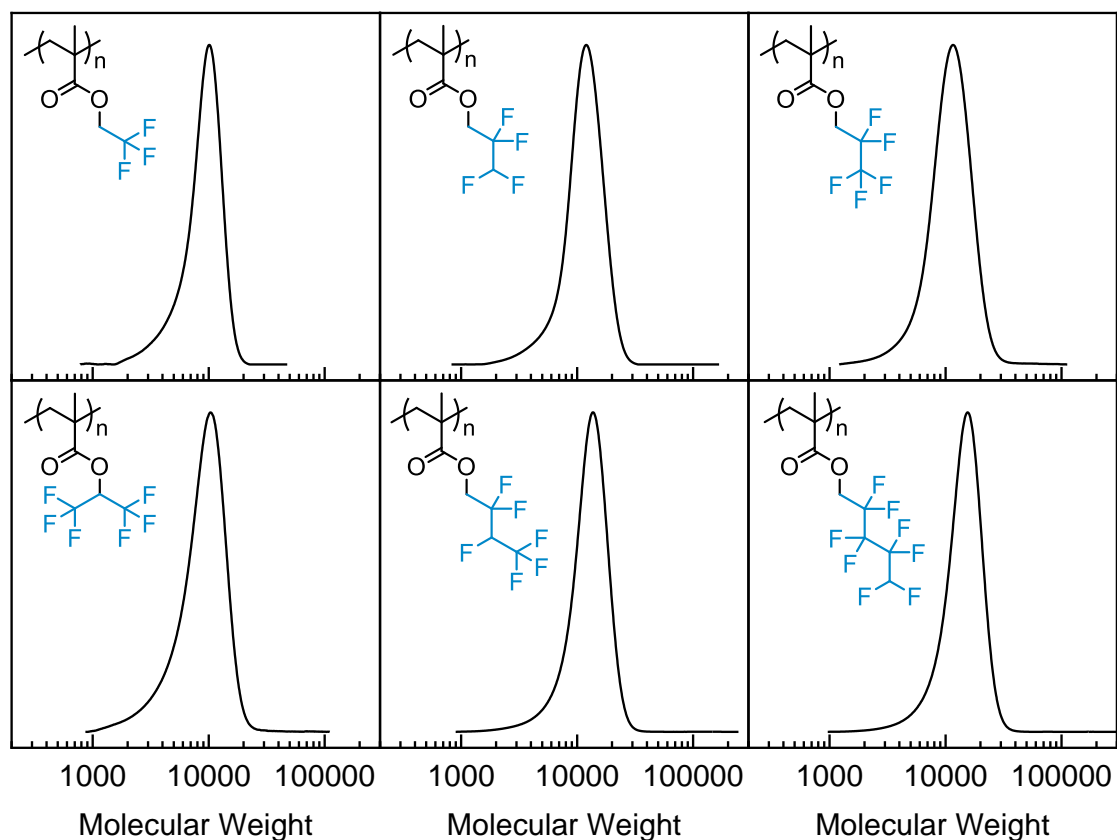
Figure 94. SEC traces of semi-fluorinated monomers polymerized by Fe-catalyzed ATRP in. Reaction conditions: [M]/[EBPA]/[FeBr$_3$]/[TBABr] = 50/1/0.04/0.08 in 50 vol% TFE (TFE/anisole = 9/1). Irradiated under blue light (465 nm, 12 mW/cm^2) for 24 h.

Table 20. Results of Fe-catalyzed ATRP of semi-fluorinated methacrylate monomers in different solvents [a]

Entry	Monomer	Solvent	Conversion (%)	$M_{n,th}$	M_n	$Đ$
1	TFEMA	TFE	90	7800	7900	1.16
2	TFEMA	Anisole	94	8200	8600	1.17
3	TFEMA	MeCN	92	8000	8300	1.21
4	TFPMA	TFE	91	9400	10000	1.17
5	TFPMA	Anisole	94	9600	9300	1.15
6	TFPMA	MeCN	92	9500	9300	1.25
7	PFPMA	TFE	92	10200	9900	1.19
8	PFPMA	MeCN	93	10400	9500	1.23
9	HFPMA	TFE	70	8500	7700	1.22
10	HFBMA	TFE	95	11900	11400	1.16
11	OFPMA	TFE	94	14100	12800	1.17

[a] Reaction conditions: [M]/[EBPA]/[FeBr$_3$]/[TBABr] = 50/1/0.04/0.08 in 50 vol% solvent, irradiated under blue LEDs (465 nm, 12 mW/cm^2) for 24 h.

Temporal control:

Temporal control was demonstrated in Fe-catalyzed ATRP of TFEMA by by applying or removal of blue light. Figure S4 shows the kineitcs of temporal control of TFEMA in the presence of 2 and 4 mol % of the Fe catalyst (with respect to initiator). Polymerization was switched on/off multiple times with only negligible monomer conversion observed in the dark periods. Notably, in the presence of low amounts of the catalyst (2 mol %) temporal control was even better compared to standar conditions using 4 mol % catalyst.
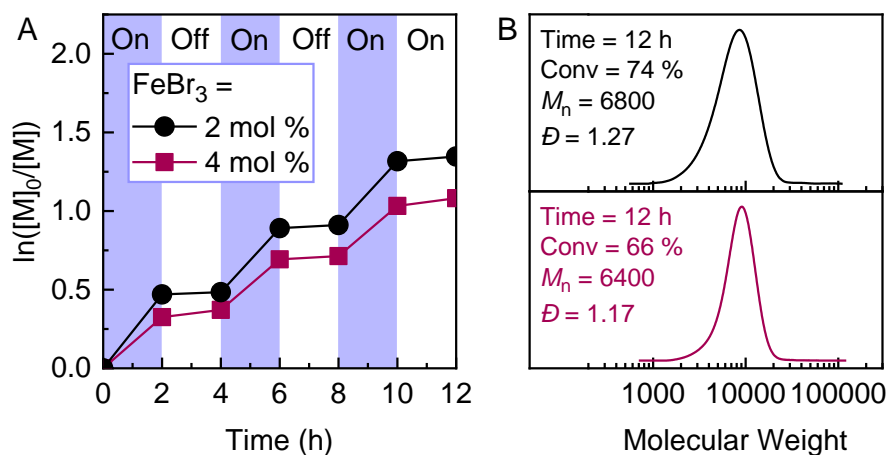
Figure 95. Temporal control in photoinduced Fe-catalyzed ATRP of TFEMA. (A) Kinetics of temporal control and (B) SEC results of PTFEMA obtained in temporal control. Reaction conditions: [TFEMA]/[EBPA]/[FeBr$_3$]/[TBABr] = 50/1/x/2x (x = 0.02 or 0.04) in 50 vol% solvent (TFE/anisole = 9/1).

Keeping the reactions in the dark for a longer period of time showed minimal monomer conversion in the early stages after which the polymerization stopped, confirming that the photochemical generation of the Fe^{II} activator resulted in the initiation of the polymerization and that the growth of polymer chains can be mediated in a temporal control manner by light. Decreasing the concentration of the catalyst from 4 to 2 mol % showed perfect temporal control as no monomer conversion was observed in the dark periods.
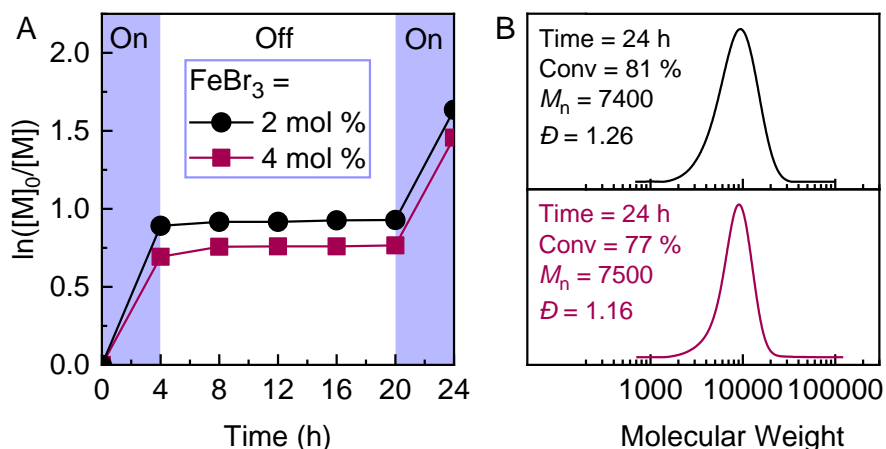
Figure 96. Temporal control in photoinduced Fe-catalyzed ATRP of TFEMA. (A) Kinetics of temporal control and (B) SEC results of PTFEMA obtained in temporal control. Reaction conditions: [TFEMA]/[EBPA]/[FeBr$_3$]/[TBABr] = 50/1/x/2x (x = 0.02 or 0.04) in 50 vol% solvent (TFE/anisole = 9/1). Irradiated under blue LED during the first and last 4 h.

Analysis of transesterification between semi-fluorinated monomer and solvent

Pentafluoropentyl methacrylate (PFPMA, 100 µL, 0.58 mmol, 1 equiv.) was added to TFE (2 equiv.) followed by addition of a stock solution of FeBr$_3$ (0.137 mg, 4.63 × 10^{-4} mmol) and TBABr (0.3 mg, 9.26 × 10^{-4} mmol) in anisole (10 µL). Samples were analyzed by NMR at 0 and 24 h.
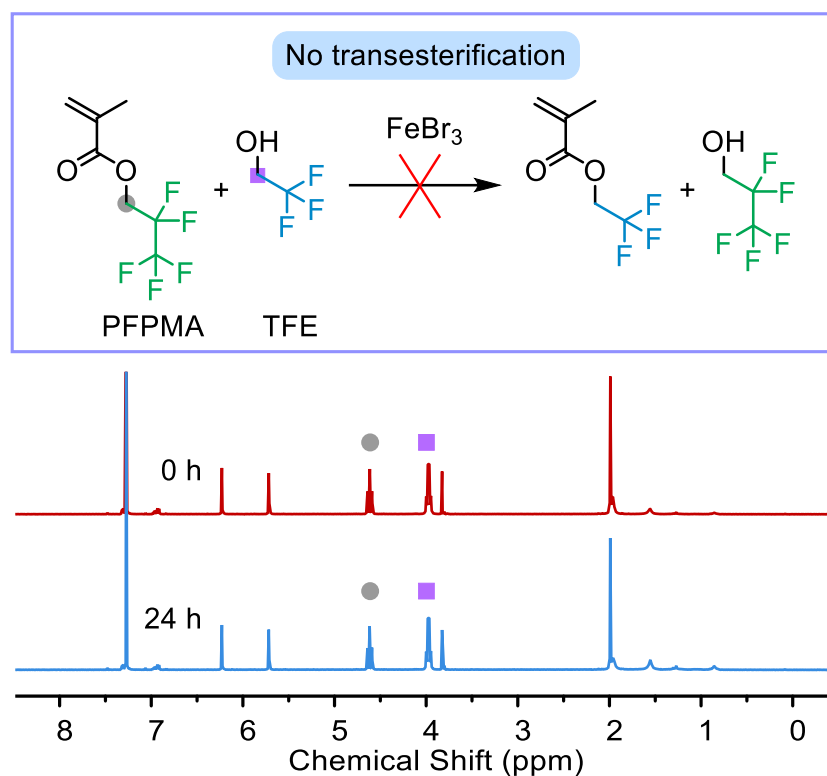
Figure 97. ^{1}H NMR spectra of the solution of PFPMA in TFE in the presence of FeBr$_3$ demonstrating no transesterification promoted under Fe-catalyzed ATRP conditions.

4.4.6 References

1. Pan, X.; Malhotra, N.; Zhang, J.; Matyjaszewski, K. Photoinduced Fe-Based Atom Transfer Radical Polymerization in the Absence of Additional Ligands, Reducing Agents, and Radical Initiators. *Macromolecules* **2015,** 48 (19), 6948-6954.

2. Xue, Z.; He, D.; Noh, S. K.; Lyoo, W. S. Iron(III)-Mediated Atom Transfer Radical Polymerization in the Absence of Any Additives. *Macromolecules* **2009,** 42 (8), 2949-2957.

3. Khan, M. Y.; Chen, X.; Lee, S. W.; Noh, S. K. Development of New Atom Transfer Radical Polymerization System by Iron (III)-Metal Salts Without Using any External Initiator and Reducing Agent. *Macromol. Rapid Commun.* **2013,** 34 (15), 1225-1230.

4. Yao, W.; Li, Y.; Huang, X. Fluorinated poly(meth)acrylate: Synthesis and properties. *Polymer* **2014,** 55 (24), 6197-6211.

5. Vitale, A.; Bongiovanni, R.; Ameduri, B. Fluorinated Oligomers and Polymers in Photopolymerization. *Chem. Rev.* **2015,** 115 (16), 8835-8866.

6. Babudri, F.; Farinola, G. M.; Naso, F.; Ragni, R. Fluorinated organic materials for electronic and optoelectronic applications: the role of the fluorine atom. *Chem. Commun.* **2007,** (10), 1003-1022.

7. Ameduri, B. Fluoropolymers: The Right Material for the Right Applications. *Chem. Eur. J.* **2018,** 24 (71), 18830-18841.

8. Cuthbert, J.; Martinez, M. R.; Sun, M.; Flum, J.; Li, L.; Olszewski, M.; Wang, Z.; Kowalewski, T.; Matyjaszewski, K. Non-Tacky Fluorinated and Elastomeric STEM Networks. *Macromol. Rapid Commun.* **2019,** 40 (10), 1800876.

9. Hirao, A.; Sugiyama, K.; Yokoyama, H. Precise synthesis and surface structures of architectural per- and semifluorinated polymers with well-defined structures. *Prog. Polym. Sci.* **2007,** 32 (12), 1393-1438.

10. Ameduri, B. Controlled Radical (Co)polymerization of Fluoromonomers. *Macromolecules* **2010,** 43 (24), 10163-10184.

11. Yang, Q.; Guerre, M.; Ladmiral, V.; Ameduri, B. Thermal and photo-RAFT polymerization of 2,2,2-trifluoroethyl α-fluoroacrylate. *Polym. Chem.* **2018,** 9 (24), 3388-3397.

12. Gong, H.; Zhao, Y.; Shen, X.; Lin, J.; Chen, M. Organocatalyzed Photocontrolled Radical Polymerization of Semifluorinated (Meth)acrylates Driven by Visible Light. *Angew. Chem. Int. Ed.* **2018,** 57 (1), 333-337.

13. Anastasaki, A.; Oschmann, B.; Willenbacher, J.; Melker, A.; Van Son, M. H. C.; Truong, N. P.; Schulze, M. W.; Discekici, E. H.; McGrath, A. J.; Davis, T. P.; Bates, C. M.; Hawker, C. J. One-Pot Synthesis of ABCDE Multiblock Copolymers with Hydrophobic, Hydrophilic, and Semi-Fluorinated Segments. *Angew. Chem. Int. Ed.* **2017,** 56 (46), 14483-14487.

14. Xia, J.; Johnson, T.; Gaynor, S. G.; Matyjaszewski, K.; DeSimone, J. Atom Transfer Radical Polymerization in Supercritical Carbon Dioxide. *Macromolecules* **1999,** 32 (15), 4802-4805.

15. Wang, J.-S.; Matyjaszewski, K. Controlled/"living" radical polymerization. atom transfer radical polymerization in the presence of transition-metal complexes. *J. Am. Chem. Soc.* **1995,** 117 (20), 5614-5615.

16. Matyjaszewski, K.; Xia, J. Atom Transfer Radical Polymerization. *Chem. Rev.* **2001,** 101 (9), 2921-2990.

17. Samanta, S. R.; Cai, R.; Percec, V. SET-LRP of semifluorinated acrylates and methacrylates. *Polym. Chem.* **2014,** 5 (18), 5479-5491.

18. Discekici, E. H.; Anastasaki, A.; Kaminker, R.; Willenbacher, J.; Truong, N. P.; Fleischmann, C.; Oschmann, B.; Lunn, D. J.; Read de Alaniz, J.; Davis, T. P.; Bates, C. M.; Hawker, C. J. Light-Mediated Atom Transfer Radical Polymerization of Semi-Fluorinated (Meth)acrylates: Facile Access to Functional Materials. *J. Am. Chem. Soc.* **2017,** 139 (16), 5939-5945.

19. Poli, R.; Allan, L. E. N.; Shaver, M. P. Iron-mediated reversible deactivation controlled radical polymerization. *Prog. Polym. Sci.* **2014,** 39 (10), 1827-1845.

20. Xue, Z.; He, D.; Xie, X. Iron-catalyzed atom transfer radical polymerization. *Polym. Chem.* **2015,** 6 (10), 1660-1687.

21. Matyjaszewski, K.; Wei, M.; Xia, J.; McDermott, N. E. Controlled/"Living" Radical Polymerization of Styrene and Methyl Methacrylate Catalyzed by Iron Complexes. *Macromolecules* **1997,** 30 (26), 8161-8164.

22. Ando, T.; Kamigaito, M.; Sawamoto, M. Iron(II) Chloride Complex for Living Radical Polymerization of Methyl Methacrylate. *Macromolecules* **1997,** 30 (16), 4507-4510.

23. Xue, Z.; Linh, N. T. B.; Noh, S. K.; Lyoo, W. S. Phosphorus-Containing Ligands for Iron(III)-Catalyzed Atom Transfer Radical Polymerization. *Angew. Chem. Int. Ed.* **2008,** 47 (34), 6426-6429.

24. Wang, Y.; Zhang, Y.; Parker, B.; Matyjaszewski, K. ATRP of MMA with ppm Levels of Iron Catalyst. *Macromolecules* **2011,** 44 (11), 4022-4025.

25. Simakova, A.; Mackenzie, M.; Averick, S. E.; Park, S.; Matyjaszewski, K. Bioinspired Iron-Based Catalyst for Atom Transfer Radical Polymerization. *Angew. Chem. Int. Ed.* **2013,** 52 (46), 12148-12151.

26. Nishizawa, K.; Ouchi, M.; Sawamoto, M. Phosphine–Ligand Decoration toward Active and Robust Iron Catalysts in LRP. *Macromolecules* **2013,** 46 (9), 3342-3349.

27. Allan, L. E. N.; MacDonald, J. P.; Nichol, G. S.; Shaver, M. P. Single Component Iron Catalysts for Atom Transfer and Organometallic Mediated Radical Polymerizations: Mechanistic Studies and Reaction Scope. *Macromolecules* **2014,** 47 (4), 1249-1257.

28. Poli, R.; Shaver, M. P. ATRP/OMRP/CCT Interplay in Styrene Polymerization Mediated by Iron(II) Complexes: A DFT Study of the α-Diimine System. *Chem. Eur. J.* **2014,** 20 (52), 17530-17540.

29. Schroeder, H.; Matyjaszewski, K.; Buback, M. Kinetics of Fe-Mediated ATRP with Triarylphosphines. *Macromolecules* **2015,** 48 (13), 4431-4437.

30. Poli, R.; Shaver, M. P. Atom Transfer Radical Polymerization (ATRP) and Organometallic Mediated Radical Polymerization (OMRP) of Styrene Mediated by Diaminobis(phenolato)iron(II) Complexes: A DFT Study. *Inorg. Chem.* **2014,** 53 (14), 7580-7590.

31. Telitel, S.; Dumur, F.; Campolo, D.; Poly, J.; Gigmes, D.; Pierre Fouassier, J.; Lalevée, J. Iron complexes as potential photocatalysts for controlled radical photopolymerizations: A tool for modifications and patterning of surfaces. *J. Polym. Sci., Part A: Polym. Chem.* **2016,** 54 (5), 702-713.

32. Schroeder, H.; Buback, M.; Shaver, M. P. Kinetics of Amine–Bis(phenolate) Iron-Mediated ATRP Up to High Pressure. *Macromolecules* **2015,** 48 (17), 6114-6120.

33. Fu, L.; Simakova, A.; Fantin, M.; Wang, Y.; Matyjaszewski, K. Direct ATRP of Methacrylic Acid with Iron-Porphyrin Based Catalysts. *ACS Macro Lett.* **2018,** 7 (1), 26-30.

34. Bauer, I.; Knölker, H.-J. Iron Catalysis in Organic Synthesis. *Chem. Rev.* **2015,** 115 (9), 3170-3387.

35. Matyjaszewski, K. Atom Transfer Radical Polymerization (ATRP): Current Status and Future Perspectives. *Macromolecules* **2012,** 45 (10), 4015-4039.

36. di Lena, F.; Matyjaszewski, K. Transition metal catalysts for controlled radical polymerization. *Prog. Polym. Sci.* **2010,** 35 (8), 959-1021.

37. Coward, D. L.; Lake, B. R. M.; Shaver, M. P. Understanding Organometallic-Mediated Radical Polymerization with an Iron(II) Amine–Bis(phenolate). *Organometallics* **2017,** 36 (17), 3322-3328.

38. Wang, Y.; Matyjaszewski, K. ATRP of MMA in Polar Solvents Catalyzed by FeBr2 without Additional Ligand. *Macromolecules* **2010,** 43 (9), 4003-4005.

39. Pan, X.; Malhotra, N.; Dadashi-Silab, S.; Matyjaszewski, K. A Simplified Fe-Based PhotoATRP Using Only Monomers and Solvent. *Macromol. Rapid Commun.* **2017,** 38 (13), 1600651.

40. Dadashi-Silab, S.; Pan, X.; Matyjaszewski, K. Photoinduced Iron-Catalyzed Atom Transfer Radical Polymerization with ppm Levels of Iron Catalyst under Blue Light Irradiation. *Macromolecules* **2017,** 50 (20), 7967-7977.

41. Teodorescu, M.; Gaynor, S. G.; Matyjaszewski, K. Halide Anions as Ligands in Iron-Mediated Atom Transfer Radical Polymerization. *Macromolecules* **2000,** 33 (7), 2335-2339.

42. Dadashi-Silab, S.; Matyjaszewski, K. Temporal Control in Atom Transfer Radical Polymerization Using Zerovalent Metals. *Macromolecules* **2018,** 51 (11), 4250-4258.

4.5. Effect of Halogens in Iron-Catalyzed Atom Transfer Radical Polymerization

4.5.1 Abstract

Efficient transfer of halogen atoms is essential for controlling the growth of polymers in atom transfer radical polymerization (ATRP). However, the nature of halogens may influence the efficiency of the halogen atom transfer during the activation and deactivation processes. The effect of halogens can be associated with the C-X bond dissociation energy and the affinity of the halogens/halides to the transition metal catalyst. In this paper, we study the effect of halogens (Br *vs.* Cl) and reaction media in iron-catalyzed ATRP in the presence of halide anions as ligands. In Br-based initiating systems, polymerization of methacrylate monomers was well-controlled whereas Cl-based initiating systems provided poor control over the polymerization. The high affinity of the Cl atom to the iron catalyst renders it inefficient for fast deactivation of growing chains which generated polymers with molecular weights higher than predetermined by $\Delta[M]/[RX]_o$ and with high dispersities. Conversely, Br can be exchanged with higher efficiency and hence provides good control over polymerization. The low polarity of the reaction medium improved control over polymerizations. Polymerization in MeCN (a more polar solvent) led to polymers with larger dispersity values as opposed to the less polar solvents such as anisole, which afforded well-controlled polymers with dispersity < 1.2.
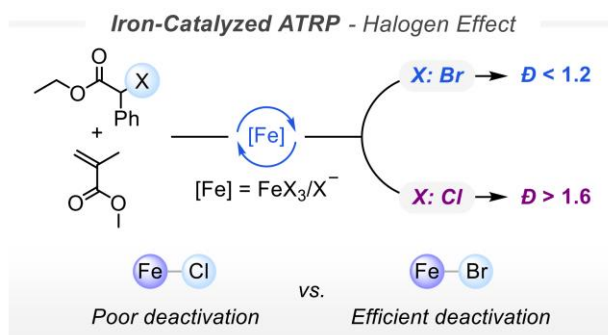
4.5.2 Introduction

The development of reversible deactivation radical polymerization (RDRP) techniques has revolutionized synthesis of well-defined polymers.[1, 2] RDRP methods offer precise control over molecular weight and dispersity, composition, and architecture of the polymers. Most common RDRP methods include atom transfer radical polymerization (ATRP),[3-5] reversible addition-fragmentation chain transfer,[6, 7] and nitroxide-mediated polymerizations.[8] While these techniques differ in their underlying mechanisms, a common feature of all RDRPs is to reduce the fraction

of terminated chains among the large pool of dormant species and provide rapid dynamic exchange between them via reversible deactivation processes.

In ATRP, catalysts are employed to provide control over the growth of polymer chains. ATRP catalysis is a redox process that involves reversible transfer of halogen atoms through activation of dormant polymer chains by the lower oxidation state catalyst (activator, L/Mt^n) as well as deactivation of the growing radicals by the higher oxidation state catalyst bonded to a halogen atom (deactivator, L/Mtn+1-X).[9] Therefore, the efficiency of the halogen atom transfer in both activation and deactivation steps is essential for promoting polymerization and gaining control in ATRP.

Activation of halogen-capped chain ends depends on dissociation energy of the C-X bond as well as the activity and halogenophilicity of the catalyst, which defines the affinity of the activator catalyst to abstract a halogen atom. For different halogens, C-X bond dissociation energy changes in order of F > Br > Cl > I, with the C-F bond being so strong that renders activation slow and inefficient.[10] On the other hand, for copper based systems, the catalyst-halogen bond (L/Mtn+1-X) becomes stronger moving from I to F. Therefore, because of the low affinity of the catalyst to iodine and high bond dissociation energy of the C-F bond, ATRP with I and F functionalities by metal catalysts is less successful.[11] Although polymerizations in the presence of alkyl iodides using Cu complexes can be challenging, the I functionality can be used in conjunction with iodide salts,[12, 13] amines,[13] or some iron complexes[14, 15] to catalyze well-controlled polymerizations which may also proceed through the degenerative transfer process.[16]

The strong bond between the catalyst and halogen atom in the deactivator (L/Mt^{n+1}-X) may hamper fast deactivation of propagating chains and therefore result in polymers with higher dispersity. For example, because of the strong bond between Cl and the catalyst, Cl-based ATRP systems typically show slower deactivation and results in polymers with relatively larger dispersity. Thus, Br is the most reactive chain end functionality in ATRP that balances the opposing factors of bond dissociation energy of C-X and catalyst halogenophilicity, hence provides fast and well-controlled ATRP.

In this paper, we aim to study the influence of halogen nature in iron-catalyzed ATRP in the presence of halide anions as ligands. Iron-based complexes form an important class of ATRP catalysts.[17-19] Research in iron catalysis has been focused on developing new efficient ligand

families that can provide control over polymerizations. Ligands such as nitrogen[20, 21] or phosphorus-containing compounds,[22-28] imines,[29-32] amine-bis(phenolate)s[33-35] and salts with halide anions[36-45] are among the widely used ligands in iron-catalyzed ATRP. Halide salts form anionic iron species that have higher catalytic activity in ATRP than their neutral or cationic counterparts. Polar solvents may also promote formation of cationic iron species that do not participate in catalysis. Therefore, control in low ppm iron-catalyzed ATRP may be compromised in polar media.

Despite the breadth of research in developing diverse ligand families in iron-catalyzed ATRP, the effect of halogens and reaction media on polymerization control has not been fully explored in these systems. Here we study these parameters in ATRP using low concentration of iron halides in the presence of salts with halide anions as ligands. We show that the high affinity of Cl to Fe resulted in lower deactivation efficiency and therefore poor control over polymerization of methacrylate monomers. However, Br-based initiating systems yielded well-defined polymers with low dispersities.

4.5.3 Results and Discussion

We began our studies by analysis of the iron catalysts using UV-Vis spectroscopy in the presence of both Br and Cl anions. Solutions of $FeBr_3$ or $FeCl_3$ in anisole or acetonitrile (MeCN) were titrated by addition of tetrabutylammonium bromide (TBABr) or tetrabutylammonium chloride (TBACl) salts as ligands. In the absence of additional halide salts, both $FeBr_3$ and $FeCl_3$ formed neutral species in anisole as this solvent does not allow disproportionation/dismutation and/or formation of ionic species (Figure 98). Addition of halide salts resulted in a change in the UV-Vis spectra of the catalyst as two absorbance maxima appeared, indicating formation of anionic FeX_4^- species. $FeCl_3$ showed absorption mainly in the UV region below 400 nm, whereas $FeBr_3$ absorbs in visible region > 550 nm. Addition of TBACl to $FeCl_3$ resulted in the formation of two absorbance peaks, whereas in the presence of TBABr added to $FeCl_3$, the spectra showed a tailing toward higher wavelengths (Figure 98-A and B) but still contained the same peak maxima as observed in Figure 1-A. Further increase of TBABr did not change the absorption spectra indicating that Cl preferably binds to Fe over Br. Upon addition of TBABr to $FeBr_3$, its absorption changed with two maxima peaks appearing > 400 nm, attributed to the formation of the anionic $FeBr_4^-$ species (Figure 98-C). Interestingly, Figure 98-B did not show

an absorption maximum at ~470 nm, suggesting that no $FeBr_4^-$ was formed even upon addition of 4 equiv. of TBABr to $FeCl_3$. However, addition of TBACl to the solution of $FeBr_3$ significantly changed the UV-Vis spectra with a blue shift that further changed as the concentration of TBACl was increased (Figure 98-D). In the presence of 4 equiv. of TBACl with respect to $FeBr_3$, the spectra were similar to those obtained with $FeCl_3$/TBACl Figure 98-A), indicating replacement of all Br with Cl and formation of $FeCl_4^-$. No change was observed upon further addition TBACl. These observations confirm the higher affinity of the Cl atom *vs.* Br to bind to Fe, which may consequently affect the deactivation of growing chains because of the formation of a strong Fe-Cl bond.

In MeCN, the UV-Vis spectra of $FeCl_3$ or $FeBr_3$ showed two absorption peaks which is attributed to the formation of anionic iron species in the absence of any additional halide salt ligands (Figure 98-E and G, respectively). Polar solvents such MeCN can stabilize/promote formation of the anionic and cationic iron species via disproportionation or ligand displacement by the solvent molecules. Addition of TBABr to $FeCl_3$, slightly changed the spectra with a tailing toward higher wavelengths (Figure 98-F). Furthermore, upon addition of TBACl to $FeBr_3$ in MeCN, the UV-Vis spectra blue shifted (~100 nm) and finally in the presence of 4 equiv. of TBACl showed similar absorption to $FeCl_3$/TBACl (Figure 98-H).
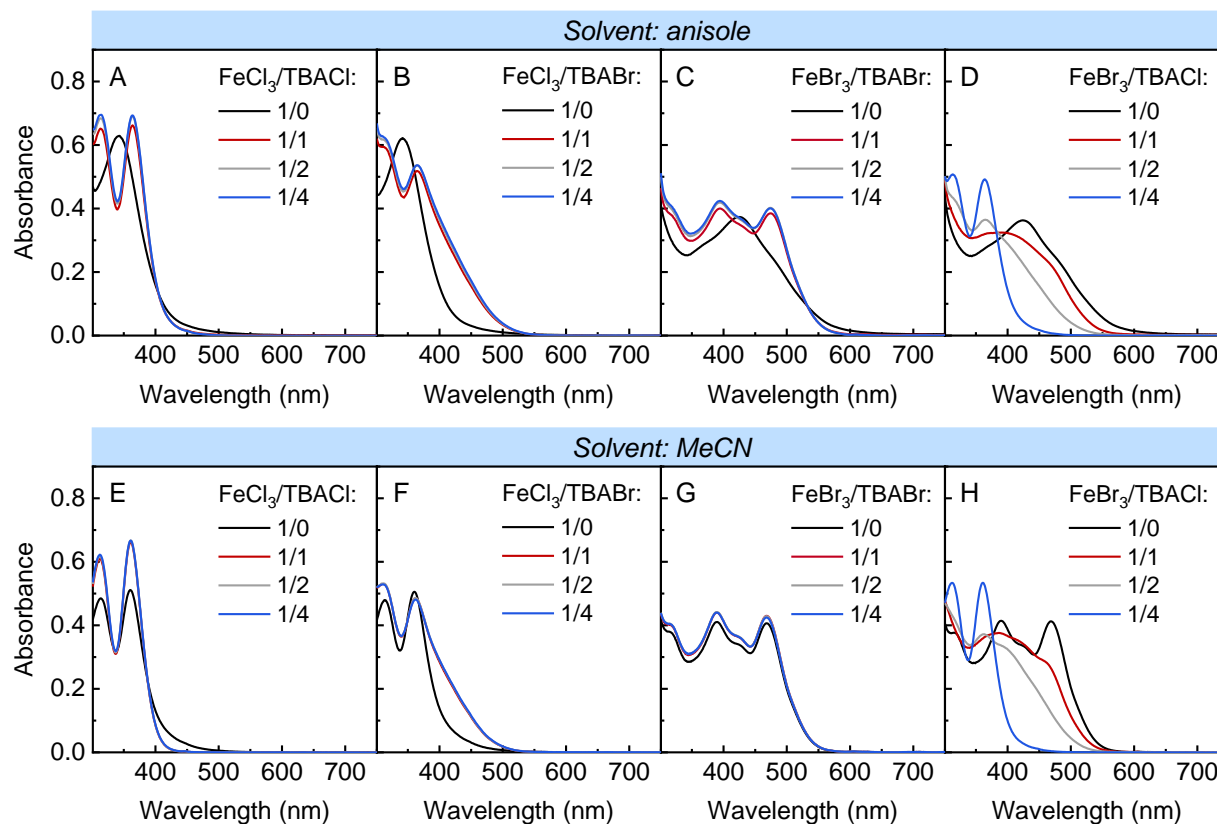
Figure 98. UV-Vis spectra of iron species with halide salts as ligands in anisole (top) or MeCN (bottom). (A) and (E) $FeCl_3$ + TBACl, (B) and (F) $FeCl_3$ + TBABr, (C) and (G) $FeBr_3$ + TBABr, and (D) and (H) $FeBr_3$ + TBACl. $[FeX_3]$ = 0.1 mM, [TBAX] = 0, 0.1, 0.2, and 0.4 mM.

These results indicate that Cl binds strongly to Fe compared to Br, and therefore may affect the deactivation process and control over polymerization. To investigate the effect of halides in iron-catalyzed ATRP, polymerization reactions were performed under ICAR (initiators for continuous activator regeneration) or photoinduced ATRP conditions in the presence of different halides in both initiator and the catalyst (Scheme 20).

Iron-Catalyzed ATRP - *Effect of Halogens*

ICAR ATRP

Photoinduced ATRP

X = Br or Cl

[Fe] = FeBr$_3$/L or FeCl$_3$/L, L = TBABr or TBACl
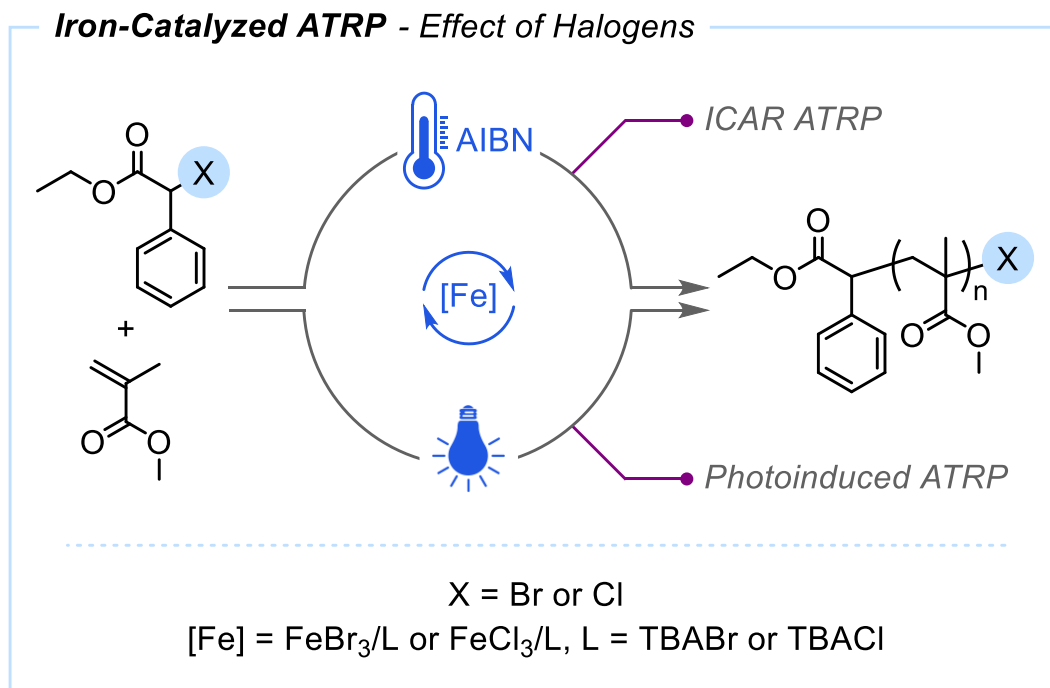
Scheme 20. Iron-catalyzed ATRP under ICAR or photoinduced ATRP conditions (TBA = tetrabutylammonium cation).

ICAR ATRP of methyl methacrylate (MMA) was performed using azobisisobutyronitrile (AIBN) as a radical source and Br or Cl-based initiators and catalysts. The Br-based initiating system used ethyl α-bromophenylacetate (EBPA) as the initiator and FeBr$_3$/TBABr as the catalyst (4 mol% with respect EBPA, i.e., 400 ppm *vs.* MMA). In the absence of additional TBABr, polymerization of MMA in anisole provided low monomer conversion (Table 21, Table 1). The importance of TBABr in affording a highly active iron catalyst was shown in ATRP of MMA with the FeBr$_3$/TBABr catalyst that yielded high monomer conversion (95%) with controlled molecular weight and low dispersity of 1.16 (Table 21, Entry 2). Using MeCN as a solvent under the same conditions, the polymers showed a higher dispersity of 1.68 (Table 21, Entry 3). Further increasing the ratio of TBABr from 1 to 4 (with respect to Fe) did not improve control (Table 21, Entry 4). Thus, a polar medium may diminish deactivation rate, especially when using low concentration of catalyst, in contrast to high catalyst concentration systems.[46]

The effect of MeCN in iron-catalyzed ATRP was further demonstrated by performing the UV-Vis analysis of the catalyst and polymerization of MMA with varying ratios of anisole and

MeCN as solvents. Addition of MeCN to a solution of $FeBr_3$ in anisole resulted in a progressive change in the UV-Vis spectra of the solution showing absorption peaks at ~390 and ~470 nm that resembled formation of anionic iron species upon addition of MeCN (1-10 vol% with respect to anisole) (Figure 101). In polymerization, ICAR ATRP of MMA in 100% anisole afforded well-controlled polymers using the Br-based initiating system. Increasing the volume ratio of MeCN with respect to anisole (from 0 to 25, 50, 75, and 100%), showed an increase in the dispersity of the resulting polymers, while experimental molecular weights agreed well with theoretical values. For example, in 25 vol% MeCN the dispersity of the polymers increased from 1.18 to 1.24. Further addition of MeCN in 50 or 75 vol%, afforded polymers with dispersity values of 1.28 and 1.36, respectively. In the presence of 100% MeCN, dispersity of the polymers was 1.69 (Table 23 and Figure 102). The increase in the dispersity of the polymers in iron-catalyzed ATRP of MMA with increasing amounts of MeCN may be attributed to the formation of iron species having low/poor deactivation efficacy in ATRP. The high stability of the deactivator $FeBr_4^-$ in a polar solvent such as MeCN may be responsible for the diminished deactivation rate of the growing chains.

Previous works have shown that well-controlled iron-catalyzed ATRP could be achieved in MeCN under either normal[46] or photoinduced[47, 48] ATRP conditions where equimolar ratios of the catalyst were used with respect to the initiator. Furthermore, in a recent study we showed that ATRP of semi-fluorinated monomers with ppm levels of the iron catalyst could also be controlled in MeCN.[42] Because of the high hydrophobicity of the fluorinated monomers, the overall polarity of the reaction medium containing MeCN was lowered and the deactivation of the growing radicals by $FeBr_4^-$ improved in a less polar medium.

To show the effect of the polarity of reaction medium, ICAR ATRP of a semi-fluorinated monomer, 2,2,2-trifluoroethyl methacrylate (TFEMA), was performed in MeCN. The overall polarity of the reaction medium in a mixture of TFEMA in MeCN was lower as compared to MMA in MeCN. Accordingly, ATRP of TFEMA showed well-controlled polymers with a low dispersity of 1.15 (conversion = 88%, M_n = 12000, Figure 103). These results indicate that the deactivation of growing chains by $FeBr_4^-$ in polar media is not efficient enough to yield polymethacrylates with low dispersity.

With FeCl$_3$/TBACl (4 mol%) as the catalyst and EBPA initiator, slightly higher dispersity of 1.22 was obtained compared to FeBr$_3$/TBABr and EBPA (Table 21, Entry 5 *vs.* 1). Using a Cl-based initiator, ethyl α-chlorophenylacetate (ECPA), in the presence of either FeBr$_3$/TBABr or FeCl$_3$/TBACl high dispersities were obtained (>1.7), indicating poor control over polymerization with Cl-based initiating systems in iron-catalyzed ATRP (Entries 6 and 7, Table 21). Note the total ratio Br/Cl was 1/0.16 in entry 5 but 0.16/1 in entry 6, in Table 1. Polymerizations conducted with the Cl-based initiating system in MeCN showed even larger dispersity values, suggesting worse deactivation in MeCN compared to anisole in the presence of Cl (Entries 8 and 9, Table 21).

Table 21.   Table 1. Results of iron-catalyzed ICAR ATRP of MMA with different halides [a]

Entry	R-X	Catalyst	Solvent	Conv. (%)	$M_{n,th}$	M_n	Đ
1	EBPA	FeBr$_3$/Br$^-$ (1/0)	Anisole	33	3500	3600	1.34
2	EBPA	FeBr$_3$/Br$^-$ (1/1)	Anisole	95	9700	9000	1.16
3	EBPA	FeBr$_3$/Br$^-$ (1/1)	MeCN	90	9300	8700	1.68
4	EBPA	FeBr$_3$/Br$^-$ (1/4)	MeCN	90	9300	9700	1.60
5	EBPA	FeCl$_3$/Cl$^-$ (1/1)	Anisole	91	9450	8700	1.19
6	ECPA	FeBr$_3$/Br$^-$ (1/1)	Anisole	94	9750	10300	1.68
7	ECPA	FeCl$_3$/Cl$^-$ (1/1)	Anisole	97	10000	12800	1.70
8	ECPA	FeCl$_3$/Cl$^-$ (1/1)	MeCN	96	9900	16200	1.94
9	ECPA	FeCl$_3$/Cl$^-$ (1/4)	MeCN	92	9600	22000	1.95

[a] Reaction conditions: [MMA]/[EXPA]/[FeX$_3$]/[TBAX]/[AIBN] = 100/1/0.04/0.04/0.4 (X = Br or Cl) in 50 vol% solvent at 65 °C for 18 h.

To further demonstrate the effect of Br *vs.* Cl, kinetics of polymerization of MMA under ICAR ATRP conditions was investigated using both Br-, and Cl-based initiating systems in anisole. Both systems showed similar rate of polymerization (Figure 99-A). However, molecular weight analysis of the resulting polymers showed that poor control was obtained over the polymerization in the Cl-based initiating system (Figure 99-B). Molecular weights were higher than theoretical values and decreased as polymerization progressed, suggesting poor deactivation

of the growing radicals by $FeCl_4^-$ catalyst (dispersity values ~1.6-1.8, Figure 99-C). In contrast, well-controlled polymerization of MMA was observed in the presence of the Br-based initiating system. Molecular weights increased as a function of monomer conversion in line with theoretical values. Moreover, the resulting polymers showed low dispersity values (< 1.2) suggesting a well-controlled polymerization was obtained in the presence of Br-based initiating system (Figure 104). Interestingly, when a Br-based initiator, EBPA, was used with $FeCl_4$/TBACl as the catalyst (4 mol%) polymerization of MMA was well-controlled as observed in the presence of all Br-based initiating system (both EBPA and $FeBr_4^-$). Considering the relative ratio of EBPA and $FeCl_4^-$ (1 to 0.04), Br is present in sufficient amount, resulting in efficient atom transfer and deactivation of the growing chains.
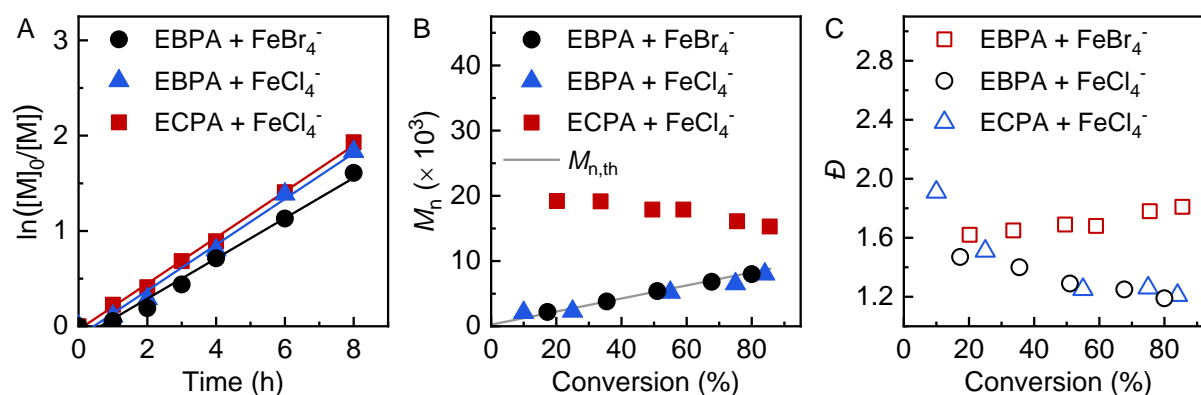
Figure 99. (A) Kinetics and evolution of (B) molecular weight (M_n) and (C) dispersity ($Đ$) in iron-catalyzed ATRP with Br or Cl-based initiating systems. Reaction conditions: [MMA]/[EXPA]/[FeX₃]/[TBAX]/[AIBN] = 100/1/0.04/0.04/0.4 (X = Br or Cl) in anisole (50 vol%) at 65 °C.

Iron-catalyzed ATRP can also be photochemically controlled via generation of the activator L/Fe^{II} under light irradiation. The Fe-Br bond in L/Fe^{III}-Br can be homolytically cleaved to generate L/Fe^{II} and Br$^•$ radicals via a ligand to metal charge transfer process. The iron catalyst with Br or Cl anions showed different absorption spectra with $FeBr_3$ absorbing in visible light and $FeCl_3$ absorbing at the UV region (below 400 nm). Therefore, photoinduced ATRP using iron catalysts was attempted under blue (460 nm) and violet (400 nm) LED lights to ensure proper photoexcitation of both species. The results of polymerization of MMA with iron in the

presence of different halides are summarized in Table 22. Polymerization of MMA using FeBr$_3$ without additional TBABr ligand showed low monomer conversion and polymers with a large dispersity of 2.18. However, when TBABr was added as a ligand, polymerization of MMA in anisole yielded well-controlled polymers. These results indicate the importance of TBABr as a ligand for obtaining the active iron catalysts. Similar to ICAR ATRP results, Br-based systems resulted in well-controlled polymerizations under both blue and violet lights (Table 22, Entries 2 and 6). However, in the Cl-based system control over polymerization was poor showing polymers with high dispersity (Table 22, Entries 5 and 7).

Table 22. Results of photoinduced iron catalyzed ATRP with different halides [a]

Entry	R-X	Catalyst	Solvent	Light	Conv. (%)	$M_{n,th}$	M_n	Đ
1	EBPA	FeBr$_3$/Br$^-$ (1/0)	Anisole	Blue	59	6100	10900	2.18
2	EBPA	FeBr$_3$/Br$^-$ (1/1)	Anisole	Blue	96	9900	11600	1.23
3	EBPA	FeBr$_3$/Br$^-$ (1/1)	MeCN	Blue	94	9700	9400	1.56
4	EBPA	FeBr$_3$/Br$^-$ (1/4)	MeCN	Blue	75	7700	8100	1.61
5	ECPA	FeCl$_3$/Cl$^-$ (1/1)	Anisole	Blue	80	8300	16800	1.75
6	EBPA	FeBr$_3$/Br$^-$ (1/1)	Anisole	Violet	96	9900	10600	1.20
7	ECPA	FeCl$_3$/Cl$^-$ (1/1)	Anisole	Violet	95	9800	7300	2.08

[a] Reaction conditions: [MMA]/[EXPA]/[FeX$_3$]/[TBAX] = 100/1/0.04/0.04 (X = Br or Cl) in 50 vol% anisole under blue (460 nm) or violet (400 nm) light irradiation for 18 h.

Block copolymerization experiments were performed to confirm the preserved chain end functionality in the resulting polymers under both ICAR and photoinduced ATRP conditions. A PMMA-Br macroinitiator was first synthesized under ICAR ATRP (M_n = 8700, Đ = 1.13). Chain extension of the PMMA-Br macroinitiator with benzyl methacrylate (BzMA) resulted in formation of the second block showing controlled block copolymer with molecular weights shifting to higher values and high blocking efficiency (M_n = 8700, Đ = 1.13, Figure 100-A). Similarly, block copolymerization was successfully achieved under photoinduced ATRP conditions (Figure 100-B).
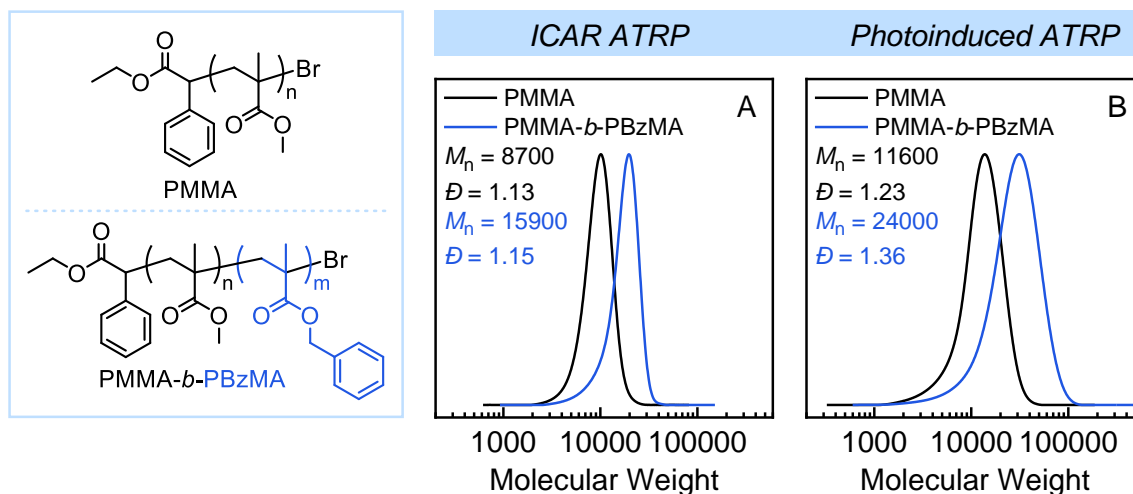
Figure 100. Chain extension experiments of PMMA with BzMA under (A) ICAR and (B) photoinduced ATRP conditions.

In summary, Cl-based initiating systems provided inferior control in iron-catalyzed ATRP in the presence of halide anions as ligands. The high affinity of Cl to iron leads to inefficient deactivation of the growing chains and therefore provides poor control over polymerization. In the presence of Br-based initiating systems, well-controlled polymerization of methacrylate monomers was achieved with well-defined molecular weights and low dispersities (< 1.2) as demonstrated in synthesis of homo and block copolymers. Furthermore, we have shown the effect of reaction medium on polymerization control wherein the deactivation may become poor/slow in polar media which yielded polymers with large dispersity. The results of this work provide further understanding of iron-catalyzed ATRP and show a delicate balance of all ATRP components including initiator, catalyst and medium needed for performing well-controlled polymerizations. Considering the great potential of iron catalysts in ATRP, future studies should expand upon mechanistic understanding of these systems as well as their utility in a wide range of monomers and reaction media.

4.5.4 Experimental Section and Supporting Information

Materials

Methyl methacrylate (MMA, Sigma-Aldrich, 99%), 2,2,2-trifluoroethyl methacrylate (TFEMA, TCI, 98%), and benzyl methacrylate (BzMA, TCI, > 98%) were purified by passing through a column of basic alumina. Azobisisobutyronitrile (AIBN, Sigma-Aldrich, 98%) was recrystallized

in methanol before use. Iron(III) bromide (FeBr$_3$, Alfa Aesar, 98%), iron(III) chloride (FeCl$_3$, Sigma-Aldrich, 97%), tetrabutylammonium bromide (TBABr, Sigma-Aldrich, 98%), tetrabutylammonium chloride (TBACl, Sigma-Aldrich, > 97%), ethyl α-bromophenylacetate (EBPA, Sigma-Aldrich, 97%), ethyl α-chlorophenylacetate (ECPA, Sigma-Aldrich, 97%), anisole, and acetonitrile (MeCN) were used as received.

Instrumentation

^{1}H nuclear magnetic resonance (^{1}H NMR) measurements were performed on a Bruker Avance™ III 500 MHz spectrometer. Molecular weight and dispersity of the polymers were measured by gel permeation chromatography (GPC). The GPC instrument used a Waters 515 pump and a Waters 2414 differential refractometer using PSS columns (SDV 10^5, 10^3, and 500 Å) with tetrahydrofuran as the eluent at 35 °C and a flow rate of 1 mL min^{-1}. Linear poly(methyl methacrylate) standards were used for calibration. UV-Vis measurements were performed using an Agilent 8453 spectrophotometer. Blue (465 nm, 12 mW/cm^2) and violet (400 nm, 10 mW/cm^2) LEDs purchased from AspectLED and mounted inside a glass container. A cooling fan was placed on top to maintain reactions at room temperature.

General procedure for iron-catalyzed ICAR ATRP of MMA

To a 2-dram reaction vial, AIBN (6.17 mg, 37.6 mmol) was added, and the vial equipped with a stir bar and sealed with a rubber septum was subjected to vacuum and backfilling with nitrogen for five times. Purified monomer and anisole were degassed by sparging with nitrogen in separate containers for 30 min. Anisole (1 mL) was added to the reaction vial followed by injection of a stock solution of FeBr$_3$ and TBABr (50 µL of the stock solution at a concentration of 75.2 mM; FeBr$_3$ = 1.11, 3.76 µmol, 0.04 equiv.; TBABr = 1.21 mg, 3.76 µmol, 0.04 equiv.) under nitrogen. MMA (1 mL, 9.4 mmol, 100 equiv.) and EBPA (16.4 µL, 94 µmol, 1 equiv.) were injected into the reaction vial and the solution was further degassed with nitrogen for ~5 min. The reaction vial was placed in pre-heated oil bath at 65 °C. Samples were taken and analyzed by NMR and GPC to determine monomer conversion and molecular weight properties.

General procedure for iron-catalyzed photoinduced ATRP of MMA

A 2-dram reaction vial equipped with a stir bar and sealed with a rubber septum was subjected to vacuum and backfilling with nitrogen for five times. Purified monomer and anisole were

degassed by sparging with nitrogen in separate containers for 30 min. Anisole (1 mL) was added to the reaction vial followed by injection of a stock solution of $FeBr_3$ and TBABr (50 µL of the stock solution at a concentration of 75.2 mM; $FeBr_3$ = 1.11, 3.76 µmol, 0.04 equiv.; TBABr = 1.21 mg, 3.76 µmol, 0.04 equiv.) under nitrogen. MMA (1 mL, 9.4 mmol, 100 equiv.) and EBPA (16.4 µL, 94 µmol, 1 equiv.) were injected into the reaction vial and the solution was further degassed with nitrogen for ~5 min. The reaction vial was irradiated in either blue or violet LED photoreactors with a cooling fan on top to maintain the reactions at room temperature. Samples were taken and analyzed by NMR and GPC to determine monomer conversion and molecular weight properties.

General procedure for synthesis of block copolymers by iron-catalyzed ICAR ATRP

To a 20-mL reaction vial, AIBN (30.85 mg, 188 mmol) was added, and the vial equipped with a stir bar and sealed with a rubber septum was subjected to vacuum and backfilling with nitrogen for five times. Purified monomer and anisole were degassed by sparging with nitrogen in separate containers for 30 min. Anisole (5 mL) was added to the reaction vial followed by injection of a stock solution of $FeBr_3$ and TBABr in anisole ($FeBr_3$ = 5.55, 18.8 µmol, 0.04 equiv.; TBABr = 6.05 mg, 18.8 µmol, 0.04 equiv.) under nitrogen. MMA (5 mL, 47 mmol, 100 equiv.) and EBPA (82 µL, 94 µmol, 1 equiv.) were injected into the reaction vial and the solution was further degassed with nitrogen for ~5 min. The reaction vial was placed in pre-heated oil bath at 65 °C. The reaction was stopped after 6 h. The reaction mixture was diluted with acetone and the catalyst was separated by passing through a column of basic alumina. Excess solvent was evaporated and the PMMA-Br macroinitiator was precipitated in cold methanol. The macroinitiator was separated by filtration and dried in vacuum (M_n = 8700, Đ = 1.13).

The PMMA-Br macroinitiator was used in block copolymerization using BzMA monomer following similar conditions and the general procedure.

UV-Vis results:

Addition of MeCN to a solution of FeBr$_3$ in anisole resulted in a progressive change in the UV-Vis spectra of the solution showing absorption peaks at ~390 and ~470 nm that resemble formation of anionic iron species upon addition of MeCN (1-10 vol% with respect to anisole) (Figure S1).
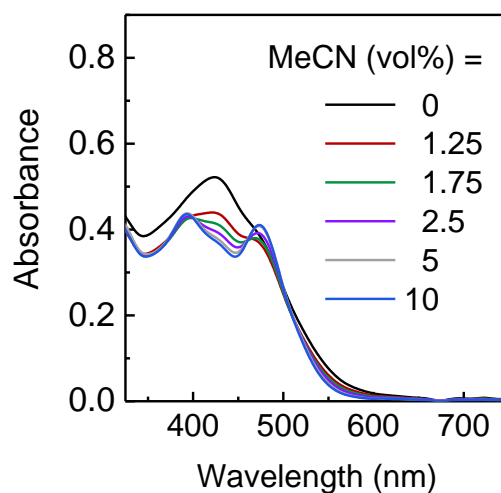
Figure 101. UV-Vis spectra of FeBr$_3$ in anisole upon increasingly addition of MeCN. The changes in the spectra are attributed to the generation of anionic iron species upon addition of MeCN. [FeBr$_3$] = 0.1 mM. In 1.25 vol%, [MeCN]/[FeBr$_3$] = 2400.

Effect of MeCN as solvent:

Iron-catalyzed ATRP of MMA showed an increase in dispersity of polymers by increasing the volume ratio of MeCN with respect to anisole as the solvent (Table S1). These results confirm the importance of the polarity of the reaction medium to obtain well-controlled polymerizations in iron-catalyzed ATRP.

Table 23. Results of iron-catalyzed ICAR ATRP of MMA with varying ratios of anisole and MeCN solvents [a]

Entry	MeCN (vol%)	Conversion (%)	$M_{n,th}$	M_n	$Đ$
1	0	96	9800	9400	1.18
2	25	97	10000	8900	1.24
3	50	93	9600	8700	1.28
4	75	95	9800	9600	1.36
5	100	92	9500	9500	1.69

[a] Reaction conditions: [MMA]/[EBPA]/[FeBr$_3$]/[TBABr]/[AIBN] = 100/1/0.04/0.04/0.4 in 50 vol% solvent (MeCN/anisole = 0-100%) at 65 °C for 18 h.
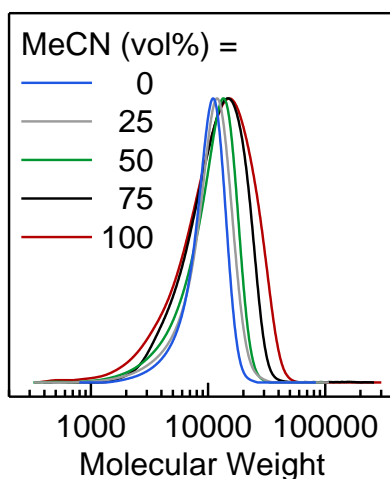
Figure 102. GPC traces of PMMA synthesizedd in iron-catalyzed ATRP with varying ratios of MeCN and anisole as the solvent. Increasing the volume ratio of MeCN resulted in broadening the molecular weight distribution of the polymers. Reaction conditions: [MMA]/[EBPA]/[FeBr$_3$]/[TBABr]/[AIBN] = 100/1/0.04/0.04/0.4 in 50 vol% solvent (MeCN/anisole = 0-100%) at 65 °C for 18 h.

ATRP of TFEMA:
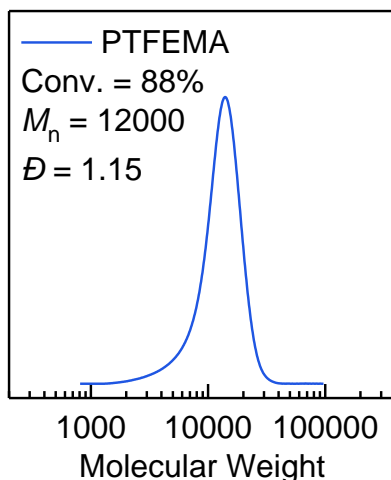
Figure 103. GPC traces of PTFEMA synthesized in iron-catalyzed ATRP in MeCN showing well-controlled properties achieved in a relatively low polar medium containing MeCN solvent impaprted by the hydrophobic nature the semi-fluorinated monomer. Reaction conditions: [TFEMA]/[EBPA]/[FeBr₃]/[TBABr]/[AIBN] = 100/1/0.04/0.04/0.4 in MeCN (50 vol%) at 65 °C.

Kinetics of ATRP of MMA with Br vs. Cl:
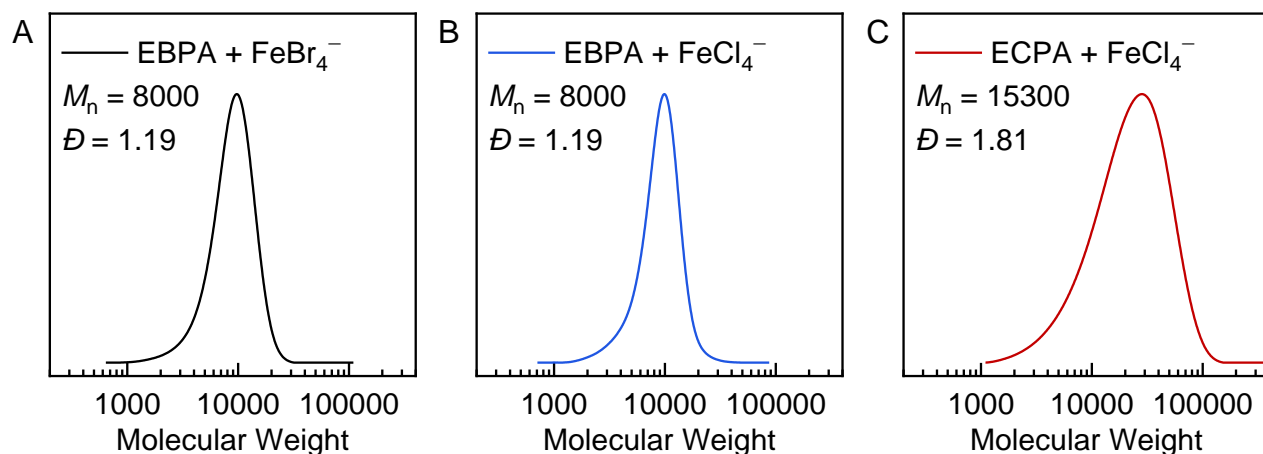
Figure 104. GPC traces of PMMA obtained in iron-catalyzed ATRP with Br or Cl-based initiating systems. Reaction conditions: [MMA]/[EXPA]/[FeX₃]/[TBAX]/[AIBN] = 100/1/0.04/0.04/0.4 (X = Br or Cl) in anisole (50 vol%) at 65 °C (full polymerization data presented in Figure 2, main text).

4.5.5 References

1. Corrigan, N.; Jung, K.; Moad, G.; Hawker, C. J.; Matyjaszewski, K.; Boyer, C. Reversible-deactivation radical polymerization (Controlled/living radical polymerization): From discovery to materials design and applications. *Prog. Polym. Sci.* **2020,** 111, 101311.

2. Parkatzidis, K.; Wang, H. S.; Truong, N. P.; Anastasaki, A. Recent Developments and Future Challenges in Controlled Radical Polymerization: A 2020 Update. *Chem* **2020,** 6 (7), 1575-1588.

3. Wang, J.-S.; Matyjaszewski, K. Controlled/"living" radical polymerization. atom transfer radical polymerization in the presence of transition-metal complexes. *J. Am. Chem. Soc.* **1995,** 117 (20), 5614-5615.

4. Matyjaszewski, K.; Xia, J. Atom Transfer Radical Polymerization. *Chem. Rev.* **2001,** 101 (9), 2921-2990.

5. Matyjaszewski, K. Atom Transfer Radical Polymerization (ATRP): Current Status and Future Perspectives. *Macromolecules* **2012,** 45 (10), 4015-4039.

6. Perrier, S. 50th Anniversary Perspective: RAFT Polymerization—A User Guide. *Macromolecules* **2017,** 50 (19), 7433-7447.

7. Chiefari, J.; Chong, Y. K.; Ercole, F.; Krstina, J.; Jeffery, J.; Le, T. P. T.; Mayadunne, R. T. A.; Meijs, G. F.; Moad, C. L.; Moad, G.; Rizzardo, E.; Thang, S. H. Living Free-Radical Polymerization by Reversible Addition−Fragmentation Chain Transfer: The RAFT Process. *Macromolecules* **1998,** 31 (16), 5559-5562.

8. Nicolas, J.; Guillaneuf, Y.; Lefay, C.; Bertin, D.; Gigmes, D.; Charleux, B. Nitroxide-mediated polymerization. *Prog. Polym. Sci.* **2013,** 38 (1), 63-235.

9. Ribelli, T. G.; Lorandi, F.; Fantin, M.; Matyjaszewski, K. Atom Transfer Radical Polymerization: Billion Times More Active Catalysts and New Initiation Systems. *Macromol. Rapid Commun.* **2019,** 40 (1), 1800616.

10. Tang, W.; Matyjaszewski, K. Effects of Initiator Structure on Activation Rate Constants in ATRP. *Macromolecules* **2007,** 40 (6), 1858-1863.

11. Lanzalaco, S.; Fantin, M.; Scialdone, O.; Galia, A.; Isse, A. A.; Gennaro, A.; Matyjaszewski, K. Atom Transfer Radical Polymerization with Different Halides (F, Cl, Br, and I): Is the Process "Living" in the Presence of Fluorinated Initiators? *Macromolecules* **2017,** 50 (1), 192-202.

12. Dadashi-Silab, S.; Szczepaniak, G.; Lathwal, S.; Matyjaszewski, K. Iodine-mediated photoATRP in aqueous media with oxygen tolerance. *Polym. Chem.* **2020,** 11 (4), 843-848.

13. Wang, C.-G.; Chong, A. M. L.; Pan, H. M.; Sarkar, J.; Tay, X. T.; Goto, A. Recent development in halogen-bonding-catalyzed living radical polymerization. *Polym. Chem.* **2020,** 11 (35), 5559-5571.

14. Onishi, I.; Baek, K.-Y.; Kotani, Y.; Kamigaito, M.; Sawamoto, M. Iron-catalyzed living radical polymerization of acrylates: Iodide-based initiating systems and block and random copolymerizations. *J. Polym. Sci., Part A: Polym. Chem.* **2002,** 40 (12), 2033-2043.

15. Chen, Z.-H.; Ma, Y.; Wang, X.-Y.; Sun, X.-L.; Li, J.-F.; Zhu, B.-H.; Tang, Y. Winning Strategy for Iron-Based ATRP Using In Situ Generated Iodine as a Regulator. *ACS Cat.* **2020,** 10 (23), 14127-14134.

16. Matyjaszewski, K.; Gaynor, S.; Wang, J.-S. Controlled Radical Polymerizations: The Use of Alkyl Iodides in Degenerative Transfer. *Macromolecules* **1995,** 28 (6), 2093-2095.

17. Poli, R.; Allan, L. E. N.; Shaver, M. P. Iron-mediated reversible deactivation controlled radical polymerization. *Prog. Polym. Sci.* **2014,** 39 (10), 1827-1845.

18. Xue, Z.; He, D.; Xie, X. Iron-catalyzed atom transfer radical polymerization. *Polym. Chem.* **2015,** 6 (10), 1660-1687.

19. Dadashi-Silab, S.; Matyjaszewski, K. Iron Catalysts in Atom Transfer Radical Polymerization. *Molecules* **2020,** 25 (7), 1648.

20. Simakova, A.; Mackenzie, M.; Averick, S. E.; Park, S.; Matyjaszewski, K. Bioinspired Iron-Based Catalyst for Atom Transfer Radical Polymerization. *Angew. Chem. Int. Ed.* **2013,** 52 (46), 12148-12151.

21. Sigg, S. J.; Seidi, F.; Renggli, K.; Silva, T. B.; Kali, G.; Bruns, N. Horseradish Peroxidase as a Catalyst for Atom Transfer Radical Polymerization. *Macromol. Rapid Commun.* **2011,** 32 (21), 1710-1715.

22. Xue, Z.; Linh, N. T. B.; Noh, S. K.; Lyoo, W. S. Phosphorus-Containing Ligands for Iron(III)-Catalyzed Atom Transfer Radical Polymerization. *Angew. Chem. Int. Ed.* **2008,** 47 (34), 6426-6429.

23. Nishizawa, K.; Ouchi, M.; Sawamoto, M. Phosphine–Ligand Decoration toward Active and Robust Iron Catalysts in LRP. *Macromolecules* **2013,** 46 (9), 3342-3349.

24. Wang, Y.; Kwak, Y.; Matyjaszewski, K. Enhanced Activity of ATRP Fe Catalysts with Phosphines Containing Electron Donating Groups. *Macromolecules* **2012,** 45 (15), 5911-5915.

25. Khan, M. Y.; Zhou, J.; Chen, X.; Khan, A.; Mudassir, H.; Xue, Z.; Lee, S. W.; Noh, S. K. Exploration of highly active bidentate ligands for iron (III)-catalyzed ATRP. *Polymer* **2016,** 90, 309-316.

26. Ando, T.; Kamigaito, M.; Sawamoto, M. Iron(II) Chloride Complex for Living Radical Polymerization of Methyl Methacrylate. *Macromolecules* **1997,** 30 (16), 4507-4510.

27. Matyjaszewski, K.; Wei, M.; Xia, J.; McDermott, N. E. Controlled/"Living" Radical Polymerization of Styrene and Methyl Methacrylate Catalyzed by Iron Complexes. *Macromolecules* **1997,** 30 (26), 8161-8164.

28. Schroeder, H.; Matyjaszewski, K.; Buback, M. Kinetics of Fe-Mediated ATRP with Triarylphosphines. *Macromolecules* **2015,** 48 (13), 4431-4437.

29. Gibson, V. C.; O'Reilly, R. K.; Reed, W.; Wass, D. F.; White, A. J. P.; Williams, D. J. Four-coordinate iron complexes bearing α-diimine ligands: efficient catalysts for Atom Transfer Radical Polymerisation (ATRP). *Chem. Commun.* **2002,** (17), 1850-1851.

30. O'Reilly, R. K.; Shaver, M. P.; Gibson, V. C.; White, A. J. P. α-Diimine, Diamine, and Diphosphine Iron Catalysts for the Controlled Radical Polymerization of Styrene and Acrylate Monomers. *Macromolecules* **2007,** 40 (21), 7441-7452.

31. Shaver, M. P.; Allan, L. E. N.; Rzepa, H. S.; Gibson, V. C. Correlation of Metal Spin State with Catalytic Reactivity: Polymerizations Mediated by α-Diimine–Iron Complexes. *Angew. Chem. Int. Ed.* **2006,** 45 (8), 1241-1244.

32. Azuma, Y.; Terashima, T.; Sawamoto, M. Self-Folding Polymer Iron Catalysts for Living Radical Polymerization. *ACS Macro Lett.* **2017,** 6 (8), 830-835.

33. Allan, L. E. N.; MacDonald, J. P.; Nichol, G. S.; Shaver, M. P. Single Component Iron Catalysts for Atom Transfer and Organometallic Mediated Radical Polymerizations: Mechanistic Studies and Reaction Scope. *Macromolecules* **2014,** 47 (4), 1249-1257.

34. Allan, L. E. N.; MacDonald, J. P.; Reckling, A. M.; Kozak, C. M.; Shaver, M. P. Controlled Radical Polymerization Mediated by Amine–Bis(phenolate) Iron(III) Complexes. *Macromol. Rapid Commun.* **2012,** 33 (5), 414-418.

35. Schroeder, H.; Lake, B. R. M.; Demeshko, S.; Shaver, M. P.; Buback, M. A Synthetic and Multispectroscopic Speciation Analysis of Controlled Radical Polymerization Mediated by Amine–Bis(phenolate)iron Complexes. *Macromolecules* **2015,** 48 (13), 4329-4338.

36. Teodorescu, M.; Gaynor, S. G.; Matyjaszewski, K. Halide Anions as Ligands in Iron-Mediated Atom Transfer Radical Polymerization. *Macromolecules* **2000,** 33 (7), 2335-2339.

37. Wang, J.; Han, J.; Xie, X.; Xue, Z.; Fliedel, C.; Poli, R. FeBr2-Catalyzed Bulk ATRP Promoted by Simple Inorganic Salts. *Macromolecules* **2019,** 52 (14), 5366-5376.

38. Rolland, M.; Truong, N. P.; Whitfield, R.; Anastasaki, A. Tailoring Polymer Dispersity in Photoinduced Iron-Catalyzed ATRP. *ACS Macro Lett.* **2020,** 9 (4), 459-463.

39. Wang, J.; Xie, X.; Xue, Z.; Fliedel, C.; Poli, R. Ligand- and solvent-free ATRP of MMA with FeBr3 and inorganic salts. *Polym. Chem.* **2020,** 11 (7), 1375-1385.

40. Wang, Y.; Zhang, Y.; Parker, B.; Matyjaszewski, K. ATRP of MMA with ppm Levels of Iron Catalyst. *Macromolecules* **2011,** 44 (11), 4022-4025.

41. Dadashi-Silab, S.; Pan, X.; Matyjaszewski, K. Photoinduced Iron-Catalyzed Atom Transfer Radical Polymerization with ppm Levels of Iron Catalyst under Blue Light Irradiation. *Macromolecules* **2017,** 50 (20), 7967-7977.

42. Dadashi-Silab, S.; Matyjaszewski, K. Iron-Catalyzed Atom Transfer Radical Polymerization of Semifluorinated Methacrylates. *ACS Macro Lett.* **2019,** 8 (9), 1110-1114.

43. Mukumoto, K.; Wang, Y.; Matyjaszewski, K. Iron-Based ICAR ATRP of Styrene with ppm Amounts of FeIIIBr3 and 1,1′-Azobis(cyclohexanecarbonitrile). *ACS Macro Lett.* **2012,** 1 (5), 599-602.

44. Ishio, M.; Katsube, M.; Ouchi, M.; Sawamoto, M.; Inoue, Y. Active, Versatile, and Removable Iron Catalysts with Phosphazenium Salts for Living Radical Polymerization of Methacrylates. *Macromolecules* **2009,** 42 (1), 188-193.

45. Schroeder, H.; Buback, J.; Demeshko, S.; Matyjaszewski, K.; Meyer, F.; Buback, M. Speciation Analysis in Iron-Mediated ATRP Studied via FT-Near-IR and Mössbauer Spectroscopy. *Macromolecules* **2015,** 48 (7), 1981-1990.

46. Wang, Y.; Matyjaszewski, K. ATRP of MMA in Polar Solvents Catalyzed by FeBr2 without Additional Ligand. *Macromolecules* **2010,** 43 (9), 4003-4005.

47. Pan, X.; Malhotra, N.; Zhang, J.; Matyjaszewski, K. Photoinduced Fe-Based Atom Transfer Radical Polymerization in the Absence of Additional Ligands, Reducing Agents, and Radical Initiators. *Macromolecules* **2015,** 48 (19), 6948-6954.

48. Pan, X.; Malhotra, N.; Dadashi-Silab, S.; Matyjaszewski, K. A Simplified Fe-Based PhotoATRP Using Only Monomers and Solvent. *Macromol. Rapid Commun.* **2017,** 38 (13), 1600651.

Chapter 5. Phenyl benzo[b]phenothiazine as a visible light photoredox catalyst for metal-free atom transfer radical polymerization

5.1. Preface

Phenothiazine derivatives are efficient organic photocatalysts for photoinduced metal-free ATRP. Initial studies reported the use of 10-phenylphenothiazine for controlled polymerization of various monomers. In this chapter, I expanded the scope of organo-catalyzed (O-ATRP) by utilizing phenyl benzo[*b*]phenothiazine (Ph-benzoPTZ) as a visible light activated photoredox catalyst to promote ATRP of methacrylate monomers under visible light irradiation. I synthesized a core-modified phenothiazine photocatalyst by introducing a phenyl group, which resulted in a red-shift in the absorption spectra of the compound to enable metal-free ATRP under visible light.

I designed and conducted the experiments with help from Dr Xiangcheng Pan and Prof Matyjaszewski's supervision.

_____

5.2. Abstract

This paper reports use of phenyl benzo[*b*]phenothiazine (Ph-benzoPTZ) as a visible light-induced metal-free atom transfer radical polymerization (ATRP) photoredox catalyst. Well-controlled polymerizations of various methacrylate monomers were conducted under a 392 nm visible light LED using Ph-benzoPTZ to activate different alkyl halides. The use of the photocatalyst enabled temporal control over the growth of polymer chains during intermittent on/off periods. The polymerization was initiated and progressed only under stimulation by light and completely stopped in the absence of light. Block copolymers were synthesized to demonstrate high retention of chain end fidelity in the polymers and livingness of the process.
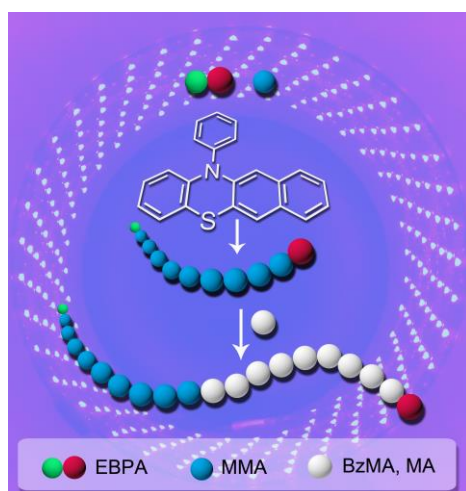
5.3. Introduction

The emergence of photoredox catalysis in the synthetic polymer community has provided unique opportunities for the synthesis of well-defined polymers.[1-6] Photochemical processes enable chemical reactions to be conducted under more environmentally benign conditions as they use light as a "green" reagent to drive a range of chemical transformations.[4] A great deal of research in the area of reversible-deactivation radical polymerization (RDRP), traditionally known as controlled radical polymerization (CRP), has been directed towards developing, and implementing, photochemical processes for the synthesis of materials with controlled polymeric structures. In this regard, atom transfer radical polymerization (ATRP),[5, 7-10] reversible addition-fragmentation chain transfer (RAFT),[11] and nitroxide-mediated polymerization (NMP)[10, 12, 13] are among the most widely used RDRP techniques and in recent years they have all adopted photochemical approaches.

ATRP predominately utilizes transition metal catalysis[12] to establish and maintain an equilibrium between dormant and growing species which in turn results in manifesting excellent control over the molecular weight (MW) and MW distribution of polymers, allowing access to well-defined polymers with complex macromolecular architecture. Recent developments have permitted diminishing catalyst concentrations to ppm levels while maintaining control over the polymerization process. This is of importance for economic reasons as well as expanding the utility of ATRP to include applications targeting biologically active materials where no, or least minimal, presence of residual transition metal catalysts is demanded. As a result, techniques including activators generated by electron transfer (AGET),[14] activators regenerated by electron transfer (ARGET),[15, 16] and use of zero-valent metals[17, 18] as supplemental activators and reducingagents ATRP (SARA ATRP),[16, 19-21] initiators for continuous activator regeneration (ICAR) ATRP,[20, 22] and electrochemically-mediated ATRP,[23-25] have been developed that use ppm levels of air-stable Cu^{II} complexes to generate *in situ* the activator Cu^I species. Similarly, owing to the fact that Cu^{II}/L complexes are photochemically active, Cu^I activators can also be (re)generated by photochemical means.[4-6, 26-34] Photoinduced ATRP has several advantages in terms of establishing spatiotemporal control over the course of the polymerization which leads to precise and facile manipulation of the growth of polymers in space and time.[34, 35]

Photoredox catalysis have been developed as a new class of catalysis for RDRP techniques for the synthesis of well-defined polymers. Advancements have been facilitated by development of photoredox catalysis for ATRP[7, 36] and RAFT[36-39] polymerizations. In addition to transition metal-based photoredox catalysts, such as Ir- or Ru- complexes, photoredox organocatalysts as recently developed transition metal-free systems are used to establish the ATRP equilibrium. In Cu-based ATRP systems an activator L/Cu^I species activates alkyl halide initiator to form initiating radicals while the L/Cu^I is oxidized to L/Cu^{II}-X (where L is a ligand and X is halogen) *via* an inner-sphere electron transfer process. In photoinduced metal-free ATRP reactions, however, a photoredox catalyst, which becomes highly reducing in its photoexcited state, is used to activate alkyl halide initiators via outer-sphere electron transfer reaction. The products of reduction of the alkyl halide by the excited state photocatalyst are organic radicals that can initiate polymerization and halide anions. At the same time, the photocatalyst is oxidized to a radical cation. The key step in establishing control over the process relies on the ability of the

catalyst radical cation, to deactivate propagating radicals forming bromine-terminated polymer chains and the initial ground state photocatalyst, thereby completing the photocatalytic cycle.

Our group recently reported a detailed mechanistic study that elucidated the mechanism of the steps involved in photoinduced metal-free ATRP reactions.[40] It was proposed that the activation step involves a photoinduced dissociative electron transfer from the excited state catalyst to the alkyl halide initiator to form initiating radicals, bromine anions, and catalyst radical cations. The deactivation process proceeds favorably through an associative electron transfer involving the radical cation, halide anion and propagating radicals to form bromine-terminated chains and regenerate the ground state catalyst.

Phenothiazine derivatives are efficient catalysts for photoinduced metal-free ATRP. Initial studies reported the use of 10-phenylphenothiazine for controlled polymerization of various monomers.[39, 41-45] Dihydrophenazine[46]- and phenoxazine[47]-based photoredox catalysts were subsequently developed to tune and enhance the polymerization efficiency in visible light regions. Polynuclear aromatic hydrocarbons including perylene,[48] anthracene, and pyrene[49] and carbazole[50]-based photoredox catalysts are also suitable for photoinduced metal-free ATRP. Furthermore, organic dyes that are oxidizing in the excited state can initiate and control the metal-free ATRP *via* a different mechanistic pathway by undergoing reductive quenching in the presence of amine electron-donor compounds.[51] In this case, the catalyst is reduced to a radical anion by accepting an electron from the electron-donor in the excited state, which can then activate the alkyl halide to form initiating radicals, a halide anion and an amine radical cation as well as regenerating the ground state catalyst. An electron transfer between the halide anion and amine radical cation regenerates the initial amine and a bromine radical that can deactivate the propagating radical.

In this communication we expand the scope of photoinduced metal-free ATRP by utilizing phenyl benzo[*b*]phenothiazine (Ph-benzoPTZ) as a visible light activated photoredox catalyst to promote ATRP of methacrylate monomers under LED irradiation. Due to more extended conjugation, with respect to phenothiazine (PTZ), the Ph-benzoPTZ photocatalyst exhibits strong absorption in the visible light region, around 400 nm.[52] In this area PTZ is transparent and shows a very weak absorption. The UV-vis spectra of the photocatalysts are shown in Figure 105.
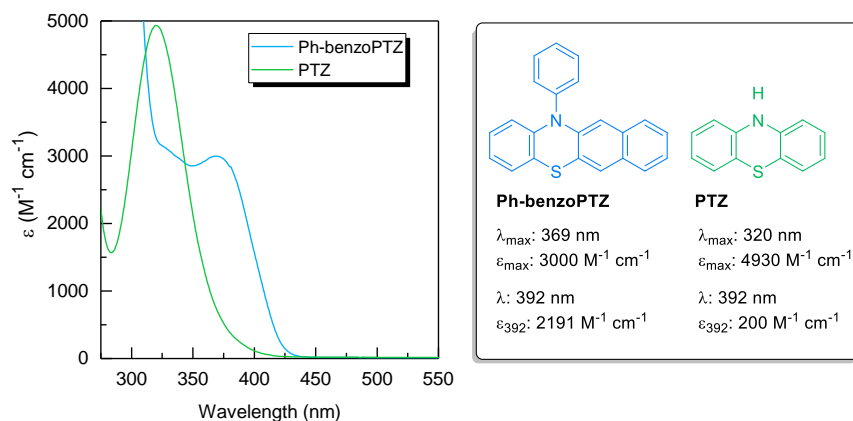
Figure 105. UV-vis spectra of photocatalysts Ph-benzoPTZ and PTZ in DMA (concentration: 3.07×10^{-4} M).

5.4. Results and Discussion

Metal-free ATRP of methyl methacrylate (MMA) was conducted using Ph-benzoPTZ with various light sources to investigate the effect of light wavelength on the kinetics of ATRP. A UV light source emitting at 365 nm with two different light intensities of 3.3 and 4.2 mW cm^{-2} and a visible light LED at 392 nm with the light intensity of 0.14 mW cm^{-2} were used. As shown in Figure 106, the kinetics of the reaction under conditions $[MMA]_0/[EBPA]_0/[Ph\text{-}benzoPTZ]_0$: 100/1/0.1 in 50 v% DMA (EBPA: ethyl α-bromophenylacetate, DMA: *N,N*-dimethylacetamide) followed a linear semilogarithmic plot of monomer consumption vs. irradiation time. As expected from the optical properties of the photocatalyst, the reaction under UV light at 365 nm was faster with respect to visible LED light at 392 nm. The use of a UV lamp with higher light intensity (4.2 mW cm^{-2}) resulted in an even faster reaction. However, the use of the UV light with higher intensity resulted in higher Đ values (1.6-2) whilst irradiation with the weaker UV lamp, or visible LED, resulted in lower Đ values reaching to 1.3.
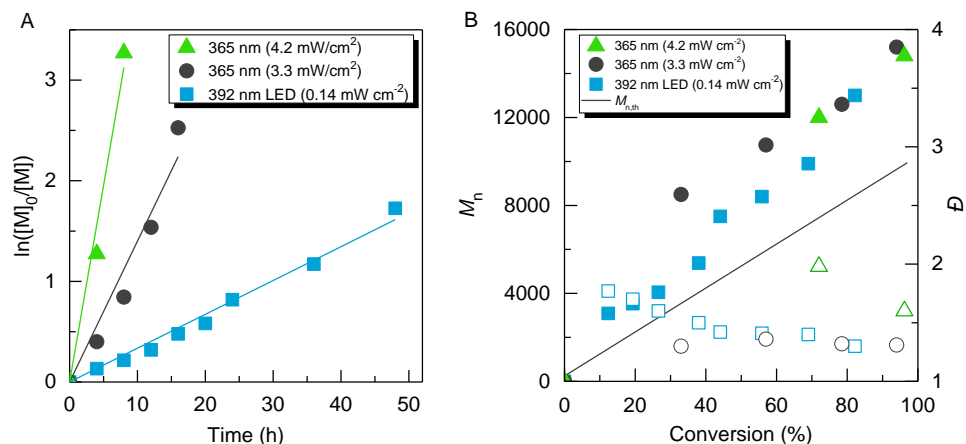
Figure 106. (A) Kinetics and (B) molecular weight properties of PMMA polymerized using Ph-benzoPTZ under various light sources. Reaction conditions: [MMA]0/[EBPA]0/[Ph-benzoPTZ]0 : 100/1/0.1 in 50 v% DMA.

Table 24. Results of photoinduced metal-free ATRP using Ph-benzoPTZ under various reaction conditions

Entry	[MMA]$_0$/[EBPA]$_0$/[Ph-benzoPTZ]$_0$	Light source	Time (h)	Conversion (%) ^{a}	$M_{n,th}$ ^{b}	M_n ^{c}	$Đ$ ^{c}	$I^{* d}$
1	100/1/0.1	365 nm (4.2 mW cm^{-2})	8	96	9843	14800	1.60	0.66
2	100/1/0.1	365 nm (3.3 mW cm^{-2})	16	94	9643	19000	1.31	0.51
3	100/1/0.1	392 nm LED (0.14 mW cm^{-2})	48	82	8443	13000	1.30	0.69
4	100/1/0.05	392 nm LED (0.14 mW cm^{-2})	48	90	9243	14700	1.34	0.63
5	100/1/0.2	392 nm LED (0.14 mW cm^{-2})	24	80	8243	17400	1.39	0.48
6	200/1/0.1	392 nm LED (0.14 mW cm^{-2})	48	71	14443	21700	1.71	0.66
7	50/1/0.1	392 nm LED (0.14 mW cm^{-2})	48	78	4143	7250	1.40	0.57

Control experiments were carried out in order to investigate the effect of various parameters. Loading the photocatalyst at the ratio of $[EBPA]_0/[Ph\text{-}benzoPTZ]_0$: 1/0.1 resulted in 82% monomer conversion after 48 h irradiation under visible light (Entry 3, Table 24) whereas decreasing the catalyst loading by half, to 100/0.05, resulted in a slightly higher conversion (90%) but lower initiation efficiency (Entry 4, Table 24). On the other hand, increasing the concentration of the catalyst by a factor of two accelerated the rate of the reaction, and it reached 80% monomer conversion within 24 h. However, the initiation efficiency was lower compared to the 100/0.1 ratio (Entry 5, Table 24). Targeting a degree of polymerization (DP) of 200 resulted in slightly higher $Đ$ (Entry 6, Table 24) whereas polymerizations targeting DPs of 100 and 50 were well-controlled (Entries 3 and 7, Table 24).

Additionally, several alkyl halide initiators and monomers were examined for photoinduced metal-free ATRP using Ph-benzoPTZ photocatalyst (Scheme 21). The polymerization results are summarized in Table 2. EBPA was the most efficient initiator in terms of initiation efficiency (0.69) and formation of polymers with low dispersity ($Đ$: 1.30). Similarly use of diethyl 2-bromo-2-methylmalonate (DEBMM) resulted in a well-controlled process with low $Đ$ and reaction faster than with EBPA (Entry 4, Table 25). Reactions with methyl α-bromoisobutyrate (MBiB) (Entry 2, Table 25) or ethyl α-bromoisobutyrate (EBiB) (Entry 3, Table 25) were not as well-controlled as they resulted in lower initiation efficiency and high $Đ$ values.

Photoinduced metal-free ATRP using Ph-benzoPTZ was also examined with a range of alkyl methacrylate monomers. The system displayed a good tolerance to various methacrylate monomers including MMA, ethyl methacrylate (EtMA), benzyl methacrylate (BzMA), and n-butyl methacrylate (n-BuMA). Polymers were synthesized in a controlled manner with the initiation efficiency ranging from 0.62-0.85 and low $Đ$.

Initiators:

EBPA　　**MBiB**　　**EBiB**　　**DEBMM**　　**BPN**

- -

Monomers:

MMA　　**EtMA**　　**BzMA**　　***n*-BuMA**
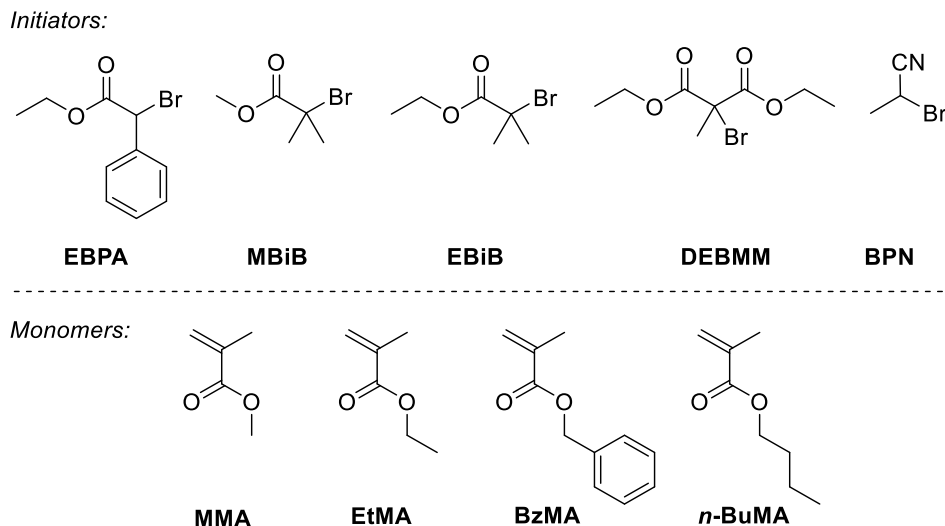
Scheme 21. ATRP initiators and monomers examined in photoinduced metal-free ATRP using Ph-benzoPTZ under visible light LED irradiation.

Table 25. The scope of ATRP initiator and monomer for photoinduced metal-free ATRP using Ph-benzoPTZ photoredox catalyst under 392 nm LED irradiation [a]

Entry	Monomer	Initiator	Time (h)	Conv. (%) [b]	$M_{n,th}$ [c]	M_n [d]	$Đ$ [d]	I^{*} [e]
1	MMA	EBPA	48	82	8443	13000	1.30	0.69
2	MMA	MBiB	36	92	9382	27700	1.69	0.34
3	MMA	EBiB	24	78	7996	45800	1.60	0.18
4	MMA	DEBMM	36	89	9154	13950	1.31	0.66
5	MMA	BPN	36	94	9535	21950	1.43	0.44
6	EtMA	EBPA	48	74	9363	14670	1.46	0.64
7	BzMA	EBPA	36	95	16963	20000	1.48	0.85
8	*n*-BuMA	EBPA	48	81	11754	17800	1.45	0.66

[a] Reaction conditions: $[M]_0/[R\text{-}X]_0/[\text{Ph-benzoPTZ}]_0$: 100/1/0.1 in 50 v% DMA, irradiation under 392 nm LED. b Conversions were calculated by 1H NMR. [c] Theoretical molecular weight ($M_{n,th}$) values were calculated based on conversions obtained by ^{1}H NMR as: $M_{n,th} = M_{R\text{-}X} + [\text{Monomer}]_0/[R\text{-}X]_0 \times \text{conversion} \times M_{Monomer}$. [d] Number-average molecular weight (M_n) and dispersity ($Đ$) were determined by GPC. [e] Initiation efficiency (I^{*}) was calculated by dividing theoretical molecular weight to experimental molecular weight measured by GPC ($M_{n,th}/M_n$).

It was also determined that the growth of polymers can be easily regulated by simply switching the light source on or off. For example, exposing a reaction mixture consisting of ([MMA]$_0$/[EBPA]$_0$/[Ph-benzoPTZ]$_0$: 100/1/0.1 in 50 v% DMA) to LED light resulted in ~20% monomer conversion after 8 h. When the light was then switched off for 8 h no polymer growth was detected during that period. Re-exposing the reaction to the light re-initiated the polymerization resulting in ~40% monomer conversion after the second 8 h illumination. This on/off cycle was repeated several times with the reaction proceeding only during the period light was on and completely stopping when the light was switched off. No conversion was observed during the dark period. Moreover, the growth of polymer chains in the light-on periods followed a linear relationship between the monomer consumption and reaction time, confirming a well-controlled process proceeding only under irradiation. This behavior clearly confirms the capability of temporal control over the system and growth of polymer chains simply by turning light on or off. Figure 107 shows the kinetic results and molecular weight properties of the resulting polymers during the light on/off periods.
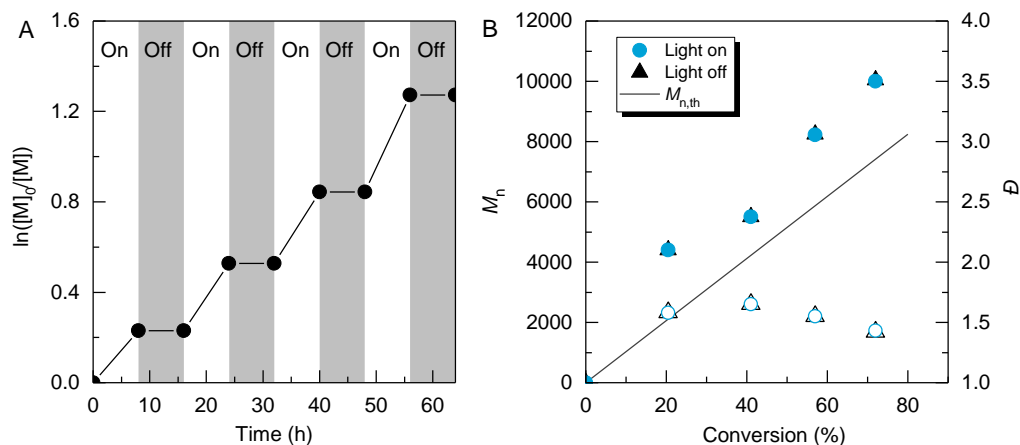
Figure 107. Evidence of temporal control in photoinduced metal-free ATRP using Ph-benzoPTZ under 392 nm LED irradiation through intermittent switching on/off the light: (A) Kinetics and (B) molecular weight and dispersity of polymers. Reaction conditions [MMA]$_0$/[EBPA]$_0$/[Ph-benzoPTZ]$_0$: 100/1/0.1 in 50 v% DMA.

The livingness of the system was also investigated and confirmed retention of chain end functionality for polymers obtained using Ph-benzoPTZ through chain extension processes (Figure 108). Thus, a PMMA macroinitiator was initially synthesized using Ph-benzoPTZ under conditions [MMA]$_0$/[EBPA]$_0$/[Ph-benzoPTZ]$_0$: 100/1/0.1 in 50 v% DMA. The synthesized

macroinitiator with Br chain-end functionality (PMMA-Br; M_n: 11800, Đ: 1.41) was used as initiator in chain extension reactions to form block copolymers in a metal-free chain extension reaction. PMMA-Br was used in the presence of Ph-benzoPTZ to polymerize BzMA under visible light LED. The GPC results, shown in Figure 4, indicate the successful formation of a P(MMA-*b*-BzMA) block copolymer as a clear and unimodal shift towards higher molecular weights was observed in the GPC traces of the polymers without any detectable dead or deactivated chains. Furthermore, the PMMA-Br macroinitiator was examined for a Cu^{II} photoinduced process to grow poly(methyl acrylate) (PMA) segment under reaction conditions [MA]$_0$/[PMMA-Br]$_0$/[CuBr$_2$]$_0$/[Me$_6$TREN]: 400/1/0.03/0.18 in DMSO (Me$_6$TREN: tris[2-(dimethylamino)ethyl]amine and DMSO: dimethyl sulfoxide) under irradiation with UV light at 365 nm. The PMMA-Br macroinitiator was successfully chain extended to form P(MMA-*b*-MA) block copolymers in a controlled manner. The resulting P(MMA-*b*-MA) block copolymers showed a unimodal peak with higher molecular weights and no dead or deactivated chains were observed. These chain extension results confirm the high retention of chain end functionality in the polymers synthesized by photoinduced metal-free ATRP using Ph-benzoPTZ. The formed macroinitiators can be readily used in different polymerization modes to form block copolymers with various functionalities.
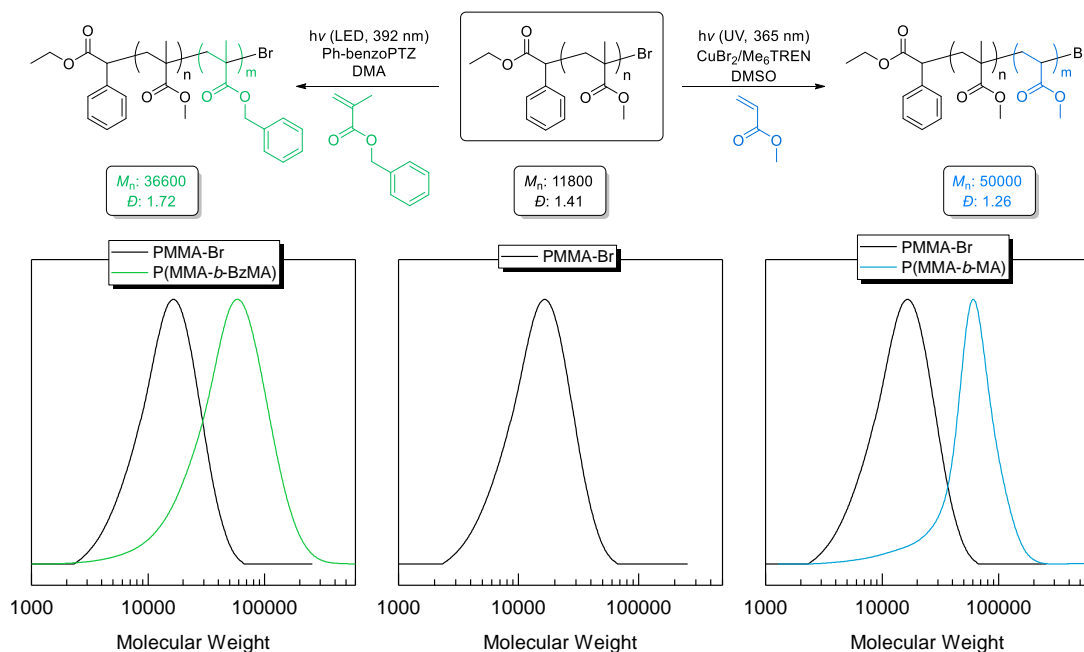
Figure 108. GPC traces of PMMA-Br macroinitiator (middle) synthesized by photoinduced metal-free ATRP using Ph-benzoPTZ (conditions: $[MMA]_0/[EBPA]_0/[Ph\text{-}benzoPTZ]_0$: 100/1/0.1 in 50 v% DMA) and its chain extension to give P(MMA-*b*-BzMA) block copolymer (left) via photoinduced metal-free ATRP (conditions: $[BzMA]_0/[PMMA\text{-}Br]_0/[Ph\text{-}benzoPTZ]_0$: 400/1/0.1 in DMA) and P(MMA-*b*-MA) (right) block copolymer prepared via Cu^{II} photoinduced ATRP (conditions: $[MA]_0/[PMMA\text{-}Br]_0/[CuBr_2]_0/[Me_6TREN]_0$: 400/1/0.03/0.18 in DMSO.

The proposed mechanism of the reaction is presented in Scheme 22 and involves initial photoexcitation of the photocatalyst Ph-benzoPTZ by visible light. In the subsequent activation step, the photoexcited state catalyst (Cat*) is quenched in an oxidative quenching reaction that reduces the alkyl halide initiator to generate initiating radicals while oxidizing the photocatalyst to a radical cation. The radicals can initiate and propagate polymerization before being deactivated by the photocatalyst radical cation and bromine anion which regenerate Br-terminated polymer chains and the initial ground state photocatalyst.
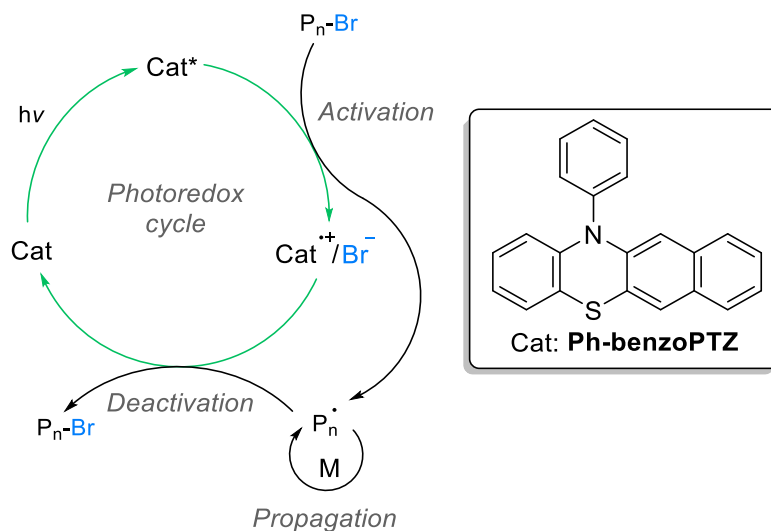
Scheme 22. Proposed mechanism for photoinduced metal-free ATRP using Ph-benzoPTZ photoredox catalyst.

5.5. Conclusions

In conclusion, we have reported results with Ph-benzoPTZ, a visible light photoredox catalyst for metal-free ATRP. Ph-benzoPTZ successfully activated polymerization of various methacrylate monomers using visible light LED illumination and several alkyl halide initiators. Well-defined polymers and block copolymers with low dispersity were synthesized, confirming a well-

controlled photoredox process. Furthermore, the polymerization using Ph-benzoPTZ could also be temporally controlled by switching the light source on/off.

5.6. Experimental Section and Supporting Information

Materials

2-Aminothiophenol (Sigma-Aldrich, 99%), 2,3-Dihydroxynaphthalene (Sigma-Aldrich, 98%), 1,2,4-trichlorobenzene (Sigma-Aldrich, anhydrous, 99%), chlorobenzene (Sigma-Aldrich, anhydrous, 99.8%), RuPhos (2- dcyclohexylphosphino-2',6'-diisopropoxybiphenyl; Sigma-Aldrich, 95%), RuPhos Pd G2 (chloro(2- dicyclohexylphosphino-2',6'-diisopropoxy-1,1'-biphenyl)[2-(2'-amino-1,1'-biphenyl)]- palladium(II); Sigma-Aldrich). Methyl methacrylate (MMA; Sigma-Aldrich, 99%), ethyl methacrylate (EtMA; Sigma-Aldrich, 99%), benzyl methacrylate (BzMA; Alfa Aesar, 98%), *n*-butyl methacrylate (*n*-BuMA; Sigma-Aldrich, 99%), and methyl acrylate (MA; Sigma-Aldrich, 99%) were passed through a basic alumina column to remove inhibitor prior to use. Ethyl 2-bromo-2-phenylacetate (EBPA; Sigma-Aldrich), methyl α-bromoisobutyrate (MBiB; Sigma-Aldrich, 99%), ethyl α-bromoisobutyrate, (EBiB; Sigma-Aldrich, 98%), diethyl 2-bromo-2-methylmalonate (DEBMM; Sigma-Aldrich, 98%), 2-bromopropionitrile (BPN; Sigma-Aldrich, 97%), phenothiazine (PTZ; Sigma-Aldrich, 98%), and tris[2-(dimethylamino)ethyl]amine (Me$_6$TREN; Alfa Aesar, 99%) were used as received. All solvents were purchased from Sigma-Aldrich and used without further purification.

Instrumentation

[1]H nuclear magnetic resonance (NMR) measurements were performed on a Bruker Avance 300 MHz spectrometer.

Gel permeation chromatography (GPC) was used to determine the molecular weight properties of polymers. The GPC system used a Waters 515 HPLC pump and a Waters 515 pump and Wyatt r-Ex differential refractometer using PSS columns (SDV 10^5, 10^3, 500 Å) with THF as eluent at 35 °C and at a flow rate of 1 mL/min. Linear PMMA/PS standards were used for calibration.

UV-vis spectra were recorded using Agilent 8453 spectrophotometer.

A custom-designed photoreactor was used for visible light-induced reactions. A 5 m long 24 W LED strip with 300 diodes (392 nm: superbrightleds.com WFLS-UV300) was mounted inside an 8 inch (203 mm) galvanized steel tube in a spiral pattern. The light intensity was measured as 0.14 mW cm^{-2}. For reactions under UV light, two UV lamps (MelodySusie® UV, www.melodysusie.com) emitting light at 365 with the light intensity of 3.3 or 4.2 mW cm^{-2} were used.

General procedure for synthesis of Ph-benzoPTZ [1]

Synthesis of benzo[b]phenothiazine
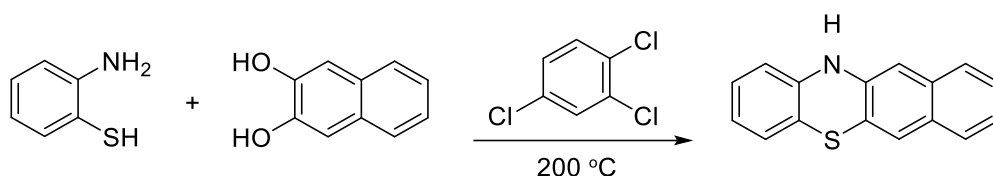
A mixture of 2,3-dihydroxynaphthalene (8 g, 0.05 mol), 2- aminothiophenol (6.25 g, 0.05 mol) and 25 mL of 1,2,4-trichlorobenzene (b.p. 215 °C) were placed in a 50 mL round bottom flask fitted with a magnetic stirrer and a vapor trap. The reaction mixture was heated to 200 °C using a sand bath and maintained at that temperature for 6 h. During that time, water was formed and collected in the trap. On cooling, the product crystallized from the reaction mixture. The product mixture was diluted with n-hexane and the yellow crystalline benzo[b]phenothiazine was collected by filtration and washed with fresh n-hexane and then ethanol. The product benzo[b]phenothiazine was obtained as yellow powder: [1] H NMR (300 MHz, CDCl₃) δ: 7.54 (2H, t, J = 8.4 Hz), 7.45 (1 H, s), 7.34-7.19 (2H, m), 7.03 (2H, t, J = 7.5 Hz), 6.87-6.80 (2H, m), 6.61 (1H, d, J = 7.8 Hz), 6.09 (1H, br s) ppm.

Synthesis of phenyl-benzo[b]phenothiazine
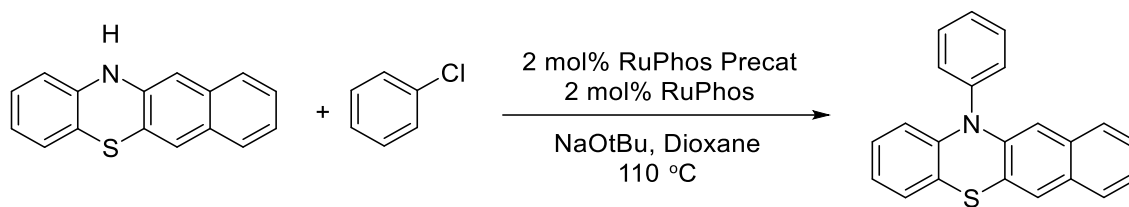
NaOtBu (268 mg, 2.8 mmol), benzo[*b*]phenothiazine (498 mg, 2 mmol), RuPhos Precat (28 mg, 0.04 mmol, 2 mol %), and RuPhos (16 mg, 0.04 mmol, 2 mol %) were added to a round bottom flask fitted with a magnetic stir bar. The vial was evacuated and backfilled with nitrogen gas three times before adding dry dioxane (2 mL) and then anhydrous chlorobenzene (286 µL, 2.8 mmol). The vial was then placed in an oil bath at 110 °C and stirred for 6 h. The vial was then cooled to room temperature, diluted with CH_2Cl_2 and the solution washed with water, brine, dried with Mg_2SO_4, and purified using column chromatography. After chromatography, the product was obtained as a yellow solid: ^{1}H NMR (300 MHz, CDCl$_3$) δ: 7.68 (2H, t, J = 7.5 Hz), 7.59-7.52 (2H, m), 7.47-7.44 (2H, m), 7.37-7.31 (2H, m), 7.22-7.19 (2H, m), 7.07 (1H, dd, J = 7.2, 1.7 Hz), 6.90-6.78 (2H, m), 6.38 (1H, s), 6.21-6.18 (1H, m) ppm.

General procedure for photoinduced metal-free ATRP

Into a 10 mL Schlenck flask MMA (2 mL, 18.72 mmol) EBPA (32.7 µL, 0.1872 mmol), Ph-benzoPTZ (6.1 mg, 0.1872 mmol) and DMA (2 mL) were added. The flask was sealed and subjected to a three freeze-pump-thaw cycles to remove oxygen before being filled back by nitrogen. The reaction mixture was then irradiated under visible light LED at 392 nm. Samples were taken periodically by a degassed syringe to calculate monomer conversion by ^{1}H NMR and molecular weight properties of the resulting polymers by GPC.

Chain Extension Experiments

Synthesis of PMMA-Br macroinitiator by metal-free ATRP

A 10 mL Schlenck flask was charged with MMA (2 mL, 18.72 mmol), EBPA (32.7 µL, 0.1872 mmol), Ph-benzoPTZ (6.1 mg, 0.1872 mmol) and DMA (2 mL). The flask was sealed and subjected to a three freeze-pump-thaw cycles to remove oxygen before being filled back by nitrogen. The reaction mixture was then irradiated under visible light LED at 392 nm. The reaction was stopped and the polymer mixture was precipitated into excess methanol to yield white PMMA-Br. The resulted polymer was analyzed by ^{1}H NMR (Figure S1) and GPC. M_n: 11800, Đ: 1.41.
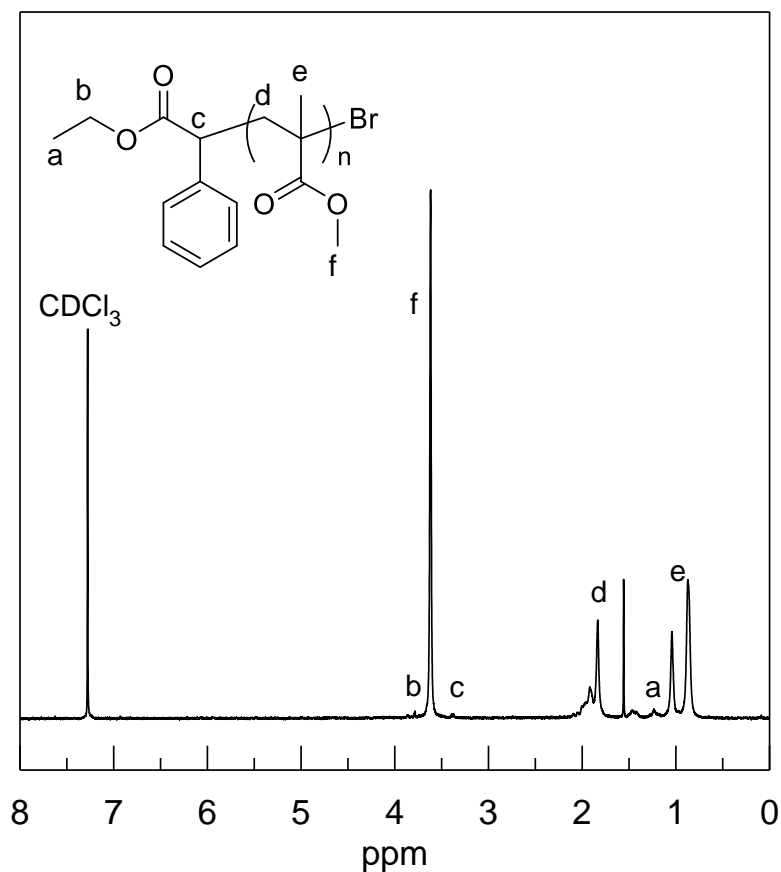
Figure 109. ^{1}H NMR spectra of PMMA macroinitiator synthesized by photoinduced metal-free ATRP using Ph-benzoPTZ

Metal-free chain extension

In a 10 mL Schlenk flask PMMA-Br (200 mg, 0.017 mmol) was dissolved in 2 mL DMA and BzMA (1.15 mL, 6.8 mmol) and Ph-benzoPTZ (0.6 mg, 0.0017 mmol) were added. The flask was sealed and purged of oxygen by subjecting to a three freeze-pump-thaw cycles followed by filling with nitrogen. The reaction was irradiated under 392 nm LED illumination for 24 h and was analyzed by GPC and NMR (Figure S2). M_n: 36600, Đ: 1.72.
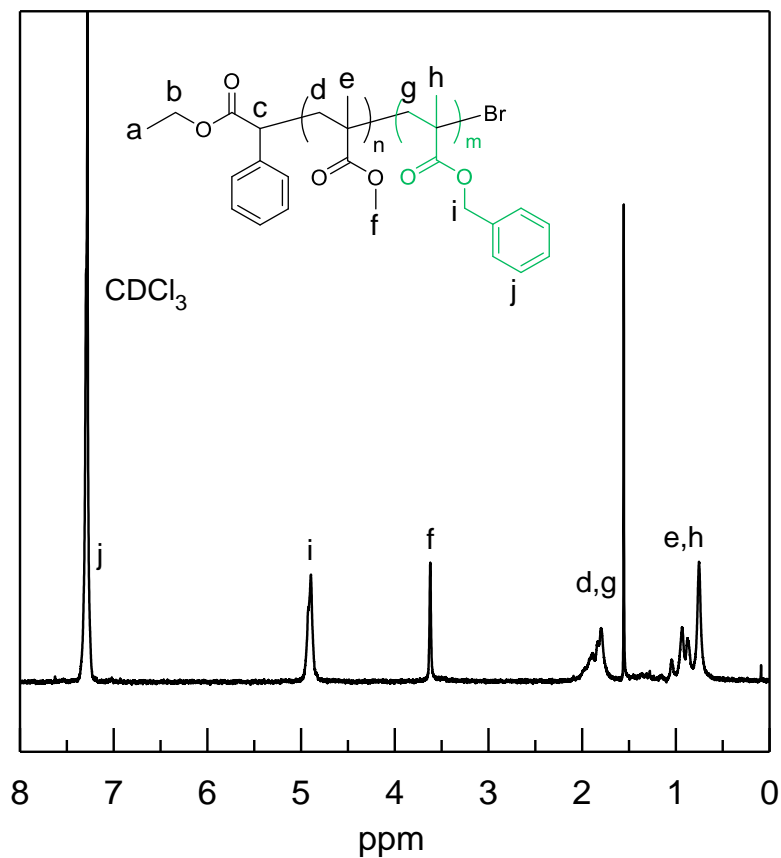
Figure 110. ^{1}H NMR spectra of P(MMA-*b*-BzMA) macroinitiator synthesized by photoinduced metal-free ATRP using Ph-benzoPTZ

Cu^{II} photoinduced chain extension

In a 10 mL Schlenk flask PMMA-Br (200 mg, 0.017 mmol) was dissolved in 4 mL DMSO and MA (0.612 mL, 6.75 mmol), CuBr$_2$ (0.12 mg, 0.00051 mmol), and Me$_6$TREN (0.85 µL, 0.00318 mmol) were added. The flask was sealed and purged of oxygen by subjecting to a three freeze-pump-thaw cycles followed by filling with nitrogen. The reaction was irradiated under a UV lamp (365 nm, 2.1 mW cm^{-2}) and after 1 h irradiation the resulting polymer was analyzed by GPC and NMR (Figure S3). *M*$_n$: 50000, *Đ*: 1.26.
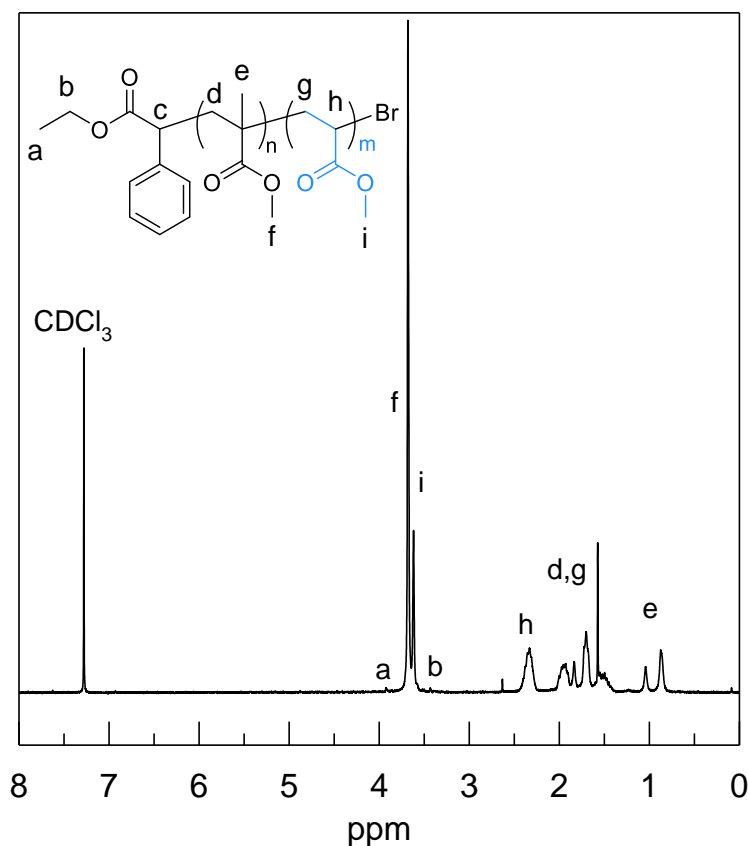
Figure 111. ^{1}H NMR spectra of P(MMA-*b*-MA) macroinitiator synthesized by Cu[II] photoinduced ATRP using CuBr$_2$/Me$_6$TREN.

5.6.1 Reference

1. Dadashi-Silab, S.; Pan, X.; Matyjaszewski, K. Photoinduced Iron-Catalyzed Atom Transfer Radical Polymerization with ppm Levels of Iron Catalyst under Blue Light Irradiation. *Macromolecules* **2017,** 50 (20), 7967-7977.

2. Dadashi-Silab, S.; Matyjaszewski, K. Temporal Control in Atom Transfer Radical Polymerization Using Zerovalent Metals. *Macromolecules* **2018,** 51 (11), 4250-4258.

3. Discekici, E. H.; Anastasaki, A.; Kaminker, R.; Willenbacher, J.; Truong, N. P.; Fleischmann, C.; Oschmann, B.; Lunn, D. J.; Read de Alaniz, J.; Davis, T. P.; Bates, C. M.; Hawker, C. J. Light-Mediated Atom Transfer Radical Polymerization of Semi-Fluorinated (Meth)acrylates: Facile Access to Functional Materials. *J. Am. Chem. Soc.* **2017,** 139 (16), 5939-5945.

4. Zivic, N.; Bouzrati-Zerelli, M.; Kermagoret, A.; Dumur, F.; Fouassier, J. P.; Gigmes, D.; Lalevee, J. Photocatalysts in Polymerization Reactions. *Chemcatchem* **2016,** 8 (9), 1617-1631.

5. Chen, M.; Zhong, M. J.; Johnson, J. A. Light-Controlled Radical Polymerization: Mechanisms, Methods, and Applications. *Chem. Rev.* **2016,** 116 (17), 10167-10211.

6. Corrigan, N.; Shanmugam, S.; Xu, J.; Boyer, C. Photocatalysis in organic and polymer synthesis. *Chem. Soc. Rev.* **2016,** 45 (22), 6165-6212.

7. Xiao, P.; Zhang, J.; Dumur, F.; Tehfe, M. A.; Morlet-Savary, F.; Graff, B.; Gigmes, D.; Fouassier, J. P.; Lalevee, J. Visible light sensitive photoinitiating systems: Recent progress in cationic and radical photopolymerization reactions under soft conditions. *Prog. Polym. Sci.* **2015,** 41, 32-66.

8. Yoon, T. P.; Ischay, M. A.; Du, J. Visible light photocatalysis as a greener approach to photochemical synthesis. *Nat. Chem.* **2010,** 2 (7), 527-532.

9. Wang, J. S.; Matyjaszewski, K. Controlled Living Radical Polymerization - Atom-Transfer Radical Polymerization in the Presence of Transition-Metal Complexes. *J. Am. Chem. Soc.* **1995,** 117 (20), 5614-5615.

10. Kato, M.; Kamigaito, M.; Sawamoto, M.; Higashimura, T. POLYMERIZATION OF METHYL-METHACRYLATE WITH THE CARBON-TETRACHLORIDE DICHLOROTRIS(TRIPHENYLPHOSPHINE)RUTHENIUM(II) METHYLALUMINUM BIS(2,6-DI-TERT-BUTYLPHENOXIDE) INITIATING SYSTEM - POSSIBILITY OF LIVING RADICAL POLYMERIZATION. *Macromolecules* **1995,** 28 (5), 1721-1723.

11. Matyjaszewski, K.; Xia, J. H. Atom transfer radical polymerization. *Chem. Rev.* **2001,** 101 (9), 2921-2990.

12. Hawker, C. J.; Bosman, A. W.; Harth, E. New polymer synthesis by nitroxide mediated living radical polymerizations. *Chem. Rev.* **2001,** 101 (12), 3661-3688.

13. Moad, G.; Rizzardo, E.; Thang, S. H. Living Radical Polymerization by the RAFT Process - A Third Update. *Aust. J. Chem.* **2012,** 65 (8), 985-1076.

14. Nicolas, J.; Guillaneuf, Y.; Lefay, C.; Bertin, D.; Gigmes, D.; Charleux, B. Nitroxide-mediated polymerization. *Prog. Polym. Sci.* **2013,** 38 (1), 63-235.

15. Tebben, L.; Studer, A. Nitroxides: Applications in Synthesis and in Polymer Chemistry. *Angew. Chem. Int. Ed.* **2011,** 50 (22), 5034-5068.

16. Jakubowski, W.; Min, K.; Matyjaszewski, K. Activators regenerated by electron transfer for atom transfer radical polymerization of styrene. *Macromolecules* **2006,** 39 (1), 39-45.

17. Min, K.; Gao, H. F.; Matyjaszewski, K. Preparation of homopolymers and block copolymers in miniemulsion by ATRP using activators generated by electron transfer (AGET). *J. Am. Chem. Soc.* **2005,** 127 (11), 3825-3830.

18. Jakubowski, W.; Matyjaszewski, K. Activators regenerated by electron transfer for atom-transfer radical polymerization of (meth)acrylates and related block copolymers. *Angew. Chem. Int. Ed.* **2006,** 45 (27), 4482-4486.

19. Matyjaszewski, K.; Coca, S.; Gaynor, S. G.; Wei, M. L.; Woodworth, B. E. Zerovalent metals in controlled "living" radical polymerization. *Macromolecules* **1997,** 30 (23), 7348-7350.

20. Anastasaki, A.; Nikolaou, V.; Nurumbetov, G.; Wilson, P.; Kempe, K.; Quinn, J. F.; Davis, T. P.; Whittaker, M. R.; Haddleton, D. M. Cu(0)-Mediated Living Radical Polymerization: A Versatile Tool for Materials Synthesis. *Chem. Rev.* **2016,** 116 (3), 835-877.

21. Konkolewicz, D.; Wang, Y.; Zhong, M. J.; Krys, P.; Isse, A. A.; Gennaro, A.; Matyjaszewski, K. Reversible-Deactivation Radical Polymerization in the Presence of Metallic Copper. A Critical Assessment of the SARA ATRP and SET-LRP Mechanisms. *Macromolecules* **2013,** 46 (22), 8749-8772.

22. Konkolewicz, D.; Krys, P.; Gois, J. R.; Mendonca, P. V.; Zhong, M. J.; Wang, Y.; Gennaro, A.; Isse, A. A.; Fantin, M.; Matyjaszewski, K. Aqueous RDRP in the Presence of Cu-0: The Exceptional Activity of Cu-I Confirms the SARA ATRP Mechanism. *Macromolecules* **2014,** 47 (2), 560-570.

23. Boyer, C.; Corrigan, N. A.; Jung, K.; Nguyen, D.; Nguyen, T. K.; Adnan, N. N. M.; Oliver, S.; Shanmugam, S.; Yeow, J. Copper-Mediated Living Radical Polymerization (Atom Transfer Radical Polymerization and Copper(0) Mediated Polymerization): From Fundamentals to Bioapplications. *Chem. Rev.* **2016,** 116 (4), 1803-1949.

24. Matyjaszewski, K.; Jakubowski, W.; Min, K.; Tang, W.; Huang, J. Y.; Braunecker, W. A.; Tsarevsky, N. V. Diminishing catalyst concentration in atom transfer radical polymerization with reducing agents. *Proc. Natl. Acad. Sci. U.S.A.* **2006,** 103 (42), 15309-15314.

25. Konkolewicz, D.; Magenau, A. J. D.; Averick, S. E.; Simakova, A.; He, H. K.; Matyjaszewski, K. ICAR ATRP with ppm Cu Catalyst in Water. *Macromolecules* **2012,** 45 (11), 4461-4468.

26. Magenau, A. J. D.; Strandwitz, N. C.; Gennaro, A.; Matyjaszewski, K. Electrochemically Mediated Atom Transfer Radical Polymerization. *Science* **2011,** 332 (6025), 81-84.

27. Magenau, A. J. D.; Bortolamei, N.; Frick, E.; Park, S.; Gennaro, A.; Matyjaszewski, K. Investigation of Electrochemically Mediated Atom Transfer Radical Polymerization. *Macromolecules* **2013,** 46 (11), 4346-4353.

28. Park, S.; Chmielarz, P.; Gennaro, A.; Matyjaszewski, K. Simplified Electrochemically Mediated Atom Transfer Radical Polymerization using a Sacrificial Anode. *Angew. Chem. Int. Ed.* **2015,** 54 (8), 2388-2392.

29. Konkolewicz, D.; Schroeder, K.; Buback, J.; Bernhard, S.; Matyjaszewski, K. Visible Light and Sunlight Photoinduced ATRP with ppm of Cu Catalyst. *ACS Macro Lett.* **2012,** 1 (10), 1219-1223.

30. Ribelli, T. G.; Konkolewicz, D.; Bernhard, S.; Matyjaszewski, K. How are Radicals (Re)Generated in Photochemical ATRP? *J. Am. Chem. Soc.* **2014,** 136 (38), 13303-13312.

31. Dadashi-Silab, S.; Tasdelen, M. A.; Yagci, Y. Photoinitiated Atom Transfer Radical Polymerization: Current Status and Future Perspectives. *J. Polym. Sci., Part A: Polym. Chem.* **2014,** 52 (20), 2878-2888.

32. Tasdelen, M. A.; Uygun, M.; Yagci, Y. Photoinduced Controlled Radical Polymerization in Methanol. *Macromol. Chem. Phys.* **2010,** 211 (21), 2271-2275.

33. Pan, X.; Malhotra, N.; Simakova, A.; Wang, Z. Y.; Konkolewicz, D.; Matyjaszewski, K. Photoinduced Atom Transfer Radical Polymerization with ppm-Level Cu Catalyst by Visible Light in Aqueous Media. *J. Am. Chem. Soc.* **2015,** 137 (49), 15430-15433.

34. Yang, Q. Z.; Dumur, F.; Morlet-Savary, F.; Poly, J.; Lalevee, J. Photocatalyzed Cu-Based ATRP Involving an Oxidative Quenching Mechanism under Visible Light. *Macromolecules* **2015,** 48 (7), 1972-1980.

35. Leibfarth, F. A.; Mattson, K. M.; Fors, B. P.; Collins, H. A.; Hawker, C. J. External regulation of controlled polymerizations. *Angew. Chem. Int. Ed.* **2013,** 52 (1), 199-210.

36. Treat, N. J.; Fors, B. P.; Kramer, J. W.; Christianson, M.; Chiu, C.-Y.; Alaniz, J. R. d.; Hawker, C. J. Controlled Radical Polymerization of Acrylates Regulated by Visible Light. *ACS Macro Lett.* **2014,** 3 (6), 580-584.

37. Poelma, J. E.; Fors, B. P.; Meyers, G. F.; Kramer, J. W.; Hawker, C. J. Fabrication of Complex Three-Dimensional Polymer Brush Nanostructures through Light-Mediated Living Radical Polymerization. *Angew. Chem. Int. Ed.* **2013,** 52 (27), 6844-6848.

38. Fors, B. P.; Hawker, C. J. Control of a Living Radical Polymerization of Methacrylates by Light. *Angew. Chem. Int. Ed.* **2012,** 51 (35), 8850-8853.

39. Xu, J. T.; Jung, K.; Atme, A.; Shanmugam, S.; Boyer, C. A Robust and Versatile Photoinduced Living Polymerization of Conjugated and Unconjugated Monomers and Its Oxygen Tolerance. *J. Am. Chem. Soc.* **2014,** 136 (14), 5508-5519.

40. McKenzie, T. G.; Fu, Q.; Uchiyama, M.; Satoh, K.; Xu, J. T.; Boyer, C.; Kamigaito, M.; Qiao, G. G. Beyond Traditional RAFT: Alternative Activation of Thiocarbonylthio Compounds for Controlled Polymerization. *Advanced Science* **2016,** 3 (9), 9.

41. Shanmugam, S.; Boyer, C. Stereo-, Temporal and Chemical Control through Photoactivation of Living Radical Polymerization: Synthesis of Block and Gradient Copolymers. *J. Am. Chem. Soc.* **2015,** 137 (31), 9988-9999.

42. Pan, X.; Fang, C.; Fantin, M.; Malhotra, N.; So, W. Y.; Peteanu, L. A.; Isse, A. A.; Gennaro, A.; Liu, P.; Matyjaszewskit, K. Mechanism of Photoinduced Metal-Free Atom Transfer Radical Polymerization: Experimental and Computational Studies. *J. Am. Chem. Soc.* **2016,** 138 (7), 2411-2425.

43. Treat, N. J.; Sprafke, H.; Kramer, J. W.; Clark, P. G.; Barton, B. E.; Read de Alaniz, J.; Fors, B. P.; Hawker, C. J. Metal-Free Atom Transfer Radical Polymerization. *J. Am. Chem. Soc.* **2014,** 136 (45), 16096-16101.

44. Pan, X.; Lamson, M.; Yan, J.; Matyjaszewski, K. Photoinduced Metal-Free Atom Transfer Radical Polymerization of Acrylonitrile. *ACS Macro Lett.* **2015,** 4 (2), 192-196.

45. Wang, J.; Yuan, L.; Wang, Z.; Rahman, M. A.; Huang, Y.; Zhu, T.; Wang, R.; Cheng, J.; Wang, C.; Chu, F.; Tang, C. Photoinduced Metal-Free Atom Transfer Radical Polymerization of Biomass-Based Monomers. *Macromolecules* **2016,** 49 (20), 7709-7717.

46. Jockusch, S.; Yagci, Y. The active role of excited states of phenothiazines in photoinduced metal free atom transfer radical polymerization: singlet or triplet excited states? *Polym. Chem.* **2016,** 7 (39), 6039-6043.

47. Yan, J.; Pan, X.; Schmitt, M.; Wang, Z. Y.; Bockstaller, M. R.; Matyjaszewski, K. Enhancing Initiation Efficiency in Metal-Free Surface-Initiated Atom Transfer Radical Polymerization (SI-ATRP). *ACS Macro Lett.* **2016,** 5 (6), 661-665.

48. Discekici, E. H.; Pester, C. W.; Treat, N. J.; Lawrence, I.; Mattson, K. M.; Narupai, B.; Toumayan, E. P.; Luo, Y. D.; McGrath, A. J.; Clark, P. G.; de Alaniz, J. R.; Hawker, C. J. Simple Benchtop Approach to Polymer Brush Nanostructures Using Visible-Light-Mediated Metal-Free Atom Transfer Radical Polymerization. *ACS Macro Lett.* **2016,** 5 (2), 258-262.

49. Theriot, J. C.; Lim, C. H.; Yang, H.; Ryan, M. D.; Musgrave, C. B.; Miyake, G. M. Organocatalyzed atom transfer radical polymerization driven by visible light. *Science* **2016,** 352 (6289), 1082-1086.

50. Pearson, R. M.; Lim, C. H.; McCarthy, B. G.; Musgrave, C. B.; Miyake, G. M. Organocatalyzed Atom Transfer Radical Polymerization Using N-Aryl Phenoxazines as Photoredox Catalysts. *J. Am. Chem. Soc.* **2016,** 138 (35), 11399-11407.

51. Miyake, G. M.; Theriot, J. C. Perylene as an Organic Photocatalyst for the Radical Polymerization of Functionalized Vinyl Monomers through Oxidative Quenching with Alkyl Bromides and Visible Light. *Macromolecules* **2014,** 47 (23), 8255-8261.

52. Allushi, A.; Jockusch, S.; Yilmaz, G.; Yagci, Y. Photoinitiated Metal-Free Controlled/Living Radical Polymerization Using Polynuclear Aromatic Hydrocarbons. *Macromolecules* **2016,** 49 (20), 7785-7792.

Chapter 6. Iodine-Mediated PhotoATRP in Aqueous Media with Oxygen Tolerance

6.1. Preface

This chapter investigated a new class of ATRP catalysts by employing iodine-mediated photoinduced polymerization in aqueous media. The choice of water as a reaction medium enabled fast and well-controlled polymerizations where control was poor in polymerizations conducted in bulk or in DMF as an organic solvent. The alkyl iodide initiator was generated ni situ by a halogen exchange reaction. Iodide salts were used as the catalyst which were readily soluble in water without requiring additional solubilizing agents. The polymerizations were conducted under a wide range of visible light irradiation (blue, green, or yellow LEDs) to gain temporal control over the growth of polymer chains. Importantly, we showed that well-controlled polymerizations could be achieved in the presence of residual oxygen without performing conventional deoxygenation processes. These results further signified the potential of this system for use in new emerging applications.

I designed and carried out the polymerization experiments with help from my collaborators Dr. Greg Szczepaniak and Dr. Sushil Lathwal under the guidance of Prof. Matyjaszewski.

———————————————————

6.2. Abstract

Water is an environmentally friendly medium for conducting reversible deactivation radical polymerizations. In this paper, we report the investigation of iodine-mediated photocontrolled atom transfer radical polymerization (photoATRP) in aqueous media. The iodine-based initiator was generated by an in situ halogen exchange from a commercially available bromine-based initiator, ethyl α-bromophenylacetate, using different iodide salts. Fast and well-controlled polymerization of a water-soluble methacrylate monomer was achieved in water under visible light irradiation, including blue, green and yellow lights. The nature of the reaction medium greatly affected the kinetics and control over the growth of polymers. Polymerizations in water resulted in a well-controlled reaction that provided high monomer conversion and polymers with low dispersities, whereas control over the polymerization was poor in bulk or in an organic solvent, *N,N*-dimethylformamide. Polymerizations were performed over a wide range of visible light in the absence of any photocatalyst. The selection of water as a reaction medium enabled use of iodide salts without the need for solubilizing agents. Moreover, iodine-mediated photoATRP was successfully performed in the presence of residual oxygen, signifying the potential of this polymerization system to tolerate oxygen without performing deoxygenation processes.
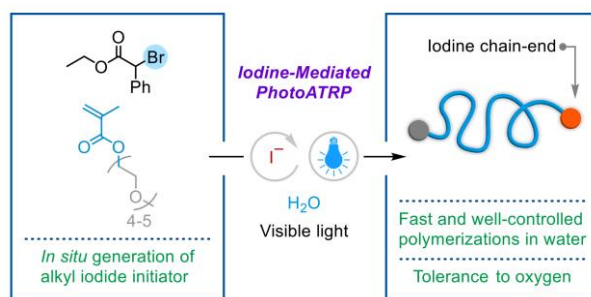
6.3. Introduction

Atom transfer radical polymerization (ATRP) is a widely used procedure for synthesizing well-defined polymers.[1, 2] In ATRP, control over the polymerization is based upon a reversible redox process using catalysts that can efficiently sustain activation and deactivation of polymer chain ends.[3-5] In this regard, copper complexes are one of the most efficient and widely used ATRP catalysts with L/Cu^I and L/Cu^{II}-X (X: Br or Cl) species being the activator and deactivator, respectively.[6-8] In addition, other transition metal-based catalysts such as iron,[9, 10] ruthenium,[11]

302

iridium[12] and also organic photoredox catalysts[11, 13, 14] are capable of catalyzing ATRP with high efficiency.[15]

In ATRP reactions, the bond dissociation energy of the carbon-halogen chain ends and affinity of the halogen atom to the catalyst are important criteria for efficient atom transfer processes to succeed. As a result, Br and Cl chain end functionalities are effective in affording well-controlled polymers in the presence of atom transfer catalysts, whereas F chain ends are not suitable due to the high energy required to cleave the C-F bonds.[16] Interestingly, C-I bonds are weaker and therefore can be cleaved easily. However, previous reports have shown low affinity of the I atom to Cu catalysts rendering inefficient ATRP catalysis in the presence of alkyl iodides.[14]

Iodine-based polymerizations typically occur via a degenerative transfer process in the presence of iodinated chain transfer agents.[17-23] The transfer and dynamic exchange of iodine between propagating radicals and dormant species affords moderate control over polymerization. However, in the presence of compounds such as amines or iodide salts that form complexes with alkyl iodides, the polymerization becomes catalytic undergoing a similar mechanism to ATRP (also referred as reversible complexation mediated polymerization, RCMP[24]) to catalyze iodine atom transfer, and consequently improves control over polymer chains.

Alkyl iodides are generally light/heat sensitive compounds that require special care for storage and handling. However, for iodine-mediated ATRP reactions, alkyl iodide initiators can be generated *in situ* from more stable alkyl bromides using iodide salts.[25] Indeed, the light sensitivity of alkyl iodides can be advantageous for developing photocontrolled iodine-mediated polymerization strategies. Scheme 23 illustrates the general mechanism of iodine-mediated photoATRP via *in situ* generation of the alkyl iodide initiator. In the presence of iodide salts that also act as a catalyst, the C-I bond can be photochemically cleaved to form initiating/propagating radicals and also generating an iodine-based radical.[26-29] The iodine radical complexes with an iodide anion to form an iodine radical anion ($I_2^{\bullet-}$) species, which serve as deactivators for propagating radicals. Furthermore, in an iodine-based polymerization, a degenerative transfer process may also be involved between the growing radicals and iodine-capped dormant species to impart control over the growth of polymer chains.
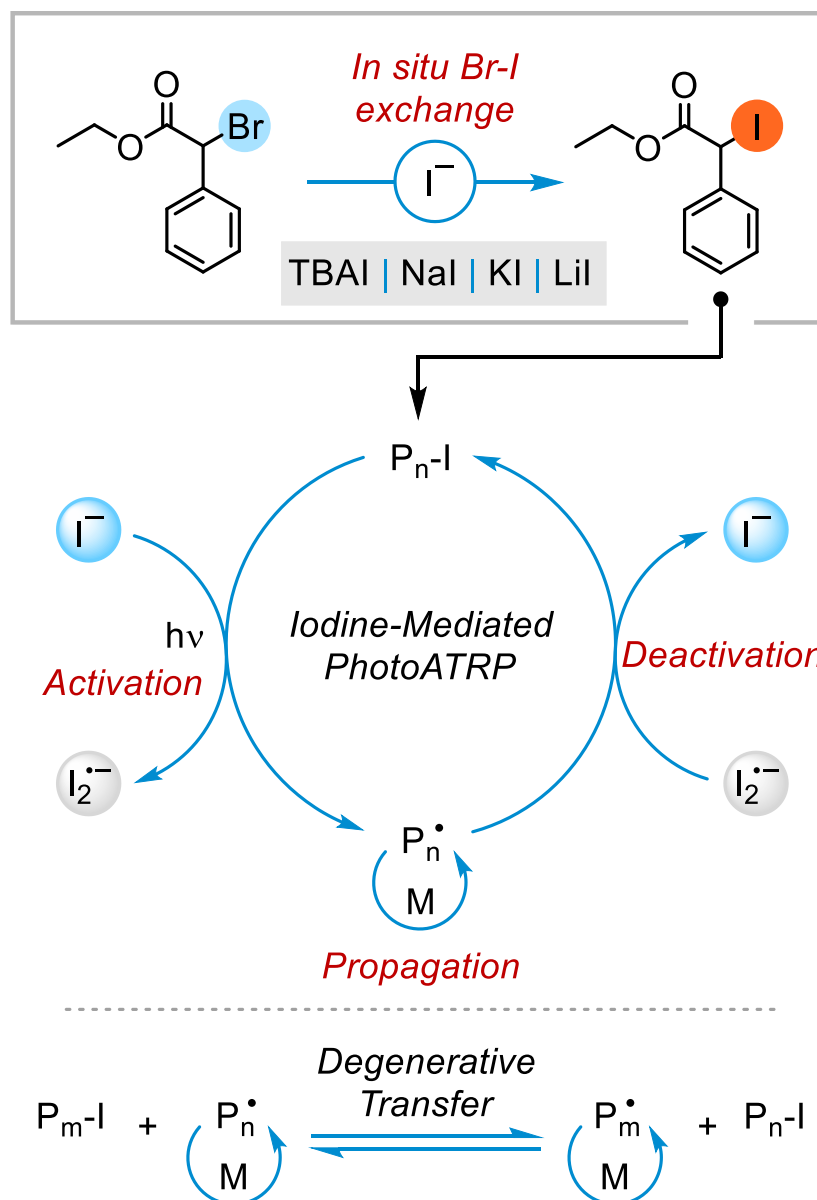
Scheme 23. Mechanism of iodine-mediated photoATRP by in situ generation of the alkyl iodide initiator using iodide salts as the catalyst.

Water is considered a green solvent for polymerizations and is compatible with different reversible-deactivation radical polymerizations (RDRP) including ATRP, RAFT and other techniques.[30-33] However, iodine-mediated polymerizations have not been fully investigated in aqueous media. Moreover, RDRP methods have been recently advanced to enable well-controlled polymerizations in the presence of oxygen.[34] Indeed, oxygen can be consumed *in situ* by applying various (photo)chemical techniques without the need for performing conventional

deoxygenation processes, thereby simplifying the synthesis of polymers with potential utility for new applications.[35-40]

In this paper, iodine-mediated photoATRP was investigated in aqueous media, which enabled fast and well-controlled polymerizations that were also tolerant to residual oxygen without the need for degassing procedures. The alkyl iodide initiator was generated *in situ* by an exchange reaction of Br to I using ethyl α-bromophenylacetate (EBPA) and various iodide salts, which also acted as the catalyst for the polymerization. Polymerizations were conducted under a wide range of visible light as external stimuli enabling temporal control over the polymerization.

6.4. Results and Discussion

Iodine-mediated photoATRP was initially attempted using poly(ethylene glycol) methyl ether methacrylate (average M_n 300, $PEGMA_{300}$) as a water-soluble monomer and ethyl EBPA under blue light irradiation in water (Scheme 24). Tetrabutylammonium iodide (TBAI) was used to generate alkyl iodide initiator by exchanging EBPA's Br to I. Table 26 shows the results of the polymerization of $PEGMA_{300}$ and the effect of concentration of different components involved on the polymerization. High monomer conversion was achieved in less than 2 h under blue light irradiation. Increasing the concentration of TBAI resulted in a well-controlled process providing polymers with low dispersity ($Đ$) values. For example, in the presence of 1 equiv. of TBAI with respect to EBPA, the polymerization of $PEGMA_{300}$ reached high monomer conversion showing molecular weights close to theoretical values, but with a high $Đ$ of 1.88. However, increasing concentration of TBAI to 2 equiv., with respect to initiator, improved control over the polymerization and provided polymers with $Đ$ of 1.43 (Entries 1 and 2, Table 26). These observations suggest that in the presence of high concentration of the iodide salt control over the polymerization was achieved mainly through an ATRP mechanism with iodide salts acting as the catalysts under photochemical conditions. In the absence of excess iodide salts, control may be attributed predominately to a degenerative mechanism.
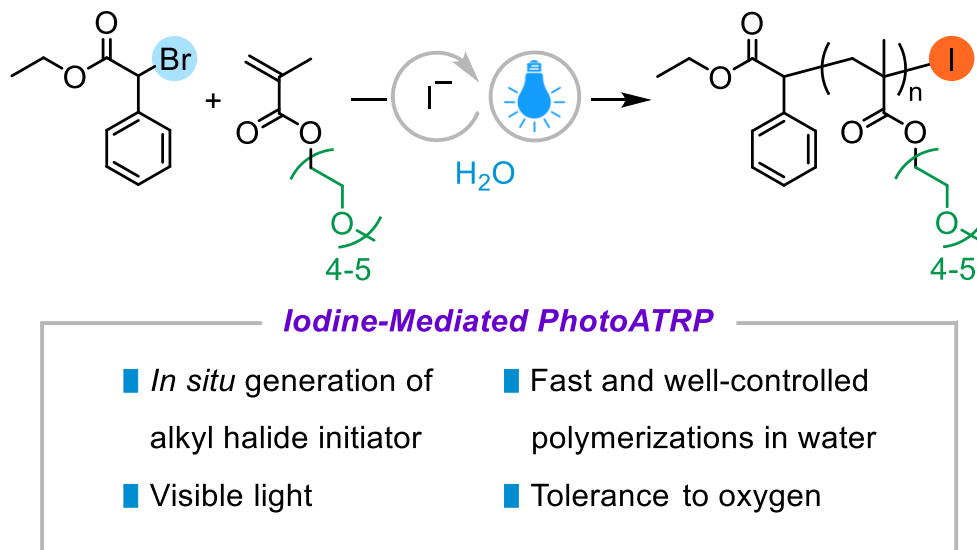
Scheme 24. Iodine-mediated photoATRP of PEGMA$_{300}$ monomer in water by *in situ* generation of the alkyl iodide initiator under visible light irradiation.

Table 26.   Results of iodine-mediated photoATRP in water ^{a}

Entry	[PEGMA$_{300}$]/[EB PA]/[I$^-$]	Iodide salt	[PEGMA$_{300}$] (vol %)	Time (h)	Conv. (%)	$M_{n,th}$	M_n	Đ
1	100/1/1	TBAI	50	2	91	27400	29900	1.88
2	100/1/2	TBAI	50	2	91	27400	30000	1.43
3	100/1/2	TBAI	33	2	90	27200	27000	1.34
4	100/1/2	TBAI	25	2	83	25100	26600	1.24
5	100/1/4	TBAI	25	2	84	25500	26800	1.18
6	100/1/4	KI	50	2	89	27000	27700	1.35
7	50/1/4	KI	50	2	94	14400	14900	1.26
8	100/1/4	NaI	25	2	83	24800	22900	1.24
9	100/1/4	LiI	25	2	84	25000	24000	1.24
10	100/0/4	TBAI	25	24	0	-	-	-
11	100/1/0	-	25	24	0	-	-	-
12	100/1/4 – in dark	TBAI	25	24	0	-	-	-

^{a} Reactions were irradiated under blue light LEDs ($\lambda_{max} = 460$ nm, 12 mW/cm^2).

Furthermore, under more dilute conditions, the rate of polymerization slightly decreased but resulted in well-controlled polymers, showing lower Đ values. For instance, in the presence of 2 equiv. of TBAI with respect to initiator, decreasing concentration of the monomer from 50 to 33

and 25 vol % in water resulted in decreasing $Đ$ from 1.43 to 1.34 and 1.24, respectively (Entries 2-4, Table 26). In the presence of 4 equiv. of TBAI and 25 vol % monomer, the polymerization was well-controlled giving low dispersity $Đ$ = 1.18 (Entry 5, Table 26). Importantly, in all these polymerizations experimental molecular weights agreed well with theoretical values, indicating high initiation efficiency. In addition, alkali metal iodide salts including potassium, sodium and lithium iodides were also used to perform and efficiently control the polymerization of PEGMA$_{300}$ in water (Entries 6-9, Table 26 and Figure 119-Figure 121). Notably, these organic and alkali metal iodide salts were readily soluble in the reaction medium and therefore were used without additional solubilizing agents, as was previously required for the *in situ* exchange of Br-I when conducting polymerization in organic media.[41]

Control experiments performed in the absence of either EBPA, iodide salts, or light did not lead to initiation of a polymerization, indicating the importance of the contributing components for a successful iodine-mediated photoATRP under visible light (Entries 10-12, Table 1).

6.4.1 Effect of polymerization medium

Using water as a solvent resulted in a well-controlled iodine-mediated photoATRP of PEGMA$_{300}$ monomer under blue light irradiation. The efficiency of polymerization in aqueous media was further demonstrated by conducting the polymerization in bulk or in an organic solvent, *N,N*-dimethylformamide (DMF). Tetrabutylammonium iodide (TBAI) was used to exchange the initiator's Br to I. Kinetics of the polymerization in bulk showed a decrease in the rate of the polymerization over time yielding 87 % monomer conversion in 6 h (Figure 112-A). Size exclusion chromatography (SEC) analysis of the polymer obtained in bulk showed a broad molecular weight distribution with a high $Đ$ of 2.16 (Figure 112-B). The uncontrolled polymerization in bulk can be related to the poor solubility of TBAI in the monomer, and consequently inefficient Br-I exchange and hence poor catalysis. Under these conditions, using DMF as an organic solvent, a decrease in the rate of polymerization was observed as the polymerization progressed with 70 % monomer conversion in 6 h. A relatively high $Đ$ of 1.43 was obtained in DMF (Figure 112-C). Fast generation of radicals under a strong blue light irradiation and relatively slow rate of propagation in DMF led to the termination of polymer chains and hence a decrease in the rate of polymerization. However, conducting the polymerization of PEGMA$_{300}$ monomer in water resulted in a fast and well-controlled process

ensured by a rapid formation of the radicals under a strong blue light and a high rate of propagation in water. Linear semi-logarithmic kinetics were observed with the polymerization reaching 94 % monomer conversion in 90 min providing polymers with low $Đ$ of 1.22 (Figure 112-D and Figure 116). Notably, SEC traces of the polymers obtained in water showed a shoulder appearing at higher molecular weights as the reaction reached high monomer conversions. The appearance of this shoulder can be attributed to the presence of di-functional impurities in the monomer, resulting in branching at higher conversions, which can be suppressed by conducting the polymerizations under dilute conditions (Figure 116-Figure 118).
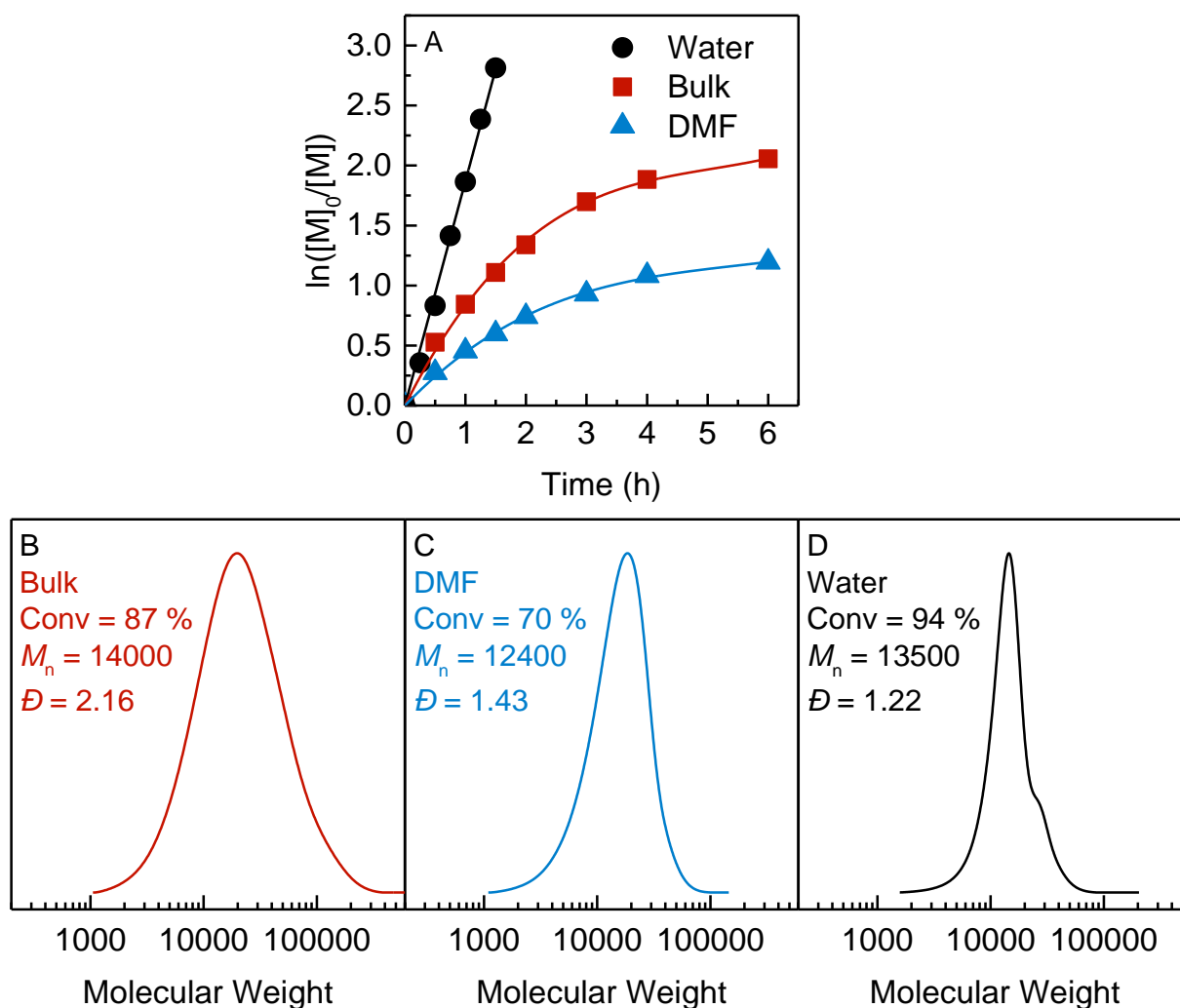
Figure 112. Iodine-mediated photoATRP of PEGMA$_{300}$ in different reaction media demonstrating a fast and well-controlled polymerization obtained in water compared to bulk or in DMF. (A) Kinetics and (B) SEC results of the

polymerizations. Reaction conditions: [PEGMA$_{300}$]/[EBPA]/[TBAI] = 50/1/4 in 50 vol % solvent (water of DMF) or bulk. Irradiated under blue LEDs (λ_{max} = 460 nm, 12 mW/cm^2).

6.4.2   Effect of light sources on polymerization

Iodine-mediated photoATRP in water was successfully initiated and controlled with a wide range of visible light sources. Figure 113-A shows the kinetics of the polymerization of PEGMA$_{300}$ monomer in the presence of TBAI under blue, green and yellow light LEDs. Irradiation under blue light LEDs (460 nm) resulted in 94 % monomer conversion in 2 h (M_n = 15 100, Đ = 1.17), Figure 113-B and Figure S3.

Under a green light (520 nm) irradiation, polymerization was slower and reached ~ 90 % monomer conversion in 6 h and provided polymers with well-controlled properties (M_n = 13300, Đ = 1.20), Figure 113-C. Polymerizations under blue and green lights showed linear semi-logarithmic kinetics with a lower rate of polymerization observed under green LEDs. Importantly, well-controlled polymerizations were achieved in both cases with molecular weights in agreement with theoretical values and Đ < 1.2. Under yellow light LEDs (595 nm), a slow polymerization of PEGMA$_{300}$ monomer was observed giving ~ 77 % conversion in 24 h, and polymers showed a Đ of 1.43, Figure 113-D. These results demonstrate the efficiency of iodine-mediated photoATRP in aqueous media achieved over a wide range of visible light in the presence of simple iodide salts.

Notably, iodine-mediated photoATRP was successfully performed in the absence of any added conventional photoinitiator/photocatalyst. Therefore, in the presence of iodide salts, direct photolysis of the labile C-I bond by visible light may be responsible for the formation of radicals and therefore successful polymerizations.
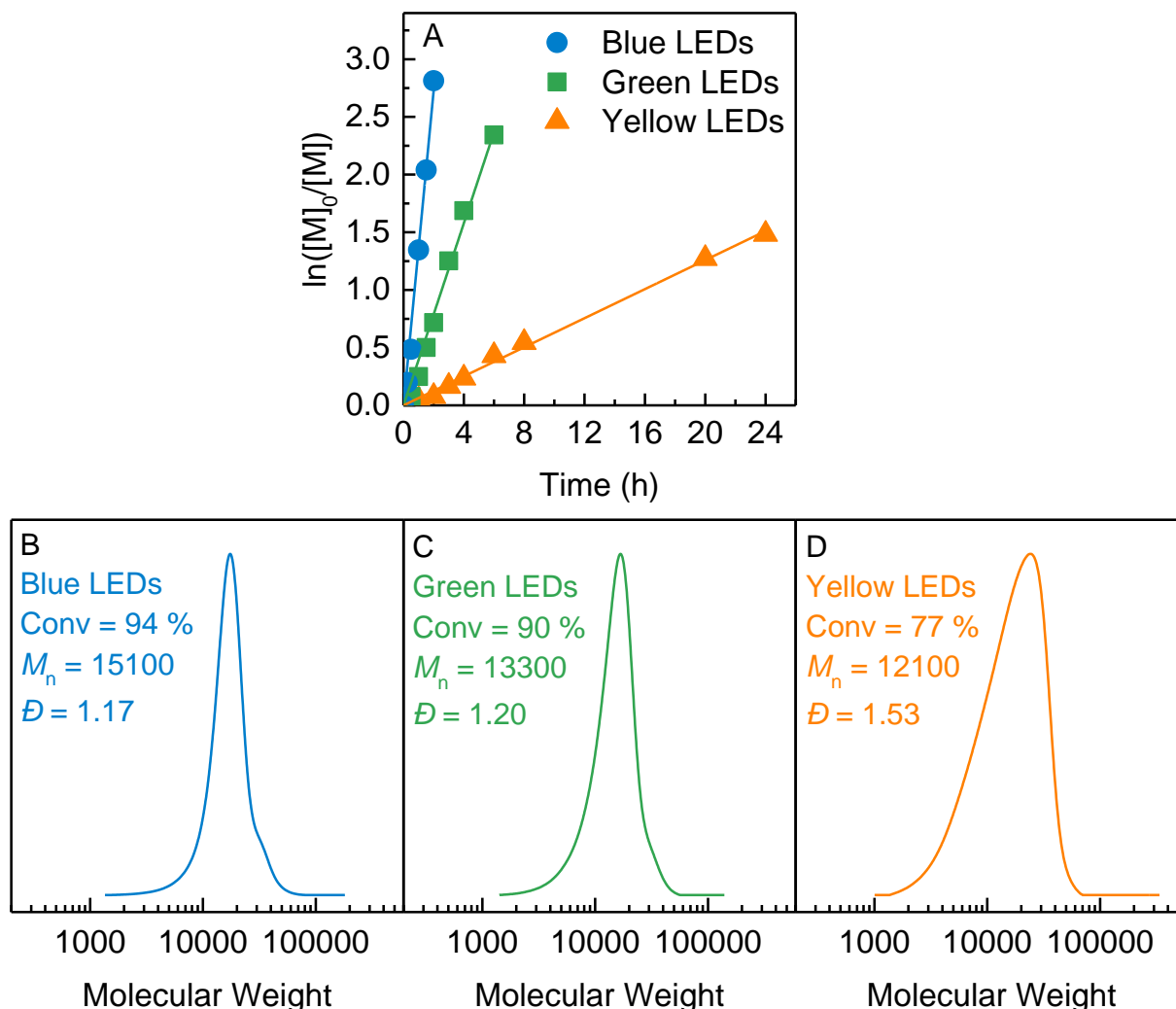
Figure 113. Iodine-mediated photoATRP of PEGMA$_{300}$ in aqueous media demonstrating well-controlled polymerizations achieved under a wide range of visible light irradiation. (A) kinetics and (B) SEC results of the polymerizations. Reaction conditions: [PEGMA$_{300}$]/[EBPA]/[TBAI] = 50/1/4, monomer 75 vol % in water, irradiated under blue (λ_{max} = 460 nm, 12 mW/cm^2), green (λ_{max} = 520 nm, 4.5 mW/cm^2), and yellow (λ_{max} = 595 nm, 0.6 mW/cm^2) LEDs.

6.4.3 Temporal control

Kinetics of the polymerization was mediated by switching the light on and off. As shown in Figure 114, iodine-mediated photoATRP of PEGMA$_{300}$ in water was activated only under blue light irradiation and was switched off by removing the light. Importantly, control over the polymerization was maintained during multiple light on/off switches with molecular weights in line with theoretical values and low $Đ < 1.2$.
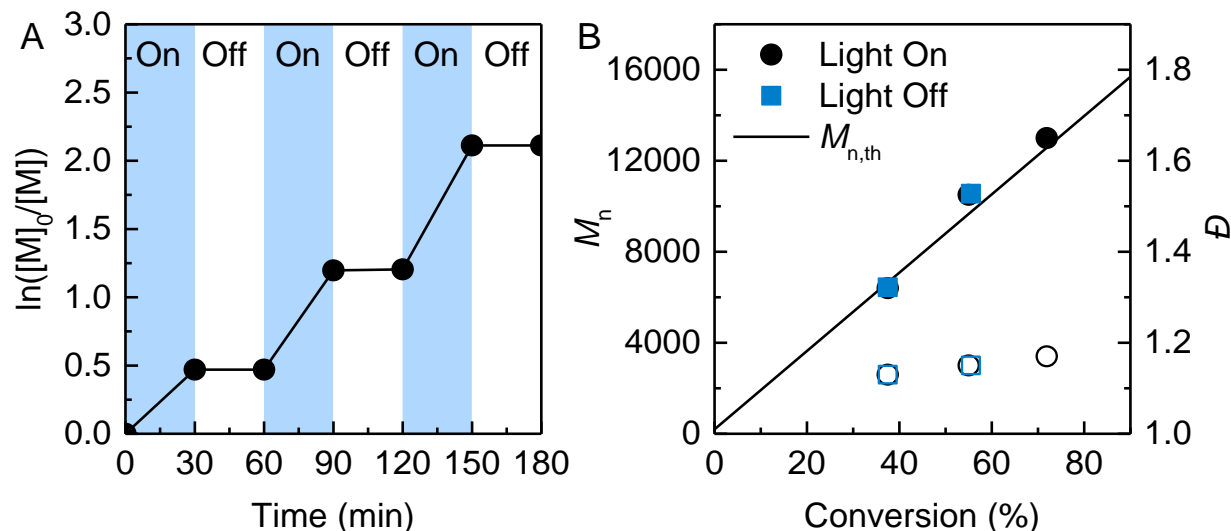
Figure 114. Temporal control in iodine-mediated photoATRP in water, demonstrating control of polymer chain growth under light irradiation. Reaction conditions: [PEGMA$_{300}$]/[EBPA]/[TBAI] = 50/1/4 in 75 vol % water. Irradiated under blue LEDs (λ_{max} = 460 nm, 12 mW/cm^2). (A) Kinetics of the polymerization upon multiple light on/off switches. (B) Number-average molecular weight (M_n, solid points) and dispersity ($Đ$, open points) as a function of monomer conversion.

6.4.4 Polymerizations in the presence of residual oxygen

Iodine-mediated photoATRP was controlled in the presence of residual oxygen without performing typical deoxygenation processes. Oxygen tolerant polymerizations of PEGMA$_{300}$ were conducted under blue light irradiation using TBAI or KI as the catalyst and targeting degrees of polymerization (DP$_t$) of 50-200. Results of the polymerizations showed well-controlled polymers obtained in the presence of residual oxygen reaching high monomer conversions and providing polymers with low $Đ$ < 1.2 (Table 27). As shown in Figure 115, the polymers synthesized in the presence of residual oxygen showed monomodal, narrow molecular weight distributions, indicating a high level of control over polymers achieved under these conditions.

Table 27.   Results of iodine-mediated photoATRP in the presence of residual oxygen (without deoxygenation)

Entry	Iodide salt	DP_t	Conv. (%)	$M_{n,th}$	M_n	$Đ$
1	TBAI	50	93	14200	15300	1.19
2	TBAI	100	85	25800	25000	1.18
3	TBAI	200	64	38600	34000	1.17
4	KI	50	74	11300	11500	1.20
5	KI	100	62	18800	17000	1.21
6	KI	200	44	26600	18500	1.20

[a] Reaction conditions: $[PEGMA_{300}]/[EBPA]/[I^-] = DP_t/1/4$ (DP_t = 50, 100, and 200) in 75 vol % water (total volume 8 mL). Irradiated under blue LEDs (λ_{max} = 460 nm, 12 mW/cm^2) for 2 h. Polymerizations were performed without deoxygenation of the solutions in full, capped vials.
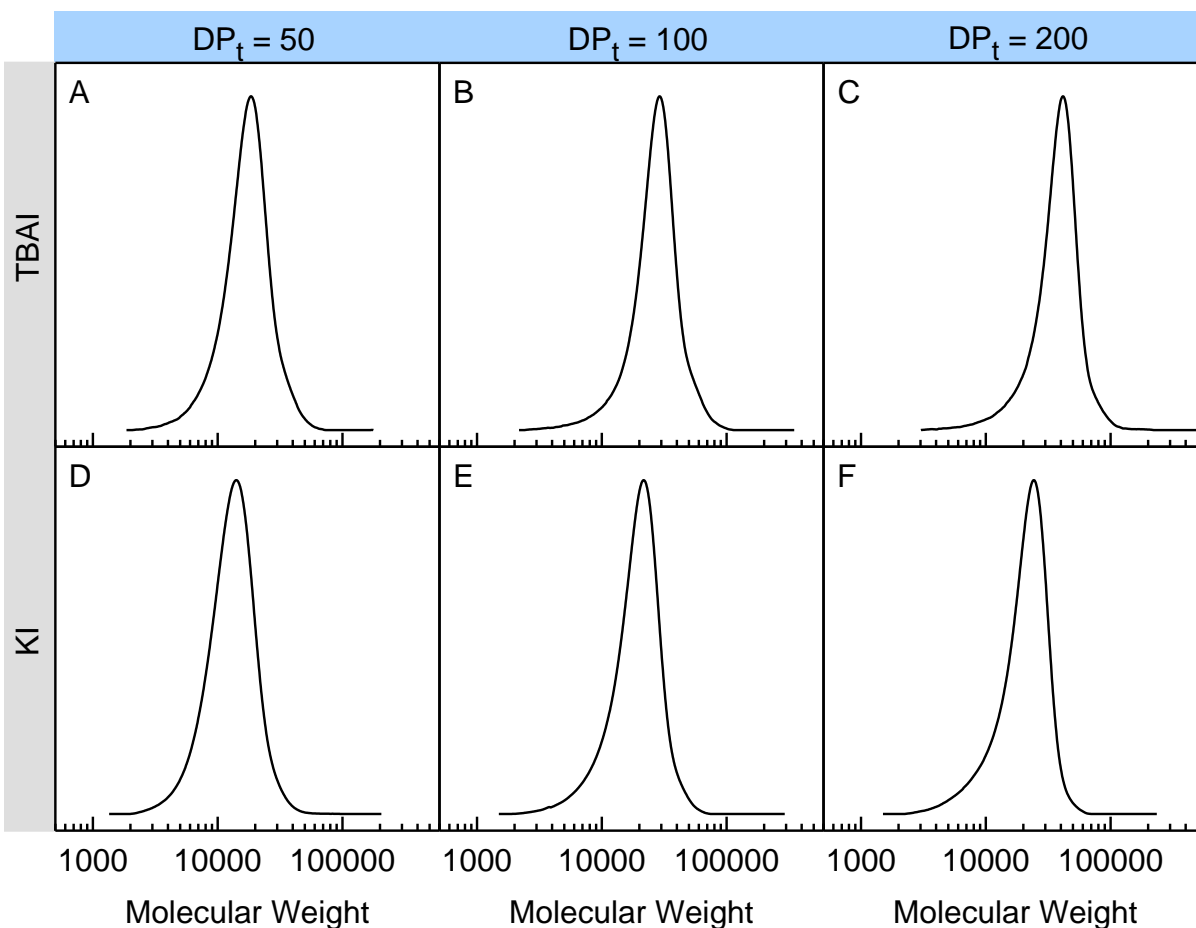
Figure 115. SEC traces of the polymers synthesized in the presence of residual oxygen. Reaction conditions: $[PEGMA_{300}]/[EBPA]/[I^-] = DP/1/4$ (DP = 50, 100, and 200) in 75 vol % water (total volume 8 mL). Irradiated under blue LEDs (λ_{max} = 460 nm, 12 mW/cm^2) for 2 h. Polymerizations were performed without deoxygenation of the solutions in full, capped vials.

6.5. Conclusions

In summary, iodine-mediated photoATRP was investigated in aqueous media. Polymerizations were catalyzed by iodide salts that were also used to initially generate alkyl iodide initiator *in situ*. Use of water as a solvent resulted in fast polymerizations, providing high monomer conversions with polymers showing well-controlled properties. Importantly, iodine-mediated photoATRP was initiated and controlled under a wide range of visible light irradiation including blue, green, and yellow lights in the absence of conventional photocatalysts. Furthermore, polymerizations were successfully controlled in the presence of residual oxygen signifying the potential of iodine-mediated photoATRP for use in applications without the need for performing deoxygenation processes.

6.6. Experimental Section and Supporting Information

Materials

Poly(ethylene glycol) methyl ether methacrylate (M_n 300, PEGMA$_{300}$, Sigma-Aldrich) was passed through a column of basic alumina to remove inhibitor. Ethyl α-bromophenylacetate (EBPA, 97 % Sigma-Aldrich), tetrabutylammonium iodide (TBAI, Fisher Chemical), potassium iodide (KI, Fisher Chemical), sodium iodide (NaI, Sigma-Aldrich), and lithium iodide (LiI, Sigma-Aldrich) were used as received.

Instrumentation

^{1}H nuclear magnetic resonance (^{1}H NMR) measurements were performed on a Bruker Avance™ III 500 MHz spectrometer. Molecular weight properties of the polymers were determined by size-exclusion chromatography (SEC). The SEC instrument was equipped with a Waters 515 pump and Waters 410 differential refractometer. SEC measurements were performed using PSS columns (Styrogel 10^5, 10^3, 10^2 Å) with DMF as an eluent at the flow rate of 1 mL/min. Linear

poly(methyl methacrylate) standards were used for calibration. Polymerizations were irradiated under blue (λ_{max} = 465 nm, 12 mW/cm^2), green (λ_{max} = 520 nm, 4.5 mW/cm^2), and yellow (λ_{max} = 595 nm, 0.6 mW/cm^2) light LEDs purchased from aspectLED.

General procedure for iodine-mediated photoATRP

Into a 2-dram vial equipped with a stir bar was added TBAI (103.4 mg, 0.28 mmol, 4 equiv.) The vial was sealed with a septum rubber and was subjected to vacuum and back filling with nitrogen for three times. PEGMA$_{300}$ monomer (1 mL, 3.5 mmol, 50 equiv.) and water (3 mL, 75 vol %) degassed with nitrogen in separate containers for 30 min were added to the vial under nitrogen atmosphere. EBPA (12.2 µL, 70 µmol, 1 equiv.) was added into the solution and the vial was irradiated under blue LEDs to start the polymerization. Samples were taken and analyzed by NMR and SEC techniques.

Supporting polymerization results:

Polymerizations using TBAI:

Figure 116. Iodine-mediated photoATRP in aqueous media. Reaction conditions: [PEGMA$_{300}$]/[EBPA]/[TBAI] = 50/1/4 in 50 vol % water. Irradiated under blue LEDs (λ_{max} = 460 nm, 12 mW/cm^2). (A) Kinetics of the polymerization. (B) Number-average molecular weight (M_n, solid points) and dispersity ($Đ$, open points) as a function of monomer conversion. (C) SEC traces.
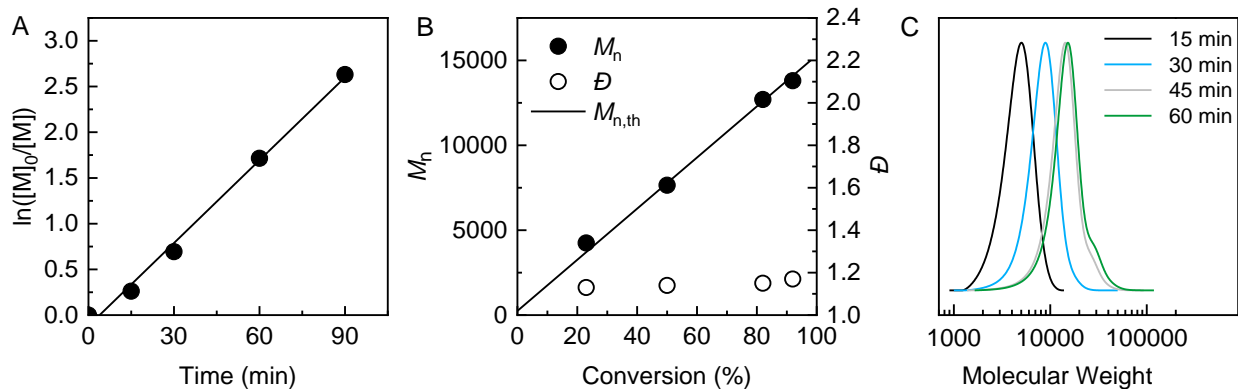
Figure 117. Iodine-mediated photoATRP in aqueous media. Reaction conditions: [PEGMA$_{300}$]/[EBPA]/[TBAI] = 50/1/4 in 67 vol % water. Irradiated under blue LEDs (λ_{max} = 460 nm, 12 mW/cm^2). (A) Kinetics of the polymerization. (B) Number-average molecular weight (M_n, solid points) and dispersity (Đ, open points) as a function of monomer conversion. (C) SEC traces.
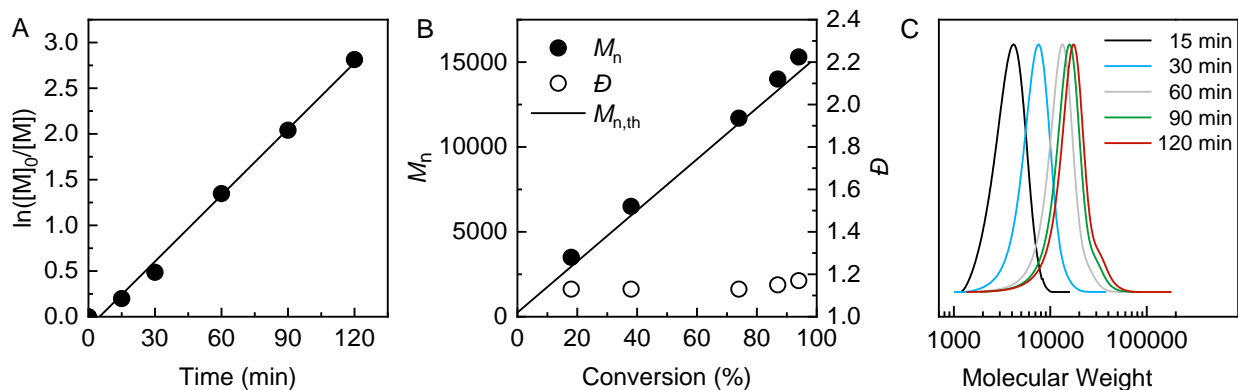
Figure 118. Iodine-mediated photoATRP in aqueous media. Reaction conditions: [PEGMA$_{300}$]/[EBPA]/[TBAI] = 50/1/4 in 75 vol % water. Irradiated under blue LEDs (λ_{max} = 460 nm, 12 mW/cm^2). (A) Kinetics of the polymerization. (B) Number-average molecular weight (M_n, solid points) and dispersity (Đ, open points) as a function of monomer conversion. (C) SEC traces.

Polymerizations using KI:
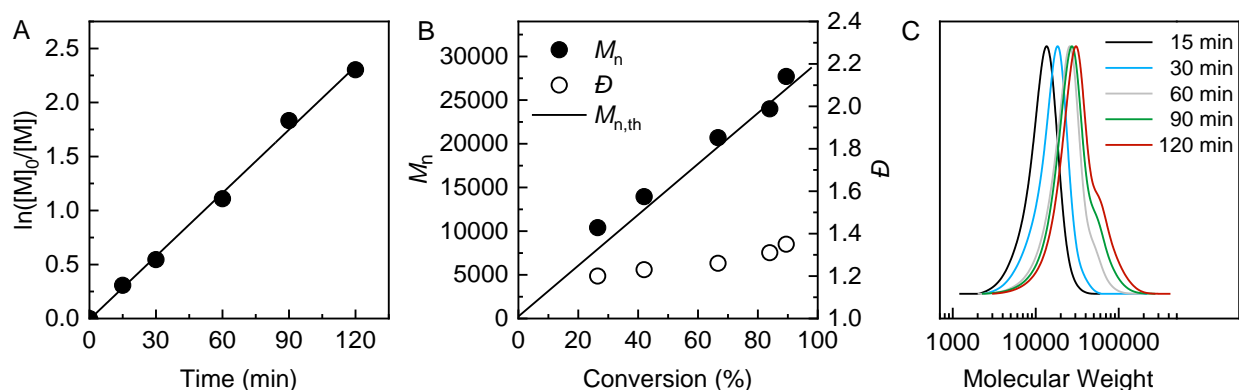
Figure 119. Iodine-mediated photoATRP in aqueous media. Reaction conditions: [PEGMA$_{300}$]/[EBPA]/[KI] = 100/1/4 in 50 vol % water. Irradiated under blue LEDs (λ_{max} = 460 nm, 12 mW/cm^2). (A) Kinetics of the polymerization. (B) Number-average molecular weight (M_n, solid points) and dispersity ($Đ$, open points) as a function of monomer conversion. (C) SEC traces.
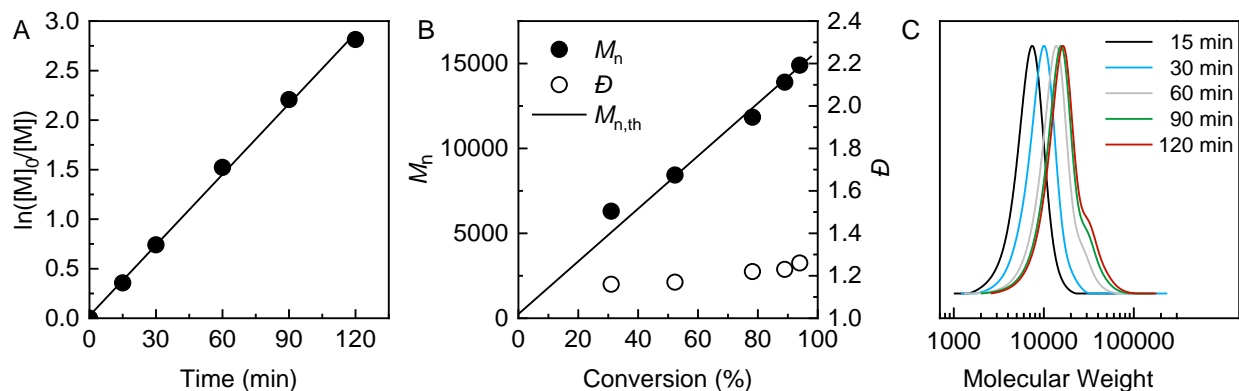
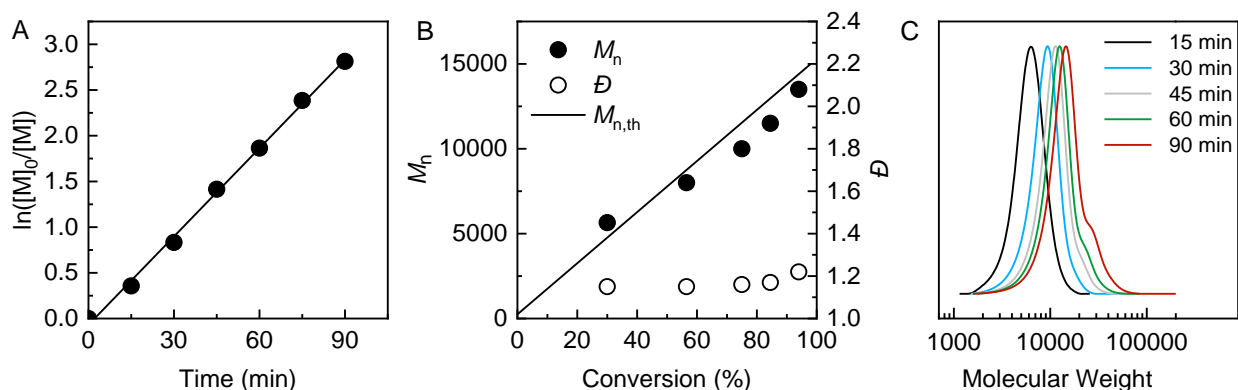**Figure 120.** Iodine-mediated photoATRP in aqueous media. Reaction conditions: [PEGMA$_{300}$]/[EBPA]/[KI] = 50/1/4 in 50 vol % water. Irradiated under blue LEDs (λ_{max} = 460 nm, 12 mW/cm^2). (A) Kinetics of the polymerization. (B) Number-average molecular weight (M_n, solid points) and dispersity ($Đ$, open points) as a function of monomer conversion. (C) SEC traces.

316
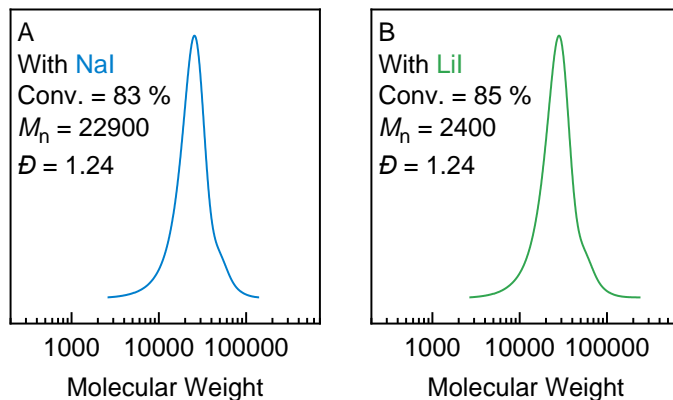
Figure 121. Results of iodine-mediated photoATRP of PEGMA$_{300}$ monomer in the presence of (A) sodium iodide (NaI) and (B) lithium iodide (LiI) salts. Reaction conditions: [PEGMA$_{300}$]/[EBPA]/[I$^-$] = 100/1/4 in 75 vol % water. Irradiated under blue LEDs (λ_{max} = 460 nm, 12 mW/cm^2) for 2 h.

6.7. References

1. Huang, Z.; Gu, Y.; Liu, X.; Zhang, L.; Cheng, Z.; Zhu, X. Metal-Free Atom Transfer Radical Polymerization of Methyl Methacrylate with ppm Level of Organic Photocatalyst. *Macromol. Rapid Commun.*

2. Kutahya, C.; Aykac, F. S.; Yilmaz, G.; Yagci, Y. LED and visible light-induced metal free ATRP using reducible dyes in the presence of amines. *Polym. Chem.* **2016,** 7 (39), 6094-6098.

3. Crivello, J. V. Benzophenothiazine and benzophenoxazine photosensitizers for triarylsulfonium salt cationic photoinitiators. *J. Polym. Sci., Part A: Polym. Chem.* **2008,** 46 (11), 3820-3829.

4. Matyjaszewski, K.; Xia, J. Atom Transfer Radical Polymerization. *Chem. Rev.* **2001,** 101 (9), 2921-2990.

5. Wang, J.-S.; Matyjaszewski, K. Controlled/"living" radical polymerization. atom transfer radical polymerization in the presence of transition-metal complexes. *J. Am. Chem. Soc.* **1995,** 117 (20), 5614-5615.

6. Matyjaszewski, K. Atom Transfer Radical Polymerization (ATRP): Current Status and Future Perspectives. *Macromolecules* **2012,** 45 (10), 4015-4039.

7. Ribelli, T. G.; Lorandi, F.; Fantin, M.; Matyjaszewski, K. Atom Transfer Radical Polymerization: Billion Times More Active Catalysts and New Initiation Systems. *Macromol. Rapid Commun.* **2019,** 40 (1), 1800616.

8. Ouchi, M.; Sawamoto, M. 50th Anniversary Perspective: Metal-Catalyzed Living Radical Polymerization: Discovery and Perspective. *Macromolecules* **2017,** 50 (7), 2603-2614.

9. di Lena, F.; Matyjaszewski, K. Transition metal catalysts for controlled radical polymerization. *Prog. Polym. Sci.* **2010,** 35 (8), 959-1021.

10. Boyer, C.; Corrigan, N. A.; Jung, K.; Nguyen, D.; Nguyen, T.-K.; Adnan, N. N. M.; Oliver, S.; Shanmugam, S.; Yeow, J. Copper-Mediated Living Radical Polymerization (Atom Transfer Radical Polymerization and Copper(0) Mediated Polymerization): From Fundamentals to Bioapplications. *Chem. Rev.* **2016,** 116 (4), 1803-1949.

11. Kato, M.; Kamigaito, M.; Sawamoto, M.; Higashimura, T. Polymerization of Methyl Methacrylate with the Carbon Tetrachloride/Dichlorotris-(triphenylphosphine)ruthenium(II)/Methylaluminum Bis(2,6-di-tert-butylphenoxide) Initiating System: Possibility of Living Radical Polymerization. *Macromolecules* **1995,** 28 (5), 1721-1723.

12. Xue, Z.; He, D.; Xie, X. Iron-catalyzed atom transfer radical polymerization. *Polym. Chem.* **2015,** 6 (10), 1660-1687.

13. Poli, R.; Allan, L. E. N.; Shaver, M. P. Iron-mediated reversible deactivation controlled radical polymerization. *Prog. Polym. Sci.* **2014,** 39 (10), 1827-1845.

14. Pan, X.; Fang, C.; Fantin, M.; Malhotra, N.; So, W. Y.; Peteanu, L. A.; Isse, A. A.; Gennaro, A.; Liu, P.; Matyjaszewski, K. Mechanism of Photoinduced Metal-Free Atom Transfer Radical Polymerization: Experimental and Computational Studies. *J. Am. Chem. Soc.* **2016,** 138 (7), 2411-2425.

15. Treat, N. J.; Sprafke, H.; Kramer, J. W.; Clark, P. G.; Barton, B. E.; Read de Alaniz, J.; Fors, B. P.; Hawker, C. J. Metal-Free Atom Transfer Radical Polymerization. *J. Am. Chem. Soc.* **2014,** 136 (45), 16096-16101.

16. Theriot, J. C.; Lim, C.-H.; Yang, H.; Ryan, M. D.; Musgrave, C. B.; Miyake, G. M. Organocatalyzed atom transfer radical polymerization driven by visible light. *Science* **2016,** 352 (6289), 1082-1086.

17. Ouchi, M.; Terashima, T.; Sawamoto, M. Transition Metal-Catalyzed Living Radical Polymerization: Toward Perfection in Catalysis and Precision Polymer Synthesis. *Chem. Rev.* **2009,** 109 (11), 4963-5050.

18. Isse, A. A.; Lin, C. Y.; Coote, M. L.; Gennaro, A. Estimation of Standard Reduction Potentials of Halogen Atoms and Alkyl Halides. *The Journal of Physical Chemistry B* **2011,** 115 (4), 678-684.

19. Lanzalaco, S.; Fantin, M.; Scialdone, O.; Galia, A.; Isse, A. A.; Gennaro, A.; Matyjaszewski, K. Atom Transfer Radical Polymerization with Different Halides (F, Cl, Br, and I): Is the Process "Living" in the Presence of Fluorinated Initiators? *Macromolecules* **2017,** 50 (1), 192-202.

20. Matyjaszewski, K.; Gaynor, S.; Wang, J.-S. Controlled Radical Polymerizations: The Use of Alkyl Iodides in Degenerative Transfer. *Macromolecules* **1995,** 28 (6), 2093-2095.

21. Gaynor, S. G.; Wang, J.-S.; Matyjaszewski, K. Controlled Radical Polymerization by Degenerative Transfer: Effect of the Structure of the Transfer Agent. *Macromolecules* **1995,** 28 (24), 8051-8056.

22. Iovu, M. C.; Matyjaszewski, K. Controlled/Living Radical Polymerization of Vinyl Acetate by Degenerative Transfer with Alkyl Iodides. *Macromolecules* **2003,** 36 (25), 9346-9354.

23. David, G.; Boyer, C.; Tonnar, J.; Ameduri, B.; Lacroix-Desmazes, P.; Boutevin, B. Use of Iodocompounds in Radical Polymerization. *Chem. Rev.* **2006,** 106 (9), 3936-3962.

24. Ni, Y.; Zhang, L.; Cheng, Z.; Zhu, X. Iodine-mediated reversible-deactivation radical polymerization: a powerful strategy for polymer synthesis. *Polym. Chem.* **2019,** 10 (20), 2504-2515.

25. Goto, A. Photo-Induced Living Radical Polymerization via Organic Catalysis. *J. Photopolym. Sci. Technol.* **2015,** 28 (1), 37-42.

26. Discekici, E. H.; Lee, I.-H.; Ren, J. M.; Bates, M. W.; McGrath, A. J.; de Alaniz, J. R.; Laitar, D. S.; Van Dyk, A. K.; Kalantar, T. H.; Hawker, C. J. Aqueous reverse iodine transfer polymerization of acrylic acid. *J. Polym. Sci., Part A: Polym. Chem.* **2019,** 57 (18), 1877-1881.

27. Goto, A.; Ohtsuki, A.; Ohfuji, H.; Tanishima, M.; Kaji, H. Reversible Generation of a Carbon-Centered Radical from Alkyl Iodide Using Organic Salts and Their Application as

Organic Catalysts in Living Radical Polymerization. *J. Am. Chem. Soc.* **2013,** 135 (30), 11131-11139.

28. Xiao, L.; Sakakibara, K.; Tsujii, Y.; Goto, A. Organocatalyzed Living Radical Polymerization via in Situ Halogen Exchange of Alkyl Bromides to Alkyl Iodides. *Macromolecules* **2017,** 50 (5), 1882-1891.

29. Liu, X.; Zhang, L.; Cheng, Z.; Zhu, X. Straightforward catalyst/solvent-free iodine-mediated living radical polymerization of functional monomers driven by visible light irradiation. *Chem. Commun.* **2016,** 52 (72), 10850-10853.

30. Ohtsuki, A.; Lei, L.; Tanishima, M.; Goto, A.; Kaji, H. Photocontrolled Organocatalyzed Living Radical Polymerization Feasible over a Wide Range of Wavelengths. *J. Am. Chem. Soc.* **2015,** 137 (16), 5610-5617.

31. Sarkar, J.; Xiao, L.; Goto, A. Living Radical Polymerization with Alkali and Alkaline Earth Metal Iodides as Catalysts. *Macromolecules* **2016,** 49 (14), 5033-5042.

32. Wang, C.-G.; Hanindita, F.; Goto, A. Biocompatible Choline Iodide Catalysts for Green Living Radical Polymerization of Functional Polymers. *ACS Macro Lett.* **2018,** 7 (2), 263-268.

33. Jones, G. R.; Anastasaki, A.; Whitfield, R.; Engelis, N.; Liarou, E.; Haddleton, D. M. Copper-Mediated Reversible Deactivation Radical Polymerization in Aqueous Media. *Angew. Chem. Int. Ed.* **2018,** 57 (33), 10468-10482.

34. Ni, Y.; Tian, C.; Zhang, L.; Cheng, Z.; Zhu, X. Photocontrolled Iodine-Mediated Green Reversible-Deactivation Radical Polymerization of Methacrylates: Effect of Water in the Polymerization System. *ACS Macro Lett.* **2019,** 8 (8), 1419-1425.

35. Fantin, M.; Isse, A. A.; Gennaro, A.; Matyjaszewski, K. Understanding the Fundamentals of Aqueous ATRP and Defining Conditions for Better Control. *Macromolecules* **2015,** 48 (19), 6862-6875.

36. Shanmugam, S.; Xu, J.; Boyer, C. Aqueous RAFT Photopolymerization with Oxygen Tolerance. *Macromolecules* **2016,** 49 (24), 9345-9357.

37. Yeow, J.; Chapman, R.; Gormley, A. J.; Boyer, C. Up in the air: oxygen tolerance in controlled/living radical polymerisation. *Chem. Soc. Rev.* **2018,** 47 (12), 4357-4387.

38. Lamb, J. R.; Qin, K. P.; Johnson, J. A. Visible-light-mediated, additive-free, and open-to-air controlled radical polymerization of acrylates and acrylamides. *Polym. Chem.* **2019,** 10 (13), 1585-1590.

39. Enciso, A. E.; Fu, L.; Russell, A. J.; Matyjaszewski, K. A Breathing Atom-Transfer Radical Polymerization: Fully Oxygen-Tolerant Polymerization Inspired by Aerobic Respiration of Cells. *Angew. Chem. Int. Ed.* **2018,** 57 (4), 933-936.

40. Enciso, A. E.; Fu, L.; Lathwal, S.; Olszewski, M.; Wang, Z.; Das, S. R.; Russell, A. J.; Matyjaszewski, K. Biocatalytic "Oxygen-Fueled" Atom Transfer Radical Polymerization. *Angew. Chem. Int. Ed.* **2018,** 57 (49), 16157-16161.

41. Dadashi-Silab, S.; Pan, X.; Matyjaszewski, K. Photoinduced Iron-Catalyzed Atom Transfer Radical Polymerization with ppm Levels of Iron Catalyst under Blue Light Irradiation. *Macromolecules* **2017,** 50 (20), 7967-7977.

Chapter 7. Summary and Outlook

External control of polymerization offers new possibilities in synthesis of well-defined polymers. In this dissertation, I undertook a comprehensive research to develop and expand the mechanistic understanding of controlling ATRP by external stimuli. This study encompassed analyzing various modes of ATRP activation and catalytic systems.

In Chapter 2, I presented a new approach for gaining temporal control in the presence of zerovalent metals. The effect of polymerization components and in particular the effect of the activity of the Cu catalysts was also in photoinduced ATRP. These studies shed light on mechanistic understanding of ATRP in response to external stimuli and achieving temporal control. The importance of developing highly active ATRP catalysts was signified in achieving excellent control over polymerization by external means. I showed that the dynamics of ATRP in the presence of highly active catalytic systems shifted the equilibrium toward deactivator and therefore in the absence of stimuli, small amounts of L/Cu^I activator were quickly consumed by radical termination reactions.

To gain on-demand control over the activity of the catalyst and hence the polymerization, I developed redox switchable ATRP, whereby the oxidation state of the Cu catalyst was altered using redox agents. In the presence of a reducing agent such as ascorbic acid, L/Cu^I activator was generated to start the polymerization. Upon addition of an oxidizing agent such as a ferrocenium salt or oxygen, the L/Cu^I activator was switched off by oxidation to L/Cu^{II} and therefore polymerization stopped. This system provided on-demand switch of polymerization between on/off states multiple times by modulating the oxidation state of the catalyst without compromising control over polymerization.

Subsequent chapters explored new ATRP catalytic systems that can be triggered and mediated by visible light.

Chapter 3 developed the dual photoredox catalysis in photoinduced ATRP to take advantage of the long wavelengths of visible light in activating ATRP. A conjugated microporous polymer composed of phenothiazine was synthesized and used as a photocatalyst. The presence of aromatic groups for crosslinking the PTZ extended the conjugation throughout the network that showed an absorption profile >600 nm. Therefore, the PTZ-CMP was used to trigger ATRP

under green or red light irradiation through generation of L/Cu^I activator to mediate the polymerization of (meth)acrylate monomers. An important feature of the heterogeneous nature of the photocatalyst was the easy separation from reaction mixture and reusability in multiple reactions without any decrease in photocatalytic efficiency.

In Chapter 4, I studied iron-catalyzed ATRP systems. I showed that through a ligand-to-metal charge transfer process, the iron activator can be generated under blue light irradiation. This system was studied in homo and copolymerization of a variety of methacrylates including semi-fluorinated monomers as well as achieving temporal control by light. A mechanistic study was undertaken to elucidate the effect of halogen and reaction media in polymerization control in iron-catalyzed ATRP. In Cl-based initiating systems, the strong bonding of Cl to the iron catalyst renders inefficient deactivation of propagating radicals and therefore provided poor control over polymerization. Polymers with poor initiation efficiency and large dispersity (>1.6) were obtained in Cl-based initiating systems. On the other hand, in Br-based initiating systems, the Br atom transfer was efficient and provided polymers with controlled molecular weights and low dispersity (<1.2) values. Moreover, I showed that a relatively low polar reaction medium was needed to achieve well-controlled polymers in iron-catalyzed ATRP even in the presence of Br-based initiating system. For example, polymerizations were well-controlled in anisole which can solubilize the catalyst with FeBr$_4^-$ anion, as well as provide control over polymerization. However, in a polar solvent such as acetonitrile, the deactivator was strongly stabilized that led to a poor deactivation of polymer chains.

In chapter 5, I showed that a core-modified phenothiazine, phenyl benzo[*b*]phenothiazine (Ph-benzoPTZ), could mediate ATRP of methacrylate monomers as a photoredox catalyst under visible light irradiation. The benzoPTZ photocatalyst showed an absorption profile extended to visible region because of its conjugated core structure. Photoexcitation of the PTZ photocatalyst generated excited state species capable of activating the dormant chains to form radicals and the oxidized form of the photocatalyst with a bromide anion. The latter species acted as a deactivator of the growing chains.

In chapter 6, I showed that ATRP could be mediated by light irradiation using an alkyl iodide initiator. The iodine mediated photoATRP used a bench stable alkyl bromide to generate the iodide initiator via a halogen exchange process. The polymerization of a water-soluble monomer

was controlled in the presence of iodide salts used as catalysts to mediate polymerization under light in aqueous media. The iodide chain end and iodide anion formed charge transfer complexes that could be activated under blue, green, or even yellow light. This system showed tolerance to residual oxygen to perform polymerization without deoxygenation processes. Iodine-mediated photoATRP offers potential in developing light-mediated polymerizations without use of metal complexes.

Outlook and future directions

Advances in RDRP and, in particular in ATRP processes, have revolutionized synthesis of well-defined polymers. In photoinduced ATRP, future studies should explore new possibilities to harness the energy of light in carrying out polymerizations. Using visible or NIR light would be of great importance. One direction is to develop dual photoredox catalytic systems in which a suitable photocatalyst or a photosensitizer active under NIR light can be used to generate activating species for ATRP. Use of NIR light with low energy and high depth of penetration can offer new opportunities in conducting ATRP.

As reported in Chapter 3, the heterogeneous photocatalysts showed efficient activation of the ATRP process via reduction of the Cu catalyst under green or red light irradiation. The hyper-crosslinking process using aromatic crosslinkers containing dimethoxy substituents holds promise in tuning the photophysical properties of the resulting network by extended conjugation. Future directions may involve investigation of the synthesis of similar heterogeneous networks using different methoxy-functional aromatic crosslinkers such as 4,4′-dimethoxybiphenyl or 2,6-dimethoxynaphthalene. This will provide access to networks with different structural properties including pore size, surface area, and many more. In addition, another possibility to control the photochemical properties of these networks would be through use of a photochemically active monomer such as porphyrins or phthalocyanines. It is anticipated that crosslinking porphyrin or phthalocyanine compounds, which absorb in the red region (<700 nm), with dimethoxy-functional crosslinkers should extend the absorption to NIR region.

Iron catalysts hold great promise in controlling ATRP processes. Improved mechanistic understanding of the catalytic properties of iron in ATRP will enable designing efficient catalytic systems. Current challenges need to be addressed to broaden the scope of iron-catalyzed ATRP and explore new ligands. For example, the anionic iron catalysts in the presence of halide anion

ligands perform poorly in polar solvents or in the presence of functional monomers. Designing new ligand families and iron complexes should provide access to carrying out ATRP in a wide range of reaction media and monomers. Potential candidates include iron complexes with macrocyclic ligands such as porphyrins or phthalocyanines, which are robust complexes and can tolerate polar media. Additionally, the porphyrin scaffold can be functionalized to potentially impart further ligating groups to modulate the catalytic properties of the complex. Furthermore, these iron complexes can be functionalized with stimuli-responsive groups such as thermoresponsive polymer arms to enable controlling their physical or catalytic properties.

Finally, many photoredox catalysts developed for organo-catalyzed ATRP were active under UV or visible light (in the UV-blue region). Furthermore, these O-ATRP systems have been mainly applied in the polymerization of methacrylate monomers with only a limited number of reports achieving polymerization of acrylates. Future research in O-ATRP should aim for designing new catalytic systems that can work for a wide range of monomers including acrylates and other monomers.

Appendix – List of Published and Submitted Papers

*Papers highlighted in **blue** are presented in this dissertation.*

* Denotes equal contribution.

20. **S. Dadashi-Silab**,* K. Kim,* K. Matyjaszewski, Halogen Effect in Iron-Catalyzed Atom Transfer Radical Polymerization, *submitted*

19. **S. Dadashi-Silab**, F. Lorandi, M. J. DiTucci, M. Sun, G. Szczepaniak, T. Liu, K. Matyjaszewski, Conjugated Cross-linked Phenothiazines as Green or Red Light Heterogeneous Photocatalysts for Copper-Catalyzed Atom Transfer Radical Polymerization, *J. Am. Chem. Soc.*, **2021**, 143, 9630–9638

18. M. R. Martinez, **S. Dadashi-Silab**, F. Lorandi, Y. Zhao, K. Matyjaszewski, Depolymerization of P(PDMS$_{11}$MA) Bottlebrushes via Atom Transfer Radical Polymerization with Activator Regeneration, Macromolecules 2021, 54, 12, 5526–5538

17. N. J. Shah, **S. Dadashi-Silab**, M. D. Galluzzo, S. Chakraborty, W. S. Loo, K. Matyjaszewski, N. P. Balsara, Effect of Added Salt on Disordered Poly(ethylene oxide)-*Block*-Poly(methyl methacrylate) Copolymer Electrolytes, *Macromolecules*, 2021, *54*, 1414–1424

16. F. Lorandi, S. Lathwal, M. R. Martinez, **S. Dadashi-Silab**, G. Szczepaniak, J. Cuthbert, Reflection on the Matyjaszewski Lab Webinar Series and the Rise of Webinars in Polymer Chemistry, *ACS Macro Lett.*, 2021, *10*, 54–59

15. G. Szczepaniak, M. Łagodzińska, **S. Dadashi-Silab**, A. Gorczyński, K. Matyjaszewski, Fully Oxygen–Tolerant Atom Transfer Radical Polymerization Triggered by Sodium Pyruvate, *Chem. Sci.*, 2020, *11*, 8809–8816

14. **S. Dadashi-Silab**,* I.-H. Lee,* A. Anastasaki, F. Lorandi, B. Narupai, N. D. Dolinski, M. L. Allegrezza, M. Fantin, D. Konkolewicz, C. J. Hawker, K. Matyjaszewski, Investigating Temporal Control in Photoinduced Atom Transfer Radical Polymerization, *Macromolecules*, 2020, *53*, 5280–5288

13. W. Yan, **S. Dadashi-Silab**, K. Matyjaszewski, N. D. Spencer, E. M. Benetti, Surface-Initiated Photoinduced ATRP: Mechanism, Oxygen Tolerance, and Temporal Control during the Synthesis of Polymer Brushes, *Macromolecules*, 2020, *53*, 2801–2810

12. **S. Dadashi-Silab**, K. Matyjaszewski, Iron Catalysts in Atom Transfer Radical Polymerization, *Molecules*, 2020, *25*, 1648 (*invited review*)

11. M. R. Martinez, J. Sobieski, F. Lorandi, M. Fantin, **S. Dadashi-Silab**, G. Xie, M. Olszewski, X. Pan, T. G. Ribelli, K. Matyjaszewski, Understanding the Relationship between Catalytic Activity and Termination in photoATRP: Synthesis of Linear and Bottlebrush Polyacrylates, *Macromolecules*, 2020, *53*, 59–67

10. **S. Dadashi-Silab**, G. Szczepaniak, S. Lathwal, K. Matyjaszewski, Iodine-Mediated PhotoATRP in Aqueous Media with Oxygen Tolerance, *Polym. Chem.*, 2020, *11*, 843–848

9. **S. Dadashi-Silab**, K. Matyjaszewski, Iron-Catalyzed Atom Transfer Radical Polymerization of Semifluorinated Methacrylates, *ACS Macro Lett.*, 2019, *8*, 1110–1114

8. Y. Wang, **S. Dadashi-Silab**, F. Lorandi, K. Matyjaszewski, Photoinduced Atom Transfer Radical Polymerization in ab initio Emulsion, *Polymer*, 2019, *165*, 163–167

7. **S. Dadashi-Silab**, F. Lorandi, M. Fantin, K. Matyjaszewski, Redox-Switchable Atom Transfer Radical Polymerization, *Chem. Commun.*, 2019, *55*, 612–615

6. Y. Wang, **S. Dadashi-Silab**, K. Matyjaszewski, Photoinduced Miniemulsion Atom Transfer Radical Polymerization, *ACS Macro Lett.*, 2018, *7*, 720–725

5. **S. Dadashi-Silab**, K. Matyjaszewski, Temporal Control in Atom Transfer Radical Polymerization Using Zerovalent Metals, *Macromolecules*, 2018, *51*, 4250–4258

4. **S. Dadashi-Silab**, X. Pan, K. Matyjaszewski, Photoinduced Iron-Catalyzed Atom Transfer Radical Polymerization with ppm Levels of Iron Catalyst under Blue Light Irradiation, *Macromolecules*, 2017, *50*, 7967–7977

3. Z. Wang, X. Pan, J. Yan, **S. Dadashi-Silab**, G. Xie, J. Zhang, Z. Wang, H. Xia, K. Matyjaszewski, Temporal Control in Mechanically Controlled Atom Transfer Radical Polymerization Using Low ppm of Cu Catalyst, *ACS Macro Lett.*, 2017, *6*, 546–549

2. **S. Dadashi-Silab**, X. Pan, K. Matyjaszewski, Phenyl Benzo[b]phenothiazine as a Visible Light Photoredox Catalyst for Metal-Free Atom Transfer Radical Polymerization, *Chem. Eur. J.*, 2017, *23*, 5972–5977

1. X. Pan, N. Malhotra, **S. Dadashi-Silab**, K. Matyjaszewski, A Simplified Fe-Based PhotoATRP Using Only Monomers and Solvent, *Macromol. Rapid Commun.*, 2017, *38*, 1600651